

The role of mechanosensing in placental vascular function

Dr Lara Catherine Morley

Submitted in accordance with the requirements for the degree of
Doctor of Philosophy

The University of Leeds

Faculty of Medicine and Health

Leeds Institute of Cardiovascular and Metabolic Medicine

Academic Unit of Obstetrics and Gynaecology

December 2020

Intellectual Property and Publication Statements

The candidate confirms that the work submitted is her own and that appropriate credit has been given where reference has been made to the work of others.

This copy has been supplied on the understanding that it is copyright material and that no quotation from the thesis may be published without proper acknowledgement.

The right of Dr Lara Catherine Morley to be identified as Author of this work has been asserted by her in accordance with the Copyright, Designs and Patents Act 1988.

© 2021 The University of Leeds and Dr Lara Catherine Morley

Acknowledgements

First and foremost I would like to thank my supervisory team: Mr Nigel Simpson and Professor David Beech. Your experience and teaching from both the clinical and scientific worlds has been invaluable to my progression, and truly inspirational.

My time in the laboratory has been a continual learning curve, and had its daunting moments. However, learning the science has been fascinating, and having fostered my willingness to learn, I hope you have seen me progress in both skills and understanding of translational research.

I have also learnt a great deal from working in the laboratory alongside Hollie Appleby, Hannah Gaunt, Peter Webster, Adam Hyman, Beth Evans and Jian Shi. Post docs Melanie Ludlow, Marjolaine Debant, Fiona Bartoli, Vincenza Caolo and Laetitia Lichtenstein have been a well of knowledge, and have been very patient in answering all of my questions!

My time at Leeds Institute of Cardiovascular and Metabolic Medicine has been a happy one, and I am very grateful for the friendships I have formed along the way. Thanks to Marc Bailey, Tom Slater and the other academic medics for all the trips to Pure cafe to indulge my pregnancy craving for iced coffee. Thanks to Hollie Appleby and Hannah Gaunt for all the chats and laughs, and making me feel welcome in lab – I'm so glad we have kept in touch. Thanks to Karen Forbes and her group, and Niamh Forde for their words of scientific wisdom and advice, and for involving me in public engagement events which were highlights of my PhD. Thanks to Sara Ibrahim for choosing to do her MRes project with us, giving me my first experience of supervision, and being a great asset to the team. Thanks to Georgia Mappa and Nic Orsi for facilitating a joint ethical approval for multiple placenta projects and for contributing to sharing resources between LICAMM and SJUH research institutes.

On the clinical side, I have been inspired to do academic obstetrics since I was a medical student. I was incredibly lucky to have been taken under the wing of Thomas Tang,

Professor Adam Balen, Professor James Walker and, of course, Nigel. This has given me fantastic opportunities, including the chance to develop a guideline for the World Health Organisation, and present my work at conferences in Manchester, London, Edinburgh, Kota Kinabalu, Florida, San Francisco and Tokyo. Special thanks go Lizzy Bonney for being a clinical inspiration, and ensuring the safe delivery of my babies.

This PhD project would not have been possible without the funding I have received from The Wellcome Trust Institutional Strategic Support Fund, the MRC and the Royal College of Obstetricians and Gynaecologists. Thanks to the doctors, theatre staff, midwives and specialist research midwives at Leeds Teaching Hospitals Trust for facilitating collection of the samples used in this project. A special thanks go to the patients who consented to be involved in our research.

My family, including my husband Sam, and my parents have been incredibly encouraging. To mum and dad – thanks for all the childcare, hot dinners and regularly starting my car (the list could go on and on...). But most of all thank you for always being there, and for being my greatest champions. Sam - we got married in the first month of starting this PhD, which was followed by the birth of Reuben Alexander, and then Iris Eloise in my final year. They turned our world upside down, but have given us so much joy and new perspectives. Thank you for being a brilliant daddy, and your unwavering support.

Abstract

Introduction

The mechanical force of blood flow is a fundamental determinant of vascular homeostasis. This frictional stimulation of cells, fluid shear stress (FSS), is increasingly recognised as being essential to placental development and function. FSS generates vasodilatation through the release of endothelial nitric oxide, a process vital for normal pregnancy vascular adaptation.

The fetus is reliant on placental perfusion to meet its circulatory and metabolic demands. Failure of the mechanisms enabling responsive interaction between fetoplacental and maternal circulations results in placental insufficiency, a cause of fetal growth restriction.

The mechanosensitive cation channel, Piezo1, is reported to be a direct sensor of FSS, and is required for murine embryonic vascular development. This study aimed to determine whether Piezo1 is important for mechanosensing in human fetoplacental endothelial cells (FpECs), in normal pregnancy and that affected by placental insufficiency.

Methods and main results

Patients were consented at Leeds Teaching Hospitals Trust. Samples were allocated as appropriately grown for gestational age (AGA), or small for gestational age (SGA), defined as birthweight <10th percentile.

FpECs were highly responsive to FSS, demonstrating alignment, upregulation of *PIEZO1*, eNOS phosphorylation, and activation of ADAM10- a downstream Notch signalling enzyme. FSS-induced alignment was suppressed by Piezo1 depletion. The Piezo1 chemical activator, Yoda1, caused strong dose-dependent elevation of the intracellular Ca²⁺ concentration. Yoda1 increased eNOS phosphorylation, and upregulated ADAM10 activity.

SGA FpECs showed increased total and phosphorylated eNOS. Expression of *PIEZO1* and Notch receptor 3 (*NOTCH3*) were upregulated in SGA. Yoda1-induced Ca²⁺ entry

was reduced in the SGA group. Furthermore, Yoda1-evoked upregulation of Notch components was strikingly blunted in SGA.

Conclusion

Piezo1 channels are present and functional in the fetoplacental endothelium. Piezo1 is important for the normal response of FpECs to FSS, and activation initiates downstream pathways with important roles in vascular regulation. In placental insufficiency, mechanisms of FSS-sensing are compromised, allowing vasoconstrictor and anti-angiogenic effects to dominate. Efforts to compensate restricted blood flow via peNOS may be insufficient due to a lack of flow responsiveness and saturated NO system. Enhanced Piezo1 activity in response to Yoda1 suggests the possibility for developing tools to manipulate mechanosensors. As such, Piezo1 is an entry point to a more nuanced understanding of placental FSS-sensing, presenting an opportunity for future intervention in placental insufficiency.

Funding

This PhD project was facilitated by a Wellcome Trust Institutional Strategic Support Fund, and Medical Research Council and Royal College of Obstetricians and Gynaecologists.

Table of Contents

Intellectual Property and Publication Statements.....	ii
Acknowledgements	iii
Abstract	v
Table of Contents.....	vii
List of Tables.....	xiii
List of Figures	xiv
Abbreviations	xix
Publications and communications.....	xxv
Additional achievements.....	xxvii
Chapter 1 Introduction	1
1.1 Placental development and vascular function	3
1.2 Epidemiology of FGR	6
1.3 Clinical sequelae of fetal growth restriction	8
1.3.1 Perinatal and early-onset	8
1.3.2 Developmental programming and later life disease	9
1.4 Risk factors and aetiology of FGR.....	11
1.4.1 Fetal.....	12
1.4.2 Maternal.....	13
1.4.3 Placental origins of FGR and pre-eclampsia.....	15
1.4.5 Clinical assessment and management.....	20
1.4.6 Placental pathology in FGR.....	22
1.5 Flow dynamics and shear stress	23
1.6 Shear stress sensing in pregnancy	25
1.6.1 Pre-implantation	25
1.6.2 Post-implantation and early pregnancy	26
1.6.3 Flow-mediated regulation of fetoplacental blood flow.....	28
1.6.4 Regulation of uteroplacental blood flow	33
1.7 Fluidic shear stress sensors.....	34
1.7.1 Cell structures	36
1.7.2 Mechanosensor complexes.....	37
1.7.4 Ion channels.....	37
1.7.5 Piezo ion channel subunit	38
1.8 Summary	42
1.9 Hypothesis, aims and objectives	44

1.9.1 Hypothesis	44
1.9.2 Aims	44
1.9.3 Objectives	44
Chapter 2 Materials and methods.....	46
2.1 Patient recruitment and consent.....	46
2.2 Ethical approval, data management and storage	47
2.3 Sampling and processing placental tissue.....	47
2.4 Isolation of fetoplacental endothelial cells (FpECs)	49
2.5 Isolation of human umbilical vein endothelial cells (HUVECs).....	51
2.6 Culture of FpECs and HUVECs.....	51
2.7 Isolation of chorionic plate artery endothelial cells	52
2.8 Immunostaining	53
2.9 Functional assays.....	54
2.9.1 Angiogenesis.....	54
2.9.2 Migration assay	55
2.9.3 Proliferation	56
2.10 RNA isolation and quantitative RT-PCR.....	57
2.10.1 RNA isolation	57
2.10.2 Reverse transcription	60
2.10.3 QPCR (quantitative polymerase chain reaction)	60
2.10.4 Effect of Yoda1 treatment on mRNA abundance	64
2.10.5 Gel electrophoresis	65
2.11 Intracellular calcium (Ca ²⁺) measurements	65
2.11.1 Yoda1 experiments using the FlexStation 3.....	68
2.11.2 Osmotic stress response.....	69
2.12 Short-interfering RNA transfection.....	71
2.12.1 Live dead cell assay.....	73
2.13 Protein isolation	74
2.13.1 Protein quantification.....	74
2.13.2 Western blotting	75
2.13.3 Imaging and analysing western blots	78
2.13.4 Effect of Yoda1 on eNOS phosphorylation in FpECs	78
2.14 Shear stress experiments.....	78
2.14.1 FpEC alignment in response to fluid shear stress	78
2.14.2 Single cell response to FSS	79
2.15 ADAM10 activity assay.....	80

2.15.1	ADAM10 activity in response to Yoda1	80
2.15.2	ADAM10 activity in response to SS.....	81
2.16	Patch clamp.....	82
2.17	Statistical analysis	83
Chapter 3 Isolating and characterising fetoplacental endothelial cells from the human placenta		84
3.1	Introduction.....	84
3.2	Patient recruitment	84
3.3	Demographic data	85
3.4	Validating the phenotype of placental samples	90
3.4.1	Macro- and microscopic appearance of placental samples...90	
3.4.2	Differential gene expression in whole placental tissue	95
3.4.3	Microscopic appearance and immunofluorescence	96
3.5	FpECs show properties of migration, proliferation and tube formation 99	
3.5.1	Migration	100
3.5.2	Proliferation.....	102
3.5.3	Angiogenic properties of fetoplacental endothelial cells.....	102
3.6	FpECs are responsive to stimulation with shear stress and VEGF104	
3.7	Discussion of results and limitations.....	106
Chapter 4 Presence and functional activity of Piezo1 and other mechanosensors in the human placenta		111
4.1	Introduction.....	111
4.2	Selecting reference genes for QPCR studies	117
4.3	<i>PIEZO1</i> mRNA is consistently expressed in placental tissue	121
4.3.1	Expression of <i>PIEZO1</i> in whole villous tissue from AG control and SGA placentas	121
4.3.2	Expression of <i>PIEZO1</i> in first trimester pregnancy tissue ...	123
4.3.3	Expression of <i>PIEZO1</i> is increased in FpECs from SGA samples.....	126
4.4	Piezo1 channel activity in placental ECs	134
4.4.1	Exposure to FSS increases the expression of Piezo1 mRNA and protein in FpECs	134
4.4.2	Endothelium freshly isolated from placental arterial ECs showed dominant FSS-activated Piezo1 channels.....	137
4.5	Piezo1 channel activity can be investigated by <i>PIEZO1</i> silencing	140
4.5.1	Piezo1 is required for FpEC alignment to FSS.....	142
	Figure 4.16 The response to FSS in FpECs is Piezo1 dependent...143	

4.5.2	Piezo1 is not required for FpEC viability or substrate attachment	144
4.6	Chemical activation of Piezo1 using Yoda1.....	146
4.6.1	Piezo1-dependent Ca ²⁺ -entry in FpECs.....	149
4.6.2	Yoda1-induced Ca ²⁺ is reduced in FpECs from SGA placentas	152
4.7	Expression of additional mechanosensors in the placenta.....	158
4.7.1	Expression of <i>PIEZO2</i> in the placenta.....	158
4.7.2	Expression of GPR68 in the placenta.....	160
4.8	Discussion.....	163
4.9	Summary.....	175
Chapter 5 Interplay between Piezo1 activity, nitric oxide- and purinergic signalling in FpECs.....		176
5.1	Introduction.....	176
5.2	Total eNOS and peNOS are increased in SGA placentas.....	179
5.3	Chemical and FSS-evoked Piezo1 activation is coupled to eNOS phosphorylation.....	181
5.4	FpECs respond to ATP but P2Y ₂ receptors are not a requirement for eNOS phosphorylation.....	188
5.5	Hypotonic stress induces a rise in intracellular Ca ²⁺ in FpECs.....	197
5.5.1	Hypotonic stress-induced intracellular Ca ²⁺ mobilisation in FpECs is mediated, at least in part, by Piezo1 channels.....	198
5.5.2	Antagonising P2 receptors partially inhibits intracellular Ca ²⁺ entry evoked by hypotonic stress.....	204
5.6	Summary of findings.....	208
5.7	Discussion.....	209
5.7.1	Nitric oxide signalling in endothelial cells.....	209
5.7.2	Nitric oxide signalling in fetal growth restriction.....	211
5.7.3	Piezo1 channel activity and ATP activation in FpECs.....	213
Chapter 6 Notch signalling via Piezo1 in the placenta.....		216
6.1	Introduction.....	216
6.1.1	Notch signalling in endothelial cells.....	216
6.1.2	Function and importance of Notch signalling.....	218
6.1.3	Notch signalling in human disease.....	220
6.1.4	Shear stress regulation of Notch signalling.....	220
6.2	Notch signalling gene expression in human placentas.....	222
6.2.1	Notch genes are expressed in FpECs from AG control and SGA placentas.....	222

6.2.2	Expression of notch genes in whole villous tissue from AG control and SGA placentas	226
6.2.3	Notch genes are expressed in early pregnancy tissue	232
6.3	Chemical activation of Piezo1 upregulates parts of the Notch signalling pathway in FpECs	236
6.4	Effect of Piezo1 depletion on Yoda1-stimulated Notch gene expression in FpECs	241
6.5	ADAM10 functional activity in FpECs can be stimulated by shear stress and Yoda1	244
6.6	Summary of findings.....	247
6.7	Discussion	247
6.7.1	Notch signalling in placental development and function	247
6.7.2	Notch signalling in pregnancy complications.....	250
6.7.3	Notch signalling and Piezo1	252
Chapter 7 Conclusion and future directions		256
7.1	Summary of key findings	256
7.1.1	Significant findings in FpECs from AGA placentas.....	256
7.1.2	Differential results between AGA and SGA FpECs	258
7.1.3	Significant findings in whole villous tissue from AGA placentas 259	
7.1.4	Differential results between AGA and SGA whole villous tissue 259	
7.2	Hypotheses based on significant findings.....	259
7.3	Final discussion.....	260
7.3.1	Piezo1 is a functionally active mechanosensor in the human placenta	260
7.3.2	Shear stress sensing and Piezo1 signalling are dysregulated in placental insufficiency	263
7.4	Future direction	268
7.4.1	<i>Ex vivo</i> studies of placental villous tissue and FpECs.....	268
7.4.2	Animal models.....	275
7.4.3	Modelling shear stress in the placenta	276
7.5	Clinical placental research considerations.....	279
7.6	Targeting mechanosensory pathways for FGR	280
7.6.1	Blood flow mimetics	280
7.6.2	Downstream modulators	282
7.6.3	Approaches to target the NO pathway	283
7.7	Conclusion.....	286

List of references	287
Appendix 1: Data collection proforma	304
Appendix 2: Sample databases	306

List of Tables

Table 1 Key research questions	2
Table 2 International definitions of fetal growth restriction	8
Table 3 Placental phenotypes associated with adult disease. Adapted from Myatt and Thornburg, 2018.	10
Table 4 Risk assessment for FGR. Adapted from RCOG, 2014.	12
Table 5 Antibodies used for immunostaining	54
Table 6 Primer Sequences and expected amplicon sizes.	64
Table 7 Chemicals used in experiments on the FlexStation.	67
Table 8 Hypotonic solutions used to test osmotic stress in FpECs.	70
Table 9 siRNA sequences.	72
Table 10 Primary antibodies used in Western blotting.....	77
Table 11 Demographic data of patients for whom placental tissue was sampled	87
Table 12 Birth and placental weights in AGA and SGA groups at term.	89
Table 13 Weight percentile and pathology reports for selected SGA placentas	94
Table 14. RNA concentration and purity ratios corresponding to the representative spectral images shown in Figure 4.1 A-H.....	115
Table 15. Patient samples used to generate the data presented in Figure 4.9 and Figure 4.10.	134
Table 16 Representative cycle threshold and minus reverse transcriptase values for Notch pathway and reference genes.....	226
Table 17 A summary of key follow up experiments	271
Table 18 Mother and baby details for samples collected for pilot study (2016)	306
Table 19 Mother and baby details for samples collected in 2017 (ethics: 13/YH/03/44).....	309
Table 20. Mother and baby details for samples collected in 2018-2020 (ethics: 18/LO/0067).....	319

List of Figures

Figure 1.1 Schematic representation of blood flow through the placenta, with contributions from the uteroplacental and fetoplacental circulations.....	5
Figure 1.2 Current management of SGA.....	22
Figure 1.3 Cross-sectional diagram of a vessel showing FSS produced by blood flow.....	24
Figure 1.4 Components of the EC, each with postulated roles in mechanosensing.	35
Figure 1.5 Structure and importance of Piezo1 for murine vascular development.....	40
Figure 1.6 Yoda1 chemical structure.	41
Figure 2.1 Isolation of FpECs.....	50
Figure 2.2 Clamped umbilical cord.....	51
Figure 2.3 Isolation of chorionic plate artery endothelial cells.....	53
Figure 2.4 Scratch WoundMaker™.....	56
Figure 2.5 Protocol for RNeasy Plus Mini Kit (Qiagen).....	58
Figure 2.6 Representative compound plate layout for the FlexStation 3.	69
Figure 2.7 Representative compound plate showing hypotonic solutions and Yoda1 being tested.....	71
Figure 2.8 Representative layout for transfection experiments.....	73
Figure 2.9 Representative BSA curve and worked example.	75
Figure 2.10 Experimental set up for pulsatile fluid shear stress ADAM10 assay.....	82
Figure 3.1 Summary demographic data.....	88
Figure 3.2 Representative images showing reduced comparative size of SGA placentas and macroscopic abnormalities.....	91
Figure 3.3 Reduced expression of both arterial and venous markers, but not CD31, in AGA versus SGA samples.	96
Figure 3.4 Isolated cells from placenta had the visual appearance expected of cultured ECs.....	97
Figure 3.5 Protein and structural markers of FpECs.	99
Figure 3.6 Normal FpECs migrate over time to close a scratch wound.	101
Figure 3.7 Normal FpECs proliferate in culture.....	102
Figure 3.8 FpECs form tubular structures when grown on suitable substrate.....	103
Figure 3.9 VEGF evokes Ca ²⁺ entry in FpECs.....	105

Figure 3.10 Normal FpECs respond to FSS by aligning in the direction of flow.	106
Figure 4.1. High quality nucleic acid obtained from placental tissue and cells under normal and experimental conditions.	114
Figure 4.2 QPCR reactions were performed using efficient primers for <i>PIEZO1</i> and <i>PIEZO2</i> , with single products detected during the melting phase of the reaction.	116
Figure 4.3 <i>ACTB</i> , <i>CYC-1</i> and <i>YWAZ</i> primer pairs were of suitable quality to use in QPCR reactions, as determined by efficiency and specificity.	118
Figure 4.4 Primer pairs of unsuitable quality to use in QPCR reactions, as determined by efficiency and specificity.	119
Figure 4.5 Stable expression levels of reference genes in the FpECs undergoing investigation.	121
Figure 4.6 <i>PIEZO1</i> mRNA is expressed in whole villous tissue.	122
Figure 4.7 No significant difference in <i>PIEZO1</i> expression between AGA and SGA villous tissue samples.	123
Figure 4.8. <i>PIEZO1</i> , <i>PIEZO2</i> and <i>GPR68</i> mRNA is expressed in early pregnancy tissue.	125
Figure 4.9. <i>PIEZO1</i> mRNA is present in cultured FpECs, with increased expression in SGA samples.	128
Figure 4.10 <i>PIEZO1</i> gene expression by subgroup analysis of maternal smoking in pregnancy, mode of delivery, and fetal sex.	131
Figure 4.11. FSS induces upregulation of Piezo1 mRNA that is significant in AG samples but not SGA FpECs.	135
Figure 4.12 Western blot for FpEC lysate probed with Proteintech anti-Piezo1 antibody after exposure to FSS.	136
Figure 4.13 Western blot for FpEC lysate probed with Beec4 anti-Piezo1 antibody after exposure to FSS.	137
Figure 4.14. Piezo1 channels are membrane-delimited sensors of FSS in freshly-isolated endothelium of human placental artery.	139
Figure 4.15 Piezo1 silencing confirmed by reduced mRNA and protein expression.	141
Figure 4.16 The response to FSS in FpECs is Piezo1 dependent.	143
Figure 4.17 FSS induces a change in Ca ²⁺ in FpECs, which is abolished by Piezo1 silencing.	144
Figure 4.18 Piezo1 is not a requirement for cell viability or attachment to the substrate.	145
Figure 4.19 Dose-dependent Ca ²⁺ entry occurs response to Yoda1 stimulation.	147
Figure 4.20 Dose-dependent Ca ²⁺ entry occurs response to Ionomycin stimulation.	148

Figure 4.21. Yoda1 induced Ca ²⁺ -entry in FpECs is inhibited by the Piezo1 channel antagonist, Gd ³⁺	150
Figure 4.22. Yoda1 induced Ca ²⁺ -entry in FpECs is inhibited by Piezo1 knockdown.	151
Figure 4.23 Example Ca ²⁺ measurement traces from AGA FpECs in response to Yoda1 stimulation.....	154
Figure 4.24 Example Ca ²⁺ measurement traces from SGA FpECs in response to Yoda1 stimulation.....	155
Figure 4.25. The baseline of Ca ²⁺ measurement traces does not differ between healthy or SGA FpECs, and there is no Yoda1 response in the absence of FpECs.	156
Figure 4.26 Pooled data showing reduced Yoda1-evoked Ca ²⁺ entry in SGA FpECs.....	157
Figure 4.27 Piezo2 is expressed in FpECs and whole villous tissue. .	159
Figure 4.28. Increased mRNA expression of GRP68 in SGA FpECs ...	162
Figure 4.29 FSS-evoked redistribution of Piezo1 in HUVECs (adapted from Li et al., 2014, extended data Figure 6).	167
Figure 4.30 Effect of intra-peritoneal administration of Calpain-2 inhibitor on days 4-7 of pregnancy (Reproduced from Kaneko et al. 2014).	169
Figure 4.31 Expression of <i>PIEZO</i> in FpECs and whole villous tissue.	171
Figure 5.1 Piezo1 channel activity is coupled to eNOS.....	177
Figure 5.2 SGA placentas show raised expression of eNOS and phosphorylated eNOS proteins.	180
Figure 5.3 FSS evokes S1177 eNOS phosphorylation.....	182
Figure 5.4 Yoda1 rapidly increases S1177 eNOS phosphorylation in FpECs.	184
Figure 5.5 Yoda1 increases S1177 eNOS phosphorylation in FpECs from AGA and SGA placentas.	186
Figure 5.6 Schematic depicting Yoda1 activation of Piezo1 channels evoking Ca ²⁺ entry and eNOS activation.	188
Figure 5.7 Intracellular Ca ²⁺ increase is stimulated by Yoda1 and ATP, with an early additive effect when both are applied to FpECs in combination.	191
Figure 5.8 Suramin inhibits ATP evoked Ca ²⁺ entry via an effect on P2Y ₂ receptors.	192
Figure 5.9 Suramin pre-treatment does not significantly reduce Yoda1-evoked Ca ²⁺ entry or blunt eNOS phosphorylation.....	194
Figure 5.10 ATP evoked Ca ²⁺ entry is not dependent on Piezo1 and nor does inhibition of P2Y ₂ channels prevent Yoda1 induced Ca ²⁺ entry in FpECs.	196

Figure 5.11 Hypotonic stress induces a change in the intracellular Ca ²⁺ concentration of FpECs.	198
Figure 5.12 Yoda1 strongly potentiates hypotonic responses in FpECs.	199
Figure 5.13 Hypotonicity-evoked increase in intracellular Ca ²⁺ entry in FpECs is suppressed by gadolinium (Gd ³⁺).	201
Figure 5.14 Piezo1 depletion reduces the hypotonicity-evoked rise in intracellular Ca ²⁺ entry in FpECs.	203
Figure 5.15 Hypotonicity mediated Ca ²⁺ entry in FpECs is partially blunted by suramin.	205
Figure 5.16 Depletion of Piezo1 and inhibition of P2 receptors prevented Ca ²⁺ increase in response to hypotonic FpEC swelling.	207
Figure 5.17 Schematic illustrating possible mechanisms by which FSS activation of Piezo1 and other mechanosensors in FpECs results in vasodilatation through the production of NO.	210
Figure 6.1 Notch signalling pathway schematic.	218
Figure 6.2 Notch pathway genes are expressed in FpECs.	223
Figure 6.3 Notch signalling genes are present in cultured FpECs from both AGA and SGA placentas, with increased expression of <i>NOTCH3</i> in SGA FpECs.	224
Figure 6.4 Notch pathway gene expression in whole villous tissue. ..	227
Figure 6.5 Notch signalling genes are present in whole villous tissue from AGA versus SGA placentas, with reduced expression of <i>ADAM10</i> in SGA samples.	228
Figure 6.6. <i>ADAM10</i> relative mRNA abundance is downregulated in tissue from SGA placentas.	231
Figure 6.7 Notch pathway genes are expressed in 1 st trimester pregnancy tissue.	232
Figure 6.8 Notch pathway genes are present in placentas from 1 st and 3 rd pregnancy trimesters with significant differential expression of <i>JAG1</i> and <i>HEY1</i>	234
Figure 6.9 Threshold cycle of detection values for <i>JAG1</i> and <i>HEY1</i> are lower in the first trimester compared with the 3 rd trimester.	235
Figure 6.10 Yoda1 did not induce a significant difference in the expression of Notch receptor genes 1 to 4 in either AG for SGA FpECs.	237
Figure 6.11 Yoda1 upregulates <i>HEY1</i> , <i>HES1</i> and <i>DLL4</i> , with differential expression between AG and SGA FpECs.	240
Figure 6.12 <i>PIEZO1</i> depletion blunts the effect of Yoda1 on the expression of <i>NOTCH4</i> , <i>HEY1</i> , <i>HES1</i> , <i>DLL1</i> and <i>DLL4</i>	243
Figure 6.13 The application of shear stress and Yoda1 potentiate the activity of the <i>ADAM10</i> enzyme in FpECs.	246

Figure 6.14 Localisation of Notch signalling proteins within the placental villi.....	250
Figure 6.15 Schematic of proposed mechanism of Piezo1 interaction with the canonical Notch signalling pathway in FpECs.	255
Figure 7.1. Schematic for our final hypothesis.	267

List of Equations

Equation 1 Beer-Lambert equation.	59
Equation 2 The $2^{-\Delta\Delta Ct}$ (Livak) method for calculating relative expression of mRNA.	61
Equation 3 Efficiency calculation	64

Abbreviations

Ab	Antibody
ACTB	β -actin
ADAM10	A Disintegrin and Metalloprotease
AGA	Appropriately grown for gestational age
ATP	Adenosine triphosphate
B2M	Beta-2-microglobulin
BMI	Body mass index
BNP	B-natriuretic peptide
bp	Base pair
BSA	Bovine Serum Albumin
Ca ²⁺	Calcium
CD31	Cluster of differentiation 31
cDNA	Complimentary DNA
cGMP	Cyclic guanosine monophosphate
CMV	Cytomegalovirus
CSL	CBF1, Suppressor of Hairless, Lag-1
Ct	Cycle threshold
CTG	Cardiotocography
CYC1	Cytochrome c-1
DAPT	Small molecule γ -secretase inhibitor
DLL	Delta-like ligand

DMSO	Dimethyl sulfoxide
DOHaD	Developmental origins of adult disease
DSL	Delta, Serrate or Lag-2
DV	Ductus venosus
EDHF	Endothelial derived hyperpolarising factor
eNOS	Endothelial nitric oxide synthase
EBM	Endothelial basal medium
EGM	Endothelial growth medium
EFNB2	Ephrin-B2
EFNB4	Ephrin-B4
EC	Endothelial cell
EP	Early pregnancy
Eph	Erythropoietin-producing hepatocellular
ER	Endoplasmic reticulum
FGR	Fetal growth restriction
FMV	Flow-mediated vasodilatation
FpEC	Fetoplacental endothelial cell
FRET	Fluorescence resonance energy transfer
FSS	Fluidic shear stress
GAPDH	Glyceraldehyde-3-phosphate dehydrogenase
Gd ³⁺	Gadolinium chloride hexahydrate
GDM	Gestational diabetes mellitus
GROW	Gestation related optimal weight

GTP	Guanosine triphosphate
hCAT-1	High affinity cationic amino acid transporter 1
HES	Helix-loop-helix
HEY	Hairy/enhancer of split-related
hFGF	Human fibroblast growth factor
HIF	Hypoxia-inducible factor
HPRT	Hypoxanthine phosphoribosyltransferase
HUAEC	Human umbilical artery endothelial cell
HUVEC	Human umbilical vein endothelial cell
i	Ionised
IGF	Insulin-like growth factor
IGFBP	Insulin-like growth factor binding protein
ISSHP	International Society for the Study of Hypertension in Pregnancy
IVS	Intervillous space
KLF8	Kruppel like factor 8
LGA	Large for gestational age
LICAMM	Leeds Institute of Cardiovascular and Metabolic Medicine
L-NAME	Nw-Nitro-L-arginine methyl ester hydrochloride
L-NMMA	NG-Monomethyl-L-arginine acetyl
LSCS	Lower segment caesarean section
LTHT	Leeds Teaching Hospitals Trust
MACS	Magnetically-activated cell sorting
MAPK	Mitogen-activated protein kinase

MLV	Murine leukaemia virus
MCA	Middle cerebral artery
MT	Mock transfected
NHDF	Normal human dermal fibroblasts
NICD	Notch intracellular domain
NO	Nitric oxide
NT	Non-transfected
OEF	Oxygen extraction fraction
OOC	Organs on a chip
PAPP-A	Pregnancy associated plasma protein A
PBS	Phosphate Buffered Saline
PECAM	Platelet/endothelial cell adhesion molecule
peNOS	Phosphorylated endothelial nitric oxide synthase
PET	Pre-eclamptic toxemia
P1.si	Piezo1 short interfering RNA
PI	Pulsatility index
PK	Protein kinase
PIGF	Placental-like growth factor
PO ₂	Partial pressure of oxygen
QPCR	Quantitative polymerase chain reaction
RCOG	Royal College of Obstetricians and Gynaecologists
RI	Resistance index
ROS	Reactive oxygen species

rpm	Revolutions per minute
RT	Reverse transcription
RWD	Relative wound density
SB 4x	Sample loading buffer (4x)
SBS	Standard Bath Solution
Sc.si	Control short interfering RNA
SDS	Sodium dodecyl sulphate
SEM	Standard error of the mean
sFLT	Soluble receptor for VEGF
SGA	Small for gestational age
siRNA	Short interfering RNA
SLB	Standard lysis buffer
SSP	Staurosporine
TAE	Tris-acetate-EDTA
TBP	TATA box-binding protein
TBS-T	Tris buffered saline with Tween
THU	Transmembrane helical unit
T _m	Melting temperature
TOP1	DNA topoisomerase 1
TRP	Transient receptor potential
UPR	Unfolded protein response
US	Ultrasound
UV	Ultraviolet

VEGF	Vascular endothelial growth factor
VEGFR	Vascular endothelial growth factor receptor
Veh	Vehicle
WHO	World Health Organisation
w/v	Weight per volume
vWF	Von Willebrand factor
YWHAZ	Tyrosine 3-monooxygenase/tryptophan 5-monooxygenase activation protein, zeta polypeptide
ZP	Zona pellucida

Publications and communications

Publications during PhD

Morley LC, Debant M, Walker JJ, Beech DJ, Simpson NAB. Placental blood flow sensing and regulation in fetal growth restriction. *Placenta*. 2021 Jan 18:S0143-4004(21)00015-1. doi: 10.1016/j.placenta.2021.01.007. Online ahead of print.

Morley LC, Walker JJ, Beech DJ, Simpson, NAB. New horizons review: Emerging concepts of shear stress in placental development and function. *Mol Hum Reprod*. 2019; 25:329-339

Morley LC, Shi J, Gaunt HJ, Hyman AJ, Webster PJ, Williams C, Forbes K, Walker JJ, Simpson NAB, Beech DJ. Piezo1 channels are mechanosensors in human fetoplacental endothelial cells. *Mol Hum Reprod*. 2018; 24:510-520

Morley LC, Walker JJ. Preeclampsia: Update. *British Medical Journal Best Practice*. Access at: <http://bestpractice.bmj.com/topics/en-gb/326> (Last update Oct 2020)

Rode B, Shi J, Endesh N, Drinkhill MJ, Webster PJ, Lotteau SJ, Bailey MA, Yuldasheva NY, Ludlow MJ, Cubbon RM, Li J, Futers TS, Morley L, Gaunt HJ, Marszalek K, Viswambharan H, Cuthbertson K, Baxter PD, Foster R, Sukumar P, Weightman A, Calaghan SC, Wheatcroft SB, Kearney MT, Beech DJ. Piezo1 channels sense whole body physical activity to reset cardiovascular homeostasis and enhance performance. *Nat Commun*. 2017; 8:350

Morley LC, Tang TMH, Balen AH on behalf of the Royal College of Obstetricians and Gynaecologists. Metformin Therapy for the Management of Infertility in Women with Polycystic Ovary Syndrome. *Scientific Impact Paper No. 13. BJOG*. 2017; 124:e306–e313

Balen AH, Morley LC, Misso M, Franks S, Legro RS, Wijeyaratne CN, Stener-Victorin E, Fauser BC, Norman RJ, Teede H. The management of anovulatory infertility in women

with polycystic ovary syndrome: an analysis of the evidence to support the development of global WHO guidance. *Hum Reprod Update*. 2016; 22:687-708

Morley LC, Simpson NAB. The principles of screening tests as applied to obstetrics and gynaecology. *Obstetrics, Gynaecology & Reproductive Medicine*. 2016; 26:1-6

Communications

Morley LC, Shi J, Gaunt H, Hyman A, Webster P, Forbes K, Walker JJ, Simpson NAB, DJ Beech. Piezo1 mechanosensitive ion channels are required for shear stress sensing in placental vasculature. *Placenta*. 2018; 69: E15-E15

LC Morley, P Webster, J Li, K Forbes, NAB Simpson, JJ Walker, DJ Beech. Mechanical sensing in placental vascular endothelium. *Placenta*. 2017; 57: 272-273

Additional achievements

Awards

- 2019 1st prize oral presentation. North of England Obstetrical and Gynaecological Society meeting, St James's University Hospital, Leeds, UK
- 2019 1st prize oral presentation. Postgraduate research symposium, Wellcome Trust Brenner building, St James's University Hospital, Leeds, UK (£150)
- 2018 Elsevier New Investigator Travel Award for abstract excellence. The International Federation of Placenta Associations, Tokyo, Japan (\$500)
- 2018 1st prize postgraduate research poster presentation. Health Education Yorkshire and the Humber, UK
- 2017 Runner up for the MRC Max Perutz science writing award: '*At the Placenta of Everything*'. Royal Institution, London, UK (£400)
- 2016 Gold medal presentation. '*Piezo1 in the placenta*'. Medico-Chirurgical Society meeting, Leeds, UK

Teaching and mentoring

Throughout my time at the Faculty of Medicine and Health, University of Leeds, I have taken an active role in teaching through developing and delivering tutorials both to students studying science and medicine. These have covered placental anatomy and physiology, endocrinology of the reproductive cycle, contraception and fertility, alongside practical teaching sessions using simulation equipment. I have supervised medical student projects, including the MRes undertaken by Sara Ibrahim, and have acted as an examiner. Following these activities I was recognised as a Fellow of the Higher Education Authority (FHEA).

Public engagement

- 2019 Be Curious: University of Leeds public engagement event attended by over 1,000 members of the public. Our stall entitled the 'Gestation Station' had multiple interactive features, including games and a competition, as well as models and microscopy.
- 2019 Pint of Science national festival: Our evening of talks entitled 'The Centre of the Womb-iverse' was a sell-out event.

Chapter 1 Introduction

As the critical interface between mother and fetus, the placenta undergoes constant vascular expansion and differentiation in order to maintain the dynamic interplay between the uteroplacental and fetoplacental circulations throughout pregnancy. The fetus is reliant on placental perfusion to meet its circulatory and metabolic demands. Failure of normal vascular adaptation can compromise effective gas exchange and nutrient supply leading to pregnancies being complicated by disorders such as pre-eclamptic toxemia (PET) and fetal growth restriction (FGR) (Kingdom et al., 2000).

Affected pregnancies are associated with an increased risk of perinatal morbidity and mortality (Alfirevic et al., 2015). The lack of available treatment for FGR often necessitates delivering the baby in order to prevent fetal demise, which may result in iatrogenic prematurity. Long term impacts of placental dysfunction include an increased risk of obesity and metabolic and cardiovascular disease into adulthood (Crispi et al., 2018). Efforts to develop therapies for FGR are hampered by a lack of knowledge of the molecular mechanisms responsible for regulating blood flow through the placenta.

Central to the development of effective therapies for FGR is understanding the molecular mechanisms responsible for placental haemoregulation, and how they may be manipulated.

Together with the maternal uteroplacental circulation, the fetoplacental vasculature is required for placental perfusion and is therefore a critical determinant of fetal growth and a successful pregnancy outcome (Kingdom et al., 2000, Su, 2015). Given the lack of placental autonomic innervation, fetoplacental endothelial function is controlled by haemodynamic forces, and the release of paracrine and vasoactive mediators, adapting according to circumstance (Tropea et al., 2018, Learmont and Poston, 1996).

A trigger for the release of vasoactive mediators from the endothelium is the frictional force of fluidic shear stress (FSS). This is the mechanical force generated by blood flow during each cardiac cycle. FSS has long been recognised as being vital for processes

including angiogenesis, vasculogenesis and control of vascular tone (Ando and Yamamoto, 2013). However, knowledge of the molecular mechanisms underpinning how cells respond to FSS and how this translates into biochemical signals is only now coming to the fore.

The ion channel subunit Piezo1 was first discovered in 2010 (Coste et al., 2010). Since then this mechanosensitive membrane protein has risen to prominence as a major player in FSS sensing (Hyman et al., 2017). Piezo1 channels are critical to vascular development and survival in mouse models with a disrupted endogenous *Piezo1* gene (Li et al., 2014). These FSS-sensitive channels are increasingly being investigated in a variety of cell types, and mutations of the *PIEZO1* gene have been found in human genetic disease (Lukacs et al., 2015, Fotiou et al., 2015).

This thesis presents the most up to date evidence of mechanosensing in placental vascular function and aims to address key challenges in the field (Table 1). My research has focussed on the role of recently identified mechanosensors, such as Piezo1, as regulators of fetoplacental circulatory flow and the implications for fetal wellbeing.

Fetoplacental endothelial cells (FpECs) were isolated and cultured from placentas where the baby was appropriately grown for gestational age (AGA), and those defined as small for gestational age (SGA), to provide an *in vitro* method for investigating the presence, and function of Piezo1. This is in addition to the study of whole villous tissue, human umbilical vein endothelial cells (HUVECs), human placental arterial cells from the chorionic plate, and first trimester pregnancy tissue.

- | |
|--|
| <ul style="list-style-type: none">- How is fluidic shear stress (FSS) sensed and transduced in the placenta?- Does aberrant FSS drive or contribute to placental dysfunction?- Could identifying the molecular complexes responsible for the FSS response provide novel targets for therapeutic agents to treat placental dysfunction? |
|--|

Table 1 Key research questions

1.1 Placental development and vascular function

A successful pregnancy outcome is dependent upon effective placentation. This occurs within the first half of pregnancy and describes the development of two distinct but independent circulatory systems involving both the mother (uteroplacental) and baby (fetoplacental). Human placentation is haemochorial, developing so that maternal blood is in contact with the chorion frondosum, consisting of epithelial placental villi, rather than direct mixing with the fetal circulation (Brugger et al., 2020).

The foundations for this process are laid down prior to implantation, when the morula divides into an inner (embryoblast) and outer (trophoblast) cell mass. Data from animal studies suggest that during early implantation, placentation is stimulated by endometrial gland secretions of growth factors and nutrients triggering progenitor trophoblast cells (Burton et al., 2019). These trophoblasts form the syncytiotrophoblast, which rapidly proliferates, and is replenished from the stem cell pool of cytotrophoblasts (Wang and Zhao, 2010). The resulting primary villi are composed of a cytotrophoblastic core surrounded by syncytiotrophoblasts. At the distal end of these villi, cytotrophoblasts breach the outer layer of syncytiotrophoblast and become known as extra-villous trophoblasts (Brugger et al., 2020). These cells have an integral role in spiral artery remodelling - the process of extra-villous trophoblast migration and invasion of spiral arterioles in the maternal decidua (Kingdom, 1998). This induces morphological changes that include the loss of smooth muscle and elastin, which transforms these narrow high resistance vessels into wider low resistance conduits.

Endovascular trophoblasts migrate into the spiral artery lumina forming occlusive plugs, protecting the early conceptus from high flow (discussed in more detail in sections 1.6.1 and 1.6.2). Eventually, the extra-villous trophoblast becomes embedded in the inner third of the myometrium (Burton et al., 2019). This remodelling prevents vessel collapse under the pressure of the inflowing maternal circulation, and reduces the velocity and pulsatility of blood to prevent villous damage (Wang and Zhao, 2010, Burton et al., 2019).

Oxygen and nutrient-rich maternal blood is then propelled into the evolving intervillous space (IVS) (Figure 1.1).

At the same time, the fetoplacental vasculature is developing through vasculogenesis and branching angiogenesis within the chorionic villi (Kingdom et al., 2000). The arborisation which starts with the umbilical arteries branching into chorionic vessels ultimately results in 60-100 individual villous trees (Clark et al., 2015). Terminal branching produces a capillary network enabling maximal gas exchange, nutrient and waste transfer across the IVS (Clark et al., 2015). This transfer is facilitated across the syncytiotrophoblastic membranes: the microvillous membrane facing the IVS and basement membrane on the side of the fetoplacental endothelium (Gaccioli and Lager, 2016).

In the second trimester, 10-15 generations of stem villi are formed from branching angiogenesis of immature intermediate villi (Kingdom, 1998). The major inducers of this angiogenesis are the vascular endothelial growth factor (VEGF) family of proteins (VEGF-A, VEGF-B, VEGF-C, VEGF-D and placenta-like growth factor (PLGF)) (Shah and Khalil, 2015). The most dominant of these is VEGF-A, referred to as VEGF unless otherwise stated. VEGF binds to VEGF-specific tyrosine kinase receptors: VEGF receptor 1 and 2 (VEGFR-1, VEGFR-2) on the FpECs. The activation of these receptors by phosphorylation triggers a signalling cascade recruiting multiple proteins with angiogenic activity.

From around 24 weeks of gestation, progressive differentiation by non-branching angiogenesis produces a vast network of mature terminal villi. Such is the degree of vascular expansion, that by term there is a 10-fold increase in the villous volume occupied by vasculature (Myatt, 2006). The circulation is completed by the umbilical arteries transporting deoxygenated blood and waste to the villous tree, to enable replenishment by the maternal supply and returned to fetus via the umbilical vein (Figure 1.1).

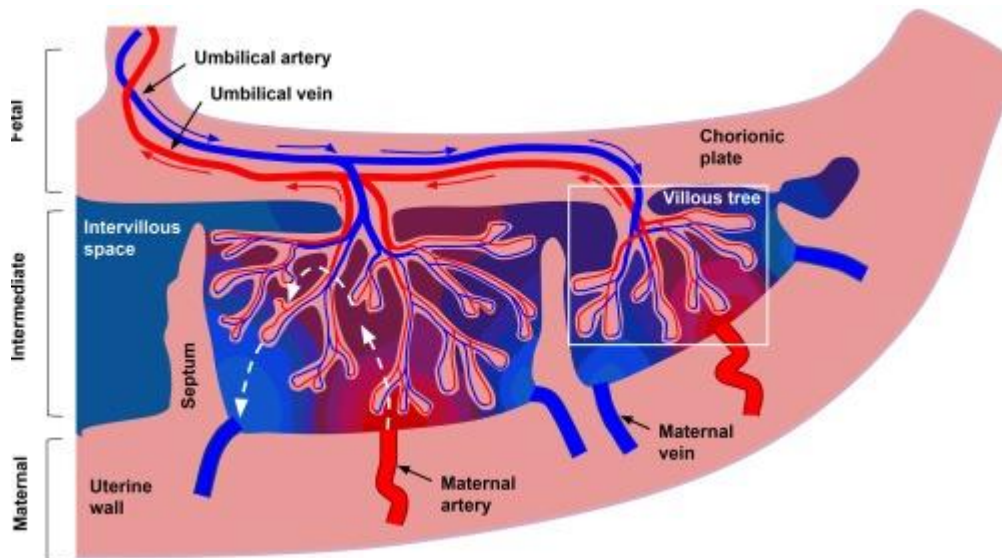


Figure 1.1 Schematic representation of blood flow through the placenta, with contributions from the uteroplacental and fetoplacental circulations. Blue and red arrows show the flow directions of oxygenated (red) and deoxygenated (blue) blood. The white box highlights the villous tree. Vascularisation from progressive branching within the fetal circulation forms capillaries in the terminal villi, which are the functional sites of maternal-fetal exchange. Dashed white arrows demonstrate the maternal blood flow through the IVS. The red-to-blue colour gradient represents oxygenation status. Figure from (Slator et al., 2018). The establishment and remodelling of this dense vascular bed results in a high flow and low resistance circuit, enabling perfusion in the absence of hypertension (Sprague et al., 2010). Effective and responsive gas and nutrient exchange is therefore dependent upon blood flow which can adapt and vary according to circumstance (Kingdom, 1998). Central to the capacity of vessels to respond and adapt to flow is the endothelium. This is the highly specialised single cell lining of all vessels that is in direct contact with blood flow.

To support fetal circulatory and metabolic requirements, blood flow to the uterus increases progressively with advancing gestation. Maternal cardiac output is increasingly directed to the uterus secondary to falling vascular resistance and haemodynamic changes in the systemic circulation (Osol and Moore, 2014). The uterine arteries of the

endometrium that feed the spiral arterioles must therefore undergo vasodilatation and remodelling to accommodate these profound changes in perfusion (Park et al., 2017).

In addition to oxygenation, the placenta is an absolute requirement for fetal nutrition. Nutrient transfer occurs through a combination of diffusion (simple or facilitated), active transport, and receptor mediated endocytosis (Myatt, 2006). Alongside maternal nutrient composition, the surface area for exchange is also a major determinant of nutrient transfer. This will be impacted by aspects of placental morphology, such as the available area of vascularised villi, blood flow rate, and the concentration gradient between maternal and fetal circulations. This is in addition to the quantity and function of villous transporter proteins and the production of endocrine signals (Sandovici et al., 2012).

Half of the glucose taken up by the placenta is used to support its own array of metabolic functions, including synthesis of peptide and steroid hormones, and to sustain its own growth until the end of the pregnancy. The placenta also has a vital role in preventing the transmission of infection, and also as an immune interlocutor preventing rejection of the semi-autologous fetal allograft (Myatt, 2006).

1.2 Epidemiology of fetal growth restriction

Fetal growth restriction (FGR) is a common pregnancy complication, affecting an average of 3-9% of maternities in high-income countries (Audette and Kingdom, 2018, Miller et al., 2016). The incidence is harder to quantify in low- and middle-income countries, but may affect up to 25% of pregnancies. This is most notable for babies born in the Asian subcontinent, which accounts for the majority of the world's cases, followed by Africa and South America (Malhotra et al., 2019, de Onis et al., 1998).

A 2016 consensus defined FGR as where a fetus 'does not meet its biological growth potential as a consequence of placental insufficiency, which may be due to a variety of factors' (Gordijn et al., 2016). This expert panel acknowledged that it was difficult to separate FGR from babies who are constitutionally small. Those that are small for gestational age (SGA) are identified by the statistical deviation of fetal size from either

population-based or customised charts, with lower limit thresholds at the 10th, 5th and 3rd percentiles. Although useful for screening, a proportion of the SGA group will be physiologically small rather than FGR, and therefore at lower risk of a poor fetal outcome. Likewise, a normal growth measurement does not exclude underlying placental insufficiency. As such, the 2016 consensus-based definition of FGR combines predicted birthweight <10th percentile with ultrasound (US) assessment of placental haemodynamic function (Gordijn et al., 2016). However, there is still international variation in these diagnostic criteria. Classification may also be based upon gestational age at detection. Accordingly, FGR can be either early-onset (<32 weeks of gestation) or late-onset (≥32 weeks) (Audette and Kingdom, 2018).

Royal College of Obstetricians and Gynaecologists (RCOG)	Abdominal circumference (AC) or estimated fetal weight (EFW) <10 th percentile, severe if <3 rd percentile
Canadian Maternal-Fetal Medicine Committee (Lausman et al., 2013)	EFW <10 th percentile due to a 'pathological process'
European TRUFFLE (Trials of Randomised Umbilical and Fetal Flow in Europe) consortium	AC <10 th percentile with abnormal placental blood flow
American College of Obstetricians and Gynecologists (American College of and Gynecologists, 2013)	EFW <10 th percentile
Barcelona Centre for Maternal-Fetal and Neonatal Medicine (Miranda et al., 2017)	Postnatal diagnosis of newborn birthweight <10 th percentile with abnormal placental blood flow, or <3 rd percentile
2016 Delphi consensus (multiple expert groups) (Gordijn et al., 2016)	EFW <10 th percentile with abnormal placental blood flow

Table 2 International definitions of fetal growth restriction

1.3 Clinical sequelae of fetal growth restriction

1.3.1 Perinatal and early-onset

FGR is a common antecedent to intrauterine fetal death and stillbirth (Gardosi et al., 2005). A retrospective re-analysis of stillbirth classification found FGR to be present in 43% of previously unexplained UK cases (International Stillbirth Alliance Collaborative for Improving Classification of Perinatal et al., 2017). Given the lack of treatments to improve placental insufficiency, iatrogenic delivery (commonly preterm) is often required

to prevent fetal demise. FGR is also an independent risk factor for spontaneous preterm birth (Zeitlin et al., 2000). As such, there is a degree of overlap between the clinical consequences of FGR and that of prematurity. However, FGR remains associated with worse perinatal outcomes independent of gestation at delivery when compared to normally-grown controls. The level of risk to the fetus corresponds to their estimated birthweight percentile, whereby extremes of growth (EFW <25th or >84th percentile), are associated with increased perinatal mortality (Iliodromiti et al., 2017). The highest rate of stillbirth occurs in those <3rd percentile, who represent the most at-risk group (Audette and Kingdom, 2018).

Serious morbidity can include intraventricular haemorrhage, bronchopulmonary dysplasia, necrotising enterocolitis, infection, pulmonary haemorrhage, hypothermia and hypoglycaemia (Alfirevic et al., 2015). Growth restriction is also a risk factor for hypoxic-ischaemic encephalopathy, defined as perinatal asphyxia (Apgar <5 at 5 min and umbilical artery pH <7) and abnormal neurological examination within 28 days from birth (Rossi and Prefumo, 2019). A recent study found higher mean cerebral oximetry values in neonates with FGR compared to normally-grown controls (Cohen et al., 2019). This suggests that early in the neonatal period, FGR neonates display impaired cerebrovascular autoregulation, which may predispose them to brain injury. This occurs despite the so-called 'brain-sparing' effect, whereby an adaptive response in FGR results in the redistribution of blood to vital organs including the brain, myocardium and adrenal glands (Miller et al., 2016, Malhotra et al., 2019). It is not yet known whether this persists or is linked to the neurodevelopmental outcomes discussed below.

1.3.2 Developmental programming and later life disease

It has long been recognised that disruptions to normal fetal growth and development are associated with an increased risk of disease in later life. This was initially known as the 'Barker hypothesis', after the initial observation from medical records that deaths from coronary heart disease in different parts of the UK paralleled the death rates of newborn babies in those areas (Barker, 2007). This led to the theory that *in utero* malnutrition

permanently changes the body's structure, function and metabolism in ways that lead to cardiovascular disease in later life (Barker, 2007). This is now a growing area of research, becoming known as 'fetal origins of adult disease' in the 1990s and now 'developmental origins of adult disease' (DOHaD). As such, placental insufficiency (and consequently FGR) are central to this concept of fetal programming.

It is now well established that FGR is linked to a wide range of non-communicable disease in adults, including hypertension, dyslipidaemia, diabetes mellitus, cardiovascular and cerebrovascular disease, and a variety of cancers (Audette and Kingdom, 2018). Even gross morphological features of the placenta have been independently associated with disease (Table 3). Barker also proposed the 'U-shaped' relationship between placental weight and adult cardiovascular disease, suggesting that placentas excessively light or heavy represented those most at risk (Myatt and Thornburg, 2018). These associations may be secondary to alterations in the villous structure of the placenta with resulting compromise to oxygenation or nutrient transport.

Phenotype	Disease
Placental thinness	Sudden cardiac death
Small placental area	Heart failure
Number of lobes	Hypertension
Low placental weight	Diabetes
Large or small placenta	Lung cancer
Placental ovality	Colorectal cancer
Short placental length	Hodgkin's lymphoma

Table 3 Placental phenotypes associated with adult disease. Adapted from Myatt and Thornburg, 2018.

Evidence is also emerging describing a link between FGR and poor neurodevelopmental outcomes. A review of human and animal studies found FGR to be associated with a reduction in cortical volume and structure, myelination defects, reduced dendritic processes and neuronal migration deficits (Miller et al., 2016). Moreover, school-age children born with FGR show cognitive impairments in memory and attention and gross motor proficiencies (Miller et al., 2016). It is also proposed that *in utero* compromise may be linked to the development of ADHD and depression, as well as Parkinson's and Alzheimer's disease (Myatt and Thornburg, 2018).

The molecular mechanisms through which a prenatal insult leads to a 'programming' event that increases the risk of adult-onset disease remain incompletely understood. *In utero* compromise and subsequent FGR may also cause epigenetic change in the placenta. This is alongside the effects of inflammation, oxidative and nitrative stress, and other reactions to hypoxia (Myatt and Thornburg, 2018).

1.4 Risk factors and aetiology of FGR

The aetiology of FGR is complex and multifactorial, where multiple different risk factors may contribute to each individual's case. Exposures that can lead to placental dysfunction include endocrine abnormalities, environmental toxins, physical and psychological stressors, altered nutrition, and a compromised intrauterine environment due to maternal medical conditions (Myatt and Thornburg, 2018).

Whilst nulliparity is a recognised risk factor, pregnancy history should also be taken into account, whereby previous SGA, stillbirth, PET, short or long pregnancy interval make subsequent FGR more likely. Based on the estimate measures of risk (odds and risk ratios) established from multiple studies, the RCOG guideline categorises factors as minor or major, which influences their management (Table 4) (RCOG, 2014). For simplicity, the causes of FGR have been presented here as fetus-derived, maternal and uteroplacental, and are not reviewed in their entirety.

Minor risk factors	Major risk factors
Maternal age ≥ 35 years	Maternal age >40
IVF singleton pregnancy	Smoker ≥ 11 cigarettes/day
Nulliparity	Maternal or paternal SGA
BMI <20	Cocaine
BMI 25-34.9	Daily vigorous exercise
Smoker 1-10 cigarettes/day	Previous SGA or stillbirth
Low fruit intake pre-pregnancy	Chronic hypertension
Previous pre-eclampsia	Diabetes with vascular disease
Pregnancy interval <6 or >60 months	Renal impairment
	Antiphospholipid syndrome
	Heavy bleeding during pregnancy
	Low placenta-associated plasma protein A (PAPP-A) (<0.4 MoM)

Table 4 Risk assessment for FGR. Adapted from RCOG, 2014.

1.4.1 Fetal

Placenta-independent causes of FGR include chromosome anomalies such as triploidy and trisomies 18 and 9 (RCOG, 2014, Audette and Kingdom, 2018). Inborn errors of metabolism, congenital cardiac defects, and vertically-transmitted infections, such as Zika virus and ToRCH (toxoplasmosis, rubella, cytomegalovirus, herpes) are also associated with FGR. In the case of cytomegalovirus, infections are also associated with abnormal placental development, with histological findings of avascular villi alongside inflammation (Pereira et al., 2014).

1.4.2 Maternal

1.4.2.1 Nutrition

Poor maternal nutrition will alter the supply and composition of nutrients crossing the placenta (Myatt and Thornburg, 2018). Food poverty occurring in both high and low-income countries is therefore likely to be a contributory factor to FGR being associated with low maternal BMI and social deprivation. This was highlighted by the INTERGROWTH-21ST study which demonstrated that under optimal nutritional conditions, fetal growth is similar in different parts of the world (Audette and Kingdom, 2018, Villar et al., 2014). Reduced availability of nutrients to the fetus may also occur in hyperemesis gravidarum, short interpregnancy intervals and adolescent pregnancy, where there is a conflict for nutrition between mother and baby (Gaccioli and Lager, 2016).

Maternal obesity can lead to babies born large for gestational age (LGA) due to increased nutrient supply. Paradoxically, high calorie diets with low nutritional content can also result in relative malnutrition in FGR. The placental environment is altered by maternal obesity, giving rise to chronic low-grade inflammation secondary to changes in the endocrine, cytokine and adipokine milieu (Myatt and Thornburg, 2018). Inflammation subsequently increases oxidative stress, negatively impacting on mitochondrial respiration of the villous trophoblasts and therefore impairing nutrient transport across the fetoplacental endothelium (Myatt and Thornburg, 2018).

1.4.2.2 Environmental exposure

Consumption of moderate or higher alcohol intake, illicit drug use, teratogenic prescription medication, and smoking tobacco in pregnancy are associated with FGR (RCOG, 2014). The inverse relationship between smoking, birthweight and other poor fetal and neonatal outcomes was first recorded after World War 2. Despite this, approximately 10% of babies are currently exposed to smoke *in utero*.

There is a dose-dependent relationship between smoking and fetal growth, which also includes smaller exposures through passive smoking, as measured by levels of cotinine

in hair strands (Reeves and Bernstein, 2008). Due to the number of components in cigarette smoke, such as carbon monoxide, there are a range of effects on the placenta. This includes disruption of oxygen binding, reduced mitochondrial function and amino acid transport, and a lower number of fetoplacental capillaries (Reeves and Bernstein, 2008). This also applies to cocaine use where the drug reduces the transport of several key amino acids (Gaccioli and Lager, 2016).

Several studies have investigated differences in the fetal outcomes of pregnant women living at high versus low altitude. Finding comparatively larger placental size relative to the fetus at high altitude suggests an adaptive response. Here, increased villous branching and diameter of blood vessels, and thinner villous membranes may promote placental diffusion (Gaccioli and Lager, 2016). Placental adaptations to suboptimal conditions are also seen in maternal anaemia, where placentas from affected mothers show increased capillary and villous volume, proportional to the severity of disease (Kingdom and Kaufmann, 1997).

Globally, malarial infection during pregnancy is a common cause of FGR. This occurs due to *Plasmodium falciparum*-infected erythrocytes binding to receptors on the fetoplacental endothelium via a placental-specific cell surface antigen (Morley, 2012). This induces a selective pressure for its clonal expansion resulting in preferential sequestration in the fetoplacental vascular bed (Morley, 2012). This parasite burden reduces blood flow, resulting in hypoxia and impaired nutrient transport.

1.4.2.3 Pre-existing health conditions

The maternal medical conditions most associated with an increased risk of FGR are those with a cardiac and/or vascular phenotype. This includes diabetes with vascular disease, hypertensive renal impairment, antiphospholipid syndrome, chronic hypertension and advanced maternal age. Systemic lupus erythematosus and cyanotic congenital heart disease are also associated with FGR although evidence is limited.

Women with type 1 diabetes are at increased risk of systemic vascular disease, such as retinopathy, renal impairment and hypertension. Correspondingly, in pregnancy, patients are predisposed to pre-eclampsia and FGR. The pathophysiology of this centres on oxidative stress caused by hyperglycaemia, reactive oxygen species (ROS) production and inflammation (Gauster et al., 2017). Increased exposure to these insults in early pregnancy may lead to placental vascular maladaptation, with secondary effects on blood flow, oxygen and nutrient transfer.

1.4.3 Placental origins of FGR and pre-eclampsia

1.4.3.1 Uteroplacental

In the absence of intrinsic fetal or maternal disease, idiopathic placental dysfunction may be the cause of FGR. This placental insufficiency may stem from defective placentation and remodelling of the uterine spiral arteries in early pregnancy, the process described in section 1.1. This is particularly evident in the development of early-onset FGR. Abnormal uterine-trophoblast interaction in the first trimester decreases blood flow through the spiral arteries, reducing perfusion of the IVS. The resulting ischaemia of the syncytiotrophoblast causes a hypoxia/reperfusion injury. This produces a stress response in the syncytiotrophoblast characterised by inflammation and oxidative stress (Shah and Khalil, 2015).

Oxidative stress is induced by an imbalance in the production of reactive oxygen species (ROS), such as superoxide, hydrogen peroxide and hydroxyl ions, which may impair a variety of cell signalling pathways. ROS depletes intracellular stores of Ca^{2+} and ATP, causing stress on the endoplasmic reticulum (ER). This results in the production of unfolded non-essential proteins, to which the cell mounts a defence: the unfolded protein response (UPR). This can inhibit normal protein production and initiate apoptosis (Myatt and Thornburg, 2018, Shah and Khalil, 2015). A degree of oxidative stress can be tolerated by the syncytiotrophoblast, which when healthy, can upregulate the production of anti-oxidants such as the vasoactive mediator nitric oxide (NO). However, if this

adaptation is inadequate, mitochondrial damage will occur (Schoots et al., 2018). The net result is compromised blood flow plus an altered placental environment, resulting in chronic hypoxia.

Hypoxia is damaging to the development of oxygen-sensitive villi and impairs branching angiogenesis (Kingdom, 1998). This is evident from the increased secretion of the anti-angiogenic factor soluble fms-like tyrosine kinase-1 (sFlt-1). This protein is expressed on trophoblast as an alternatively spliced variant of VEGFR-1. Under hypoxic conditions, the transcription factor, hypoxia-inducible factor 1 (HIF-1), binds the *FLT-1* gene promoter increasing its expression (Shah and Khalil, 2015). sFlt-1 antagonises both VEGF and PlGF, therefore reducing circulating levels of these pro-angiogenic proteins. Trisomy 13 is associated with an additional copy of *FLT-1* (Shah and Khalil, 2015). The severe FGR in these babies, and high rates of hypertension in their mothers, illustrates the importance of these circulating factors.

Abnormal angiogenesis disrupts the normal development and maintenance of the vascularised terminal villi, resulting in increased capillary-mediated vascular impedance (Shah and Khalil, 2015). Underperfusion induces the dedifferentiation of smooth muscle cells of the stem villous vessels to form a proliferative phenotype (Burton and Jauniaux, 2018). This causes thickening of vessel walls and luminal narrowing, leading to increased vascular resistance (Su, 2015). Oxygenation is therefore impaired due to compromised blood flow and a reduced surface area for gas exchange (Kingdom, 1998). This is alongside alterations in the expression of glucose, amino acid, and fatty acid transporters in the trophoblast (Myatt and Thornburg, 2018), the result of which is compromised transfer of oxygen and nutrients to the fetus.

The disrupted production of important anabolic hormones will also impact on fetal growth. For example, insulin-like growth factors -I and -II (IGF-I and IGF-II) are involved in cell proliferation, differentiation, protein and glycogen synthesis and are particularly important for brain development (Malhotra et al., 2019). Insulin-like growth factor binding protein (IGFBP) is cleaved by the placentally-secreted PAPP-A protease. IGFBP-4 is a

potent inhibitor of IGF production, and furthermore, decreased serum IGF-1 is associated with FGR. Correspondingly, low PAPP-A inhibits the disruption of IGFBP-4 and is associated with FGR. As such low PAPP-A on first trimester screening is regarded as a major risk factor for FGR (Table 4).

As pregnancy progresses there is therefore a growing mismatch between supply and fetal and placental metabolic demands resulting in impaired growth (Burton et al., 2019). The failure of early uteroplacental vascular adaptation classically presents as early-onset FGR, with features of abnormal placental blood flow on USS (Kingdom and Kaufmann, 1997). Paradoxically, other cases of FGR present at a later gestation and may have normal Doppler flow measures. This reinforces the concept of placental vascular adaptation.

1.4.3.2 Fetoplacental

Even in normal pregnancy, as gestation progresses the trophoblast barrier thins and capillary surface area increases. These measures promote both passive exchange and the capacity for transporter proteins to support the fetus to term (Sandovici et al., 2012). It is thought that the placenta can respond to hypoxia by increasing trophoblast proliferation and angiogenesis. Increased villous vascularity can be identified histologically as villous chorangiomas (Schoots et al., 2018, Kingdom and Kaufmann, 1997). This adaptation leads to a compensatory lowering of fetoplacental capillary-mediated vascular resistance. This demonstrates the capacity of the placenta to 'sense' changes in its environmental conditions and respond to those changes in a dynamic fashion (Sandovici et al., 2012). As such, failure of its adaptive capacity may lead to fetal hypoxia. Likewise, a primary significant defect in the structure or function of the fetoplacental vasculature causes 'postplacental hypoxia', where the placenta is failing to adequately oxygenate the fetus despite normally oxygenated blood entering the IVS from the maternal circulation (Kingdom and Kaufmann, 1997). Alongside vascular development through angiogenesis, the ability of the fetoplacental endothelium to

regulate blood flow is critical to meeting fetal demand (discussed in more detail in section 1.6.3).

The fetus also acts as a promoter for its own growth, whereby the fetal genome is a key regulator of fetoplacental function through the production of 'demand signals' (Sandovici et al., 2012). In response to physiological stressors, the expression of imprinted genes changes, with subsequent alterations to multiple cellular and metabolic processes (Myatt and Thornburg, 2018). There are multiple imprinted genes, which are either expressed on the maternal or paternal chromosome. Multiple studies have highlighted the importance of these genes for the regulation and homeostasis required for placentation and fetal growth (Myatt and Thornburg, 2018). For example, the insulin-like growth factor gene *IGF-2*, which is paternally expressed, promotes transfer to the fetus, whereas maternally-expressed *GRB10* limits this transfer to protect maternal health (Myatt and Thornburg, 2018). Studies of imprinted genes are predominantly in animal models but highlight that maternal dietary and environmental alterations can induce genetic changes that alter placental metabolic functions. These gene modifications may contribute to the fetal programming that results in long-term harm from FGR (Myatt and Thornburg, 2018, Sandovici et al., 2012).

1.4.3.3 Pre-eclamptic toxemia (PET)

PET is defined by the International Society for the Study of Hypertension in Pregnancy (ISSHP) as new onset hypertension in pregnancy (systolic >140 mmHg and diastolic >90 mmHg) with one or more of the following:

- proteinuria
- maternal organ dysfunction (liver, kidney, neurological)
- haematological dysfunction
- FGR
- abnormal uteroplacental blood flow on US

The pathogenesis of PET centres on deficient remodelling of the spiral arteries and is therefore intrinsically linked to FGR. It is therefore unsurprising that the two conditions often co-exist, and share many of the same consequences, namely previous poor pregnancy outcomes and a vasculopathic phenotype. PET is increasingly being classified as early- or late-onset, corresponding to the gestation of FGR recognition (Audette and Kingdom, 2018).

PET may represent a severe end of the placental dysfunction spectrum, characterised by high levels of oxidative stress. Severe ER stress worsens the UPR, triggering apoptosis. Trophoblastic apoptotic remnants are secreted into the maternal circulation and a pro-inflammatory, anti-angiogenic cascade is triggered. This induces systemic endothelial dysfunction, particularly in women with a clinical and genetic predisposition to vascular disease. The resulting clinical syndrome manifests as hypertension and organ dysfunction secondary to inflammation, vasospasm, abnormal clotting, and plasma volume contraction.

The ability to detect sFlt and PlGF in the maternal circulation has led to the development of predictive tests for women presenting with symptoms of PET, which are now being used in clinical practice (Triage PlGF test, Elecsys immunoassay sFlt-1/PlGF ratio, DELFIA Xpress PlGF 1-2-3 test, and BRAHMS sFlt-1 Kryptor/BRAHMS PlGF plus Kryptor PE ratio) (NICE, 2019). Early diagnosis of PET enables enhanced surveillance of at-risk babies, although there is no independent diagnostic test for FGR. Likewise, treatments are available to control hypertension and thereby ameliorate the likelihood of maternal complications such as stroke and eclampsia (NICE, 2019). However, the impact of underlying placental dysfunction for the fetus remains.

1.4.5 Clinical assessment and management

In vivo assessment of placental haemodynamics using Doppler US quantifies the 'differences between the peak systolic and the end-diastolic velocity within blood vessels of interest in each cardiac cycle' (Alfirevic et al., 2015). This is given as the pulsatility index (PI) or resistance index (RI). These measurements reflect vascular resistance within the placenta, and the fetal redistribution of blood flow in response to hypoxia, which may be detected as abnormal flow in the umbilical, middle cerebral artery (MCA) and/or ductus venosus (DV) (Malhotra et al., 2019).

1.4.5.1 Umbilical artery velocimetry

US of the umbilical arteries demonstrates flow velocity waveforms from the fetoplacental circulation. The pattern is dependent on fetal cardiac contractility, blood viscosity, vessel wall elasticity and placental vascular resistance (Alfirevic et al., 2017). In normal pregnancy umbilical arterial Doppler indices suggest a high flow and low resistance circulation, with forward flowing blood throughout the cardiac cycle. In those affected by FGR, high umbilical artery resistance is commonly observed, with the degree of abnormality corresponding to the level of placental compromise (Malhotra et al., 2019). This may result in reduced, absent or reversed blood flow at the end of diastole, indicating a fetus at high risk of FGR and stillbirth (Alfirevic et al., 2017).

By contrast, umbilical artery flow may be normal, particularly in late-onset FGR. This may represent milder placental insufficiency, or a partial compensation. Here, successful adaptations may result in sustained placental function, and therefore fetal growth, until later in the pregnancy (Malhotra et al., 2019, Kingdom and Kaufmann, 1997).

An updated Cochrane review of the use of Doppler umbilical artery US in at-risk patients found a significant reduction in perinatal death (16 studies, 10,225 babies, number needed to treat 203, moderate evidence) (Alfirevic et al., 2017). The results for stillbirth followed the same trend, although there was no statistical evidence of a difference.

1.4.5.3 Fetal blood vessel velocimetry and vascular maladaptation

Paradoxically, abnormalities in umbilical artery flow may progress to a fall in vascular resistance in the MCA. This response to hypoxia reflects the redistribution of blood to preferentially oxygenate vital organs. This 'brain-sparing' effect is the result of compensatory vasodilatation in cerebral vascular beds (Malhotra et al., 2019).

Although referred to as 'brain-sparing', babies with FGR that demonstrate this alteration in cerebral blood flow are at higher risk of brain injury and poor outcomes (Malhotra et al., 2019). It is not yet clear whether this redistribution reflects the severity of FGR or is an independent cause of neuropathology (Stampalija et al., 2020). Some authors have advocated that combining umbilical and cerebral blood flow measurements (using the cerebroplacental ratio, CPR) may be a useful prognostic marker to guide the management of FGR (Monteith et al., 2019). However, the issue remains under debate due to the confounding effects of prematurity associated with severe FGR (Lees 2020).

Chronic hypoxia and high placental vascular resistance can both affect the fetal myocardium and cause cardiac dysfunction. This has been reported in both early- and late-onset FGR, indicating that cardiac programming can occur throughout gestation. This can be demonstrated by the increasing presence of markers of cardiac injury, such as serum B-natriuretic peptide (BNP) corresponding to the severity of fetal compromise (Malhotra et al., 2019). High resistance increases afterload in the fetal venous circulation raising the intraventricular pressure (Alfirevic et al., 2017). Over time, this increases cardiac wall stress, leading to hypertrophy and abnormal ventricular compliance. This can be measured as increased resistance in the DV and inferior vena cava. The TRUFFLE study found that using abnormalities in DV flow alongside computerised cardiotocography (CTG) to determine management of FGR improved neurodevelopmental outcomes (Frusca et al., 2018).

Given the lack of pharmacotherapy to treat FGR when it is detected, Doppler velocimetry and other assessments of fetal wellbeing such as CTG are used to guide timing of iatrogenic delivery. Current recommendations are that a baby with an EFW <10th

percentile should undergo increased US surveillance, with progressive Doppler measurements until delivery is deemed necessary (Figure 1.2) (RCOG, 2014).

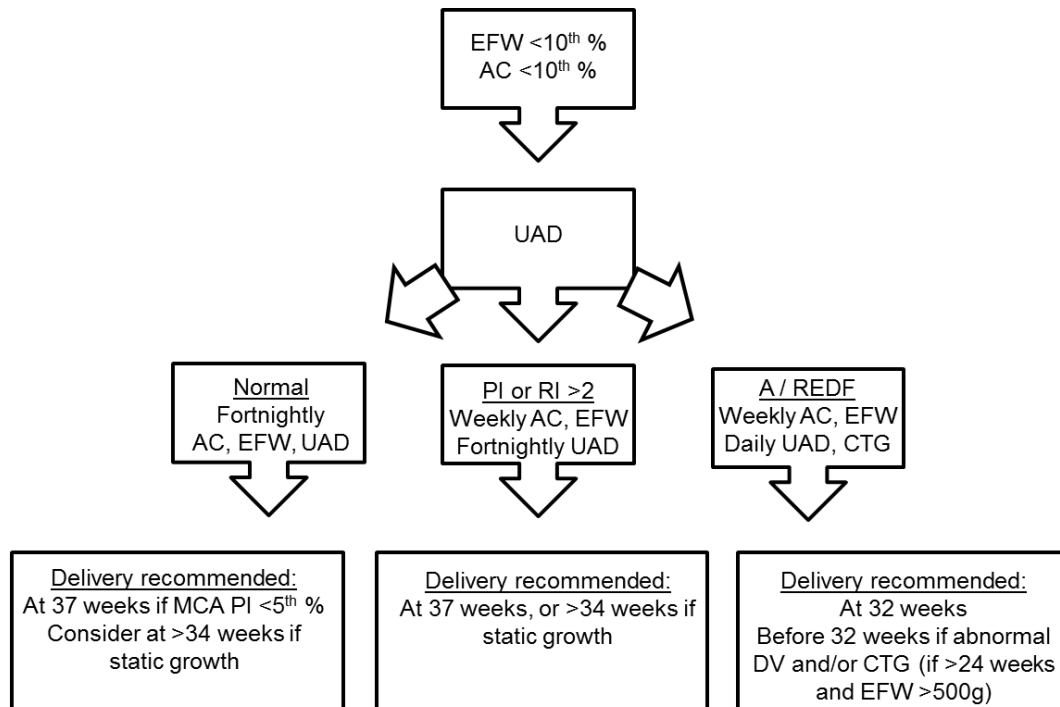


Figure 1.2 Current management of SGA. Appreciating the importance of haemodynamics in the fetoplacental circulation by assessing flow velocity waveforms on Doppler US improves fetal outcomes by improving the timing of iatrogenic delivery (Alfirevic et al., 2017). Abbreviations: AC abdominal circumference, EFW estimated fetal weight, UAD umbilical artery Doppler, PI pulsatility index, RI resistance index, MCA middle cerebral artery, A / REDFV absent or reduced end-diastolic flow, DV ductus venosus, CTG computerised cardiotocography. Figure adapted from RCOG, 2014.

1.4.6 Placental pathology in FGR

Pathological findings in placentas from FGR-affected pregnancies are varied, but are broadly indicative of hypoperfusion and high vascular resistance. Characteristically, these placentas are small with reduced numbers of villi, avascular villi and distal villous hypoplasia with fewer branches (Kingdom et al., 2000, Mifsud and Sebire, 2014, Su, 2015). Alongside these structural vascular abnormalities are reactive changes secondary to hypoxia, including fibrinoid necrosis and areas of infarction (Schoots et al., 2018).

The degree and type of abnormality found on placental assessment is proportionate to the placental compromise (Alfirevic et al., 2017). For example, wall thickening and luminal obliteration of stem villous vessels is associated with absent or reduced end-diastolic flow (AEDFV / REDFV) on Doppler US, where the 'percentage of abnormal vessels directly correlates with fetoplacental vascular resistance' (Su, 2015). The severe umbilical resistance with AEDFV associated with preterm FGR leads to an increased proportion of extracellular matrix and reduction in vascularised villi seen on histology (Kingdom and Kaufmann, 1997). When in conjunction with PET, more syncytial knots are observed, suggestive of apoptosis (Kingdom and Kaufmann, 1997).

However, FGR with preserved end-diastolic flow, or FGR at term, may have a histological phenotype suggestive of adaptive change, as well as lesions associated with hypoxia. This includes increased capillary volume. This is termed villous chorangiomas when 10 or more capillaries in 10 or more terminal villi in 10 or more areas of the placenta can be visualised using a 10× microscope objective. It is believed that this 'hypercapillarisation' is induced by VEGFs and cytokines as a response to chronic hypoxia (Schoots et al., 2018). It is thought that chorangiomas takes weeks to develop and is therefore an adaptive mechanism, designed to maximise oxygen extraction from the IVS (Schoots et al., 2018).

1.5 Flow dynamics and shear stress

From as soon as the embryonic heart starts beating, haemodynamic force is critical to the vasculogenesis and angiogenesis required for effective placental development, as described in section 1.1. Mice with a disrupted heartbeat show a lack of yolk sac vascularisation alongside lethality (Hyman et al., 2017, Huang et al., 2003). As pregnancy progresses, blood vessels are constantly exposed to the friction of blood flow, both in the uteroplacental and fetoplacental circulations. This mechanical force is fluidic shear stress (FSS), which can be quantified using measurements of the inner diameter of the vessel, velocity of flow and blood viscosity (Figure 1.3) (Wareing, 2012, Rodriguez and Gonzalez, 2014).

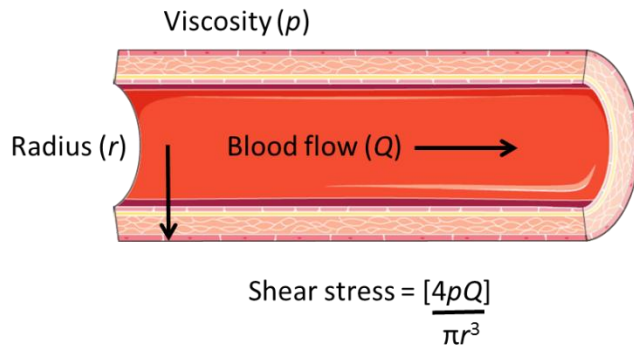


Figure 1.3 Cross-sectional diagram of a vessel showing FSS produced by blood flow. FSS in force/unit area (dyne/cm²) can be calculated using the equation $FSS = (4pQ)/\pi r^3$, where r is the vessel radius (μm), Q is blood flow velocity ($\mu\text{L/s}$), and p is blood viscosity in poise (dyne.s/cm³). 10 dyne/cm² = 1 Pascal. Adapted from (Wareing, 2012, Morley et al., 2019).

Efforts to accurately quantify FSS in the placenta have been complicated by its inaccessibility for *in vivo* high resolution imaging (Clark et al., 2015). This is in addition to the challenges posed by the pulsatile nature of flow, the viscosity of blood contents and complex placental vascular architecture (Baratchi et al., 2017b). Variations in umbilical cord insertion point and vessel branching pattern, for example, will produce differing intraluminal forces, with flow that may be laminar or turbulent (Clark et al., 2015).

The effect of FSS is friction exerted on the endothelial lining of blood vessels during each cardiac cycle (Sprague et al., 2010). This shearing is sensed by the endothelium, and the mechanical force transduced by the cell in a process known as mechanotransduction. This activates multiple downstream signalling pathways in the EC which can result in the release of vasoactive mediators, such as NO. The endothelium is therefore dynamic, responding to local cues to control vascular homeostasis (Chatterjee, 2018). As such, the type and magnitude of FSS has a significant impact on the endothelial phenotype (Malek et al., 1999).

In the systemic circulation, ECs exposed to physiological FSS show increased production of vasodilators and anti-oxidants, with a reduction in vasoconstrictors and inflammatory mediators (Malek et al., 1999). Likewise, disruption of normal FSS, for example at sites of turbulent flow is considered pro-atherosclerotic (Baratchi et al., 2017b). Indeed, an impaired response to FSS has been linked to a variety of cardiovascular disease processes such as aneurysms, thrombosis and hypertension (Ando and Yamamoto, 2013).

Furthermore, in addition to the endothelium, mechanosensing is now being widely reported in multiple cell types that are subjected to fluid flow, including villous tissue. It is therefore no surprise that FSS and the subsequent cellular response is postulated to have multiple roles in homeostasis from acute modulation of vasomotor tone to angiogenesis and vasculogenesis (Baratchi et al., 2017b).

1.6 Shear stress sensing in pregnancy

1.6.1 Pre-implantation

From the moment of conception, a preimplantation embryo is subjected to the force of fluid flow as it traverses the uterus by peristalsis. To determine if embryos can sense FSS, Xie et al., exposed mouse embryos to either FSS or static conditions (Xie et al., 2006). They found no surviving embryos after 24 hours of FSS at 1.2 dyne/cm^2 and reduced blastocyst cell numbers. An increase in apoptotic markers and stress-activated protein kinase (mitogen-activated protein kinase, MAPK) suggested that shear was transduced prior to lethality (Xie et al., 2006). Shear-induced lethality after removal of the zona pellucida (ZP) suggests that the ZP may protect the embryo from mechanical force. This has implications for embryo handling in assisted conception transfer procedures, although transient FSS caused by repeated pipetting did not affect development, despite increased MAPK phosphorylation (Xie et al., 2007).

The mechanosensitive ion channel subunit Piezo1 has been identified in murine embryonic stem cells (Del Marmol et al., 2018). This raises the question of whether Piezo1 activation by FSS is important for cell differentiation. The lack of lethality in *Piezo1* knockout mouse models until mid-gestation suggests that Piezo1 is not critical for early development but may have fine-tuning roles that are not yet fully identified (Del Marmol et al., 2018).

1.6.2 Post-implantation and early pregnancy

Transfer of oxygen to the fetus is critically dependent on the flow past, and effective diffusion across, the trophoblast as discussed in section 1.1 (Kingdom, 1998). Despite the importance of FSS, extra-villous trophoblast cells also form plugs within the spiral arteries, effectively preventing the flow of maternal blood to the IVS (James et al., 2018). It is well known that a hypoxic environment is important for early development. For example, in cases of miscarriage, erythrocytes have been found prematurely in the IVS (Jauniaux et al., 2000). Alongside regulation of oxygen tension, the presence of plugs will also impact on haemodynamics. Until recently, it was thought that plugs prevented any blood from entering the IVS until the end of the first trimester. However, evidence now suggests that capillary-sized channels enable a small, constant influx of blood that increases dramatically after 12 weeks of gestation (Roberts et al., 2017). Nevertheless, low FSS conditions of <2 dyne/cm² (<0.2 Pa) are produced in the IVS (James et al., 2018). James et al., found that at very low FSS (0.5 and 2 dyne/cm²) trophoblasts did not undergo migration (James et al., 2012). However, at increased FSS (4 and 6 dyne/cm²) migration in the direction of flow occurred. This suggests that high FSS at this early stage would damage vascular remodelling by stimulating migration away from the site of invasion (James et al., 2012). Low FSS may therefore be protective of the delicate villi by preventing physical and oxidative stress. Breakdown of plugs coincides with the end of the first trimester, where increasing blood flow elevates FSS, encouraging trophoblast migration (James et al., 2018).

Scanning electron microscopy has been used to demonstrate minimal villous growth in BeWo cells and cultured human villous trophoblast (HVTs) under static conditions. By contrast, when exposed to FSS, villi formation started at 1 hour. Miura et al., found short villous projections at high FSS but these protrusions were longer ($> 2 \mu\text{m}$) at low FSS, increasing over 12 hours. If, however, FSS was stopped, the villi decreased (Miura et al., 2015). This therefore suggests that placental villi sense and respond to flow in their fluidic environment. Furthermore, there is a minimum requirement for FSS as a 'critical external cue' for villous formation (Miura et al., 2015).

When investigating the mechanism behind FSS-induced villi formation, Miura et al., found that application of FSS to BeWo cells increased intracellular calcium concentration (Ca^{2+}). Correspondingly, culturing cells in the presence of a Ca^{2+} -chelator inhibited villous growth (Miura et al., 2015). They suggest that the Ca^{2+} channel TRPV6, a member of the TRP family, is a candidate mechanosensor here. Silencing TRPV6 using short interfering RNA (siRNA) resulted in loss of the FSS-induced intracellular Ca^{2+} response. They hypothesised that activation of TRPV6 results in re-localisation of EZRIN (a protein linking the membrane and cytoskeleton) within the cell. Rapid EZRIN phosphorylation, but a lack of change in gene expression in response to FSS, suggests that trophoblast cells are hyper-responsive to their dynamic fluid environment.

This interplay between the uteroplacental and fetoplacental circulations occurs throughout pregnancy, whereby FSS produced by the flow of maternal blood in the IVS continues to affect the villous trophoblast (Brugger et al., 2020). Exposing trophoblast cells from term placentas to FSS at 1 dyne/cm^2 resulted in increased secretion of PIGF and intracellular Ca^{2+} influx (Lecarpentier et al., 2016a). The dose-dependent rise in PIGF associated with increasing flow is suggestive of an important stimulatory role for FSS in angiogenesis (Brugger et al., 2020, Lecarpentier et al., 2016a). MRI of term pregnancies has revealed maternal blood flow velocity of $0.94 \pm 0.14 \text{ mm/s}$, which has been used to estimate FSS values of $\sim 5 \text{ dyne/cm}^2$ in the IVS (Lecarpentier et al., 2016b). This computer modelling suggests that at term, maintaining low FSS at the maternal-

fetal interface remains important, and may promote maximal exchange of nutrients and waste.

1.6.3 Flow-mediated regulation of fetoplacental blood flow

It has long been established by chorionic plate artery myography and *ex vivo* placental perfusion models that incremental increases in flow decrease vascular resistance (Jones et al., 2015, Larmont and Poston, 1996). This flow-mediated vasodilatation (FMV) is associated with the release of vasoactive mediators from the endothelium, such as nitric oxide (NO) (Wieczorek et al., 1995). Given the lack of autonomic innervation of fetoplacental vasculature, the release of these factors is of critical importance for regulating vasomotor tone and therefore blood flow.

1.6.3.1 Release of vasoactive mediators

Nitric oxide (NO)

FSS is the most powerful physiological stimulator of endothelial nitric oxide synthase (eNOS), which when activated, leads to synthesis of NO (Sprague et al., 2010). This constitutively produced vasoactive mediator is known to be a potent vasodilator within placental vasculature (Larmont and Poston, 1996).

Alternate mechanisms of eNOS activation are via FSS being sensed by the endothelium (flow-dependent), and via receptors for a variety of ligands on the EC (receptor-mediated). The activity of eNOS is dependent on Ca^{2+} , both from rapid and transient release from endoplasmic reticulum storage, and sustained influx across the plasma membrane (Wang et al., 2016). As such, placental Ca^{2+} transport and regulation is a critical determinant of adaptive cell signalling in pregnancy, and in particular NO-driven vasodilatation (Belkacemi et al., 2005).

When quiescent, eNOS is bound to caveolae, co-localised with the amino acid transporter proteins, hCATs. Increasing intracellular Ca^{2+} results in the liberation of eNOS from the caveolae (Boeldt et al., 2011). Further association of eNOS with kinases,

such as AKT (protein kinase B) and protein kinase (PK) A, induces phosphorylation and thereby activation of eNOS at serine residue 1177 (Boeldt et al., 2011).

The conversion of L-arginine, NADPH and oxygen to L-citrulline, NADP⁺ and H⁺ is catalysed by eNOS, with NO formed as a by-product. Once synthesised, NO binds to the guanylate cyclase enzyme on smooth muscle cells, catalysing the dephosphorylation of GTP to produce cyclic GMP (Sprague et al., 2010). Sustained Ca²⁺ influx into the EC is therefore required to maintain eNOS in the cytosol (Boeldt et al., 2011).

Multiple downstream pathways lead to vasodilatation, including the activation of protein kinase G (PKG), and subsequently, myosin phosphatase. This triggers the release of Ca²⁺ from the smooth muscle cell intracellular stores. Conversely, phosphodiesterases convert cGMP back to GTP, blocking the NO signalling cascade.

In the placental perfusion model, flow stimulated NO release (Learmont and Poston, 1996). Correspondingly, pre-treating chorionic arteries with the eNOS inhibitors, L-NAME or L-NMMA (Nw-Nitro-L-arginine methyl ester hydrochloride, NG-Monomethyl-L-arginine acetyl salt) significantly reduced FMV (Sprague et al., 2010). Furthermore, this could be reversed by adding the eNOS substrate, L-arginine (Sprague et al., 2010).

Flow stimulates the production of other vasoactive mediators from uterine artery ECs including prostacyclin, endothelium-derived hyperpolarising factor (EDHF) and natriuretic peptides, although there is little evidence to support their role in fetoplacental vasodilatation (Sprague et al., 2010, Wieczorek et al., 1995).

Vascular endothelial growth factor (VEGF)

The interplay between VEGF activity and NO bioavailability in fetoplacental vasculature is complex and incompletely understood. Animal model data from systemic tissue show that L-arginine supplementation increases VEGF expression and subsequently, angiogenesis, suggesting that vascular remodelling via VEGF involves the NO pathway (Rodriguez and Gonzalez, 2014).

In HUVECs, VEGF treatment produced a concentration-dependent rise in cGMP that was inhibited by L-NAME (Papapetropoulos et al., 1997). Correspondingly, incubation with VEGF increased eNOS protein, and angiogenesis (tube formation), which were both inhibited by L-NAME. Furthermore, inhibiting tyrosine kinases and applying Ca^{2+} chelators attenuated VEGF-induced NO release (Papapetropoulos et al., 1997).

More recent HUVEC data suggest that VEGF receptors are flow activated as part of a FSS-sensing complex with vascular endothelial cadherin (VE-cadherin) and platelet endothelial cell adhesion molecule (PECAM-1) (Wang et al., 2016, Coon et al., 2015). This sensing results in phosphorylation of VEGFR-2, activating AKT kinase and the signalling cascade which produces NO (Wang et al., 2015).

Adenosine triphosphate (ATP)

HUVEC data demonstrate that endothelial ATP release can be stimulated by flow (Wang et al., 2015). Correspondingly, apyrase, which degrades ATP, inhibits the FSS-induced Ca^{2+} influx. ATP binds to the P2Y_2 receptor on endothelial cells (ECs), which is coupled to G_q and G_{11} proteins. Endothelial $\text{P2Y}_2 / \text{G}_q / \text{G}_{11}$ subsequently activates the VE-cadherin, PECAM-1 and VEGFR-2 triad, leading to AKT kinase phosphorylation and NO release (Wang et al., 2015). Although it is evident that flow-induced ATP release is a mechanism upstream of NO vasodilatation, little is known about its role in the fetoplacental endothelium.

1.6.3.2 Abnormal flow-mediated vasodilation in FGR

Abnormal blood flow velocity and pulsatility on Doppler US of the umbilical artery are indicative of increased vascular resistance, often associated with FGR. Structural abnormalities associated with FGR including altered villous branching and reduced vessel calibre secondary to vasoconstriction may raise the transmural pressure in fetoplacental vasculature (Krause et al., 2013).

Using computational models of placental microvasculature, Tun et al., estimated FSS to be increased in FGR (0.5 dyne/cm² in the normal placenta versus 2.0 dyne/cm² in severe FGR), representative of a five-fold elevation in total placental vascular resistance (Tun et al., 2019).

Increased FSS in FGR is supported by *ex vivo* perfusion model data. In placental samples from normal pregnancies, the lowest measures of *in vivo* resistance on umbilical artery Doppler velocimetry correlated with maximal flow from the villous side of perfused tissue (Jones et al., 2015). This highlights the importance of fetoplacental vasculature in determining total placental resistance, although there was no clinical correlation with chorionic plate artery myography data (Mills et al., 2005). In the perfusion experiment, increasing flow reduced fetal-side hydrostatic pressure, demonstrative of FMV (Jones et al., 2015). In FGR samples, baseline vascular resistance was markedly elevated, and furthermore, FMV was substantially reduced or absent (Jones et al., 2015).

Myography of chorionic arteries demonstrated vasoconstriction to a thromboxane mimetic (U46619), and relaxation in response to the NO donor sodium nitroprusside (SNP) (Mills et al., 2005). Vessels from FGR placentas showed enhanced vasoreactivity, displaying both increased contraction in response to U46619, and dilatation with the donated NO. In the perfusion model, inhibiting eNOS with L-NAME in FGR placentas caused an increase in vascular resistance which far outweighed the response in normal tissue (Jones et al., 2015). As such, Jones et al., argued that ‘...vessels from dysfunctional placentae have the capacity to vasodilate over-and-above those from a healthy pregnancy’ (Jones et al., 2015). Chorionic artery ECs produced nitrite, and thus NO, proportionate to the level of FSS. The nitrite concentration was significantly greater in FGR cells when exposed to high FSS (Jones et al., 2015). Increased eNOS protein expression in FGR has also been demonstrated in numerous studies (Myatt, 2006, Jones et al., 2015, Giannubilo et al., 2008).

Taken together, the findings from whole vessels and ECs imply that despite impaired FMV, FGR placental vasculature shows increased responsivity to NO. This enhanced

sensitivity is suggestive of an adaptive physiological mechanism for overcoming deficiencies in the fetoplacental circulation (Giannubilo et al., 2008). However, when endothelial dysfunction is severe enough to prevent this response to increased FSS, flow-induced NO compensation will be insufficient and FGR may worsen (Jones et al., 2015, Morley et al., 2019). Also for consideration is the impact of NO at high concentrations combining with superoxide to form peroxynitrite. This leads to production of nitrotyrosine, known to cause nitrate stress and inflammation (Salvolini et al., 2019).

The success of compensatory flow-induced NO in FGR is dependent upon the production and response to vasoactive mediators by the endothelium. Krause et al., found reduced eNOS activation in FGR, and suggest that despite elevated expression, the eNOS is inactive (Krause et al., 2013). Their group found reduced gene expression of the hCAT proteins involved in eNOS activation (Casanello and Sobrevia, 2002). In addition, they showed inhibited L-arginine transport and reduced production of L-citrulline in FGR (Casanello and Sobrevia, 2002). Furthermore, exposing HUVECs to hypoxia increased activity of arginase-2, the enzyme competitor of eNOS, thus influencing the bioavailability of L-arginine for NO production (Krause et al., 2013). However, in FGR, neither inhibition of arginase nor supplementation with L-arginine have had clinically beneficial effects (Krause et al., 2013). This suggests deficiencies in eNOS function or the ability to mount a NOS-dependent vasodilatory response in FGR.

Also contributing to abnormal vasodilatation in FGR are increased circulating vasoconstrictors such as endothelin-1, and lower prostanoid synthesis related to altered endothelial expression of oestrogen receptor- β (Su, 2015). This highlights the complexity of factors influencing both flow-mediated and flow-independent vasoregulation.

The relationship between hypoxia and activation of FSS sensors remains to be determined. Placental perfusion data suggest that hypoxia increases vascular resistance, an effect which could be enhanced or inhibited by modulators of the oxygen-sensitive K^+ channels previously described (Wareing, 2014, Wareing et al., 2006a). In the systemic circulation, altering K^+ channel activity is associated with hypertension

secondary to vasoconstriction. K^+ channels can be regulated by reactive oxygen species (ROS), which are known to be elevated in the FGR placenta (Wareing, 2014). Further exploration is therefore required to determine whether differential expression of these, or other mechanosensitive ion channels in FGR, is a cause or effect of the hypoxic environment.

1.6.4 Regulation of uteroplacental blood flow

The production of endothelial NO alongside prostacyclin and endothelial hyperpolarizing factor has also been recognised as essential for the vasodilatory component of the expansive remodelling in the uteroplacental circulation (Osol and Moore, 2014). This can be demonstrated in uterine arteries, where an eightfold increase in eNOS activity was observed in normal pregnancy (Nelson et al., 2000). This has also been shown in animal models where eNOS inhibition prevented uterine artery remodelling (Ko et al., 2018). The augmentation of NO in pregnancy may be secondary to FSS generated by the increase in blood flow through the uterine vasculature. This is in conjunction with growth factors such as VEGF, PlGF, and endocrine signals (Osol and Moore, 2014). Successful vascular adaptation normalises the FSS, although definitive values for FSS in human uterine vessels both in normal and in gestational disorders remain to be determined.

The response of uterine artery ECs to FSS can be demonstrated by their alignment in the direction of flow (10-20 dyne/cm², based on an assumption of physiological arterial FSS in the systemic circulation of 6-40 dyne/cm²) (de la Paz et al., 2012). Alongside the morphological change in response to FSS, Park et al., (2017) showed increased expression of VEGF receptor 3 (VEGFR-3) in human uterine artery ECs. This receptor is thought to be involved in angiogenesis and its expression in response to flow occurred independently of its ligand. Although alterations in flow through the uterine vessels may contribute to vascular remodelling, the mechanisms transducing FSS into the expression of growth factors remains unknown. *Piezo1* mRNA has been detected in the uterine artery endothelium of the rat (John et al., 2018). It is therefore possible that *Piezo1*

channel activation may induce NO production, alongside expression of VEGFs, but this requires confirmation.

A low sodium diet was used to generate a rat model of FGR characterised by reduced uteroplacental perfusion (Bigonnesse et al., 2018). Impaired blood flow velocity and increased resistance occurred secondary to reduced uterine vessel diameters. In these hypoperfused placentae, increased NO activity was observed, leading the authors to conclude that enhanced production was compensating for vasoconstriction (Bigonnesse et al., 2018). This feeds into our hypothesis that alterations in FSS are detected by sensors of mechanical force (mechanosensors) leading to the release of NO as a compensatory mechanism.

Analysis of placental bed biopsies showed that increasing intraluminal flow led to dilatation of the small myometrial resistance arteries. By contrast, in women with PET, the FSS response was blunted, with absent FMV (Kublickiene et al., 2000). Inhibiting eNOS increased myogenic- and norepinephrine-induced tone in arteries from both controls and PET (Kublickiene et al., 2000). As such, NO may still have a role in regulation of vascular tone in PET, but the *FSS-mediated* NO release appears to be absent. Failure of FSS-induced vasodilatation may therefore contribute to impaired uteroplacental blood flow (Kublickiene et al., 2000, Osol and Moore, 2014).

1.7 Fluidic shear stress sensors

For FSS to activate multiple cell-signalling pathways, the force must first be detected and then transmitted from the vessel lumen to the interior of the endothelium. Understanding the mechanisms underpinning *how* cells in the placenta sense their haemodynamic environment and transduce signals is therefore essential. A growing body of literature is dedicated to identifying mechanosensors including a variety of proteins, receptors, transmembrane channels and components of the cell architecture (Fels and Kusche-Vihrog, 2020) (Figure 1.4). These candidate mechanosensors may also be co-

dependent, with several FSS sensors working in conjunction and forming a mechanosome complex (Chatterjee, 2018).

There is a paucity in the literature of studies investigating the role of mechanosensors responsible for the sensing and adaptive response to FSS in the fetoplacental endothelium. Köhler et al., first described 'stretch-activated cation channels' in HUVECs and found that they were involved in Ca^{2+} influx (Kohler et al., 1998, Brakemeier et al., 2002). Although the channel identity remained unknown in their study, they found a doubling in the density of the channels in HUVECs from pregnancies affected by PET (Kohler et al., 1998). Understanding the mechanisms through which FSS is sensed and how FpECs respond will provide novel insights into the control of placental vascular tone and therefore blood flow.

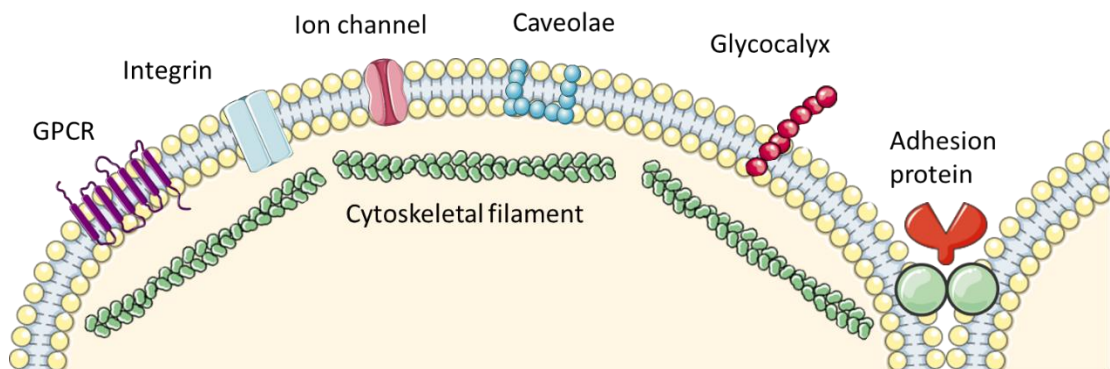


Figure 1.4 Components of the EC, each with postulated roles in mechanosensing.

G-protein coupled receptors (GPCRs) are membrane-spanning receptors e.g. GPR68 (Xu et al., 2018). Integrins are membrane-spanning receptors linking cytoskeletal proteins to the cell matrix. Ion channels may be rapidly activated in response to flow. Examples include members of the TRP family and Piezo1, which are both non-selective cation channels. Caveolae are membrane invaginations abundantly expressed on ECs. The glycocalyx is a matrix composed of glycoprotein and glycolipid moieties that covers and protects the cell membrane. Adhesion molecules include cell surface proteins (e.g. platelet adhesion cell adhesion molecule), which are expressed on cell-cell junctions. The cytoskeleton includes microtubules, microfilaments and intermediate protein filaments (Chatterjee, 2018). Created using SMART Servier Medical Art (LES LABORATOIRES SERVIER, SAS, France), adapted from (Shihata et al., 2016, Morley et al., 2019).

1.7.1 Cell structures

The surface of ECs has been described as a 'flexible signalling hub' (Fels and Kusche-Vihrog, 2020). The cytoskeletal scaffold encompasses a variety of protein filaments, such as vimentin, that may be deformed by shear on the cell surface. This impacts on cellular components, such as integrins (membrane spanning receptors), focal adhesion proteins and the extracellular matrix, where the force is transduced (Chatterjee, 2018). Integrins themselves may also sense FSS, affecting the cytoskeletal filaments directly (Chatterjee, 2018, Baratchi et al., 2017b). Force may also be transmitted to the cytoskeleton via the heparan sulfate, chondroitin sulfate, and hyaluronic acid moieties of the glycocalyx on the EC membrane. As such, friction-induced deformation of the cytoskeleton may result in EC reorganisation and remodelling (Chatterjee, 2018).

Caveolae plasma membrane invaginations are abundantly expressed on the surface of ECs, but not in the trophoblast (Shihata et al., 2016, Rodriguez and Gonzalez, 2014). *CAV-1* gene expression has been found in both HUVECs and microvascular FpECs (Rodriguez and Gonzalez, 2014). In systemic ECs, exposure to FSS increased both the amount of caveolae, and *cav-1* expression. In HUVECs and ovine FpECs, *CAV-1/cav-1*

knockdown reduced the production of vasodilatory NO, and VEGF-induced angiogenesis (tube formation). The link between this and the NO pathway, may lie in the co-localisation of eNOS with its chaperone protein, hCAT-1, in the caveolae (Rodriguez and Gonzalez, 2014, Casanello and Sobrevia, 2002, Guzman-Gutierrez et al., 2014).

1.7.2 Mechanosensor complexes

The most studied mechanosensory complex is the PECAM-1, VE-cadherin, VEGFR-2 triad (Chatterjee, 2018, Tzima et al., 2005). As discussed above, flow induces changes in cytoskeletal structures, altering the force applied across endothelial cell-cell junctions (Sak et al., 2013). PECAM-1 junctional proteins are thought to act as the direct sensor, transmitting force to the VE-cadherin junction receptor, which functions as an adaptor, and VEGFR-2 (Tzima et al., 2005). Alongside integrin activation, this triggers kinase phosphorylation, leading to downstream NO production.

Cytoskeletal components disturbed by flow include intermediate filaments, such as vimentin, which alter tension on PECAM-1 (Sak et al., 2013). Although the role of mechanosensory complexes in human placenta remains unknown, of interest is the finding of increased villous immunostaining for vimentin in samples from women with severe PET (Sak et al., 2013).

1.7.3 Ion channels

The endothelium expresses an array of ion channels, although the identification of those that sense haemodynamic force in the placenta is still an emerging area of research. Wareing et al., have demonstrated several subtypes of K⁺ channels expressed in chorionic plate vessels and villous homogenate, including voltage-gated (K_v), large conductance Ca²⁺ (BK_{Ca}), and ATP-sensitive (K_{ATP}) channels, which are oxygen sensitive (Wareing et al., 2006a). In HUVECs, insulin-induced L-arginine transport and membrane hyperpolarisation were attenuated by a K_{ATP} blocker (Rodriguez and Gonzalez, 2014). However, a role for K⁺ channels in placental mechanosensing remains to be determined.

In the systemic circulation, TRP (Transient Receptor Potential) channels have been widely studied. Ca^{2+} influx through these channels produces smooth muscle contractility, alterations in vascular permeability and remodelling (Baratchi et al., 2017a). However, in murine models, TRP channel knockout either did not affect survival, or caused delayed lethality, suggesting they are not essential for early vascular development (Hartmannsgruber et al., 2007, Garcia-Gonzalez et al., 2010).

1.7.4 Piezo ion channel subunit

The Piezo family of proteins comprises of two mechanosensitive ion channels: Piezo1 and Piezo2. They have been discovered to be important for mechanically-evoked Ca^{2+} entry in a variety of cell types. Piezo1 and Piezo2 differ in the sites of their expression, physiological roles, and biophysical properties. Whilst Piezo1 is a mediator of FSS, stretch and pressure in non-neuronal cells such as erythrocytes, epithelial cells, chondrocytes and the endothelium, Piezo2 is expressed predominantly in sensory neurones (Taberner et al., 2019). Piezo2 is thought to be important for proprioception, light touch, thermo-tactile regulation and detection of noxious stimuli such as pain (Zheng et al., 2019). This research has therefore focused on Piezo1 and its role in placental vasculature.

1.7.4.1 Piezo1 structure and function

In 2014, our group first reported that Piezo1 channels respond to FSS in a variety of EC types, including HUVECs (Li et al., 2014). Since then, Piezo1 has risen to prominence as a major player in FSS sensing (Beech and Kalli, 2019). The channels are composed of Piezo1 proteins assembled as a large trimer of approximately 0.9 million Daltons in the cell membrane (Coste et al., 2010, Saotome et al., 2018, Guo and MacKinnon, 2017). These distinctive proteins of over 2,500 amino acids lack sequence homology with any other class of ion channels (Zhao et al., 2019). Cryo-electron microscopy has revealed the structure of Piezo1 to be composed of nine repetitive units consisting of four transmembrane helical units (THUs) that are assembled into a triskelion structure, resembling a propeller blade (Figure 1.5A) (Zhao et al., 2018).

The 'pore module' of Piezo1 contains the extra-cellular C-terminal domain (Cap), transmembrane pore and the intracellular C-terminal domain. The pore is hydrophobic, with fenestrated sites and side portals that determine its properties. The pore is permeable to both monovalent (Na^+ and K^+) and divalent cations, with a preference for Ca^{2+} (Coste et al., 2010, Saotome et al., 2018, Guo and MacKinnon, 2017).

Each blade of the triskelion is composed of 3 major components: peripheral transmembrane helices, an anchoring region connecting the inner aspect of the cell membrane with the outer helices, and a long beam structure (Zhao et al., 2019). This beam bridges the membrane, acting as a lever connecting the THUs to the pore module, anchoring domain and outer helix, and the inside of the cell (Zhao et al., 2018). If single residues in the beam or extracellular loops of the THUs are mutated or deleted, the mechanosensory function of Piezo1 is lost (Zhao et al., 2018).

Piezo1 channels are thought to sense FSS directly via the highly flexible blade regions. These blades are deformable by flow, and their activation is thought to directly modulate membrane tension, leading to Ca^{2+} influx into the EC (Saotome et al., 2018).

To investigate the significance of Piezo1, our group generated a mouse model with a disrupted endogenous Piezo1 gene. Inheritance of the homozygous *Piezo1* deletion was embryonically lethal in 49 pups at mid-gestation (embryonic days 9.5 – 11.5). Growth restriction of the embryos was commonly observed (embryonic day 10.5), alongside reduced yolk sac vascularisation (Figure 1.5B, C and D) (Li et al., 2014). These findings were also apparent in an endothelial-specific *Piezo1* knockout murine model. Ranade et al., also found that mice homozygous for *Piezo1* disruption developed FGR before dying at mid-gestation (Ranade et al., 2014). *In vitro* assays using Piezo1 siRNA in HUVECs suppressed VEGF-induced tube formation and migration, suggesting that Piezo1 may have an important role in angiogenesis (Li et al., 2014). This raises the question of whether a common molecular pathway involving Piezo1 also features in the abnormal placental vascular function seen in FGR.

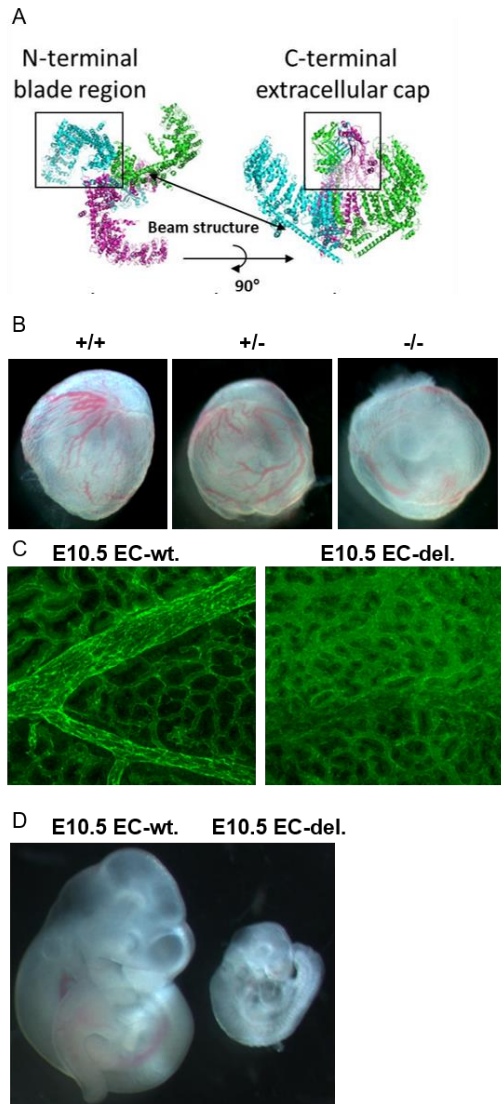


Figure 1.5 Structure and importance of Piezo1 for murine vascular development.

A., Cryo-electron microscopy Piezo1 trimeric structure produced using PyMol (Schrodinger Inc. Cambridge, UK) using PDB code 5Z10 by laboratory member Katie Simmons. Each monomer is represented as ribbons (monomer 1 cyan, monomer 2 magenta, monomer 3 green) (Zhao et al., 2018). B., Images of sibling yolk sacs (containing embryos) at E 9.5. Scale bar, 1 mm. Piezo1 wild-type (wt ++), haplotype (+/-), and homozygous knock out (-/-) are depicted. C., Dissected yolk sacs stained for CD31, showing wt, and endothelial-specific Piezo1-modified (EC-del) samples with reduced vascularization at mid-gestation. D., Sibling embryos at E 10.5. The embryo on the left was wild-type and the smaller embryo on the right contained endothelial-specific Piezo1 deletion (EC-del.). Figure showing highlights from (Li et al., 2014).

1.7.4.2 Yoda1: Piezo1 channel modulator

In addition to mechanical activation, a high-throughput screen by Syeda et al., identified Yoda1 as a synthetic compound capable of activating Piezo1 (Figure 1.6) (Syeda et al., 2015). This small molecule activates Piezo1 by prolonging the opening of the channel, leading to downstream effects via influx of Ca^{2+} and other cations into the cell. Yoda1 is able to induce Piezo1 activity when the channel is purified and isolated in a lipid bilayer (Syeda et al., 2015). This suggests that Yoda1 binds and activates Piezo1 directly. This exciting step allows us to manipulate Piezo1 function chemically. Importantly, Yoda1-evoked Ca^{2+} entry does not trigger release of intracellular Ca^{2+} stores, nor activate Piezo2 (Evans et al., 2018). However, the nature of Piezo1 activation differs from mechanical stimulation, namely slower channel inactivation. In addition, Yoda1 does not have the pharmacological properties of a drug for *in vivo* or therapeutic use. As such, Yoda1 is a useful research tool for facilitating the study of Piezo1 activation (Evans et al., 2018). The ability to develop novel chemical modulators of mechanosensors raises the possibility of new interventions targeting vascular dysfunction secondary to altered FSS, such as FGR.

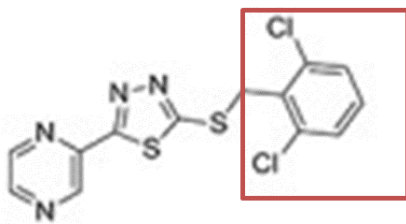


Figure 1.6 Yoda1 chemical structure. The 2,6-dichlorophenyl group of Yoda1 (red) is required for Piezo1 channel activation (Evans et al., 2018).

1.7.4.3 Piezo1 in human disease

In human disease, the most well-known *PIEZO1* mutation is autosomal dominant, where gain of function causes dehydrated xerocytosis, indicating the importance of Piezo1 for

erythrocyte stability (Zarychanski et al., 2012). Additionally, in embryonic development, an autosomal recessive Piezo1 loss of function mutation has been found in patients with generalised lymphatic dysplasia (Lukacs et al., 2015, Fotiou et al., 2015). This can present antenatally as non-immune fetal hydrops, which can result in death or pulmonary compromise at birth secondary to pleural effusions. Oedema can also recur in childhood and be generalised, affecting the face, limbs and genitals (Martin-Almedina et al., 2018). Interestingly, dehydrated xerocytosis can also present with perinatal oedema (Martin-Almedina et al., 2018). The similarity between the phenotypes of both gain- and loss of function suggests that Piezo1 has a critical role in sensing and developing the lympho-vascular flow system, although this is very much an emerging area of work (Hyman et al., 2017).

Research into Piezo1 in other areas of human disease is a fast-paced. Recent publications include findings in the pancreas, gastrointestinal tract epithelium, cardiomyocytes, chondrocytes and renal endothelium (Romac et al., 2018, Alcaino et al., 2017, Servin-Vences et al., 2017, Liang et al., 2017). One example is the role of Piezo1 in iatrogenic pancreatitis occurring secondary to the application of retractors during surgery (Romac et al., 2018). The authors describe pressure-induced Piezo1 channel activation. This was also induced by Yoda1 application and inhibited by Piezo1 antagonists (Romac et al., 2018). Despite these findings highlighting the functional importance and pathological relevance of Piezo1, to our knowledge there have been no studies investigating Piezo1 in the placenta.

1.8 Summary

The mechanical force of blood flow, FSS, is known to be a fundamental determinant of vascular homeostasis, regulating remodelling and vasomotor tone in the systemic circulation. The body of literature describing the role of FSS sensing and subsequent signalling in multiple vascular functions within the placenta is growing. Previous studies have shown that uterine arteries, FpECs, and trophoblast cells are sensitive to flow. It is becoming apparent that FSS has implications for a developing pregnancy, from

establishing the conceptus through to adequacy of placental blood supply at term (Morley et al., 2019). The role of FSS appears to be nuanced however, depending upon gestation and (potentially) cell type. This paradox stems from the threshold required for survival while preventing damage to the embryo and villi. As pregnancy progresses however, profound vasodilation and adaptation to flow are required to enable adequate placental perfusion. As such, a delicate balance in fluid forces is required for the complex processes of embryo establishment, uteroplacental remodelling, and fetoplacental vascular development. This therefore requires tight control by regulators capable of sensing and transducing force at each stage of development.

In FGR, the architecture of the placental vascular tree is altered with smaller numbers of immature villi, suggestive of impaired branching angiogenesis. This occurs alongside endothelial dysfunction, and creates a hypoxic environment (Kingdom et al., 2000). As such, subsequent increases in transmural pressure in small vessels will heighten placental vascular tone, generating greater FSS forces (Krause et al., 2013). We propose that mechanosensing has an important role in regulating placental vascular tone under normal conditions and when FSS is elevated in FGR.

When vascular resistance in the fetoplacental circulation is raised, abnormal flow velocity waveforms in fetoplacental blood vessels can be seen on Doppler US (Alfirevic et al., 2017). These changes correspond with signs of ischaemic damage on placental histopathological assessment. However, examining tissue from FGR-associated pregnancies also reveals the adaptive capacity of the placenta (Kingdom and Kaufmann, 1997). For example, evidence of a compensatory increase in branching angiogenesis and NO release in some cases of FGR. The placenta therefore has an active role in adapting its capacity to adequately oxygenate and supply nutrients to the fetus (Sandovici et al., 2012). Determining the molecular mechanisms enabling complementary, responsive interaction between the fetal, placental, and maternal circulations is a critical step towards understanding normal pregnancy and the development of treatments for FGR.

The identification of specific fast-acting placental mechanosensors which could be pharmacologically manipulated is therefore of particular interest. Piezo1 is increasingly being shown to be of fundamental importance in a variety of body systems. It has also been established that gene mutations in PIEZO1 can affect early pregnancy lympho-vascular development (Lukacs et al., 2015). Given the finding from our group that Piezo1 is critical for vascular development in the murine embryo, I sought to establish if Piezo1 has a role in human fetoplacental vasculature.

1.9 Hypothesis, aims and objectives

1.9.1 Hypothesis

Piezo1 is a mechanical sensor of critical importance in determining placental vascular function. The study of Piezo1 is therefore a useful focus for understanding and addressing problems of placental insufficiency.

1.9.2 Aims

1. To study the fetoplacental vascular endothelium through a novel method of EC isolation and culture.
2. To compare the characteristics of FpECs between patients with normal pregnancy outcomes and those with FGR.
3. To determine the contribution of Piezo1 to placental vascular function in health and disease.

1.9.3 Objectives

1. To determine the sensitivities of FpECs from normal pregnancies to FSS and establish the implications for EC properties and signalling pathways including NO mechanisms
2. To define the specific roles of Piezo1 in mediating these mechanical responses and characterise the effects of chemical activation of Piezo1 through the use of Yoda1

3. To compare the properties of healthy FpECs with those obtained from the placentas of pregnancies affected by FGR

Chapter 2 Materials and methods

2.1 Patient recruitment and consent

Due to the novel nature of researching placental vascular function at Leeds Institute of Cardiovascular and Metabolic Medicine (LICAMM), a new protocol for obtaining human placental tissue was established. Patients delivering at Leeds Teaching Hospitals Trust (LTHT) were approached to participate in either appropriately grown for gestational age (AGA) or small for gestational age (SGA) groups.

The inclusion criteria for patients in the AGA control group were women delivering by elective lower segment caesarean section (LSCS) at term (≥ 37 weeks of gestation), with no fetal growth or maternal health concerns. Examples include women undergoing LSCS due to breech presentation, previous emergency delivery or perineal trauma. Patients with a history of assisted conception, smoking, BMI > 40 Kg/m² or age ≥ 40 years were excluded.

The SGA group comprised of samples where babies weighed $< 10^{\text{th}}$ percentile at birth. This was determined using the GrowthCharts UK-WHO mobile app, a UK-specific growth chart combining data from the Neonatal and Infant Close Monitoring Growth Chart (NICM), the UK WHO 0-4 years growth chart, and the UK growth chart 2-18). Ultrasound (US) scan findings were recorded, including growth measurements and Doppler blood flow findings. All modes of delivery were included to reflect deliveries by emergency secondary to SGA with fetal compromise, and these data were recorded. All risk factors for SGA secondary to placental insufficiency were considered. As such, PET, gestational hypertension, a history of assisted conception, smoking, extremes of BMI (> 40 Kg/m²) and/or age ≥ 40 years, were included (Appendix 1 and 2). Multiple pregnancy, and babies with known genetic or congenital abnormalities were excluded from both the control and SGA groups.

In addition, samples of RNA from first trimester pregnancies were provided by Karen Forbes. These samples were obtained following surgical terminations of pregnancy.

Patient consent, tissue storage and the demographic data for these samples were handled by Karen Forbes.

2.2 Ethical approval, data management and storage

Patients were recruited at the antenatal clinic, the antenatal ward, or the delivery suite at either Leeds General Infirmary (LGI) or St James's University Hospital (SJUH). Consented patients were provided with written information and a copy of their consent form, in accordance with the approval granted by the local ethics committee (Ref 13/YH/03/44 and 18/LO/0067). Their demographic and clinical data were collected on a predesigned proforma (Appendix 1). The original consent form and proforma were assigned a number to correspond with the sample and stored in a locked filing cabinet. A copy of the consent form was placed in each woman's hospital notes. The research midwives at the Women's Clinical Service Unit collected, stored and verified these consent forms. Sample numbers were assigned chronologically, and data transcribed onto an Excel spreadsheet (Appendix 2). Patient identifiers on the spreadsheet were the NHS number, date of delivery and mother's initials. This spreadsheet was located on the University 'M' drive and access only possible after pre-arranged IT activation. All home working was carried out on Desktop Anywhere.

2.3 Sampling and processing placental tissue

Placentas were obtained within one hour of delivery, inspected for any visual abnormalities, and were weighed after removal of the umbilical cord and membranes.

Samples of placental parenchymal tissue were taken from the villous surface of the placenta, avoiding membranes, margins and any macroscopically abnormal areas. A 2 x 2 cm sample was taken from each of four quadrants and pooled.

Additional samples were obtained depending on experiment requirements. This included the umbilical cord, which was cut from the insertion point on the chorionic plate, and a

length of 10 cm obtained. Larger sections of placenta (5 x 5 cm) involving the chorionic plate were collected for the isolation of chorionic artery endothelial cells and/or myography studies of the chorionic arteries. Samples were also taken when required to support the work of Sara Ibrahim (chorionic membrane), Georgia Mappa (histological studies) and Karen Forbes (explant experiments).

All samples were transported to the laboratory on ice, in Endothelial Cell Growth Medium-2 (EGM-2; Lonza, USA) and processed immediately. EGM-2 is comprised of Endothelial Basal Medium-1 (EBM-1) supplemented with 2% fetal calf serum and the EGM-2 bullet kit (CC-3162, Lonza, USA). This kit comprises of growth factors (10 ng/mL VEGF, 5 ng/mL human basic fibroblast growth factor), 1 µg/mL hydrocortisone, 50 ng/mL gentamicin, 50 ng/mL amphotericin B, 10 µg/mL heparin and 10 µg/mL ascorbic acid.

The pooled placental sample was divided into 5 mL Eppendorf Tubes® (EP0030119401, Sigma, UK) and either snap frozen in liquid nitrogen for protein extraction, stored in RNA*later*[™] (RNA stabilisation solution, R0901, Ambion, USA) for RNA isolation, or transferred to tissue culture for immediate EC isolation.

Where placentas were required to undergo histological examination for clinical reasons, the remaining tissue was sent to pathology with a description of the samples obtained for research. Upon completion of sampling, the remaining placental tissue was disposed of in accordance with a standard operating procedure developed for this project in LICAMM. Briefly, blood was decontaminated overnight in ChemGene disinfectant sealed with Parafilm prior to disposal. Tissue and items in contact with tissue were placed in a triple-layered Biohazard bag which was autoclaved before incineration.

2.4 Isolation of fetoplacental endothelial cells (FpECs)

Isolation of FpECs was undertaken in a sterile manner, using a protocol adapted and optimised for placental tissue (van Beijnum et al., 2008). Placental tissue was hand minced and re-suspended in a dissociation solution of 0.1% Collagenase II w/v (9 mL), 2.5 units/mL Dispase w/v (1 mL), 1 μ M CaCl₂ and 1 μ M MgCl₂ in Hanks' Balanced Salts Solution. This was incubated at 37°C for 45 minutes in a MACSMix Tube Rotator (Miltenyi Biotech, UK) to provide continuous agitation (Figure 2.1). Samples were passed through a 70 μ m cell strainer to remove undigested tissue. The cell suspensions were washed in magnetically-activated cell sorting (MACS) buffer consisting of Phosphate Buffered Saline (PBS), 2 mM EDTA, and 0.1% Bovine Serum Albumin (BSA) w/v, before a 10 minute centrifugation at 1000 rpm. This wash step was repeated twice. Pellets were then re-suspended in red blood cell lysis buffer consisting of 17 mM Tris base and 140 mM NH₄Cl in PBS. Cells were washed for a final time in MACS buffer before mixing with 200 μ L of Dead Cell Removal Kit (Miltenyi Biotec). The cell suspensions were passed through a column prepared with Binding Buffer (Miltenyi Biotec) in a magnetic field (MidiMACS™ Separator, Miltenyi Biotec).

The eluate consisting of live cells was incubated with Fc receptor blocking reagent and CD31-conjugated paramagnetic microbeads under continuous agitation for 15 minutes at 4 °C. After incubation, the solution was passed through a column prepared with MACS buffer. CD31 positive cells were retained in the column, and CD31 negative cells passed through as eluate and were discarded (Figure 2.1). The magnetised column was transferred to a fresh sterile falcon for rapid elution of the CD31 positive cells. This cell mix was pelleted by centrifugation at 1000 rpm for 4 minutes. The pellet was re-suspended in 1 mL of pre-warmed EGM-2 media. One well of a 6 well tissue culture plate (Corning® Costar®) was coated with 0.1% gelatin before the 1 mL cell mix was seeded.

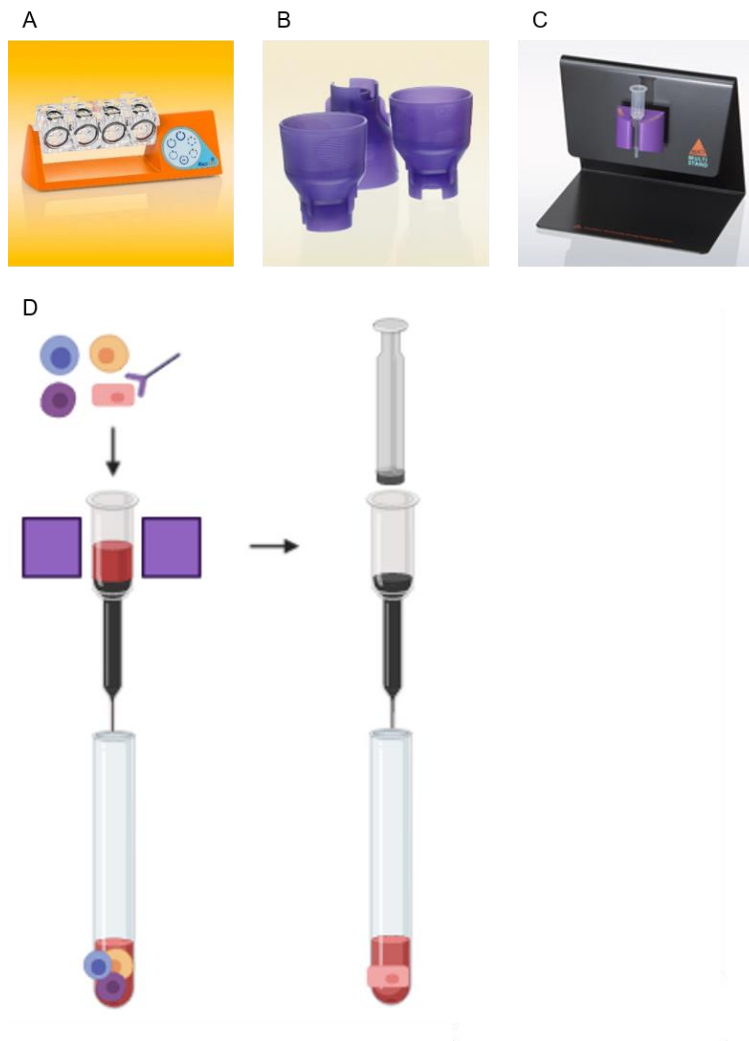


Figure 2.1 Isolation of FpECs. A., The MACSMix™ Tube Rotator (Miltenyi Biotec) used to incubate placental tissue under continuous agitation. B., Examples of 70 µm cell strainers used to sieve out undigested tissue. C., The MidiMACS™ Separator attached to a MultiStand, holding an LS Column (Miltenyi Biotec). D., Graphic adapted from Miltenyi Biotec depicting target cells being magnetically labelled with nano-sized MicroBeads (~50 nm) via antibodies and being retained in the column. The flow-through fraction of negatively labelled cells was discarded. The columns were removed from the separator. The retained positively selected cell fractions were eluted by plunging into a new falcon. Images obtained from www.miltenyibiotec.com/GB-en/products, created with BioRender.

2.5 Isolation of human umbilical vein endothelial cells (HUVECs)

Within a sterile tissue culture hood, each umbilical cord was placed in a culture dish (Corning®). The umbilical veins and artery were identified and one vein cannulated with a sterile blunt ended needle, in an adapted method (Fearnley et al., 2014). 20 mL of PBS were flushed through the cord to remove blood clots. The end of the vein was clamped before infusing with 0.1% Collagenase II w/v (9 mL) and clamping the other end (Figure 2.2). The infused cord was incubated at 37 °C for 20 minutes. The cord was suspended over a 50 mL falcon, unclamped and flushed with 20 mL of PBS, to collect to eluate. Cells were pelleted by centrifugation for 5 minutes. The pellet was re-suspended in 2 mL of pre-warmed EGM-2, before dividing between 2 wells of a 6 well plate (Corning® Costar®).



Figure 2.2 Clamped umbilical cord. Example of an umbilical cord clamped at both ends, prior to incubation. One umbilical vein is filled with Collagenase (pink tinge).

2.6 Culture of FpECs and HUVECs

24 hours after seeding FpECs and HUVECs, wells were gently washed with PBS to remove any non-adhered cells before adding fresh EGM-2. The medium was subsequently replenished every 48-72 hours. Cells were maintained at 37°C in a humidified atmosphere containing 5% CO₂ and 95% air. Cells were grown to 95%

confluency before passage. FpECs at passage 0 reached confluency in approximately 4-6 weeks, whilst HUVECs were faster growing at 1-2 weeks.

For all experiments, cells at passages 3-6 were used. Cells were passaged by washing with PBS, and application of 0.1% Trypsin-EDTA. After neutralisation with EGM-2, cells were either counted for experiments or seeded into new tissue culture flasks. Cells were counted by placing 10 μ L of cell suspension under the coverslip of a haemocytometer and averaging the number of cells per grid quadrant, when viewed at 10 x magnification on a light microscope.

Cells were frozen for future experiments at passage 3. After re-suspending the trypsinised cell pellet in freezing medium, cells were transferred to a cryovial for temporary storage in a Mr. Frosty™ freezing container at -80 °C. After 24 hours, cryovials were stored in liquid nitrogen. Cells were rapidly defrosted into pre-warmed EGM-2 when required.

2.7 Isolation of chorionic plate artery endothelial cells

From our placental samples, second order arteries from the chorionic plate were identified within one hour of the delivery (Figure 2.3A and B). The fresh isolation of primary ECs from these arteries was performed by laboratory member, Jian Shi in a method previously described and validated (Greenberg et al., 2016, Rode et al., 2017). In brief, the placental arteries were digested enzymatically in a dissociation solution of 1 mg/mL collagenase Type IA (Sigma-Aldrich, UK) with 126 mM NaCl, 6 mM KCl, 10 mM Glucose, 11 mM HEPES, 1.2 mM MgCl₂, 0.05 mM CaCl₂, with pH adjusted to 7.2. These were incubated for 14 min at 37°C before gentle trituration of the vessels to release the ECs onto a glass coverslip (Figure 2.3C).

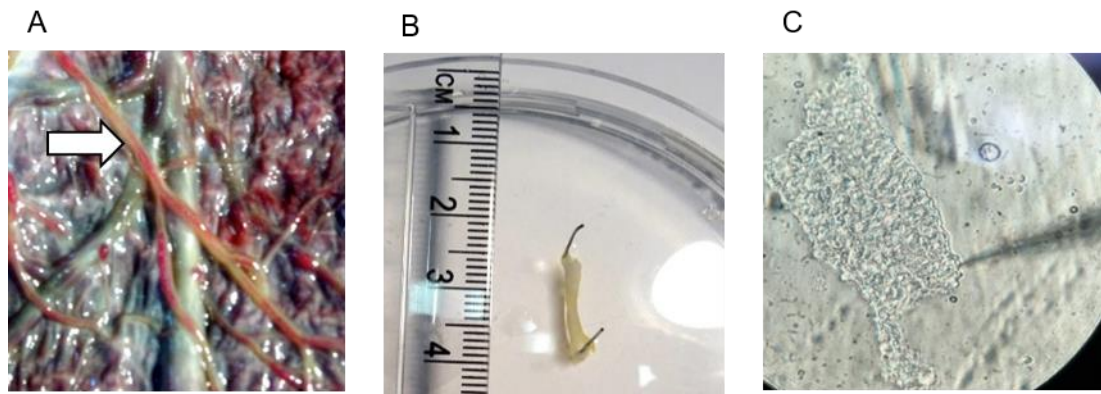


Figure 2.3 Isolation of chorionic plate artery endothelial cells. A., Identifying an artery of appropriate diameter, crossing over a vein on the placental chorionic plate (arrow). B., Dissected and cleaned chorionic artery (diameter 760 μm) in physiological solution. C., Single freshly isolated endothelial cell viewed under the light microscope. Images B and C provided by Jian Shi (Morley et al., 2018).

2.8 Immunostaining

FpECs were grown on glass coverslips in a 24 well culture plate, before fixing with 4% paraformaldehyde solution. After PBS washes, cells were permeabilised with 0.1% Triton X-100 w/v. To prevent non-specific antibody binding, cells were blocked with donkey serum (5% v/v) for 30 minutes. Cells were incubated with primary antibody in the dark for one hour (Table 5). Post washing with PBS, cells were incubated for 30 minutes with the relevant species-specific secondary antibodies conjugated with appropriate fluorophores. DAPI was used to counterstain cell nuclei. Coverslips were mounted onto slides and stored in the dark until imaging. Slides were imaged using an LSM 880 confocal microscope (Zeiss, Sweden). Image analysis was performed using ImageJ to quantify staining intensity.

Primary Ab	Dilution	Host species	Product	Secondary Ab dilution (PBS)
Anti-CD31	1:300 in 1% BSA in PBS	Mouse	JC/70A Dako USA	1:300 Alexa-488
Anti-vWF	1:200 in PBS	Mouse	F8/86	1:300
Anti-vimentin C20	1:100 in 1% BSA in PBS	Mouse	Sc-7557 Santa Cruz Biotechnology Inc., USA	1:300
Anti- α -SMA-1A4	1:100	Mouse	ab7817 Sigma, UK	1:200
Anti-cytokeratin peptide 7	1:200	Mouse	C6417 Sigma, UK	1:200

Table 5 Antibodies used for immunostaining

2.9 Functional assays

2.9.1 Angiogenesis

Angiogenesis was investigated by studying tube formation on a growth factor-reduced Matrigel® basement membrane matrix (10 mg/mL; Corning, 354234). The Matrigel® was thawed overnight at 4 °C to ensure liquidity, then kept on ice. Sterile filter tips, falcons and pipettes were also cooled prior to use. A cold 96 well tissue culture plate was

prepared with 60 μL of Matrigel® per well, taking care to avoid air bubbles. Plates were incubated at 37 °C for 15 minutes to gel the matrix. Confluent FpECs were lysed, as previously described, and counted. A total of 10,000 FpECs were seeded onto the Matrigel® in each well. The plate was placed in an IncuCyte ZOOM Kinetic Imaging System (Essen BioScience). HD-Phase Contrast images were taken immediately after seeding, and hourly for 12 hours. Cells seeded onto substrate-free wells were used as a negative control for tube formation.

In vitro tube formation was also demonstrated using an endothelial cell and fibroblast co-culture assay. Here, Normal Human Dermal Fibroblasts (NHDF, Lonza) were seeded at 6,000 cells per well in a 96 well plate (day 1, Greiner Bio-one, UK) and allowed to grow to a 100% confluent monolayer (~ day 4). FpECs were seeded on top of the fibroblast monolayer and allowed to grow into tube-like structures. On day 10, cells were fixed and CD31 immunocytochemistry was performed (as previously described). Capillary-like structures were visualised using HD-Fluorescent imaging on the IncuCyte.

2.9.2 Migration assay

The ability of FpECs to show the property of migration was assessed using a WoundMaker™ (Essen BioScience). In this cell migration assay, wells of a 96 well Essen Image Lock tissue culture plate (Essen BioScience 4379) were first coated with 0.1% gelatin. Confluent FpECs were trypsinised and counted, as previously described. FpECs were seeded at 25,000 cells per well in 100 μL of EGM-2 media. After overnight incubation, cells were checked to ensure a confluent monolayer had formed. To promote migration over proliferation, confluent cells were serum-starved with 100 μL per well of serum-free media, with added mitomycin C (1 $\mu\text{L}/100 \mu\text{L}$). After 4 hours, the WoundMaker™ was cleaned with 2 x 5 minute cycles of 70% ethanol followed by distilled water, and then prepared with PBS. A linear scratch wound was made in each well (Figure 2.4). Wells were washed in PBS and the scratch checked under the microscope. EGM-2 media containing serum was added to each well before transferring to the IncuCyte for imaging.

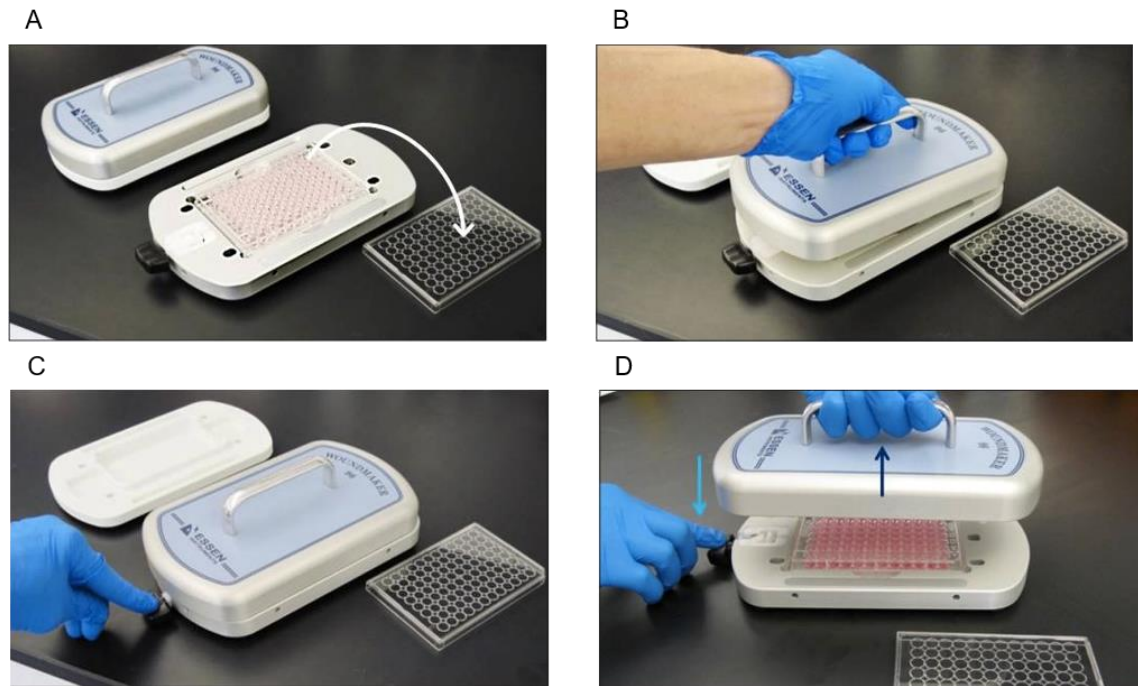


Figure 2.4 Scratch WoundMaker™. A., Plate inserted into base of the WoundMaker™ with lid removed. B., 96 well pin block carefully placed into the cell plate. C., Lever held down to create the scratch. D., Pin block carefully removed from the cell plate, prior to imaging cells and cleaning WoundMaker™. Images taken from 96 well kinetic cell migration assay user manual (EssenBioScience, 2020). HD-Phase contrast images were taken after the initial wound (0 hours), then at 2 hour intervals for 12 hours. IncuCyte™ Software was used to determine the relative wound density (RWD). RWD is a % measure of the density of the wound region relative to the density of the cell region (EssenBioScience, 2020). This accounts for background density at the initial time point, such as cell debris, and therefore RWD at 0 hours is 0%. The RWD result is generated on IncuCyte™ by using the ‘Scratch Wound Mask’ and ‘Confluence Mask’ image analysis functions. The mask was further defined to highlight cells only, filtering out unwanted dead cells, debris and other background. This Processing Definition was applied all images from the assay.

2.9.3 Proliferation

A growth curve was used to demonstrate viable FpEC cell colonies. On day 0, cells were trypsinised and counted as previously described, and seeded at 25,000 cells per well of

a 6 well plate. EGM-2 was exchanged on day 1, and then alternate days. On day 2, cells in well 1 were trypsinised, pelleted, reconstituted in 1 mL of EGM-2, and counted. This was continued to day 12, and a growth chart plotted.

2.10 RNA isolation and quantitative RT-PCR

2.10.1 RNA isolation

Prior to RNA isolation, the laboratory bench and other equipment were cleaned with RNaseZAP™ (Sigma), and sterile filter tips used throughout.

Total RNA was isolated from confluent FpECs in 6 well tissue culture plates using the RNeasy Plus Mini Kit (74134, Qiagen, UK). Cells were washed with PBS before the addition of lysis buffer (350 µL of Buffer RLT, in molecular grade ethanol plus β-mercaptoethanol, added to each well). Cells were scraped from the well, collected in an RNase-free Eppendorf, and pipetted repeatedly to ensure cell lysis. Each tube was vortexed for 30 seconds to homogenise the sample. Each lysate was transferred to a gDNA Eliminator spin column and centrifuged, to remove genomic DNA from the samples. 70% ethanol (350 µL) was added to the samples which were transferred to RNeasy spin columns and the flow-through discarded. Samples were washed on column with buffer solutions, before eluting into RNase-free water in a collection tube, using high speed centrifugation (Figure 2.5). Samples were kept on ice whilst quantifying and assessing quality, before freezing at -80 °C.

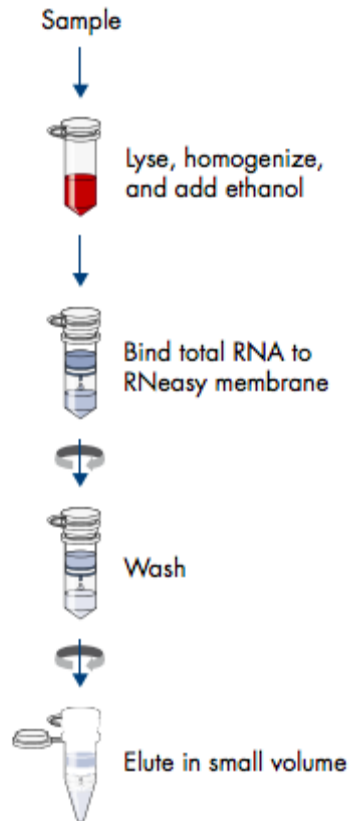


Figure 2.5 Protocol for RNeasy Plus Mini Kit (Qiagen). Overview of the RNeasy Plus Mini Kit (Qiagen) protocol showing on-column isolation and elution of total RNA.

Total RNA was extracted from whole placental tissue using TRIzol® reagent (Ambion). In this protocol, 1 mL of cold TRIzol® was added to 200 µg of frozen tissue in an RNase-free microcentrifuge tube containing a stainless steel bead, before mechanical disruption by high-speed shaking (Tissue Lyser II, Qiagen, Denmark). The homogenised tissue was pelleted by centrifugation (10,000 g, 10 minutes at 4 °C). Phase separation was achieved with the addition of chloroform (200 µL) and centrifugation. The aqueous upper phase was retained and RNA was precipitated by addition of an equal volume of ice-cold isopropanol (~450 µL). Samples were vortexed thoroughly, left on ice for 10 minutes, then centrifuged to pellet the RNA. The pellet was washed in 70% ethanol, then centrifuged before careful removal of the ethanol. The pellet was air-dried for exactly five minutes, before dissolving in 20 µL of RNase-free water.

Samples underwent DNase digestion using the TURBO DNA-free™ Kit (AM1907 Invitrogen, UK). This involved incubation of samples with RNase-free DNase enzyme and 10x reaction buffer for one hour in a water bath at 37 °C. Enzyme inactivation agent was added before centrifugation. The RNA-containing supernatant was transferred to a fresh Eppendorf for quantitative and quality assessment.

RNA was measured using a microvolume NanoDrop™ 2000 spectrophotometer and NanoDrop™ 2000 software (Thermo Fisher). The NanoDrop pedestal was first cleaned with ethanol before establishing a Blank reading using molecular grade water. This was followed by a reading of 1 µL of sample. The pedestal was cleaned and dried between samples. The absorbance of each sample was measured at 260 and 280 nm. The absorbance at 260 nm was used to calculate the RNA concentration using the Beer-Lambert equation (Equation 1):

$$c = (A * \epsilon)/b$$

Equation 1 Beer-Lambert equation. Equation modified to calculate RNA concentration in ng-cm/microliter, where c = the nucleic acid concentration in ng/µL, A = the absorbance in AU, ϵ = the wavelength-dependent extinction coefficient in ng-cm/microliter, b = the path length in cm (1.0 cm).

The spectral image and purity ratios of absorbance were used to assess sample quality. In accordance with the manufacturers guideline, a 260/280 nm ratio of ~ 2.0 was accepted as 'pure' for RNA. For the secondary purity ratio obtained from the 260/230 nm absorbance, values in the range of 1.8 - 2.2 were regarded as 'pure' RNA (Scientific, 2009). Contamination with Phenol or guanidine isothiocyanate was occasionally seen after RNA isolation using either TRIzol® or the RNeasy Plus Mini Kit, respectively, as discussed in Chapter 4, section 4.1.

Samples with ratios appreciably below these values were treated with the RNA Clean and Concentrator Kit-5 (R1013, Zymo Research, USA). In this protocol, samples were first diluted to a volume of 50 µL with molecular grade water. This was mixed with 100 µL

of RNA Binding Buffer, followed by 150 μL of 100% ethanol. Samples were transferred to the Zymo-Spin™ Column in a collection tube and centrifuged for 30 seconds at 10,000g, before discarding the flow-through. Centrifugation and discarding the flow-through was performed after addition of 400 μL of RNA Prep Buffer, and 2 washes with RNA Wash Buffer. The purified RNA was eluted from the column with 15 μL of molecular grade water. Samples then underwent repeat measurement on the NanoDrop™.

2.10.2 Reverse transcription

RNA at high concentrations was diluted to 250 ng/ μL , and re-measured. 1 μg of RNA (~4 μL) in a total volume of 10 μL (~5 μL molecular grade water) was used to reverse transcribe each sample. 2 μL of Random Primers (DNA hexamers, Promega, C1181) were added to the RNA mix before running for 7 minutes at 75 °C, to denature the DNA. Complimentary DNA (cDNA) was synthesised with the addition of Moloney Murine Leukaemia Virus (m-MLV) Reverse Transcriptase kit (Thermo Scientific, 28025013), containing m-MLV enzyme (0.5 μL), 5x Reaction Buffer (4 μL), and 0.1 M DTT (0.2 μL). RNase OUT (0.5 μL , Invitrogen, 10777-019), 10 mM deoxynucleotide triphosphates (dNTPs, 1 μL , Thermo Fisher 4387406), and molecular grade water (2.8 μL) were also added. Samples were programmed to run for 10 minutes at room temperature, 1 hour at 37 °C and 5 minutes at 95 °C. Selected samples were non reverse transcribed (-RT) in reactions which were ran in parallel to those with enzyme. The cDNA was either used immediately for QPCR or stored temporarily at 4 °C.

2.10.3 QPCR (quantitative polymerase chain reaction)

Quantitative real time-qPCR (QPCR) of the cDNA was used to assess the mRNA expression of target genes of interest, and endogenous controls (reference genes). Immediately prior to the experiment, cDNA was diluted twice. Gene-specific primers were prepared by diluting 100 μM stocks of both Forward and Reverse primers to 2 μM , in molecular grade water (Table 6). A master mix was prepared for each primer pair, consisting of Sybr green Supermix (Bio-Rad, 1725121), primers and molecular grade water. 96 well QPCR plates were prepared, whereby each well contained 2 μL of cDNA

and 18 μL of mastermix. All reactions were performed in duplicate. Plates were then sealed and centrifuged. Quantification was performed by a LightCycler® 96 Instrument (Roche, 05815916001). The reaction conditions were preincubation (600 seconds at 95°C), two step amplification (45 cycles at 95°C , 10 seconds at 95°C and 30 seconds at 60°C), melting (one cycle at 95°C , 60 seconds at 65°C and 1 second at 97°C) and cooling for one cycle (37°C for 30 seconds). Data were analysed using LightCycler® 96 Instrument software version 1.1.1.

Mean threshold cycle (Ct) values were calculated for each replicate, and the mean difference used to check for technical errors. Ct values of target genes were normalised to the reference genes results to obtain delta (Δ) Ct values. $\Delta\Delta\text{CT}$ was calculated using Equation 2. Given that primers were selected with high (>90%) efficiency for both housekeeping and target genes, the fold change in mRNA expression was calculated using the $2^{-\Delta\Delta\text{CT}}$ (Livak) method (Vandesompele et al., 2002). The specificity of QPCR was verified by analysing the –RT results, melt-curves, and confirming the amplicon size of PCR products using gel electrophoresis.

$$\Delta\text{CtC (control)} = \text{CtgTC} - \text{CtgRC}$$

$$\Delta\text{CtE (experimental)} = \text{CtgTE} - \text{CtgRE}$$

$$\Delta\Delta\text{Ct} = \Delta\text{CtE} - \Delta\text{CtC}$$

$$2^{-\Delta\Delta\text{Ct}} = 2^{\Delta\text{CtE}} / 2^{\Delta\text{CtC}}$$

Equation 2 The $2^{-\Delta\Delta\text{Ct}}$ (Livak) method for calculating relative expression of mRNA.

ΔCtC = Change in Ct control group: CtgTC = Mean Ct value of target gene in the control group, CtgRC = Mean Ct value of the reference genes in the control group. ΔCtE = Change in Ct the experimental group: CtgTE = Mean Ct value of the target gene in the experimental group, CtgRE = Mean Ct value of the reference genes in the experimental group. $\Delta\Delta\text{Ct}$ = relative expression, $2^{-\Delta\Delta\text{Ct}}$ = normalised expression ratio.

Gene	Reference	Primer sequence 5' – 3'	Size (bp)	Source
Reference genes				
<i>ACTB</i>	NM_001101.5	R: CACGCAGCTCATTGTAGAAG F: ATCCTCACCCCTGAAGTACCC	97	VC
<i>YWHAZ</i>	NM_145690.3	F: ACTTTTGGTACATTGTGGCTTCA A R: CCG CCA GGA CAA ACC AGT AT	94	(Drewlo et al., 2012)
<i>CYC1</i>	XM_024447072. 1	F: CAG ATA GCC AAG GAT GTG TG R: CATCATCAACATCTTGAGCC	93	(Drewlo et al., 2012)
Genes of interest				
<i>PIEZO1</i>	NM_001142864. 4	F: CGTCTTCGTGGAGCAGATG R: GCCCTTGACGGTGCATAC	76	VC
<i>PIEZO2</i>	NM_022068.3	F: CCTTTCTGCTGGTGTGCATT R: GGCCAGTCTGTAGATGGTGTG	113	Design
<i>NOTCH1</i>	NM_017617.5	F: CTGGAGGACCTCATCAACTC R: TTCTTCAGGAGCACAACCTGC	119	VC
<i>NOTCH2</i>	NM_024408.4	F: CTTGCTGTTGCTGTTGTCAT R: GCGAAGAGTGAAACCTTCAG	111	VC
<i>NOTCH3</i>	NM_000435.3	F: GTGGCCCTCATGGTATCTGC R: TTCAGGCATGGGTTGGGGTC	121	Design
<i>NOTCH4</i>	NM_004557.4	F: GTGGGTATCTCTGCCAGTGT R: CTCAGGTTTGGGAGTACAG	116	Design
<i>JAG1</i>	NM_000214.3	F: GCGTTGCCCACTTTGAGTAT R: GCCTTCCATGCAAGTTTTGT	146	VC
<i>DLL1</i>	NM_005618.4	F: CGGATCTCGAGAACAGCTAC R: GTCATGGCACTCAATTCACA	76	VC
<i>DLL4</i>	NM_019074.4	F: ACAACTTGTCGGACTTCCAG R: CAGCTCCTTCTTCTGGTTTG	77	VC
<i>ADAM 10</i>	NM_001320570. 2	F: TTGCCTCCTCCTAAACCACT R: AGGCAGTAGGAAGAACCAA	153	VC
<i>HEY1</i>	NM_001040708. 1	F: GCGTGGGAAAGGATGGTTG R: TCCGCTCTCGGCTGCTTG	85	VC

<i>HES1</i>	NM_005524.4	F: CCAAAGACAGCATCTGAGCA R: GCCGCGAGCTATCTTTCTT	133	VC
<i>CD31</i>	XM_005276882.1	F: AGACTGAACCTGTCCTGCTC R: CTGTCCGACTTTGAGGCTAT	119	VC
<i>EPHRIN B2</i>	NM_005251.3	F: CACCTTGAACGGCATCTACC R: GCCGTTCTCGAACATGTTG	199	VC
<i>EPHRIN B4</i>	NM_004444.5	F: GACCCTGCTGAACACAAAAT R: CACGTCACACACTTCGTAGG	136	VC
<i>GPR68</i>	NM_001177676.2	F: TGTACCATCGACCATACCA R: GGTAGCGAAGTAGAGGGACA	105	Design
Additional primers tested for efficiency and suitability				
<i>TOP1</i>		F: GATGAACCTGAAGATGATGGC R: TCAGCATCATCCTCATCTCG		(Drewlo et al., 2012)
<i>GAPDH</i>		F: AGATCATCAGCAATGCCTCC R: CATGAGTCCTCCCACGATAC		(Drewlo et al., 2012)
<i>HPRT1</i>		F: TGACACTGGCAAACAATGCA R: GGTCTTTTTACCCAGCAAGCT		(Drewlo et al., 2012)
<i>B2M</i>		F: GGCTATCCAGCGTACTCCAAA R: CGGCAGGCATACTCATCTTTTT		(Drewlo et al., 2012)
<i>SDHA</i>		F: TGGGAACAAGAGGGCATCTG R: CCACCACTGCATCAAATTCATG		(Drewlo et al., 2012)
<i>TBP</i>		F: TGCACAGGAGCCAAGAGTGAA R: CACATCACAGCTCCCCACCA		(Drewlo et al., 2012)
<i>BA</i>		F: ATTGGCAATGAGCGGTTC R: GGATGCCACAGGACTCCAT		(Meller et al., 2005)
<i>RNA18S 1</i>		F: CGATTGGATGGTTTAGTGAGG R: AGTTCGACCGTCTTCTCAGC		(Meller et al., 2005)

<i>PIEZO2</i>		F: ATGGCCTCAGAAGTGGTGTG R: ATGTCCTTGCATCGTCGTTTT	(Huang et al., 2019)
---------------	--	---	----------------------

Table 6 Primer Sequences and expected amplicon sizes. Primer sequences were either obtained from publications, or colleagues (Vincenza Caolo). Where these were unavailable or not of suitable quality, new primers were designed using Primer-BLAST (www.ncbi.nlm.nih.gov/tools/primer-blast/). Primers were selected to have a product size of 70-250 bp, specificity with no unintended gene targets, low self-complementarity, GC content of 40-60%, and a melting temperature (T_m) of 52-58 °C.

All primer pairs listed in Table 6, were tested for their efficiency in QPCR reactions. cDNA was prepared from samples of AGA FpECs (LGI007 and LGI011). A 6-fold serial dilution of the cDNA was produced from a pure sample. Efficiency was calculated by plotting log dilution against mean Ct value of 2 replicate wells. The R^2 correlation co-efficient was deemed adequate if ≥ 0.99 , and efficiency was calculated from the slope (y) (Equation 3). Primers with efficiency of 0.9 – 1.1 were regarded as suitable for use. These data, alongside analysis of melt curves was used to select the appropriate primer pairs for experiments.

$$\text{Efficiency} = \text{POWER}(10, -1/y) - 1$$

Equation 3 Efficiency calculation

2.10.4 Effect of Yoda1 treatment on mRNA abundance

To determine the effect of treating FpECs with the synthetic compound, Yoda1, on the expression of target genes (*PIEZO1*, *PIEZO2*, *NOTCH* pathway), cells were grown to $\geq 80\%$ confluency in 6 well plates. Cells were serum-starved by aspirating EGM-2 and replaced with reduced serum media (0.5%). Due to potential upregulation of the ADAM10 complex by VEGF and human fibroblast growth factor (hFGF), these were omitted from this media. After 4 hours, a 0.2 μM Yoda1 (10 mM in DMSO, Tocris, 5586) solution was

made up in starvation media, alongside a vehicle control (2 μ M DMSO). Each well was treated with either 1.5 mL of Yoda1 or vehicle solution for 2 hours, after which cells were lysed, RNA isolated and QPCR performed (as described in 2.10.1 and 2.10.3).

2.10.5 Gel electrophoresis

QPCR plates were centrifuged, and PCR products of interest were aspirated. 2% Agarose gels were made up with 1x Tris-acetate-EDTA (TAE) buffer and stained with SYBR Safe DNA gel stain (Invitrogen, S33102). Products were stained with loading dye (Sigma, R1386) and separated on the gel by running a current of 80 Volts for 45 minutes. The amplicon size of products was compared to a 100 base pair (bp) ladder (Sigma, P1473), and the expected size based on primer-BLAST software (Ye et al., 2012).

2.11 Intracellular calcium (Ca^{2+}) measurements

Changes in intracellular Ca^{2+} concentration, were measured using a FlexStation 3 (Molecular Devices) bench-top fluorometer and fluorescent probe. For this assay, a UV light-sensitive radiometric Ca^{2+} indicator dye was used. Fura-2 AM is a dual-wavelength dye, whereby upon binding to Ca^{2+} , Fura-2 AM exhibits an absorption shift in between 300 and 400 nm on the exciting spectrum, with emission at 510 nm. During the experiments incubation period, Fura-2 AM enters the cell cytoplasm. When a ligand binds to a receptor upon the application of a drug compound, Ca^{2+} is released. The dye binds to this cytoplasmic Ca^{2+} and a change in fluorescence occurs. The shift in the fluorescence spectrum is proportional to the concentration of intracellular free Ca^{2+} , and is therefore measurable.

For these experiments, FpECs were seeded onto a standard tissue culture 96 well plate at a density of 25,000 cells per well. Assays were performed the following day, after checking cells were \geq 80% confluent.

The 96-well assay plates were prepared in a dark room, and kept foil wrapped. Media was removed from the wells, and cells loaded with Fura-2 acetoxymethyl ester (AM) indicator dye (2 μM) (Thermo Fisher, F1200). This consisted of the light-sensitive radiometric Ca^{2+} indicator dye, Fura-2 AM, and 0.01% pluronic acid in Standard Bath Solution (SBS) with Ca^{2+} . 50 μL of Fura-2 AM was added to each well and incubated for 45 minutes at 37 $^{\circ}\text{C}$. The Fura-2 AM was then removed, and replaced with 100 μL per well of SBS. This SBS contained the vehicle corresponding to the compound to be tested (distilled water or Dimethyl sulfoxide (DMSO)). Plates were foil wrapped again and kept at room temperature for 30 minutes.

Compounds to be tested were prepared in Ca^{2+} SBS from the stock solutions listed in Table 7. These were prepared at double the desired concentration, accounting for the dilution occurring upon transferring the compound (100 μL per well) onto the assay plate (100 μL per well). Compounds were loaded into a 96 well round bottom plate (Corning®, 3799) at 120 μL per well, to ensure the full 100 μL volume was taken up by the automated pipette tip.

Chemical	Concentration	Product
For 500 mL of SBS with Ca ²⁺	130 mM NaCl (3.9 g) 5 mM KCl (0.18 g) 1.2 mM MgCl ₂ (600 µL) 1.5 mM CaCl ₂ (750 µL) 8 mM d-glucose (0.72 g) 10 mM HEPES buffer (1.19 g) pH to 7.4, with addition of 4M NaOH	Made up from communal laboratory stocks purchased from Sigma.
Fura-2 AM	1 mM (1:500 in SBS)	Thermo Fisher, F1200
Pluronic acid	10% w/v in DMSO (1:1000 in SBS)	Sigma, P2443
VEGF	30 µg/mL in H ₂ O (30 ng/mL)	Sigma, V7259
ATP	20 mM in H ₂ O (10 µM)	Sigma, FLAAS
Ionomycin	1 mM in DMSO (0.1-10 µM)	Sigma, 10634
Yoda1	10 mM in DMSO (0.1–20 µM)	Tocris, 5586
Gd ³⁺	100 mM in H ₂ O (30 µM)	Sigma, 439770
Glucose	1 M in H ₂ O	Sigma, G8270
D-Mannitol	0.5 M in H ₂ O (30-270 mM)	Sigma, M4125
Sucrose	0.5 M in H ₂ O (30-270 mM)	Sigma, 84100
Suramin	10 mM in H ₂ O (10 µM)	CalBiochem, 574625

Table 7 Chemicals used in experiments on the FlexStation. Storage stock solutions given, with working concentrations in brackets. Unless otherwise stated, SBS solutions contained Ca²⁺, as described here.

The FlexStation 3 was loaded with a tip box (96 pipette tips). The assay plates were then placed into the FlexStation 3 reader to monitor fluorescence before and after the addition of the drugs in the compound plate (Figure 2.6). Temperature on the fluorimeter was checked to ensure consistency (21 ± 2 °C).

Settings were adjusted using the Softmax Pro 4.7.1 software, to match the excitation and emission wavelengths of Fura-2 AM (340-380 and 510 nm, respectively). The machine was programmed to do one transfer of 100 μ L of compound into the corresponding well on the assay plate. Baseline fluorescence ratios were recorded before the addition of the compound solution to the assay plate after 30 seconds, with recordings at 6 second intervals, for a total of 350 seconds. Both the absolute baseline and a baseline subtracted data were saved. Unless otherwise stated, the baseline subtracted data were analysed, using OriginPro (version 9.1, OriginLabs, 2016). The change in Fura-2 AM fluorescence ratio (ΔF) was plotted graphically at each time point, and the mean peak Ca^{2+} entry used for statistical comparison.

2.11.1 Yoda1 experiments using the FlexStation 3

To investigate whether the application of Yoda1 stimulated an intracellular Ca^{2+} response in FpECs, increasing doses of the synthetic compound (i.e., Yoda1) were used, and compared to vehicle control (DMSO) (Figure 2.6). Raw results were analysed alongside data normalised to the response to Ionomycin. These responses were used to calculate the half maximal effective concentration (EC_{50}) of Yoda1. Prior to loading with Fura-2 AM, cells were first checked for confluency under the light microscope and confirmed by IncuCyte™ imaging. This step was also performed when investigating the response to Yoda1 in AGA FpECs and those from SGA samples, to ensure equivalent confluence.

In addition to stimulating Piezo1 in FpECs, the effect of channel inhibition on the Ca^{2+} response to Yoda1 was also investigated. Here, the blocker of voltage-sensitive Ca^{2+} channels, gadolinium chloride hexahydrate (Gd^{3+} , 30 μ M) was used for a 30 minute pre-treatment, prior to the application of Yoda1.

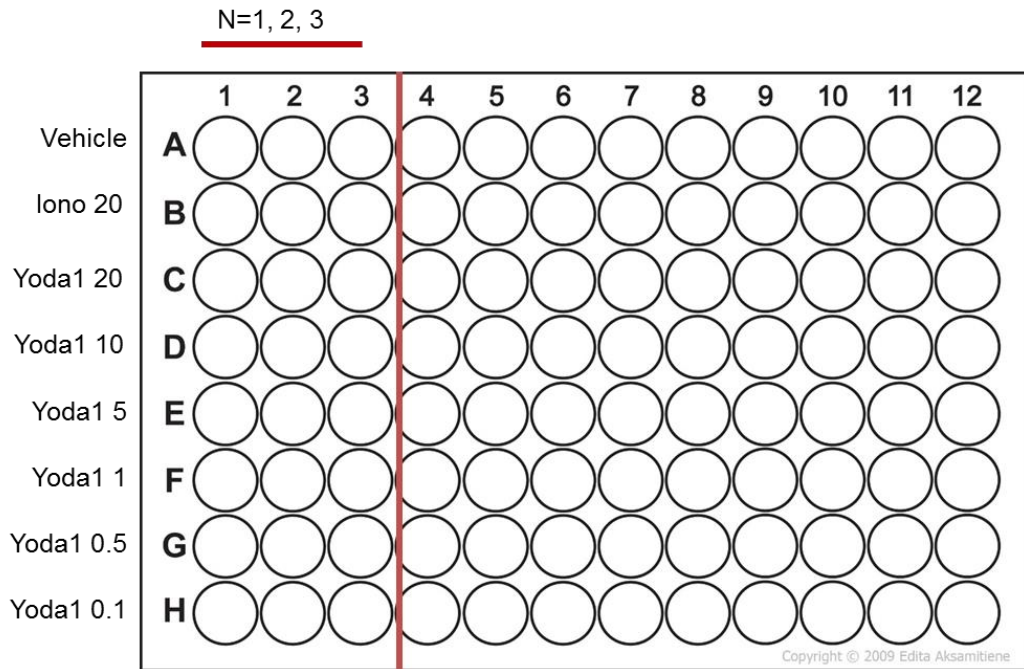


Figure 2.6 Representative compound plate layout for the FlexStation 3. Example layout for testing Ca^{2+} in response to doses of Yoda1 (μM), including vehicle (DMSO) as a negative control, and ionomycin (μM). For all FlexStation 3 experiments, each condition was tested in triplicate ($N = 3$), in a minimum of 3 independent patient samples ($n = 3$).

2.11.2 Osmotic stress response

The FlexStation 3 was used for the measurement of Ca^{2+} responses upon exposure to hypotonic solutions. Here, cells at $\geq 80\%$ confluency were incubated with Fura-2 AM loading dye, as described in section 2.11.1. Cells were then washed in SBS and incubated for 30 minutes at room temperature in 80 μL of SBS per well.

For the compound plate, a mastermix comprised of a 10 x SBS solution, without glucose or Na^+ (100 $\mu\text{L}/\text{mL}$), and 1M glucose (80 $\mu\text{L}/\text{mL}$). This mastermix was added to each 'dose' being tested (180 μL per well). Through omitting the Na^+ , the osmolarity of solutions could be varied through the addition of different quantities of 0.5 M sucrose (in distilled H_2O), to achieve the concentrations given in (Table 8). The concentration of the 1x SBS on the cells plate remained consistent (304.7 mOsm). The FlexStation 3 settings were as described in 2.11, with the exception of an 80 μL volume on both the assay and cells plate.

Compound	1	2	3	4	5	6	7	8
Plate								
Sucrose (mM)	270	210	150	120	90	60	50	30
Sucrose (μ L)	540	420	300	240	180	120	100	60
H ₂ O (μ L)	280	400	520	580	640	700	720	760
Decrease (%)	-0.16	9.67	19.51	24.43	29.34	34.26	35.9	40.26

Table 8 Hypotonic solutions used to test osmotic stress in FpECs. Volumes of solution required for each concentration of sucrose, and percentage decrease in hypotonicity were calculated by laboratory member Melanie Ludlow and myself. The concentrations given in Table 8 were selected on the basis of human plasma osmolarity ranging from 275-325 mOsm (Gagné, 2014). As such, this osmolarity maintains a transmembrane equilibrium, preventing cells undergoing hypo- or hyper-osmotic stress. 270 mM sucrose was therefore the isotonic control, with each solution becoming progressively more hypotonic. As the concentration reduces, osmotic shifts in water into the cell are expected to induce swelling and therefore tension on the cell membrane. This led to the hypothesis that increasing membrane tension would evoke the mechanical activation of Piezo1. As such, the capacity for Yoda1 to potentiate the effects of hypotonicity was investigated, through the additional application of Yoda1.

This method was initially optimised by experimenting with the hypotonic solution, type of assay plate, and well coating e.g. fibronectin (Figure 2.7). The most consistent Ca²⁺

responses on the FlexStation were produced with the use of sucrose, and culturing the cells on a Poly-D-Lysine 96 well plate (Corning® BioCoat™, 354640).

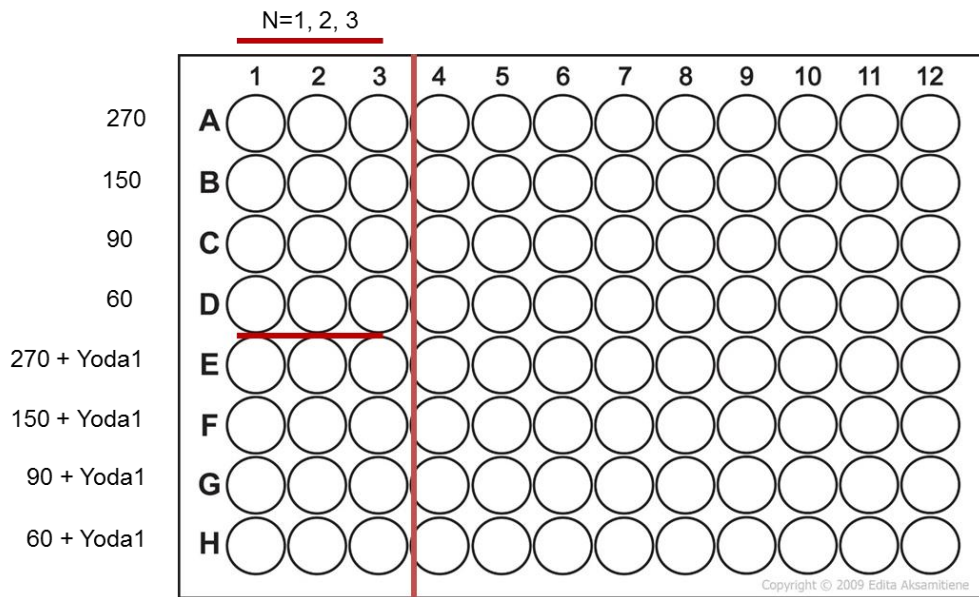


Figure 2.7 Representative compound plate showing hypotonic solutions and Yoda1 being tested. Example layout for testing Ca^{2+} in response to hypotonic solutions (mM) in the presence or absence of Yoda1 (0.1 μM). Each condition was tested in triplicate (N = 3), in a minimum of 3 independent patient samples (n = 3).

2.12 Short-interfering RNA transfection

Transfections with short-interfering RNA (siRNA) were used to investigate the effect of PIEZO1 knock down in FpECs. The transfections were performed in 6 well standard culture plates, on cells at ~80% confluency after seeding (24-48 hours). This method was optimised for FpECs by comparing the efficacy of knock down after either:

- 10 or 20 nM transfection
- using MV-media, Promocell media (- heparin) or Opti-MEM transfection media
- assay at 48 or 72 hours post-transfection

The most reproducible results were achieved by preparing the following for a 20 nM transfection of 1 well:

- 0.4 μ L of 50 μ M siRNA in 100 μ L of Opti-MEM (reduced serum media, Gibco, 31985062)
- 2 μ L of Lipofectamine™ 2000 (Invitrogen) in 100 μ L of Opti-MEM

These solutions were mixed and incubated at room temperature for 15 minutes. A separate mixture was made with control siRNA (non-targeting, scrambled, Table 9 for sequences). Additional wells underwent a ‘mock’ transfection, and were treated with Opti-MEM and Lipofectamine™ 2000 only, under the same experimental conditions (Figure 2.8).

siRNA	Gene	Sequence (5' – 3')	Product
PIEZO1 91	<i>FAM38A</i>	GCCUCGUGGUCUACAAGAU	Ambion, 4392422
PIEZO1 85	<i>FAM38A</i>	GCAAGUUCGUGCGCGGAUU AAUCCGCGCACGAACUUGC	Sigma
Scrambled	N/A	UGGUUUACAUGUCGACUAA UGGUUUACAUGUUGUGUGA UGGUUUACAUGUUUUCUGA UGGUUUACAUGUUUCCUA	Dharmacon, 001810

Table 9 siRNA sequences

Initial transfection experiments were performed using the siRNA.91 sequence. However, a more specific siRNA.85 was later provided by laboratory members Marjolaine Debant and Vincenza Caolo, with less concerns over off targets effects, such as VEGF knockdown. All experiments are labelled with the sequence used. The culture medium was removed from each well, and replaced with 800 μ L of fresh EGM-2. 200 μ L of the transfection solution was added to each well and briefly rocked to mix. After 4 hours, the mix was removed from each well and replaced with 1 mL of EGM-2. The media was changed again 24 hours after the transfection. Cells were assayed 48 hours post-transfection. PIEZO1 mRNA knock down was confirmed on QPCR and in functional experiments on the FlexStation 3.

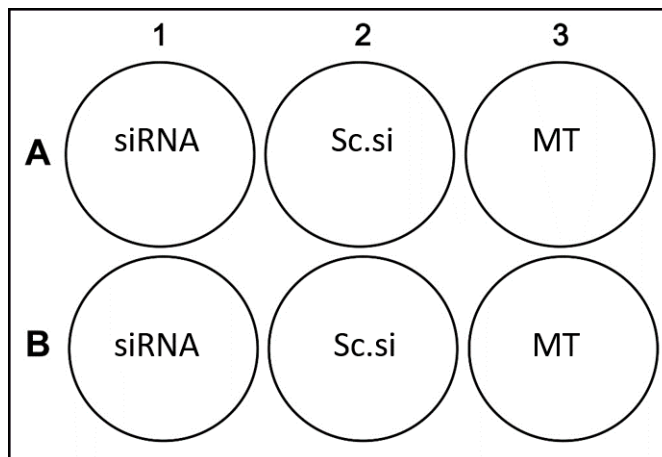


Figure 2.8 Representative layout for transfection experiments. 48 hours post-transfections with either short interfering RNA (siRNA), scrambled control siRNA sequence (Sc.si) or Lipofectamine-only mock transfection (MT), cells were prepared for assays. This included the application of cold lysis buffer and scraping cells into ice-cold Eppendorfs for RNA isolation, as described in section 2.10.1. For FlexStation 3 experiments, cells were trypsinised, counted and plated, as described in section 2.6.

2.12.1 Live dead cell assay

Cell viability post transfection was confirmed using a LIVE/DEAD™ Cell Imaging Kit (Thermo Fisher, L3224), which recognises plasma membrane integrity. Reagents stored at -20 °C were foil wrapped and defrosted in a dark tissue culture hood. 20 μ L of

compound B was added to 10 mL of PBS, followed by 5 μ L of compound A. 1 mL of this mix was added to each well of a 6 well plate, foil wrapped and incubated for 30 minutes. A dead cell control was produced by the addition of 500 μ L of staurosporine (SSP; 1 μ M in DMSO). This chemotherapeutic agent induces cell death via intrinsic apoptotic pathways (Belmokhtar et al., 2001). The IncuCyte™ was used to produce dual wavelength fluorescent images of the live and dead cells. Red and green channels were selected, and a new mask Processing Definition created in the analysis software.

2.13 Protein isolation

In preparation for protein isolation using Western blotting, lysis buffer was freshly made up, consisting of 0.5% NP-40 detergent with protease and phosphatase inhibitors (both 1:500). Media was aspirated off confluent FpECs in 6 well culture plates, and wells washed with PBS. All PBS was carefully removed, followed by the addition of 80 μ L of lysis buffer into each well. Cell scrapers were used to detach cells before transferring into cold Eppendorfs. Samples were left on ice for 30 minutes. Tubes were centrifuged at 4 °C (10 minutes, 13,000 rpm) and the supernatant containing the soluble protein was transferred to new Eppendorfs. The samples were either frozen at -20 °C or used immediately for western blotting. The same protocol was followed for the AG control and SGA samples.

2.13.1 Protein quantification

A fresh BSA curve was produced for each set of protein quantifications, on a 96 well plate. 8 BSA solutions of reducing concentration were made up from varying the quantities of BSA at 2 mg/mL, H₂O and NP-40 buffer. Each BSA concentration was loaded in duplicate (15 μ L per well) across a 96 well compound plate.

Every sample well was prepared with 10 μ L of distilled water, followed by 5 μ L of sample. A protein quantification assay was prepared with the addition of reagent A (500 μ L) plus S (10 μ L) (100 μ L per well), followed by reagent B (160 μ L per well) (*DC*™ Protein Assay

Kit, Bio-Rad, 5000111). These reagents exhibit a differential colour change according to concentration, which was measured as absorbance on a microplate reader at 750 nm.

Protein concentration in each sample was calculated using the line equation of the standard curve (Figure 2.9). This value is multiplied by 3 to account for sample dilution in H₂O, to give the concentration in µg/µL.

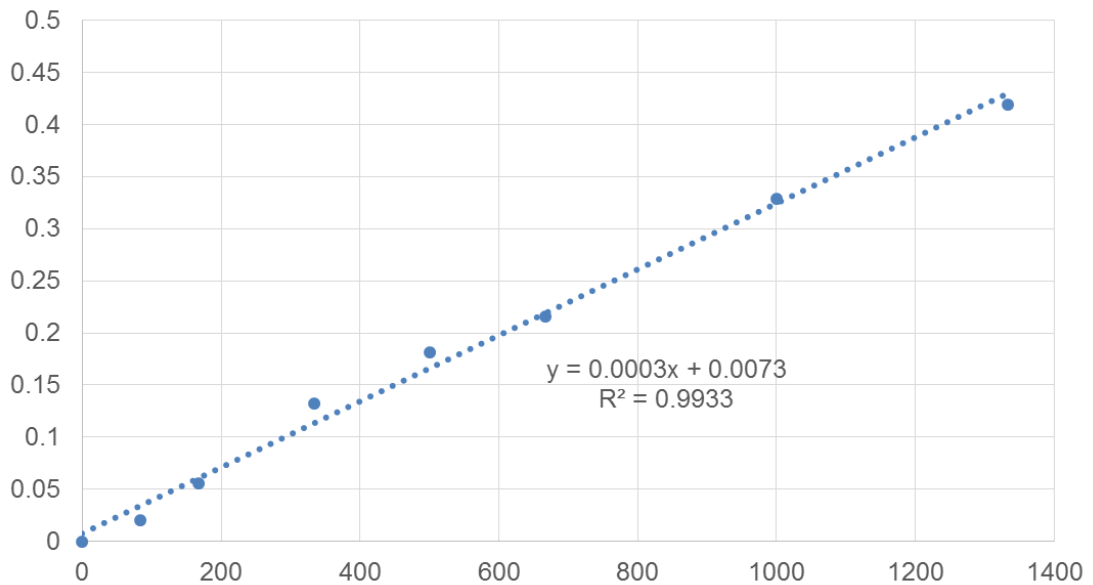


Figure 2.9 Representative BSA curve and worked example. Example standard curve, where BSA concentration (µg/mL, x axis), is plotted against the mean plate reading at each concentration (zeroed, y axis). In this example, the plate reading of sample LGI041 was 0.156. Using the line equation, $((0.156 - 0.0073) / 0.0003) \times 3 = 1.5 \mu\text{g}/\mu\text{L}$. The protein concentration was used to determine the volumes of sample lysate, sample loading buffer (SB 4x) and NP-40 SLB to use for a 20 µg western blot. SB 4x consisted of 200 mM Tris, 8% SDS, 40% glycerol, 8% mercaptoethanol and 0.1% bromophenol blue. Samples were placed on a heat block at 95 °C for 5 minutes to ensure protein denaturation. Samples being tested for Piezo1 were incubated at room temperature for 1 hour.

2.13.2 Western blotting

Gel electrophoresis tanks were prepared with 1x Tris-Glycine-SDS page running buffer (diluted from 10 x concentrate, pH 8.1, Sigma, T7777), and 4-20% gradient Mini-

PROTEAN TGX™ pre-cast SDS polyacrylamide gels (12 well, 20 μ L, Bio-Rad, 4561095). SDS is a surfactant which disrupts the non-covalent bonds in protein molecules, making them linear. It is anionic, and therefore binds to the positive charges on the protein, forming a 'coat' of negative charge. The high binding affinity means that the speed proteins move through the pores in the polyacrylamide gel web is according to size, rather than charge.

Molecular weight markers were loaded before and after each set of samples (5 μ L, PageRuler™ Plus Pre-stained protein ladder, 26620). Samples were then loaded (20 μ L per well), with all patient samples tested in duplicate. The electrophoresis was carried out at 175 Volts for 60-90 minutes. With the application of this electric current, the negatively charged proteins move towards the positively charged anode, with the molecular weight range of each protein sample being separated along the length of the gel.

For this semi-dry blotting method, polyvinylidene fluoride (PVDF) membranes (Immobilon-P, Millipore, IPVH00010) were first washed in methanol then soaked in transfer buffer alongside blotting paper. When removed from the tank, gels were carefully transferred to the membrane on a transfer machine wetted with transfer buffer, sandwiched between blotting papers. The semi-dry transfer buffer comprised of 48 mM Tris, 39 mM glycine and 20% methanol. The transfer was run at 0.05 Amps per membrane for 90 minutes.

Following the transfer, membranes were soaked in a milk solution containing 5% milk in 1x Tris buffered saline with Tween (TBS-T), for 1 hour at room temperature. 1x TBS-T is comprised of 145 mM NaCl, 20 mM Tris-base, 0.5% Tween 20, pH 7.5. This step reduces non-specific background binding, prior to labelling with primary antibody.

Primary antibodies were made up in either 5% milk in TBS-T or 5% BSA, at appropriate dilution. Each membrane was incubated overnight at 4 °C in 5 mL of primary antibody (Table 10).

Target	Dilution	Species	Product
ACTB	1:2000 Milk	Mouse	Santa Cruz sc47778
eNOS	1:1000 Milk	Mouse	BD BioScience 610296
Phospho-eNOS (S1177)	1:1000 BSA	Mouse	BD BioScience 612393
BEEC4	1:1000 Milk	Rabbit	Cambridge BioSciences N/A
Piezo1 extracellular domain	1:300 Milk	Rabbit	Proteintech 28511-1-AP

Table 10 Primary antibodies used in Western blotting. β -actin (ACTB), endothelial nitric oxide synthase (eNOS), phosphorylated endothelial nitric oxide synthase (peNOS) at phosphorylation site: serine1177, Beech laboratory antibody to Piezo1 (BEEC4), and alternative anti-Piezo1 (Proteintech). The primary antibody was removed from each membrane with 4 x 10 minute washes in TBS-T. Secondary antibodies were made up in 5% milk TBS-T solution, according to species (Horse radish peroxidase donkey anti-mouse 1:5000 for ACTB, eNOS and peNOS, anti-rabbit 1:10,000 for Piezo1, Jackson ImmunoResearch). After a 1 hour incubation at room temperature, the secondary antibody was removed with 4 x 10 minute washes in TBS-T.

To optimise Piezo1 protein detection, wet transfer was tried, alongside varying sample preparation conditions and using either the BEEC4 or Proteintech Piezo1 primary antibodies. The most reproducible results were found with protein denaturation at room temperature for 1 hour, followed by semi-dry transfer, and Proteintech Piezo1 primary antibody.

2.13.3 Imaging and analysing western blots

Proteins were visualised using the SuperSignal™ West Femto Maximum Sensitivity Substrate kit (Thermo Fisher, 34095). Membranes were imaged using a G:BOX (Syngene) with Genesis software. To determine total eNOS, membrane were stripped using RESTORE™ stripping buffer (Thermo Fisher, 21059), timed for 15 minutes. These membranes were washed in distilled water followed by TBS-T. They were blocked for 1 hour in 5% milk TBS-T solution, before returning to the primary antibody stage.

Data were analysed using Image J software (Schneider et al., 2012). Each band was selected and a histogram of colour intensity was created. The area under the curve was recorded and analysed in OriginPro.

2.13.4 Effect of Yoda1 on eNOS phosphorylation in FpECs

FpECs confluent in a 6 well plate were prepared for drug treatment with Yoda1 by serum starving. EGM-2 media was aspirated, wells were washed with SBS and 1 mL of SBS left in each well. Plates were incubated for 1 hour at 37 °C in a CO₂-free incubator. A 2 μM Yoda1 (10 mM stock) solution was made up in SBS, alongside the vehicle control (2 μM DMSO). After aspiration of SBS, cells were treated with 1 mL of either Yoda1 or vehicle for exactly 1 minute. Compounds were removed, washed with ice-cold PBS, and the plates placed on ice. Care was taken to remove all the PBS, before applying 80 μL of NP-40 lysis buffer (with protease and phosphatase inhibitors). After scraping the cells into Eppendorfs, the experiments proceeded as per the protein isolation and western blotting described above.

2.14 Shear stress experiments

2.14.1 FpEC alignment in response to fluid shear stress

Cells were seeded in a 6 well plate and cultured to 100 % confluency. Plates were placed on an orbital shaker in a 37 °C incubator, with 2 mL of EGM-2 media in each well. FSS

was achieved by setting the orbital shaker to rotate at 153 rpm, in a method previously described (Dardik et al., 2005, Li et al., 2014).

This produces tangential shear stress, resulting in cell elongation and alignment. After 48 hours, HD-Phase Contrast images of the wells were taken on the IncuCyte. 32 images per well were taken, and 4 analysed. ImageJ software was used for the analysis, where the OrientationJ plugin³⁷ quantified cell orientation relative to the direction of shear stress (<http://bigwww.epfl.ch/demo/orientation/>). A Gaussian distribution curve was fitted to each arising histogram. The baseline-subtracted frequency maximum at the mode of the distribution was determined (peak - baseline, with standard deviation).

To determine the effect of shear stress on *PIEZO1* mRNA expression, FpECs from AGA samples were lysed after no exposure to FSS (St) or after 48 hours. RNA was isolated (as described in 2.10.1), and QPCR performed to establish the mRNA expression of *PIEZO1* relative to the reference genes.

2.14.2 Single cell response to FSS

To investigate the effect of Piezo1 knockdown on FpECs response to FSS, cells were first seeded in a 6 well plate and transfected at 75% confluency (as described in section 2.12). After 48 hours, cell imaging and analysis took place, comparing FpEC alignment after Piezo1 siRNA, scrambled sequence siRNA or mock transfection.

An Ibidi shear stress chamber system was used to determine how single FpECs exposed to FSS respond to a known stimulus - VEGF. In this experiment, 1 confluent of a 6 well plate was trypsinised, pelleted and re-suspended in 150 μ L of EGM-2. 100 μ L of this cell suspension was carefully loaded into a FSS microfluidic chamber (Ibidi), and incubated for 4 hours for cells to attach. The media was then aspirated and replaced with 120 μ L of Fura-2 AM and incubated for one hour. After aspirating the Fura-2 AM, the compound solution was applied. This consisted of 30 mL of Ca^{2+} SBS with 2 μ L of VEGF (2 ng/ μ L). Single cells were identified by microscope attached to the computer and highlighted. The

microfluidic chambers were filled with SBS, and flow applied for three minutes, stopped for one minute, and re-applied for three minutes.

2.15 ADAM10 activity assay

2.15.1 ADAM10 activity in response to Yoda1

Glass slides were placed in a slide chamber and coated with fibronectin (10 $\mu\text{L}/\text{mL}$, Sigma, F0895) for 45 minutes. Slides were washed thoroughly with PBS whilst preparing cells. Confluent FpECs were trypsinised, pelleted and re-suspended in EGM-2 media. Each slide was coated with 500 μL of cell suspension and left to attach for two hours, before topping up with 4 mL of EGM-2. Once slides were confluent, cells were serum starved in reduced serum media (0.5% serum, minus VEGF and hFGF) for a minimum of four hours. FpECs were treated with or without Yoda1, in the presence or absence of the ADAM10 inhibitor, Gd^{3+} . The following solutions were made up in starvation media, and comprised:

- Yoda1 (0.2 μM)
- Vehicle (DMSO 0.2 μM)
- Gd^{3+} (30 μM for 10 minute pre-treatment), followed by Yoda1 (0.2 μM) in Gd^{3+} (30 μM)
- Gd^{3+} (30 μM for 10 minute pre-treatment), followed by DMSO (0.2 μM) in Gd^{3+} (30 μM)

Following incubation for 30 minutes at 37 $^{\circ}\text{C}$, slides were washed with PBS, trypsinised and pelleted. Samples were re-suspended in 80 μL of ice-cold buffer from the SensoLyte520 ADAM10 Activity Assay Kit (AnaSpec Inc, AS-72226). This assay uses a fluorescence resonance energy transfer (FRET) substrate to detect the activity of the ADAM10 α -secretase. When the enzyme cleaves the substrate, an increase in fluorescence occurs at excitation/emission 490/520 nm, which is measurable on the FlexStation. After keeping samples on ice for 10 minutes, then and centrifuging at 4 $^{\circ}\text{C}$, supernatants were transferred to a 96 well plate. The substrate solution was added to

the sample wells immediately before commencing the FlexStation reading. The FlexStation was set up to measure fluorescence at the appropriate wavelength, every 2.5 minutes for 60 minutes.

2.15.2 ADAM10 activity in response to SS

FpECs were prepared on glass slides as described above. The shear stress circuit system was prepared by connecting inflow and outflow tubing to the peristaltic pump, bottle of warmed starvation media and slide chambers (Figure 2.10). Slides were sealed inside glass chambers, and media-filled tubes connected, ensuring no leaks and no air bubbles. The circuit was placed inside a 37°C incubator, and flow started. After 30 minutes, flow was stopped, slides were quickly removed and placed into PBS. Cells were trypsinised to remove from the slides, pelleted, and re-suspended in 4 mL of media. After a further centrifugation, the pellet was re-suspended in assay buffer, the experiment proceeded as described above. The static control slides were kept in the same incubator, and cells processed in the same way.

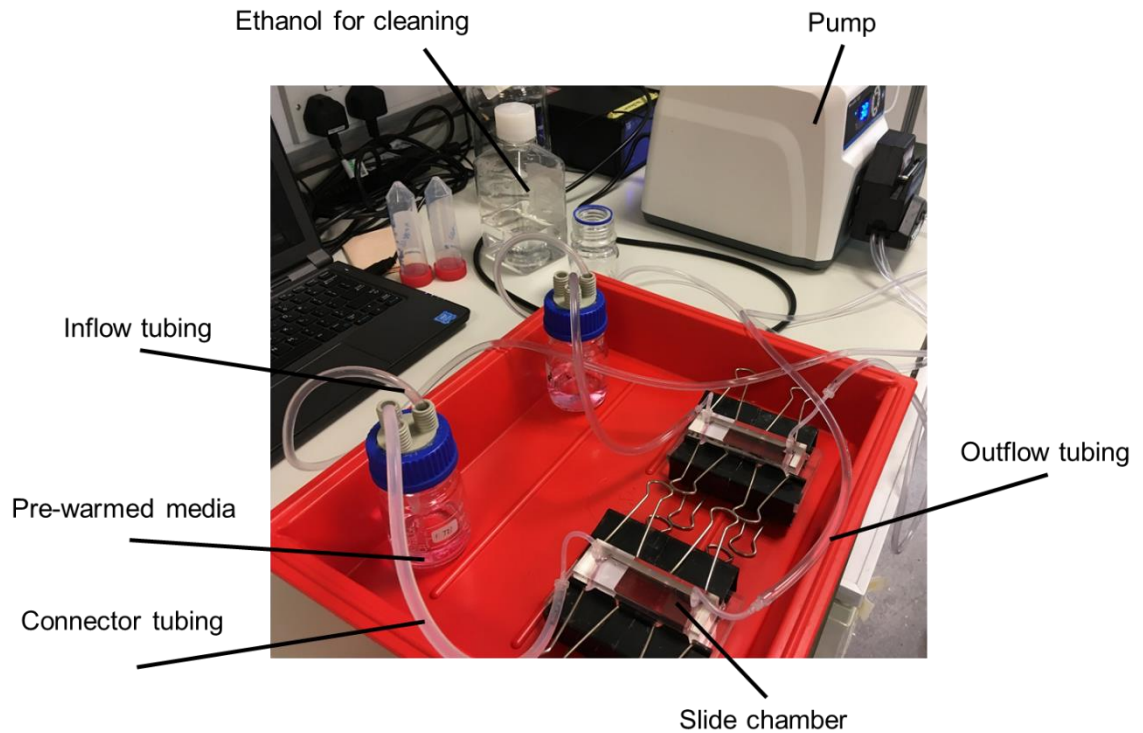


Figure 2.10 Experimental set up for pulsatile fluid shear stress ADAM10 assay.

Flow circuit used to expose FpECs to FSS. Two replicate experiments are shown in parallel, with each ‘N’ representing one confluent slide of FpECs in each chamber. Experiment designed by laboratory members Vincenza Caolo and Marjolaine Debant.

2.16 Patch clamp

Outside-out membrane patch recordings were performed on the freshly isolated human placental arterial ECs described in section 2.3. The recordings were made by Jian Shi using an Axopatch-200A amplifier (Axon Instruments, Inc., USA) equipped with Digidata 1440 A and pCLAMP 10.6 software (Molecular Devices) at room temperature, in a method previously described (Morley et al., 2018). Heat-polished patch pipettes with tip resistances between 3 and 5 M Ω were used. For the application of fluid flow, membrane patches were manoeuvred to the exit of a capillary tube with tip diameter of 350 μ m, out

of which ionic (bath) solution flowed at 20 $\mu\text{L}/\text{second}$. The external solution for recording consisted of 135 mM NaCl, 4 mM KCl, 2 mM CaCl_2 , 1 mM MgCl_2 , 10 mM glucose and 10 mM HEPES (pH 7.4) while the pipette solution was composed of 145 mM KCl, 1 mM MgCl_2 , 0.5 mM EGTA and 10 mM HEPES (pH 7.2).

2.17 Statistical analysis

Microsoft® Excel® was used to generate spreadsheets for calculations in experiments such as relative abundance in mRNA expression in QPCR, and protein quantification in Western blotting.

OriginPro® 8.6 (OriginLab, USA) software was used for data analyses and presentation. Data are expressed as mean \pm standard error of the mean (SEM). Each results plot presents data as mean \pm SEM with all raw data points superimposed. Statistical comparisons of paired data were made using the paired Student's T-test. Data sets with more than two groups were analysed by ANOVA, with post-hoc Tukey correction. Statistical significance is indicated by * ($p < 0.05$), ** ($p < 0.01$) and *** ($p < 0.001$). No significant difference is indicated by NS ($p > 0.05$). Grubbs' test was used to identify any statistical outliers. Unless otherwise stated, no outliers were removed from the analyses. The number of experiments on independent patient samples is indicated by 'n'. The number of replicates per independent experiment is denoted by 'N'.

Chapter 3 Isolating and characterising fetoplacental endothelial cells from the human placenta

3.1 Introduction

As discussed in the Methods chapter, section 2.3, a new protocol was developed for consenting patients, processing and storing the tissue to be used for the work presented in this thesis. The aim of this chapter is to demonstrate that placentas were sampled from pregnancies affected by SGA, and those where the baby was appropriately grown for gestational age (AGA). These samples were used successfully for a variety of experiments, involving whole villous tissue and cultured FpECs.

After recruiting patients antenatally into either the AGA (control) or SGA arms based on EFW, the allocation was reviewed postnatally according to the baby's birthweight percentile on a growth chart. After sampling the tissue, the individual phenotypes were further investigated by comparing placental weight and the relative mRNA abundance of the vascular markers, cluster of differentiation 31 (*CD31*), ephrin-B2 (*EFNB2*) and ephrin-B4 (*EFNB4*).

After culturing CD31-positive cells using the FpEC isolation protocol, they were validated through a series of experiments. These included morphological assessment and functional assays. These experiments were designed to ensure that the FpECs showed the expected properties of viable ECs, such as migration, proliferation and angiogenesis (tube formation). I also assessed how these cells responded to stimulation with a chemical mediator (VEGF) and FSS.

3.2 Patient recruitment

A total of 110 patients were consented at LGI between 18th June 2018 (LGI001) and 30th January 2020 (LGI110). Consent was taken primarily by myself. In 2018, MRES student Sara Ibrahim (SI) also took consent and sampled placental tissue as part of her project. Likewise, PhD students (Maggie Kennedy, Kate Timms, Katy Walsh and Rachel Quilang) under the supervision of Karen Forbes started consenting and collecting tissue from

2018 onwards, focusing on comparisons between AGA placentas and from pregnancies affected by gestational diabetes mellitus (GDM) or large for gestational age (LGA) babies. Of these, 8 placentas were discarded prior to sampling (LGI009, LGI014, LGI015, LGI054, LGI062, LGI070, LGI074, LGI078). Nine samples were excluded from the control group, as further assessment of the patient and/or delivery notes revealed the inclusion criteria were not met, such as fetal distress pre-delivery (LGI018, LGI019, LGI056, LGI057, LGI068, LGI073, LGI084, LGI109). Likewise, two samples were excluded from the SGA group as baby was born > 10th percentile (LGI006, LGI100).

Two samples were discarded post-sampling as the original consent form could not be located in the patient's hospital notes (LGI017, LGI099). In addition, the placental samples collected from women with GDM (n = 11) or LGA babies (n = 3) were not included in this study.

After these exclusions, 54 AGA and 23 SGA placentas were sampled for use in this study. This is in addition to the 22 AGA and nine SGA placentas collected for the initial experiments (previous ethical approval, samples prefixed with 'LM', 2016 – 2017). A further 10 placental samples had been collected for pilot experiments during a six month Wellcome Trust supported laboratory placement in 2015. The data obtained from these experiments were used for PhD funding applications. The full patient databases are provided in Appendix 2: Table 18, Table 19 and Table 20.

3.3 Demographic data

The characteristics of all patients whose tissue was sampled are summarised in Table 11. Analysis of these data reveals that mothers with SGA babies were significantly younger than those in the AGA group ($p < 0.01$). The weight of babies in the SGA group was significantly lower than those who were AGA ($p < 0.01$). Placental weight, when trimmed of umbilical cord and membranes, was also significantly reduced in the SGA group ($p < 0.01$) (Figure 3.1). Maternal ethnicity and fetal sex were equally distributed between the two groups. There were no significant differences in gravidity or parity.

There was no significant difference in maternal BMI between the groups, however, the SGA groups featured women at more extremes of weight, as the AGA control group was restricted to those with a BMI of 18-40 Kg/m² (15.7-39 versus 18-36.7 kg/m², respectively). Other women with clinical risks predisposing to placental dysfunction in the SGA group included three patients with PAPP-A <0.4 mom (LGI005, LGI016, LGI050), two patients with PET (LGI004, LGI040), one patient with chronic hypertension (LGI058), one patient with pre-existing cardiac disease (LGI063) and one IVF pregnancy (LGI021).

Demographic data (mean ± SEM, median ± range, %)	AGA (n = 76)	SGA (n = 31)	Difference (significance denoted by *)
Maternal age	32.3 (0.7)	27.7 (1.5)	0.0018** (mean difference 4.57, 95% CI 1.76 - 7.38)
Maternal ethnicity ⁱ %			
White	82.6	89.7	
Mixed	0.0	3.5	
Asian	8.7	0.00	
Black	7.3	3.5	
Other	1.5	3.5	
Maternal BMI (Kg/m ²)	26.3 (0.5)	24.2 (1.2)	0.062 (mean difference 2.06, 95% CI - 1.09 - 4.23)
Smoking in pregnancy (%)	0.0	61.6	N/A ⁱⁱ
Parity (number of previous births, zero if primiparous) (median, range)	1(0-5)	1 (0-4)	0.105 (mean difference 0.51, 95% CI - 0.11 to 1.12)

Gravidity (including current pregnancy) (median, range)	2(1-6)	2 (1-5)	0.199 (mean difference 0.50, 95% CI - 0.27 to 1.26)
Gestation (days)	274.49 (0.67)	256.23 (5.61)	N/A
Mode of delivery (%)			
SVD	2.77 ⁱⁱⁱ	52.00	N/A
EI LSCS	97.22	40.00	N/A
Em LSCS	0.00	8.00	N/A
Other	0.00	0.00	N/A
IOL for FGR	0.00	32.00	N/A
Baby weight (g)	3499.2 (45.2)	2186.3 (131.3)	< 0.0001*** (mean difference 1312.91, 95% CI 1095.88 - 1529.94)
Percentile (UK-WHO GrowthCharts) ⁱⁱⁱ	51.72	3.23	< 0.0001*** (mean difference 48.48, 95% CI 39.8 to 57.17)
Fetal Sex			
Female %	57.5	59.3	
Male %	42.5	40.7	
Placenta weight (trimmed, g)	521.0 (16.1)	332.3 (25.8)	< 0.0001*** (mean difference 188.70, 95% CI 127.94 - 249.47)

Table 11 Demographic data of patients for whom placental tissue was sampled

ⁱ Ethnic groupings were selected from the UK government recommendation (UKGov, 2011). ⁱⁱN/A refers to where data are not suitable for statistical comparison due to not being matched between groups. ⁱⁱⁱWhere percentile was < 0.4th, mean difference was calculated as for a percentile of 0.4.

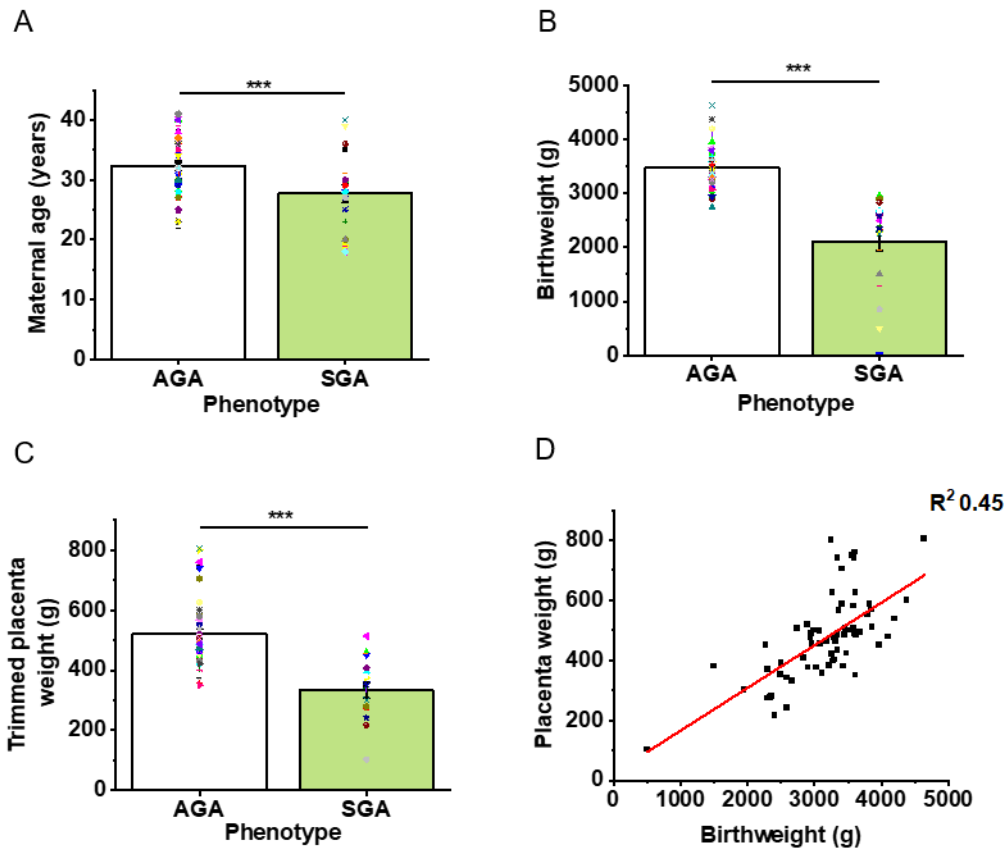


Figure 3.1 Summary demographic data. A., Maternal age: mothers of the SGA babies were significantly younger than those of appropriate birthweight. B., Birthweight: samples assigned to the SGA group were from significantly lower weight babies than the AGA group. C., Placental weight: samples assigned to the SGA group were from significantly lighter placentas than those of the AGA babies. D., Weak positive correlation between birthweight and placental weight. A-C: Unpaired *t* test.

Gestation was significantly reduced in the SGA group ($p = 0.0001$, 95% CI 10.56 – 25.97 days). However, the groups were not matched, and as such these data were not suitable for comparison. Deliveries at all gestation were included in the SGA group, but were limited to term deliveries by elective LSCS in the AGA group. This therefore also applies to mode of delivery, whereby SGA babies born by any method were included.

A subset of seven babies in the SGA group were also born preterm, accounting for the reduced mean gestational age (Quinn et al., 2016). This included one extremely preterm

infant (LGI040), four very preterm (LGI063, LGI004, LGI005, LM13) and three late preterm deliveries (LM16, LM18, LM30). Within the SGA group, abnormal blood flow on Doppler US was recorded in 29% of patients (7/24). 62% of mothers in the SGA group disclosed smoking during their pregnancies, whereas only non-smokers were included in the AGA control arm.

To consider the effect of gestational age on the mean birth and placental weights a subgroup analysis was performed. After including only SGA babies born at term (>37 completed weeks), birthweight remained significantly lower than in the AGA group (Table 12). The difference in placental weight remained significant between the two groups.

Demographic data (mean ± SEM)	AGA (n = 47)	SGA (n = 17)	Difference (significance denoted by *)
Birthweight (g)	3465.26 (54.8)	2509.41 (66.17)	p< 0.0001*** (95% CI -1155 - 756)
Placenta weight (trimmed, g)	524.7 (17.25)	412.5 (37.9)	p = 0.003** (95% CI 185 - 38.53)

Table 12 Birth and placental weights in AGA and SGA groups at term.

Depending on the research requirements for this, and related projects (Sara Ibrahim, Karen Forbes's group), not all samples underwent FpEC isolation, and nor were all cultured FpECs used in every experiment described in this thesis. Similarly, not all FpECs were cultured successfully or were suitable for use. As such, for individual comparative experiments, demographic data are discussed in subgroup analyses. For each experiment, the identifying placental sample number is provided in the figure legend.

3.4 Validating the phenotype of placental samples

3.4.1 Macro- and microscopic appearance of placental samples

Placentas were inspected prior to sampling, and those allocated to the SGA group appeared smaller than the normal control tissue (Figure 3.2). This is reflected by the significant difference in placental weight between the two groups (Figure 3.1C).

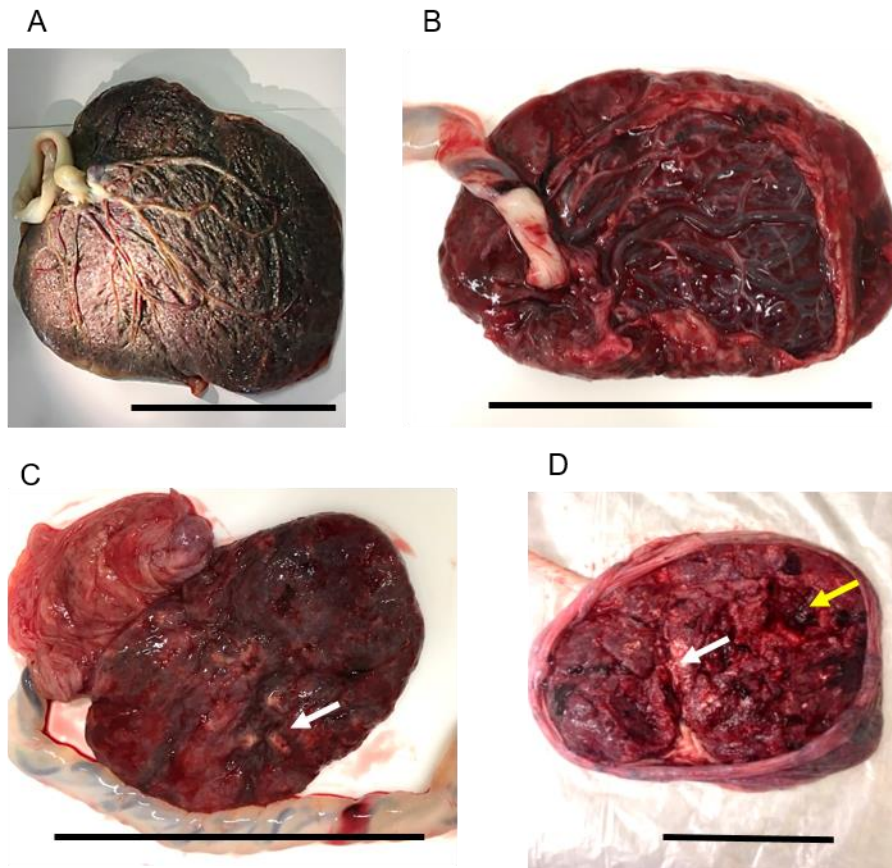


Figure 3.2 Representative images showing reduced comparative size of SGA placentas and macroscopic abnormalities. All scale bars 100 mm. A., Fetal surface of a normal placenta (LM19). B., Chorionic surface of a SGA placenta (LGI003). C., Villous surface of a small SGA placenta, arrow to area of calcification (LGI003). D., Villous surface of an SGA placenta, arrows to areas of calcification (white) and thrombosis (yellow) (LGI040). See Table 13 for corresponding histology.

All placentas in the control group appeared macroscopically normal and therefore none were sent to pathology. Histopathological reports were available for 10 placentas in the SGA group (Table 13). These revealed a wide variation in placental weight percentile. These were calculated from population-based, fetal sex- and gestational age-specific curves (Thompson et al., 2007).

The pathology reports highlight the heterogeneous findings in SGA placentas, as discussed in Chapter 1, section 1.4.6. Common themes included macroscopic findings of a small, thin placenta with fibrin deposition, and microscopic features

of villous ischaemia and infarction (Table 13). Two samples were from women with PET (LGI004 and LGI040). Their histological findings correspond with the maternal hypoperfusion associated with uteroplacental hypoxia, namely ischaemia, vasculopathy, infarction and syncytial knotting (Kingdom and Kaufmann, 1997). Figure 3.2 shows representative examples of the gross morphological appearance of these placentas.

Two patients had no cause for FGR on placental examination (LGI063, LGI038) but with distinct clinical histories. Sample LGI063 is from a baby born <5th percentile and prematurely at 28+3 weeks of gestation, with AEDF on Doppler US, and a mother with cardiac disease. Sample LGI038 is from a baby born at term <3rd percentile, with a normal placental weight percentile, but a maternal history of heavy smoking.

Sample	Histopathology findings	Placental weight percentile
LGI004	<p>Macroscopic</p> <ul style="list-style-type: none"> - irregular shape - marked thinning of the disc to a few millimetres in several areas - subchorionic fibrin plaques and fibrin deposition - large area of infarction 5 x 1.5 x 1.5cm <p>Microscopic</p> <ul style="list-style-type: none"> - retromembranous haematoma - RBC cytolysis and fibrin strands adjacent to infarcted villi - multiple acute and old intervillous haematomas - widespread ischaemic villi with increased syncytial knotting - focal calcifications <p>Summary</p> <ul style="list-style-type: none"> - significant maternal malperfusion changes, including established infarction and decidual vasculopathy. Clinically PET 	50

LGI097	Macroscopic	<3
	<ul style="list-style-type: none"> - maternal surface friable fibrinous deposits and white chalky calcification - pale white marbled patches lying beneath the maternal surface that extend to the fetal surface 	
	Microscopic	
	<ul style="list-style-type: none"> - mild, patchy chorionic vasculitis, indicating stage 1 fetal inflammatory response 	
	Summary	
	<ul style="list-style-type: none"> - very small placenta 	
LGI063	<ul style="list-style-type: none"> - no significant histological abnormalities 	<3
	Summary	
	<ul style="list-style-type: none"> - low placenta weight of unclear cause 	
LGI030	Macroscopic	5
	<ul style="list-style-type: none"> - succenturiate lobe and velamentous cord insertion 	
	Microscopic	
	<ul style="list-style-type: none"> - focal maternal malperfusion with increased syncytial knotting - patchy clumping of the villi and foci of established infarction - thinning parenchyma with ischaemic change in surrounding villi - acute chorioamnionitis with focal accumulation of neutrophils in the subchorionic fibrin 	
	Summary	
	<ul style="list-style-type: none"> - small placenta with maternal malperfusion and focal infarction 	
LGI005	Macroscopic	10 - 50
	<ul style="list-style-type: none"> - small subchorionic fibrin plaques 	
	Microscopic	
	<ul style="list-style-type: none"> - mild acute subchorionitis (Stage 1 maternal inflammatory response) - accelerated villous maturation 	
	Summary	
	<ul style="list-style-type: none"> - mild acute inflammation, and accelerated villous maturation suggestive of maternal vascular hypoperfusion 	
LGI003	Macroscopic	<3
	<ul style="list-style-type: none"> - 20% of the disc at the periphery is thinned to 0.4cm 	

Figure 3.2	Microscopic - perivillous fibrin deposition	
	Summary - perivillous fibrin at the periphery	
LGI058	Macroscopic - old organising retroplacental blood clot	<3
	Microscopic - mild ischaemic changes: small terminal villi with increased intervillous space	
	Summary - small placenta with patchy ischaemia - old retroplacental haematoma	
LGI040 Figure 3.2	Macroscopic - two lesions: 2cm firm red lesion and a 1cm firm pale lesion near periphery	<3
	Microscopic - accelerated villous maturation with increased syncytial knots - established infarcts, some with haematomas	
	Summary - small placenta with multifocal ischaemic change and infarction (maternal malperfusion)	
LGI033	Macroscopic - some areas of fibrin deposition	<3
	Microscopic - mild acute stage II chorioamnionitis	
	Summary - fetally-derived chronic inflammatory vasculitis	
LGI038	- no cause for FGR identified	10 - 50

Table 13 Weight percentile and pathology reports for selected SGA placentas

3.4.2 Differential gene expression in whole placental tissue

Phenotypic differences in the vascular nature of placental tissue between AGA and SGA placentas were investigated by measuring the relative mRNA abundance of *CD31*, *EFRNB2* and *EFRNB4*. CD31, also referred to as PECAM-1, is a differentiation antigen expressed on the surface of vascular cells (Lertkiatmongkol et al., 2016). PECAM-1 is thought to have multiple roles in thrombosis and inflammation, and as a potential mechanosensor. The ubiquitous location of this protein at endothelial cell-cell junctions, serving to maintain the permeability barrier, makes CD31 a useful measure of EC identity, and vascular cell volume within the tissue.

The erythropoietin-producing hepatocellular (**Eph**) receptors are the largest family of human receptor tyrosine kinases (Wolf et al., 2019). Within this family, the Eph-B4 receptor and its ephrin-B2 ligand are of critical importance for the differential development of arterial and venous vasculature. Animal models have shown that ephrins arise early in embryonic development (embryonic day 9 in the mouse), and they continue to be expressed on mature vessels. Their permanent differential expression makes these ephrins molecular markers of vessel identity, whereby Eph-B4 is exclusively venous and ephrin-B2 denotes arterial endothelium (Wolf et al., 2019). As such, their relative abundance was used as a marker of the vascular proportions in AGA and SGA placental tissue (Figure 3.3). For this analysis the mRNA expression was normalised to the mean of three placental reference genes (*ACTB*, *CYC-1* and *YWHAZ*). The rationale for using these particular housekeepers is discussed in Chapter 4, section 4.2.

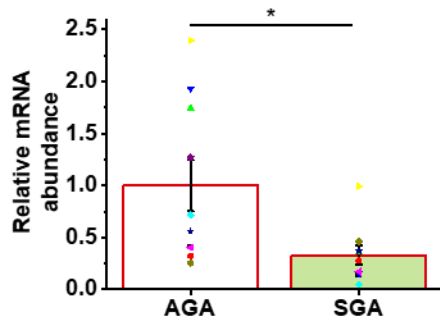
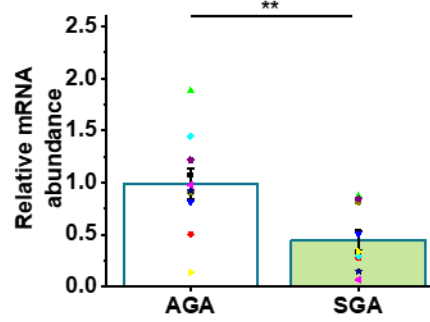
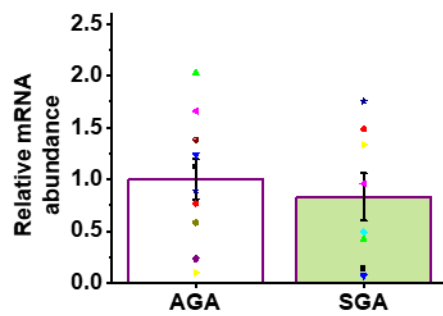
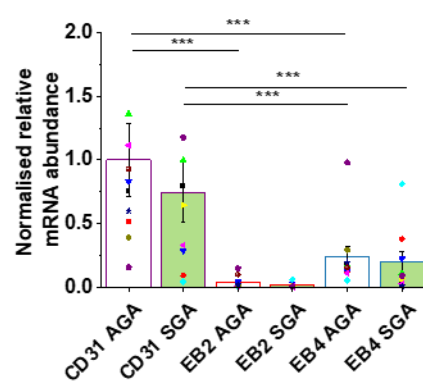
A: *EFRNB2*B: *EFRNB4*C: *CD31*D: Normalised to *CD31*

Figure 3.3 Reduced mRNA expression of both arterial and venous markers, but not *CD31*, in AGA versus SGA samples. When normalised to the mean of *ACTB*, *CYC-1* and *YWHAZ* reference genes, *EFRNB2* (arterial) and *EFRNB4* (venous) are significantly reduced in SGA versus normal tissue (AGA $n = 10/N = 2$: LGI022, LGI036, LGI037, LGI041, LGI043, LGI045, LGI046, LGI069, LGI071, LGI082. SGA $n = 9/N = 2$: LGI004, LGI006, LG026, LGI027, LGI030, LGI051, LGI055, LGI058, LGI063). No significant difference in *CD31* between groups. A: *EFRNB2* $p = 0.026$. B: *EFRNB4* $p = 0.007$. C: *CD31* NS. D: Increased expression of *CD31* compared to *EFRNB2* and *B4*, in both normal and SGA groups. However, no evidence of a difference between expression of *EFRNB2* or *B4* between the AGA vs SGA groups, when normalised to abundance of *CD31*. A-C: Unpaired *t* test, D: ANOVA.

3.4.3 Microscopic appearance and immunofluorescence

Endothelial cell cultures were successfully established and maintained. In culture, both the FpECs isolated from AGA placental parenchyma and from SGA samples had the

visual appearance expected of ECs, and did not look different (Figure 3.4). HUVECs cultured isolated from umbilical cord samples from AGA and SGA also showed characteristic ‘cobblestone’ morphology when viewed under the light microscope, and imaged with the IncuCyte™ (Ulrich-Merzenich et al., 2002). The yield of HUVECs was higher than for FpECs, and confluency was reached more quickly. As such, the HUVECs were primarily used for optimising experiment methods.

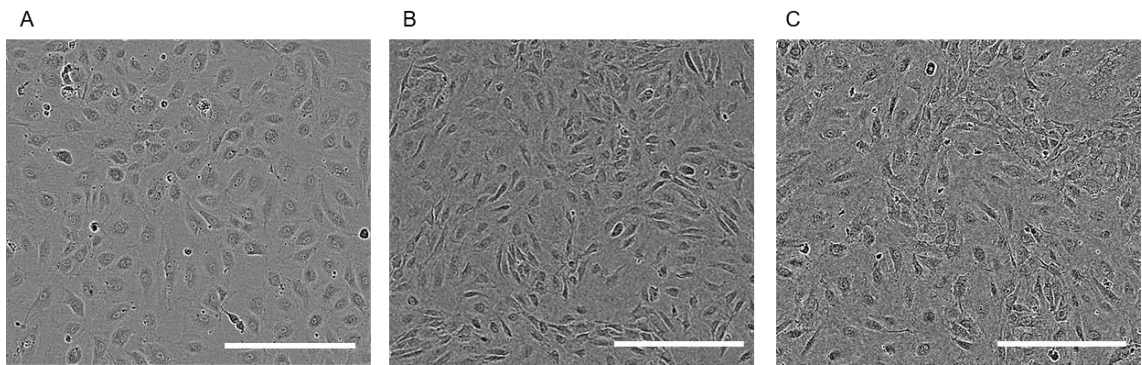


Figure 3.4 Isolated cells from placenta had the visual appearance expected of cultured ECs. Representative phase contrast images of cells, showing monolayers growing in culture, imaged using the IncuCyte™, scale bar 300 μm. A, AGA HUVECs (LM4). B, AGA FpECs (LGI008). C, SGA FpECs (LGI016).

Immunofluorescent staining of FpECs confirmed the expression of the endothelial marker CD31/PECAM-1 with its characteristic subcellular localisation at the plasma membrane and adherens junctions (Figure 3.5A). They also expressed von Willebrand factor (vWF) in the expected punctate structures expected of Weibel-Palade Bodies, which carry vWF factor and are specific to ECs (Figure 3.5B). Furthermore, they showed the characteristic expression of vimentin (Figure 3.5C). As discussed in the Chapter 1, section 1.7.2, increased villous vimentin staining has been demonstrated on histology from samples of women with PET (Sak et al., 2013). However, the role of this filamentous protein in placental mechanosensing remains unexplored. Fluorescence was reduced in controls in which primary antibodies for these endothelial proteins were excluded (Figure 3.5D-F). Expression of the trophoblast marker cytokeratin 7, and of the

fibroblast/smooth muscle marker α smooth muscle actin, was not detected. These data suggest that FpECs share the fundamental and unique proteins and structures of the general EC classification.

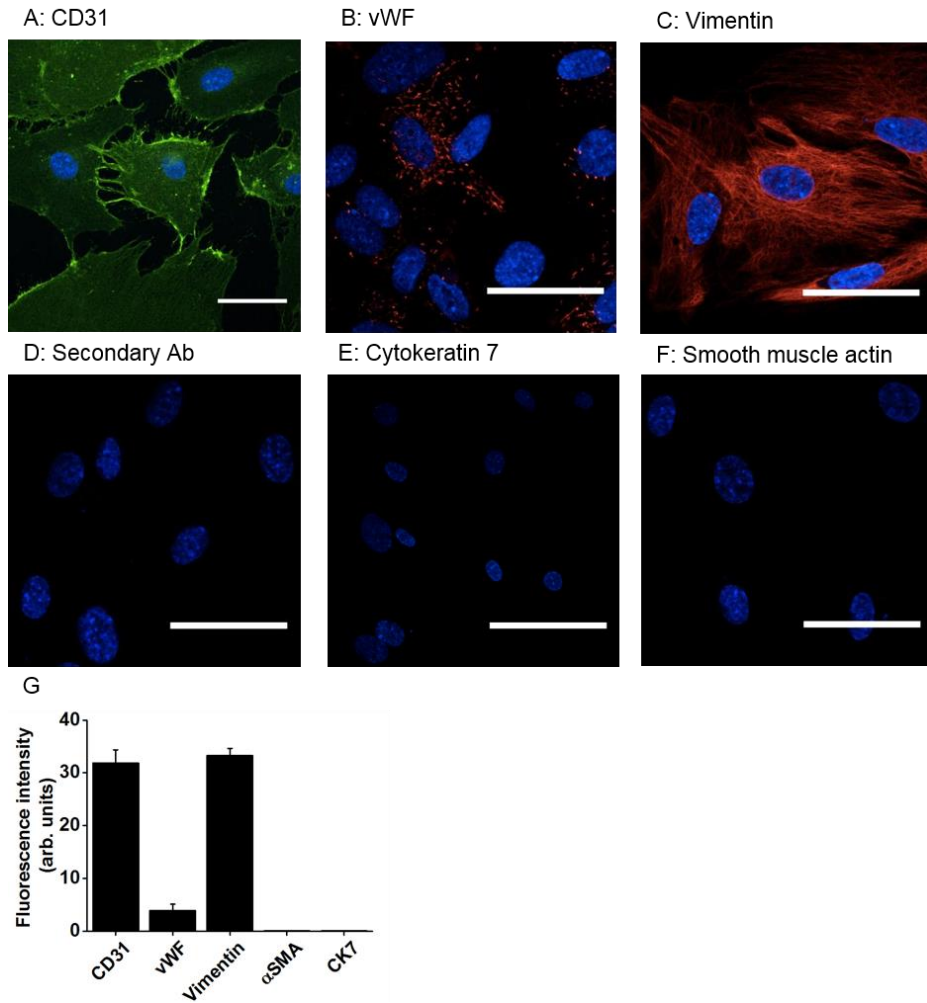


Figure 3.5 Protein and structural markers of FpECs.

AGA FpECs stained with: A., CD31 (green); B., von Willebrand factor (red); C., Vimentin (red); D., Secondary antibody only (red, not visible). Scale bars, 50 μm . E., Negative staining for the trophoblast marker cytokeratin 7 (CK7) (red, not visible). F., Negative staining for the fibroblast marker $\alpha\text{-SM}$ actin (red, not visible). A–F, Cell nuclei labelled with DAPI (blue). G, Quantification of FpEC staining intensity.

3.5 FpECs show properties of migration, proliferation and tube formation

To determine if the CD31 positive cells isolated from the placental parenchyma were viable and behaved as expected of ECs, a number of functional assays were performed. These included investigating whether the cultured FpECs from AGA placentas showed properties of sprouting angiogenesis. This early angiogenic process is characterised by

sprouts of ECs, eventually leading to new vessel formation. Briefly, the steps of sprouting angiogenesis include enzymatic degradation of the capillary basement membrane, EC proliferation, migration of ECs, tube formation, vessel fusion, vessel pruning, and pericyte stabilization (Adair, 2010). As such, I next assessed the capability of FpECs to migrate, proliferate and form tubes.

3.5.1 Migration

To investigate the endothelial properties of cultured FpECs, a scratch wound assay was performed. At time point 0, a linear scratch wound was made through confluent FpECs and imaged 2 hourly post-wounding (Figure 3.6). The progressive closure of the wound through the cells migrating into the scratch indicates that FpECs can migrate, as would be expected for ECs cultured from the systemic circulation. The culture media used for this experiment contained low serum (0.2%) and mitomycin to limit proliferation and ensure migration was the dominant process being assessed.

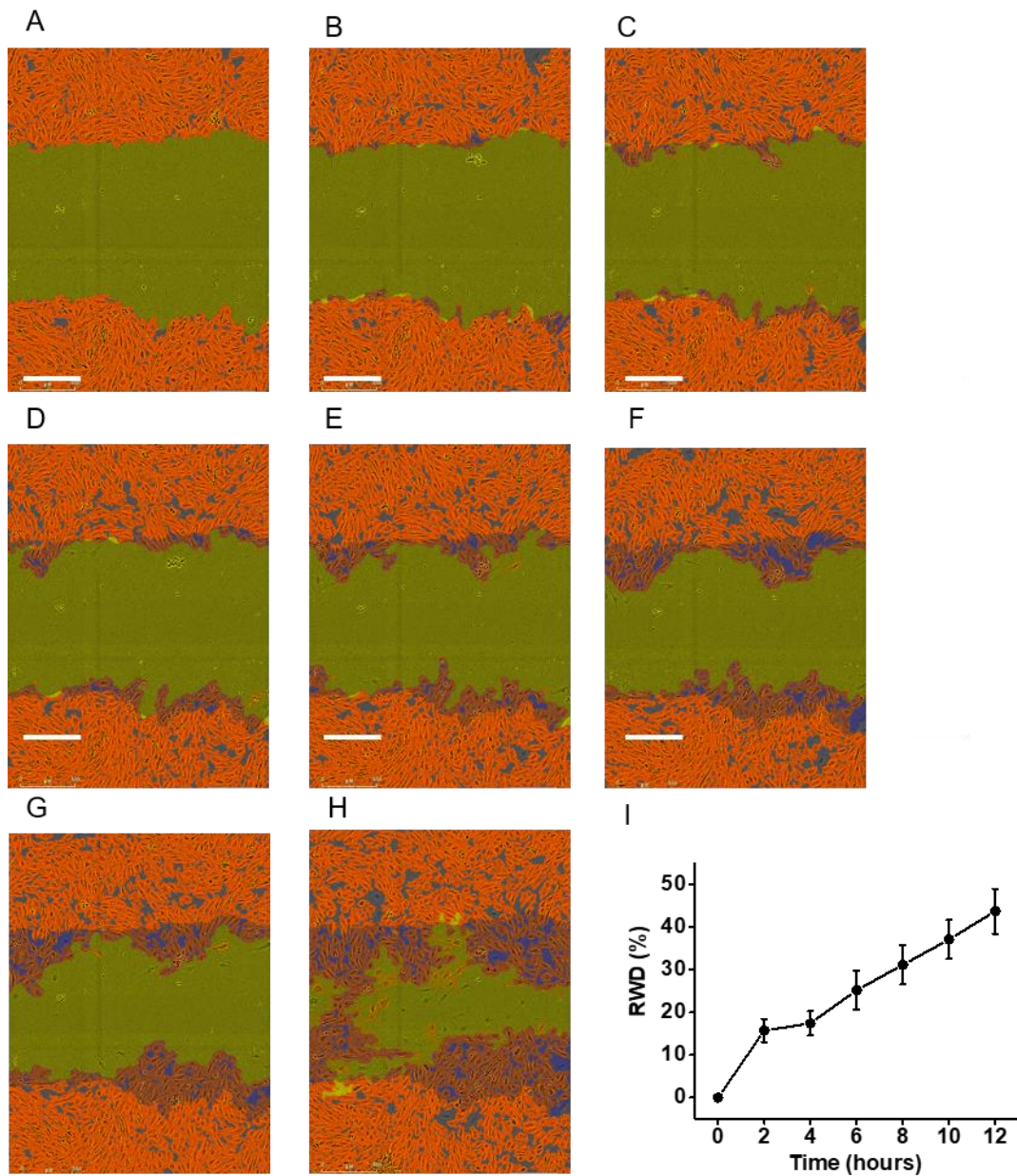


Figure 3.6 Normal FpECs migrate over time to close a scratch wound. Representative scratch wound images with IncuCyte mask analysis applied. Images taken immediately after scratch (0 hours, A), then 2 hourly until 12 hours (B-G). Final image taken at 24 hours post wounding (H). Purple is the original scratch, yellow is the residual wound, orange is the cell mask (scale bars 300 μm). I., Cumulative data for Relative wound density (RWD) showing migration across the scratch wound with time. Data from AGA sample (LG1039), N = 3.

3.5.2 Proliferation

To determine whether FpECs grown in culture were proliferative, cells were seeded at time point 0. Adjacent wells were split and counted every 48 hours up to day 12. All wells showed an increase in cell number, with a mean doubling time of 1.63 days (Figure 3.7). Cells left longer than 10 days in culture were noted to apoptose. Doubling time was as described by (Roth, 2006).

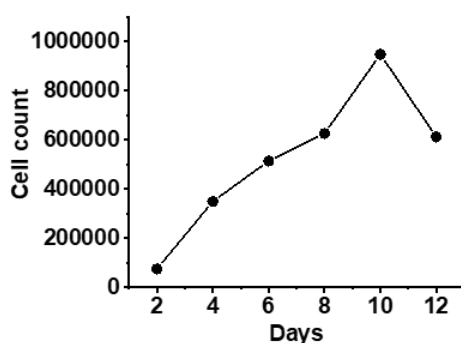


Figure 3.7 Normal FpECs proliferate in culture. Representative growth curve, where FpECs were counted 48 hours after seeding, and every 48 hours until day 12 (LM10). Experiment performed on AGA FpECs, n = 3 (LM9, LM10, LM11).

3.5.3 Angiogenic properties of fetoplacental endothelial cells

The formation of capillary-like structures on the artificial basement membrane extracellular matrix Matrigel® is a hallmark of ECs (Arnaoutova et al., 2009). In the presence of Matrigel® FpECs rapidly formed these capillary-like structures (Figure 3.8A-D). In the absence of Matrigel® FpECs grew into a confluent monolayer, and no tube formation was observed (Figure 3.8E). An alternative assay assessed tube formation on a confluent layer of fibroblasts. After 5 days, the FpECs grew into tubular structures that could be detected with anti-CD31 immunofluorescent staining (Figure 3.8F).

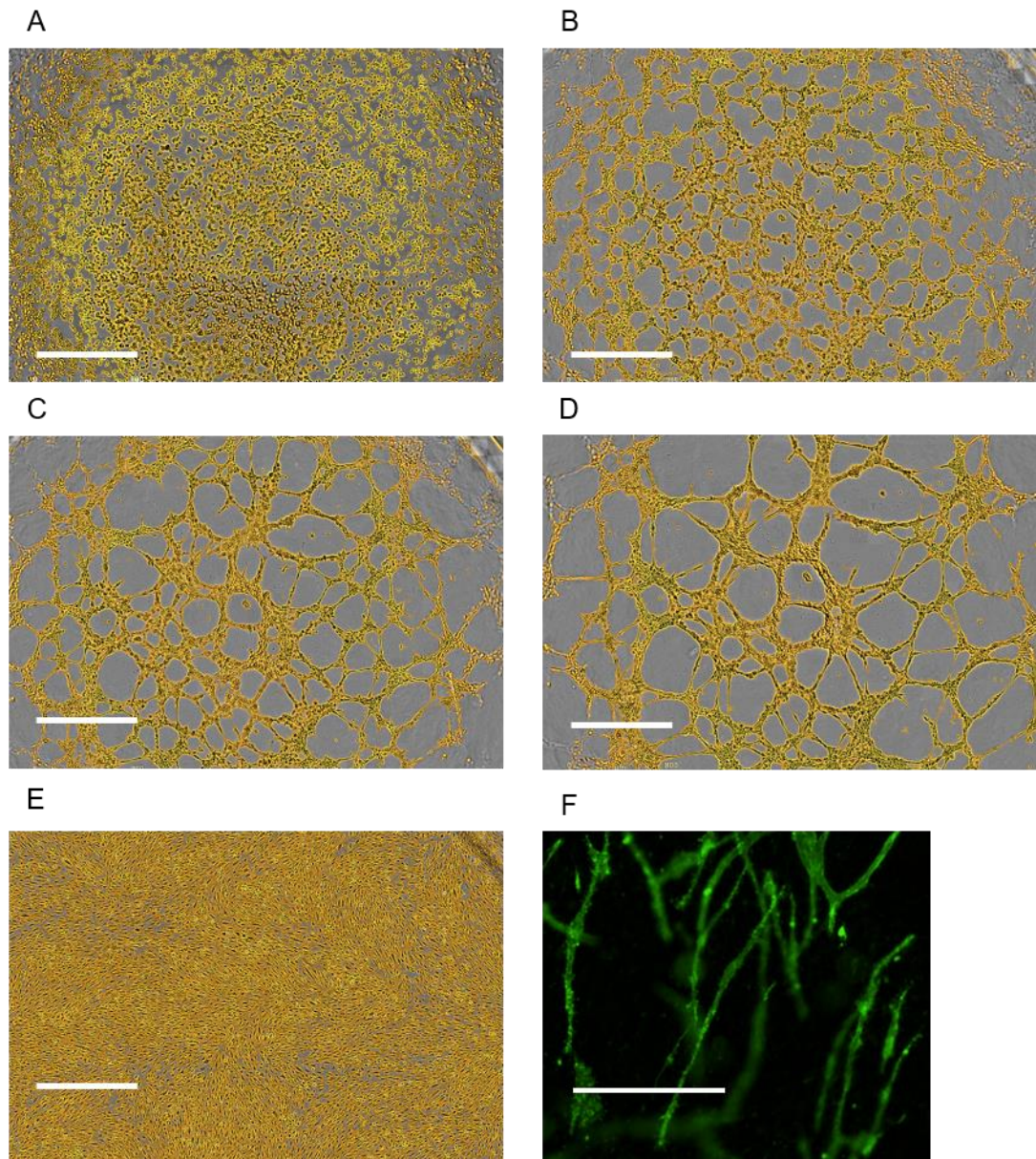


Figure 3.8 FpECs form tubular structures when grown on suitable substrate. Representative image of tube formation in the presence of Matrigel® (n = 2 / N = 4 (LM23, LM34), scale bar, 800 μ m). Images taken immediately post seeding cells (0 hours) A., then 2 hourly (B., C.) until 12 hours (D). E., Negative control without Matrigel® membrane showing confluent FpECs without tube formation. F., Example image of tube formation in co-culture with fibroblasts. The FpECs were labelled with anti-CD31 antibody (green). Fibroblasts are not visible in the image (n = 2/N = 4 (LM23, LM34), scale bar, 300 μ m).

3.6 FpECs are responsive to stimulation with shear stress and VEGF

Functional experiments showed that FpECs exhibited intracellular Ca^{2+} elevation in response to the application of VEGF (Figure 3.9). The effect of repeated passaging on the phenotype of FpECs in culture was considered. To determine this, the response to VEGF was tested on a single sample of control FpECs as they were repeatedly split and grown to confluence in a 96 well plate. This showed an equivalent rise in intracellular Ca^{2+} in cells from passage 2-5 (Figure 3.9E). As such, cells at these passages were used for subsequent experiments.

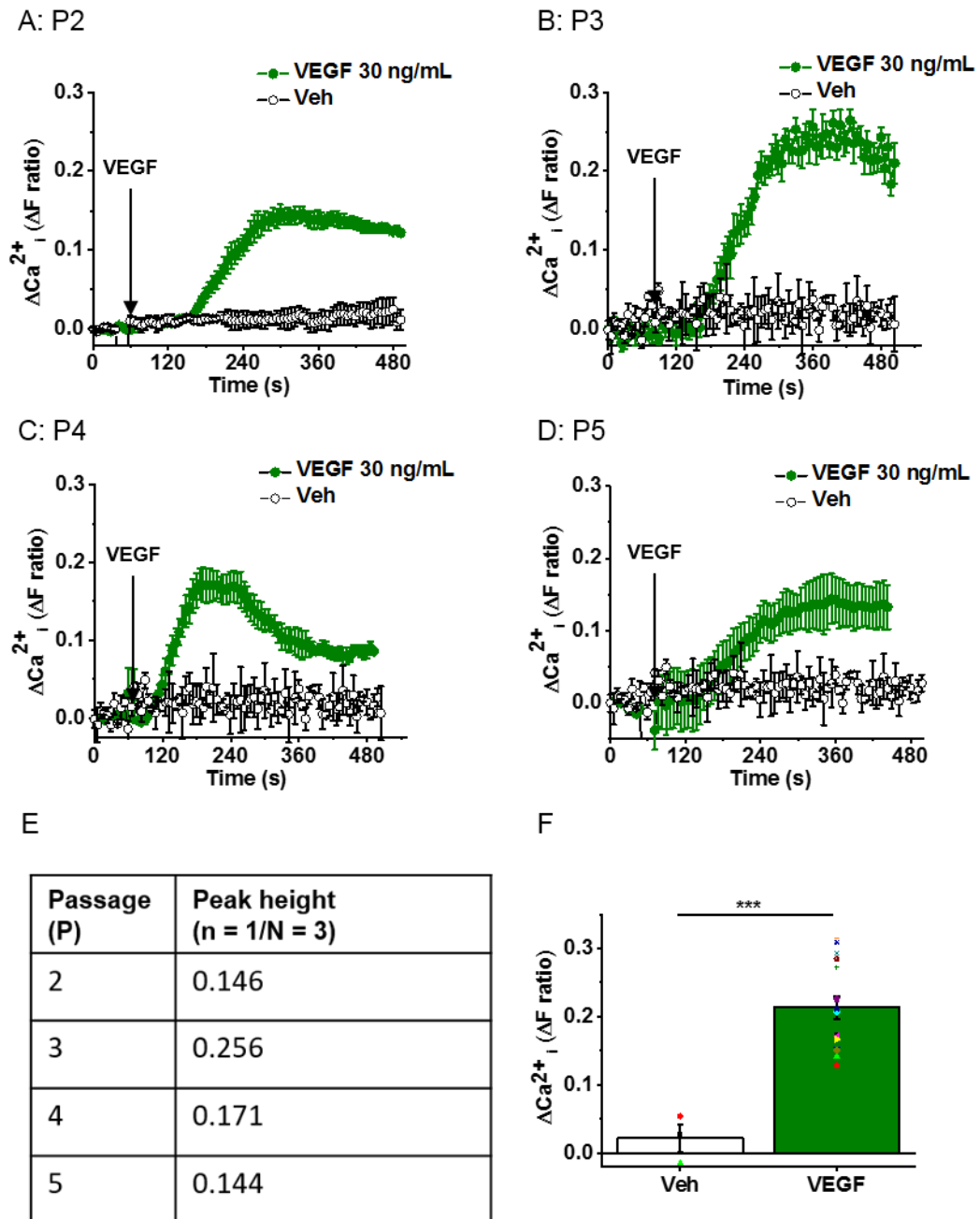


Figure 3.9 VEGF evokes Ca^{2+} entry in FpECs. A., B., C., D., Response of FpECs to VEGF (30 ng/mL) demonstrated by the intracellular Ca^{2+} elevation in multiple wells of a 96 well plate on a fluorescence plate-reader at passages (P) 2, 3, 4, 5, respectively (n = 1/N = 3, LM34). E., Maximal height of Ca^{2+} elevation in response to VEGF at different passages. Data obtained from the experiment shown in A., B., C., D with baseline subtraction performed. F., VEGF response quantified against vehicle (Veh) control (H_2O) in three AGA patient samples $p < 0.0002$ (n = 3/ N = 5, LM10, LM11, LM34). F: Unpaired *t* test.

Another common characteristic of ECs is their alignment to FSS, a process occurring physiologically in blood vessels as a result of blood flow (Li et al., 2014). In static conditions, FpECs grew into a confluent monolayer, with a typical morphological appearance for ECs grown *in vitro*. In contrast, 48 hrs of FSS led to striking alignment of the FpECs to the direction of flow (Figure 3.10). Analysis of FpECs exposed to FSS demonstrated a peak in the number of cells orientated to the direction of flow (0°) confirming alignment.

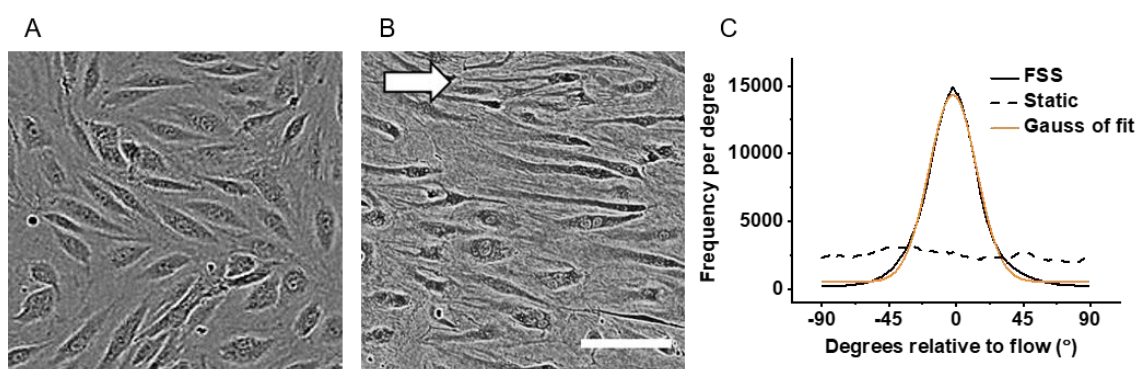


Figure 3.10 Normal FpECs respond to FSS by aligning in the direction of flow. A., FpECs from the control group grew to confluence in static culture. B., FpECs from the same patient sample after exposure to 48 hours of FSS caused by an orbital shaker at 153 rpm, showing alignment in the direction of flow (arrow depicts direction of flow, scale bar 100 μm). C., Orientation analysis for images of the type shown in A and B: solid line: cells exposed to flow (FSS), dashed line: cells in static control, orange line: Gaussian fit curve.

3.7 Discussion of results and limitations

Over the course of this project, all women approached by myself to take part in the study gave their consent for placental sampling and data collection. Many patients were interested in the study, and their willingness highlights the importance of research investigating poor fetal growth for women and their families.

The SGA group comprised of samples where babies weighed <10th percentile on the GrowthCharts UK-WHO mobile app. This algorithm customises for fetal sex, birthweight

and gestation at delivery. The WHO-based growth chart is based upon birthweight data collected from 1,387 women at 10 international centres (Kiserud et al., 2017). Percentiles were calculated on the basis of singleton pregnancies with no fetal concerns and mothers with no current or past risk factors for FGR (Kiserud et al., 2017). Birth percentiles were cross checked against each patient's antenatally generated customised gestation related optimal weight (GROW) chart to ensure the categorisation was consistent.

In our study, mothers in the SGA group were significantly younger than the AGA (control) group (18-28 years versus 22-40 years, respectively). There were four teenagers in the SGA group, aged 18 and 19 years. Two of these women smoked during their pregnancies, and another had PET. Overall in the SGA group, 62% of the women were smokers. Pathology reports available for the placentas of the women who smoked showed fibrin deposition and vasculitis (LGI033) or no cause found for placental dysfunction (LGI038). Both young maternal age and smoking are both known to be risk factors for SGA. As discussed in Chapter 1, section 1.4.2, low maternal age can cause a nutritional conflict between mother and baby. Likewise, smoking reduces placental amino acid transport, disrupts mitochondrial function and impairs oxygen transport to the baby. However, whether poor nutrition and smoking affect shear stress in placental vasculature remains unknown. This study is underpowered to determine a conclusive relationship between any specific risk factors for SGA and the expression and function of mechanosensors in the fetoplacental endothelium.

A limitation of this study is the lack of matching between the study and control groups. This applies to mode of delivery, maternal smoking and gestation at delivery. However, the primary outcome for the project was to determine the presence and function of mechanosensors in healthy placental tissue firstly, followed by those with SGA. As such, the control group was designed to include no maternal or fetal health concerns, extremes of maternal age, BMI or smokers.

Only patients delivering by elective LSCS were recruited to the control group, due to the potential for numerous confounding variables associated with labour. For example,

evidence from immunostaining of villous tissue post vaginal delivery shows an increase in markers of ER stress and phosphorylation of certain proteins, when compared to those after elective LSCS (Cindrova-Davies, 2009, Veerbeek et al., 2015).

The challenges of matched controls in obstetrics research was discussed by Burton, who describes the variables introduced by labour, such as intermittent perfusion due to contractions, and maternal administration of opioids and other therapeutics (Burton et al., 2019). The effect of labour, and resulting impact on the placental transcriptome, metabolome and stress response on FSS in the placenta and the expression of mechanosensors is another unknown entity. This difficulty also applies to matching gestation at delivery, whereby babies delivered preterm due to SGA do not have an appropriate control (Burton et al., 2019). For example, normally-grown preterm births may have their own predisposing pathology related to the cause and gestation of birth.

As expected, babies in the SGA group were significantly lighter than the AGA controls. The placentas also weighed significantly less, an effect maintained when including only those in the SGA group born at term. Many of the babies in the SGA group had normal placental blood flow on Doppler US. Likewise, the SGA babies delivered at term all had good Apgar scores, with none requiring resuscitation. This suggests that some patients in the SGA group had a relatively mild degree of placental dysfunction, and / or may have been constitutionally small. However, the available pathology reports from the SGA placentas did demonstrate features of ischaemia and infarction (Table 13). These correspond to the histological abnormalities associated with placental dysfunction described in the literature, as discussed in the Introduction chapter section 1.4.5.

As described in the Chapter 2, section 2.3, the placentas used in this study were sampled systematically, avoiding the periphery and any visible sites of infarction, calcification or thrombosis. The pathological changes in SGA-associated placentas have been described as heterogeneous (Kingdom and Kaufmann, 1997). This may be secondary to focal areas of hypoxia due to localised impairments in perfusion. As such, sampling a

single area may not be representative of the placenta as a whole, which is a disadvantage of culture-based methods of laboratory work.

Studying the gene expression in whole villous tissue sampled from the placentas in this study showed a significant reduction in both arterial and venous markers (Ephrin-B2 and B4, respectively). This is suggestive of a global reduction in vasculature in the SGA placentas, although there was no statistically significant decrease in CD31. These findings are explored in more detail in the next chapter.

In the systemic vasculature, the molecular identity of blood vessels can change following surgery. For example, vein grafts show a loss of venous identity, with less Eph-B4 expression, and arteriovenous fistulae show gain of dual arterial-venous identity, with both Eph-B4 and ephrin-B2 expression (Wolf et al., 2019). Some vascular pathologies including arteriovenous malformations and Kaposi's sarcoma, are also characterised by mutations or aberrant expression of vascular identity markers (Wolf et al., 2019). This phenomenon highlights vascular plasticity even in mature vessels, whereby arteries and veins exhibit context-dependent gain of identity (Wolf et al., 2019).

The relationship between vascular identity and FSS is incompletely understood, and no studies have investigated this in the placenta. *In vitro* research has demonstrated that FSS induces murine EC differentiation, regulating arterial-venous specification (Masumura et al., 2009). Exposing murine ECs to FSS increased the gene and protein expression of ephrin-B2 dose-dependently, with a corresponding reduction in Eph-B4. It is therefore apparent that ephrins are not just passive markers but determinants of vascular identity linked to FSS signalling pathways (Masumura et al., 2009). The altered expression of ephrins in the placenta could therefore reflect changes in vascular molecular identity corresponding to structural, flow, or other abnormalities in FGR placentas that remain to be determined. Taken together, these findings indicate that the placental samples assigned to the SGA group in this project did have both macro- and microscopic changes, and alterations in gene expression.

The decision to focus primarily on the investigation of FpECs rather than HUVECs stems from the phenotypic and epigenetic differences between microvascular cells, and those from conduit vessels. This includes higher expression of vascular mediators in microvascular cells and differential gene expression (Lang et al., 2003). Importantly, sampling tissue from within the placental cotyledon includes ECs from the gas-exchanging terminal villi (Kingdom et al., 2000).

The cultured FpECs were viable, attached and functionally active. They could be identified by their morphological appearance, and expression of endothelial protein markers, namely CD31, vWF and vimentin. Their colonies showed properties of migration and proliferation. Culturing FpECs on Matrigel® basement membrane or a bed of human fibroblasts led to the formation of tube-like structures. These data show that FpECs have mechanisms for angiogenesis, and for the sensing of shear stress (as demonstrated by their alignment to the orientation of that FSS). Furthermore, FpECs respond to the application of VEGF, exhibiting an intracellular Ca^{2+} response that does not diminish with passaging. This process of characterising the cultured cells validates the use of these FpECs as a model to study mechanosensing in fetoplacental endothelium. As such, these cells are used in a variety of experiments in the following chapters.

Chapter 4 Presence and functional activity of Piezo1 and other mechanosensors in the human placenta

4.1 Introduction

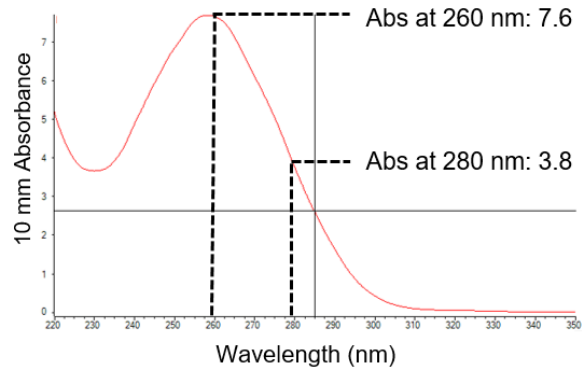
The initial aim of this chapter was to establish whether the *PIEZO1* gene was expressed in the human placenta. QPCR was performed on mRNA isolated from cultured FpECs. The effect of EC isolation, culture and passage on the expression of *PIEZO1* was also considered. The expression of *PIEZO1* was measured in whole villous tissue sampled and stored promptly after delivery. Furthermore, human placental arterial cells from the chorionic plate were used to determine the presence of Piezo1 channels in freshly isolated ECs. In addition, *PIEZO1* expression was measured in samples of whole tissue from the 1st trimester of pregnancy. These samples were obtained from women having an elective termination of pregnancy at less than 12 weeks of gestation, and were used to determine if Piezo channels were present in early, as well as late pregnancy. Next, comparisons were made between the relative abundance of *PIEZO1* mRNA in the AGA versus SGA groups, in both whole villous tissue and FpECs.

Although the focus of the data presented in this thesis is on establishing the presence and function of Piezo1 channels in the human placenta, the expression of other candidate mechanosensors was also considered. A specific G_{q/11}-protein coupled receptor, GPR68, has been highlighted as having an important role in FSS sensing in blood vessels (Xu et al., 2018). There are numerous different GPCRs, with a range of reported sensory functions including mediating olfactory, light and gustatory stimuli (Storch et al., 2012). GPR68 was identified as a potential mechanosensor following a high-throughput mechanical stimulation assay (Xu et al., 2018). Evidence supporting its function stemmed from its expression in murine small resistance arteries, and also in HUVECs (Xu et al., 2018). Correspondingly, myography studies of mesenteric vessels found absent FMV in 3rd order arteries from *grp68* knock out mice. Likewise, overexpressing *gpr86* in naïve HEK293T cells induced sensitivity to FSS with demonstrable Ca²⁺ responses (Xu et al., 2018). With the application of FSS, GPR68 is

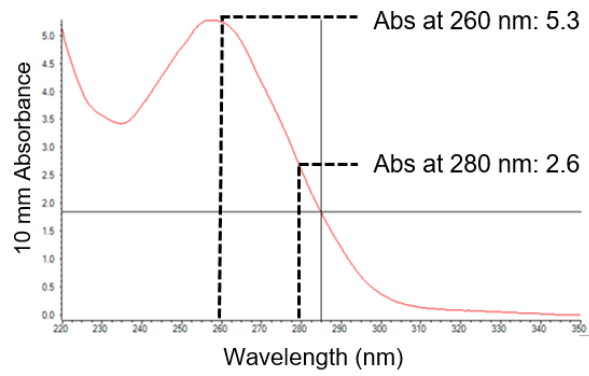
thought to undergo a conformational change which interacts with the EC cytoskeleton (Xu et al., 2018). This has the potential to trigger a number of signalling events, although the exact mechanotransduction pathway downstream of flow-induced GPR68 activation remains unknown.

Alongside GPR68, the potential for the sensory channel, Piezo2, to have as yet unrecognised roles in placental vasculature was also considered. As such, the relative abundance of *PIEZO2* and *GPR68* mRNA in FpECs and whole villous tissue was quantified.

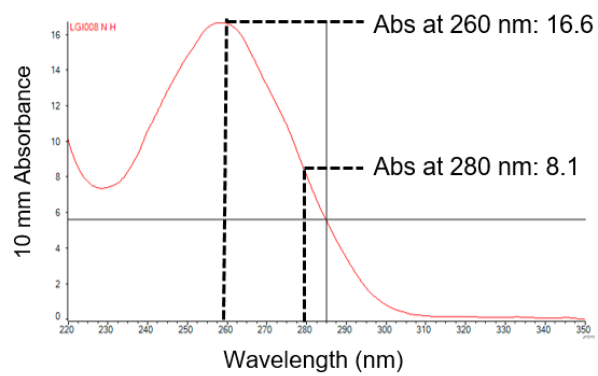
The quality of the data obtained from QPCR is dependent upon the purity and integrity of the RNA. As such, all RNA samples were measured using a NanoDrop™ 2000 spectrophotometer. The spectral image and purity ratios of absorbance were used to assess sample quality, whereby a 260/280 nm ratio of ~ 2.0 was accepted as 'pure' for RNA. For the secondary purity ratio obtained from the 260/230 nm absorbance, values in the range of 1.8-2.2 were regarded as 'pure' RNA (Scientific, 2009). Figure 4.1 gives representative examples of the high quality RNA yielded from ECs and placental tissue from both clinical groups. The RNA quality was unaffected by exposing the cells to experimental conditions, such as treatment with Yoda1 or FSS (Figure 4.1 and Table 14).

A: 3rd trimester tissue (LGI006)

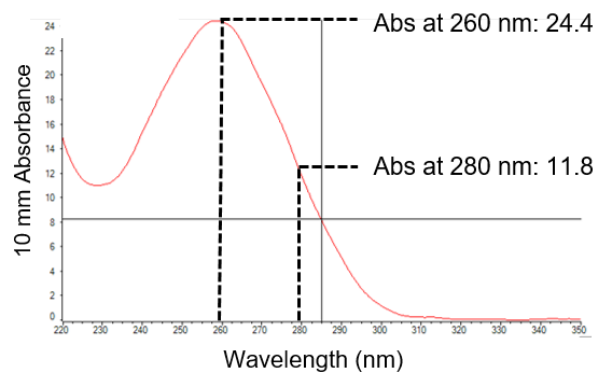
B: 1st trimester tissue (EP200)



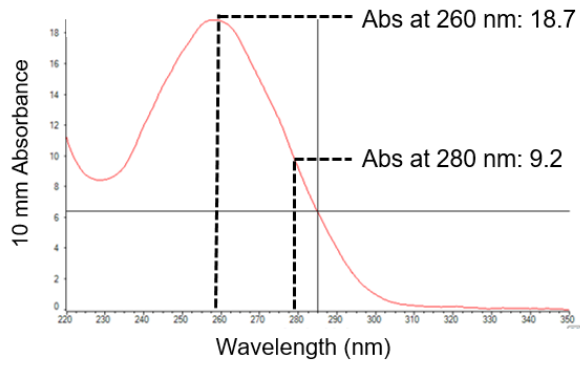
C: HUVEC (LGI008)



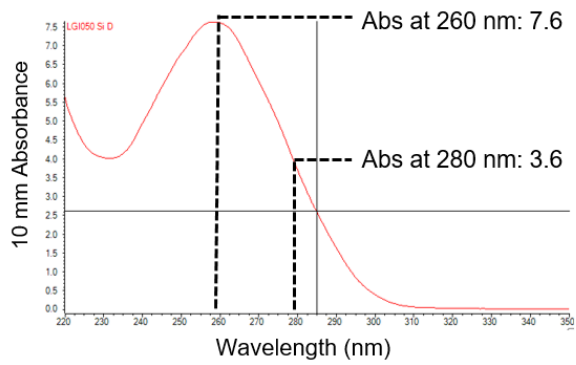
D: AGA FpEC (LGI049)



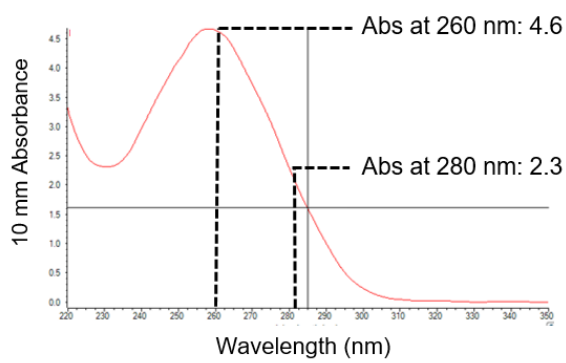
E: SGA FpEC (LGI016)



F: P1.si FpEC (LGI050)



G: Y1-treated FpEC (LGI050)



H: FSS-treated FpEC (LGI020)

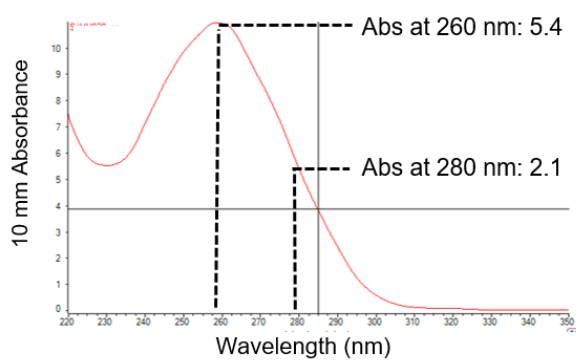


Figure 4.1. High quality nucleic acid obtained from placental tissue and cells under normal and experimental conditions.

A., Representative nucleic acid spectrum from a sample of whole villous tissue (LGI006). B., Spectrum from a sample of 1st trimester pregnancy tissue (EP200) showing some phenol-related absorbance. C., Spectrum from AGA HUVEC RNA (LGI008). D., Spectrum from AGA FpEC RNA (LGI049). E., Spectrum from SGA FpEC RNA (LGI016). F., Spectrum from FpEC RNA isolated post Piezo1 knock down with siRNA (LGI050). G., Spectrum from FpEC RNA isolated post Yoda1 treatment (LGI050). H., Spectrum from FpEC RNA isolated post FSS application (LGI020).

Sample	Group / treatment	RNA (ng/ μ L)	260/280	260/230
LGI006	3 rd trimester tissue	306.0	2.03	2.10
EP200	1 st trimester tissue	210.1	2.02	1.47
LGI008	HUVEC	664.3	2.05	2.25
LGI049	AGA FpEC	250.0	2.02	2.07
LGI016	SGA FpEC	751.4	2.02	2.23
LGI050	Piezo1 siRNA FpEC	304.4	2.05	1.89
LGI050	Yoda1-treated FpEC	215.3	2.07	1.58
LGI020	FSS-treated FpEC	438.2	2.02	1.99

Table 14. RNA concentration and purity ratios corresponding to the representative spectral images shown in Figure 4.1 A-H.

The accuracy of the gene expression data is also dependent on the efficiency of the QPCR reaction, and therefore the suitability of the primers selected for the primary genes of interest (*PIEZO1*, and *PIEZO2*). Gene sequences were selected from high quality studies and verified (Li et al., 2014, Huang et al., 2019). The quality of the primer pairs was assessed by measuring the QPCR reaction efficiency, and detection of a single gene product (Figure 4.2).

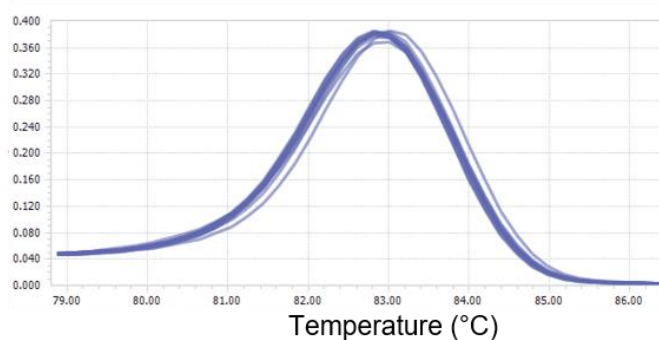
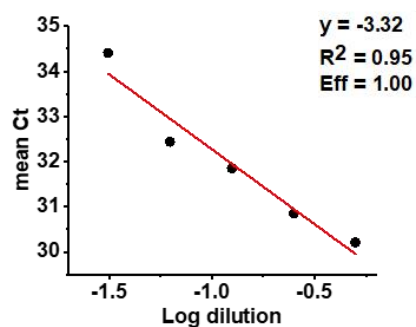
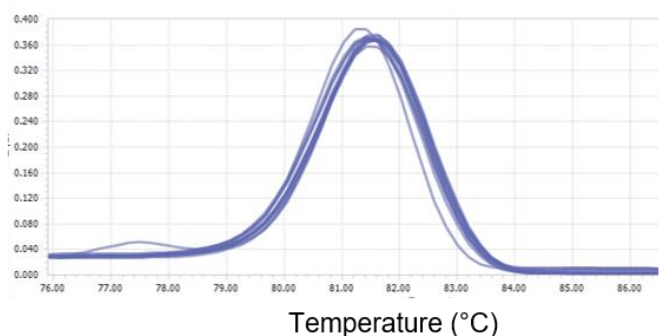
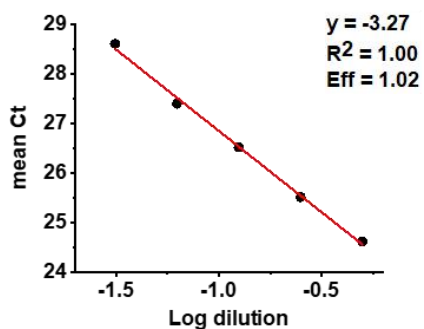
A: *PIEZO1*B: *PIEZO2*

Figure 4.2 QPCR reactions were performed using efficient primers for *PIEZO1* and *PIEZO2*, with single products detected during the melting phase of the reaction.

Primer efficiency calculated from the slope of the graph (y), and tested on 2 independent AGA samples ($n = 2/N = 2$: LGI007, LGI011). A., *PIEZO1* primer efficiency (Eff) (LGI007). B., *PIEZO2* primer efficiency (LGI007). C and D., Single melting curves for *PIEZO1* and *PIEZO2* (LGI007). The second aim of this chapter was to determine whether the presence of *PIEZO1* mRNA led to functional channel activity in FpECs. This was investigated using the synthetic Piezo1 channel agonist Yoda1 as a useful tool for studying chemical activation of Piezo1. Gene expression was also studied after exposure

to FSS to more closely simulate the *in vivo* placental environment. In addition, the effect of Piezo1 inhibition in FpECs was studied via blockade of the channel using Gd^{3+} , and depletion using siRNA.

4.2 Selecting reference genes for QPCR studies

To enable the comparison of steady-state gene transcription between the AGA and SGA clinical groups, reference genes were used as internal controls. A validation process was performed to determine the reference genes with optimal precision for our specific cell population and experimental setup. The candidate genes were selected from high quality studies, and the gene sequences verified (Drewlo et al., 2012, Meller et al., 2005, Bakhashab et al., 2014). If no sequences were available, primers were designed as described in Chapter 2, section 2.10.3. The quality of the primer pair was assessed by measuring the efficiency of the QPCR reaction, and detection of a single gene product (Figure 4.3 and Figure 4.4).

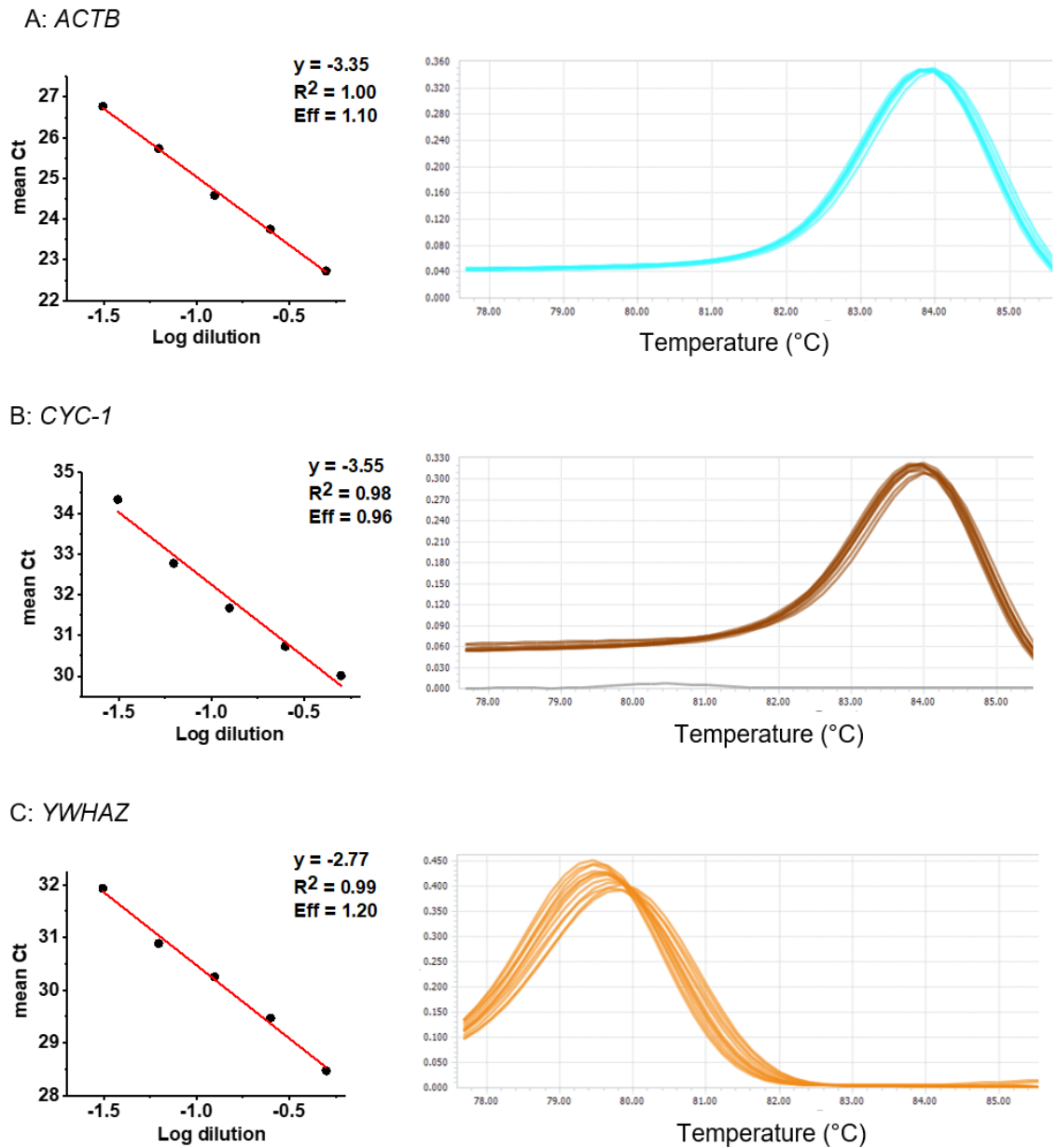
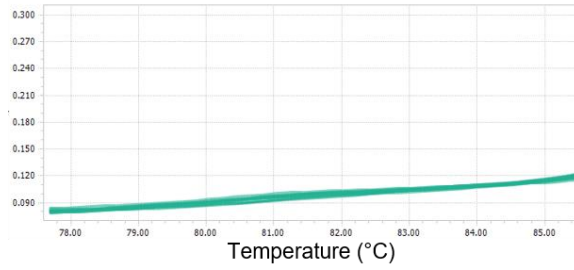
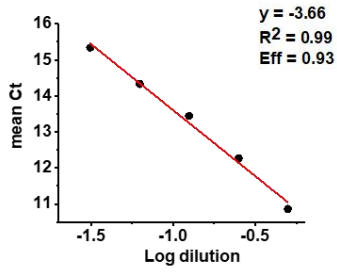
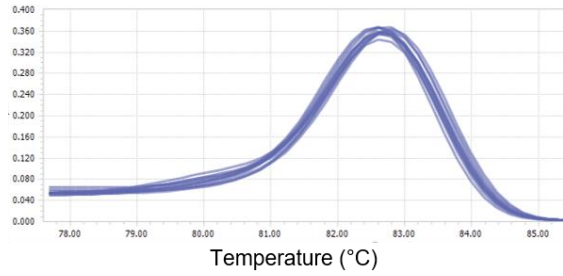
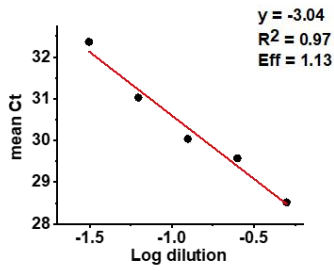


Figure 4.3 *ACTB*, *CYC-1* and *YWAZ* primer pairs were of suitable quality to use in QPCR reactions, as determined by efficiency and specificity. A., B., C are standard curves where y = slope, R^2 = correlation coefficient, Eff = efficiency. Single peak melting curves for each gene denotes primer specificity. A., β -actin (*ACTB*). B., *Cytochrome c-1* (*CYC-1*). C., *Tyrosine 3-monooxygenase/tryptophan 5-monooxygenase activation protein, zeta polypeptide* (*YWAZ*).

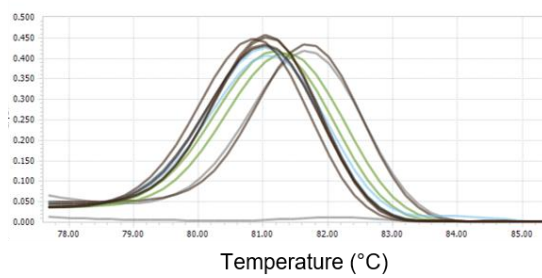
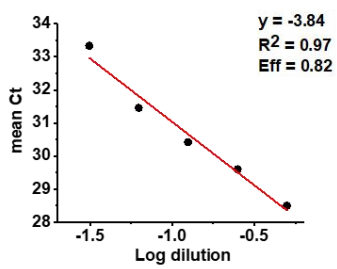
A: *RNA18S*



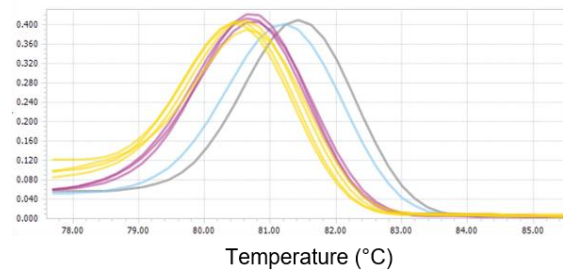
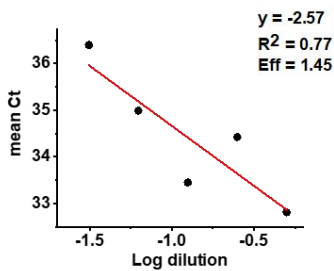
B: *GAPDH*



C: *B2M*



D: *HPRT*



E: *TOP1*

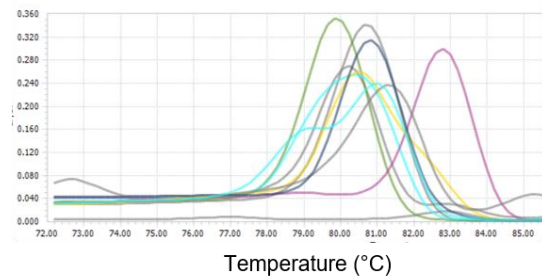
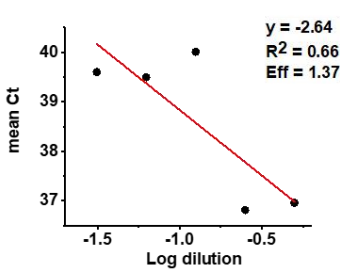


Figure 4.4 Primer pairs of unsuitable quality to use in QPCR reactions, as determined by efficiency and specificity.

A., B., C., D., E are standard curves as described in Figure 4.3 legend. A., *RNA18S*, with product detection at low Ct values. B., *Glyceraldehyde-3-phosphate dehydrogenase (GAPDH)*. C., D., E *β -2-microglobulin (B2M)*, *TATA box-binding protein (TBP)* and *DNA topoisomerase 1 (TOP1)* respectively, showed poor efficiency and specificity.

The data in Figure 4.4 are from genes that were rejected as potential housekeepers. Of these, the *RNA18S* and *GAPDH* primers had good efficiency and melt curves. However, the mean Ct values of *RNA18S* were several cycles different from those of the target genes. There is some evidence to suggest that *GAPDH* expression is oxygen-sensitive, and may therefore not be a suitable reference gene for comparisons with SGA placental samples. This was found in a study of HUVECs where exposure to hyperglycaemia and hypoxia upregulated the expression of *GAPDH*, but not *ACTB* (Bakhashab et al., 2014).

To enable the genes of interest to be normalised to the selected reference genes, their stability of expression across the AGA samples and SGA FpECs was assessed (Figure 4.5). This process was also performed using whole villous tissue as part of the project undertaken by Sara Ibrahim. The geometric means of three good quality primers (*ACTB*, *CYC-1* and *YWHAZ*) were stable across both clinical groups and were therefore selected as the reference genes for the QPCR data presented in this thesis. These findings are similar to a previous study of reference genes in whole placental tissue from control, PET and/or FGR cases delivered vaginally or by LSCS (Drewlo et al., 2012). After testing *TBP*, *HPRT*, *SDHA*, *TOP1*, *CYC-1*, *YWHAZ* and *B2M*, these authors found *TOP1*, *CYC-1* and *YWHAZ* to be the most stable.

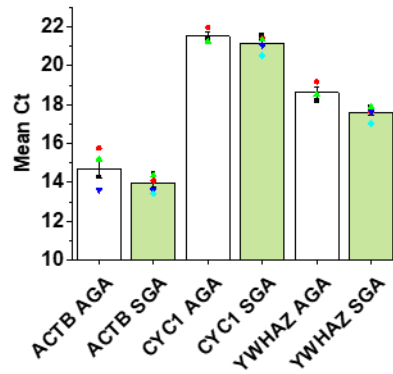


Figure 4.5 Stable expression levels of reference genes in the FpECs undergoing investigation. No statistically significant difference in mean Ct between AGA samples (AG) compared to SGA. $n = 3/N = 2$ each group (AGA: LGI004, LGI007, LGI045; SGA: LGI003, LGI030, LGI058). ANOVA.

4.3 *PIEZO1* mRNA is consistently expressed in placental tissue

4.3.1 Expression of *PIEZO1* in whole villous tissue from AG control and SGA placentas

Whole villous tissue was initially used to demonstrate *PIEZO1* gene expression in the human placenta. *PIEZO1* mRNA was readily detected in nine samples from AGA placentas. This expression was confirmed by demonstrating the amplified QPCR products using gel electrophoresis (Figure 4.6). When comparing the relative abundance of *PIEZO1* normalised to the three reference genes, there was no significant difference in expression between the AGA and SGA samples (Figure 4.6C and D). A subgroup analysis including only SGA samples with A/REDF also demonstrated no evidence of a difference compared with the AGA controls, although this was subset was limited to four patients (Figure 4.7).

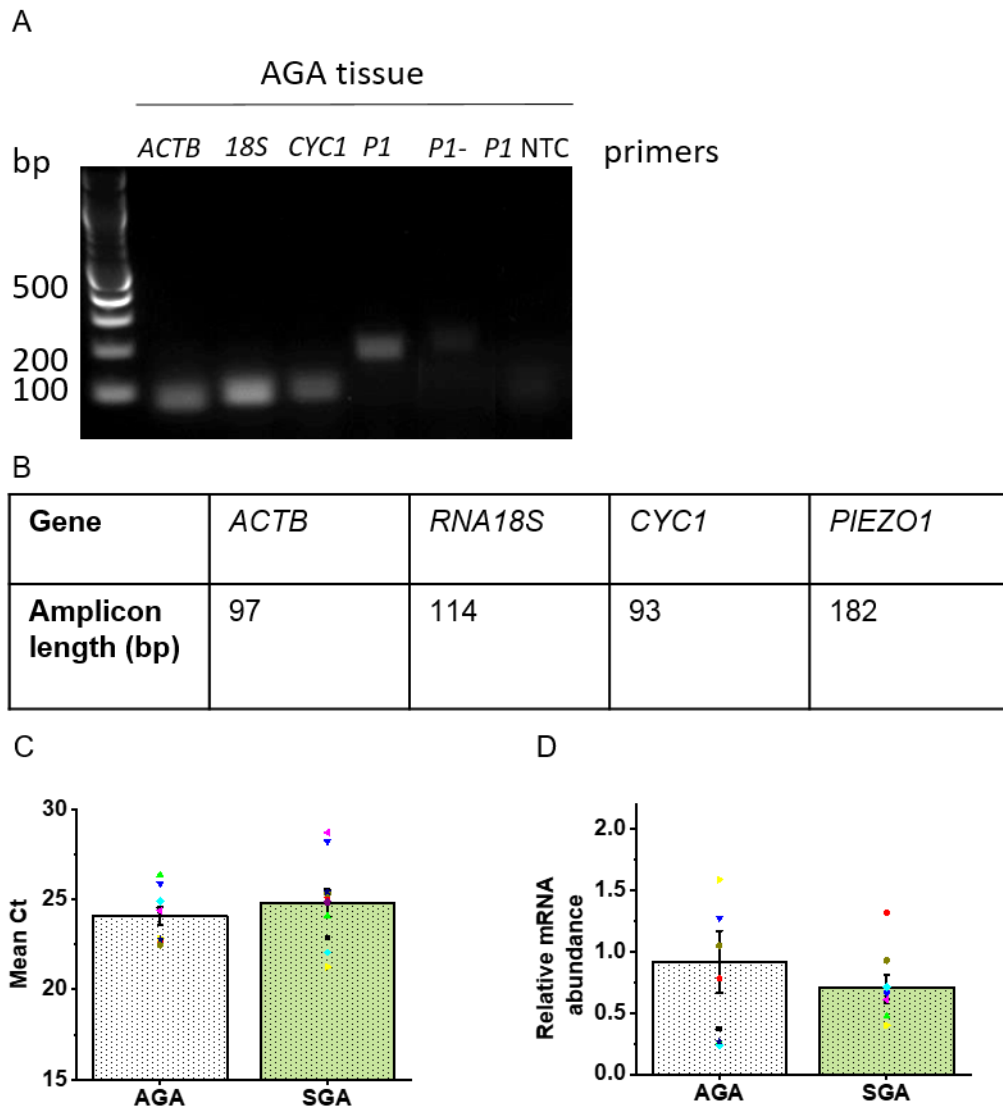


Figure 4.6 *PIEZO1* mRNA is expressed in whole villous tissue. A., Gel electrophoresis image of amplified products following QPCR, showing reference genes (*ACTB*, *RNA18S*, *CYC-1*) and *PIEZO1*. Abbreviations: bp base pair, NTC no template control, P1- minus reverse transcriptase control for *PIEZO1*. Gel produced by SI (AGA control sample LGI069). B., Expected amplicon sizes (bp). C., Summarised mean \pm SEM Ct values for *PIEZO1* expression. D., Summarized mean \pm SEM QPCR data showing no significant difference in *PIEZO1* between groups. AGA $n = 9/N = 2$: LGI022, LGI037, LGI043, LGI045, LGI046, LGI065, LGI069, LGI071, LGI082. SGA $n = 10/N = 2$: LGI004, LGI005, LGI006, LGI026, LGI027, LGI038, LGI051, LGI055, LGI058, LGI063. C and D: Unpaired *t* test.

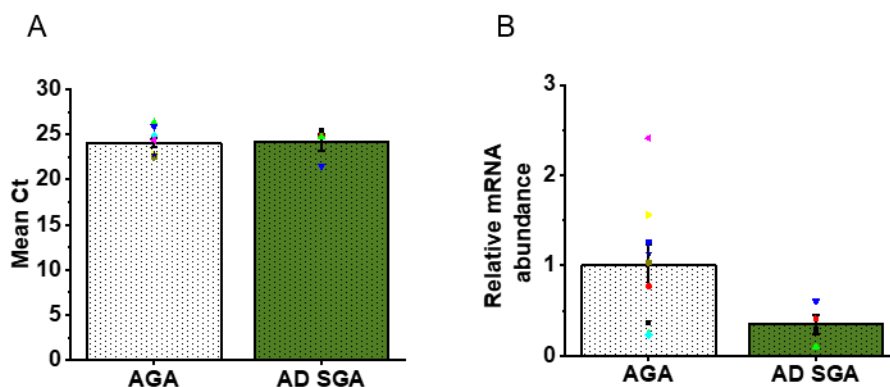


Figure 4.7 No significant difference in *PIEZO1* expression between AGA and SGA villous tissue samples. Subgroup analysis including AGA tissue (n = 9, as per Figure 1.6) and only SGA samples with abnormal Doppler (AD) blood flow detected on US scan (n = 4: LGI004, LGI027, LGI051, LGI063). One statistical outlier was removed from the AGA group (LGI082, $2\Delta\Delta Ct$ 8.86). A and B: Unpaired *t* test.

4.3.2 Expression of *PIEZO1* in first trimester pregnancy tissue

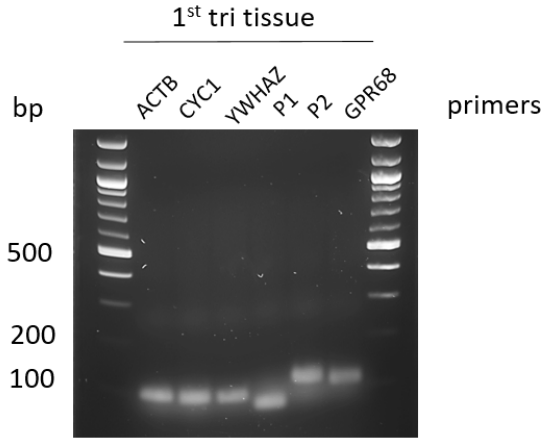
As discussed in the introduction sections 1.6.1 and 1.6.2, the body of evidence suggesting that finely tuned FSS has a critical role in early pregnancy is increasing (James et al., 2018). However, knowledge of specific mechanosensors involved in the sensing and transducing of FSS in the first trimester remains lacking.

Loss of function mutations in human *PIEZO1* can result in early pregnancy loss secondary to fetal hydrops (Fotiou et al., 2015). However, in both the global and endothelial-specific *piezo1* knock out murine model, loss of *piezo1* did not result in lethality until mid-gestation (embryonic day 9.5-11.5) (Li et al., 2014). The finding of *piezo1* expression in murine embryonic stem cells suggests that FSS-induced Piezo1 channel activation is important for cell differentiation. As such, Piezo1 may have fine-tuning roles that are not yet fully identified (Del Marmol et al., 2018).

The relative abundance of *PIEZO1* in early pregnancy (EP) tissue was investigated. In addition, expression or otherwise of the mechanosensitive receptor GPR68 in the first

trimester of pregnancy was also assessed (Figure 4.8). The mRNA expression of these mechanosensors, and that of Piezo2, was confirmed using gel electrophoresis (Figure 4.8A). There was no significant difference in the expression of *PIEZO1* between tissue obtained from the first trimester of pregnancy, and the AGA tissue from the third trimester. In addition, *GPR68* was detected in both first and third trimester tissue samples, with no significant difference in relative abundance (Figure 4.8E and F). In contrast, *PIEZO2* was expressed in greater abundance in the first trimester (Figure 4.8G and H). However, this analysis is likely to be limited by the use of heterogeneous tissue comprising differing cell types and quantities. Piezo2 and GPR68 are discussed in more detail in sections 4.7.1 and 4.7.2).

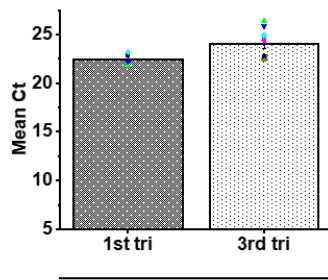
A



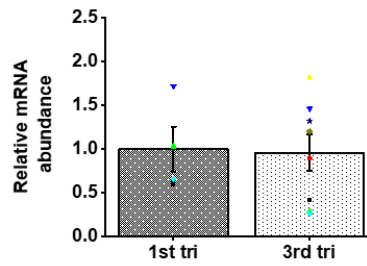
B

Gene	<i>ACTB</i>	<i>CYC1</i>	<i>YWHAZ</i>	<i>PIEZO1</i>	<i>PIEZO2</i>	<i>GPR68</i>
Amplicon length (bp)	97	93	94	76	113	105

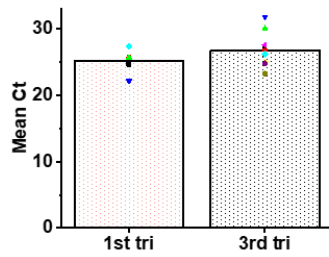
C: *PIEZO1*



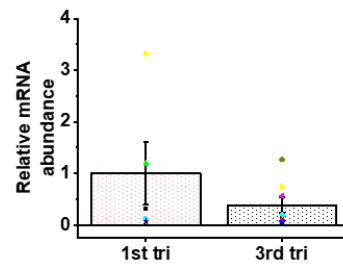
D



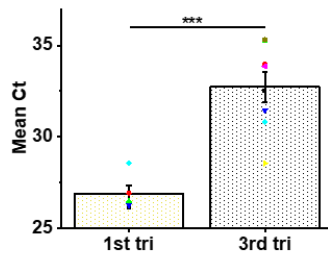
E: *GPR68*



F



G: *PIEZO2*



H

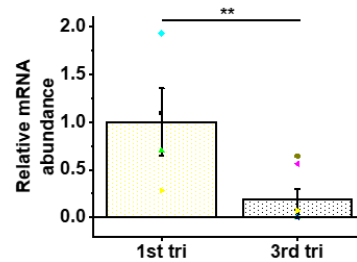


Figure 4.8. *PIEZO1*, *PIEZO2* and *GPR68* mRNA is expressed in early pregnancy tissue.

A., Gel electrophoresis image of amplified products following QPCR, confirming the expression of reference genes (*ACTB*, *CYC-1*, *YWHAZ*), *PIEZO1*, *PIEZO2* and *GPR68* (EP200). B., Expected amplicon sizes (bp). C., Summarised mean \pm SEM Ct values for *PIEZO1* expression. D., Summarized mean \pm SEM QPCR data showing no significant difference in *PIEZO1* between 1st trimester tissue versus AGA tissue from the 3rd trimester. E., Summarised mean \pm SEM Ct values for *GPR68* expression F., Summarized mean \pm SEM QPCR data showing no significant difference in *PIEZO1* between 1st trimester tissue versus AGA tissue from the 3rd trimester G., Summarised mean \pm SEM Ct values for *PIEZO2* demonstrating a significant difference ($p = 0.0002$) H. Summarized mean \pm SEM QPCR data showing a significant difference in *PIEZO2* between 1st trimester tissue versus AGA tissue from the 3rd trimester ($p = 0.005$). Early pregnancy samples $n = 5/N = 2$: EP188, EP189, EP200, EP201, EP202; 3rd trimester samples $n = 9/N = 2$: LGI022, LGI037, LGI043, LGI045, LGI046, LGI065, LGI069, LGI071, LGI082. All data normalised to the mean of three reference genes. C-H: Unpaired *t* test.

4.3.3 Expression of *PIEZO1* is increased in FpECs from SGA samples

To establish whether the *PIEZO1* gene is expressed in the fetoplacental endothelium, QPCR was performed on mRNA isolated from the FpECs. *PIEZO1* expression was readily detected in an AGA sample, and confirmed using gel electrophoresis (Figure 4.9A). As before, for optimal precision data were normalised to the mean of three reference genes, also shown on Figure 4.9A.

Prior to determining the relative abundance of *PIEZO1* in both AGA and SGA group, sample size was considered. This could be calculated from an expected effect size if prior research had established a clinically meaningful deviation in Piezo1 (Kadam and Bhalerao, 2010). However, due to the novel nature of researching Piezo1 in the placenta, the biological effect size is unknown. Likewise, whilst the prevalence of our disease of interest, FGR, is well established, there is no event rate for Piezo1 abnormalities in

placental research. The most relevant previous studies were therefore considered, including research into Piezo1-mediated iatrogenic pancreatitis (Romac et al., 2018). This study used a murine model, but with similarities in experimental set up, including cell responses to Yoda1 and histology. Here, between 7 and 13 mice were used in each experiment. A human study involving patients with suspected hereditary xerocytosis investigated Piezo1 mutations (Glogowska et al., 2017). Here, 9 patient samples were used.

After considering these previous studies, a statistical measure of sample size was also used, based on an acceptable level of significance (type 1 error rate) of <0.05 , with a power of 80%. After QPCR was performed on three samples in each group, a sample size calculation was undertaken based upon the mean normalised $\Delta\Delta C_t$ values and standard deviation of these samples (Chow, 2008). This suggested that 11 samples per group would be sufficient to detect a difference in the means of the two groups.

A pragmatic decision was therefore taken to measure Piezo1 abundance in a 15 samples in each group. Data are available for 15 AGA and 13 SGA samples. This demonstrated significantly higher relative abundance of *PIEZO1* in the SGA FpECs ($p = 0.007$) (Figure 4.9D). The results were also normalised to each reference gene independently which demonstrated a significant upregulation relative to *CYC-1* and *YWHAZ* ($p = 0.027$ and 0.014 , respectively), although the increase relative to *ACTB* was not significant ($p = 0.246$) (Figure 4.9E-G).

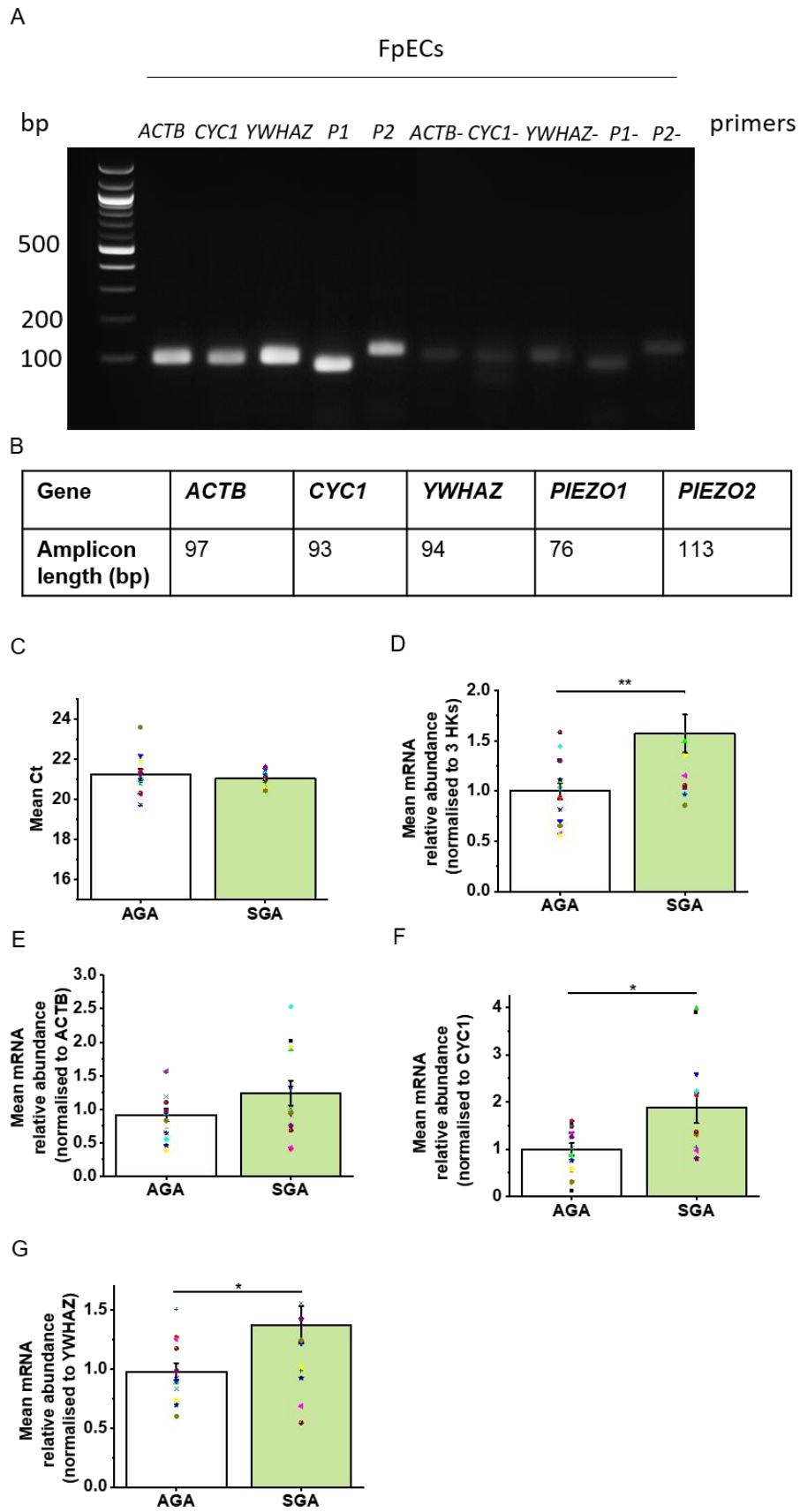


Figure 4.9. *PIEZO1* mRNA is present in cultured FpECs, with increased expression in SGA samples.

A., Gel electrophoresis image of amplified products following QPCR, confirming the expression of reference genes (*ACTB*, *CYC-1*, *YWHAZ*), *PIEZO1* and *PIEZO2* in an AGA sample (LGI096). *ACTB*-, *CYC1*-, *YWHAZ*-, *P1*- and *P2*- are minus reverse transcriptase controls. *PIEZO2* quantitative data from FpECs is presented and discussed in section 4.7.1. B., Expected amplicon sizes (bp). C., Summarised mean \pm SEM Ct values for *PIEZO1* expression in AGA (n = 15/N = 2) and SGA (n = 13/N = 2) FpECs. D., Summarized mean \pm SEM QPCR data showing significant increase in *PIEZO1* in the SGA FpECs (p <0.0078), when normalised to the mean of 3 reference genes (*ACTB*, *CYC1*, *YWHAZ*). E., F., G. As for D., showing relative abundance when normalised to each reference gene separately (p <0.05 for *CYC-1* and *YWHAZ*, p = NS for *ACTB*). Samples numbers are given in the Table 15 legend. C-G: Unpaired *t* test.

The demographic details for the patient samples included in this analysis are provided in Table 15. This subset of samples is reflective of the overall samples collected in this project, as presented in Table 11. In these FpEC samples, mothers were significantly younger in the SGA group and had significantly fewer previous children. 25% of these women were smokers during the pregnancy. As discussed previously, gestation at birth and mode of delivery varied in the SGA group. Birthweight and placental weight were significantly reduced in the SGA group versus the AG controls.

Although the samples in each group were not gestation matched, a subgroup analysis was performed including only samples from babies born ≥ 37 weeks of gestation. After excluding LGI063 (28⁺² weeks) and LM13 (30 weeks), 11 FpEC samples remained in the SGA group. *PIEZO1* mRNA expression remained significantly higher in this group versus the term-born AGA samples (p = 0.01). Subgroup analyses were also performed to investigate the effects of maternal smoking in pregnancy, and mode of delivery, on *Piezo1* gene expression (Figure 4.10). There was no significant difference in *PIEZO1* relative abundance between the smokers and non-smokers. However, given my sample size calculation requiring 11 per group, this analysis is underpowered to detect an effect (3 smokers and 10 non-smokers). Analysis by mode of delivery suggested that those

born by emergency LSCS (Em LSCS) in the SGA group had the highest *PIEZO1* expression. Severity of SGA or poor fetal condition necessitating emergency iatrogenic delivery may be indicative of the greatest degree of placental dysfunction and raised FSS, although this requires further investigation. Insufficient sample numbers were available to perform a subgroup analysis based on placental blood flow abnormalities. As such, this analysis was performed on the whole villous tissue samples (Figure 4.7). A subgroup analysis by fetal sex, suggested that expression may be higher in the placentas of female babies, although the data were not significantly different. As such, whether sexual dimorphism in the placenta is important for the response to FSS and subsequent mechanotransduction signalling warrants further investigation.

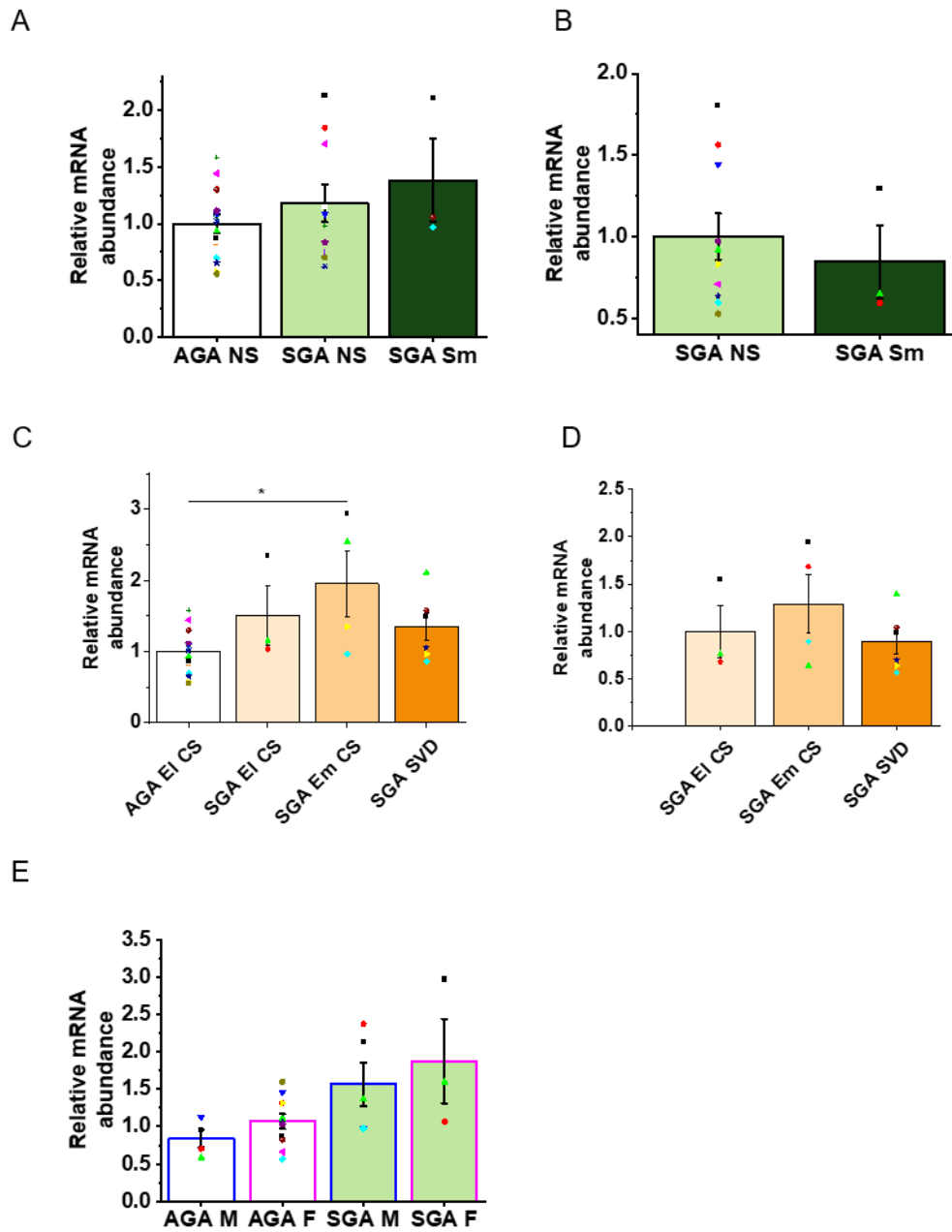


Figure 4.10 *PIEZO1* gene expression by subgroup analysis of maternal smoking in pregnancy, mode of delivery, and fetal sex.

A., Summarized mean \pm SEM QPCR data showing no significant difference in *PIEZO1* between either SGA FpECs with, or without a history of smoking, and the non-smoking AGA group. B., Summarized mean \pm SEM QPCR data showing no significant difference in *PIEZO1* between SGA FpECs with, or without a history of maternal smoking in pregnancy. C., Significant difference between SGA delivered by Em LSCS and AGA group, which were all delivered by EI LSCS ($p = 0.014$). D., No significant different in Piezo1 expression by mode of delivery within the SGA group. A., and C., Data were normalised to the AGA control group. B., and D., Data were normalised to the SGA control, SGA NS or EI CS, respectively. Abbreviations: non-smoker (NS), smoker (Sm), elective LSCS (EI CS), Emergency LSCS (Em CS), spontaneous vaginal delivery (SVD), Male (M), Female (F). FpEC samples in this analysis are provided in Table 15 legend. A, C, D, E: ANOVA, B: Unpaired *t* test.

Demographic data (mean \pm SEM, median \pm range, %)	AGA (n = 15)	SGA (n = 13)	Difference (significance denoted by *)
Maternal age	33.4 (1.46)	28.08 (1.99)	0.037* (mean difference 5.32, 95% CI -10.28 - 0.35)
Maternal ethnicity (%)			
White	73.33	83.33	
Mixed	0	0	
Asian	13.33	16.67	
Black		0	
Other	13.33	0	
Maternal BMI (Kg/m ²)	27.57 (1.35)	24.87 (1.44)	0.196 (mean difference 2.70, 95% CI -1.53 - 6.93)
Smoking in pregnancy (%)	0	25	N/A

Parity: mean number of previous births, zero if primiparous (median, range)	1(0-5)	0 (0-2)	0.043* (mean difference - 0.88, 95% CI -1.74 - -0.03)
Gravidity including current pregnancy (median, range)	2(1-6)	2(1-5)	0.138 (95% CI -2.12 - 0.32)
Gestation (days)	274.13 (0.83)	253.64 (7.64)	p = 0.005** (mean difference -20.50, 95% CI -2.12 - -0.32)
Mode of delivery (%)			
SVD	0	41.66	N/A
EI LSCS	100	25	N/A
Em LSCS	0	33.33	N/A
Other	0	0	N/A
IOL for FGR	0	16.66	N/A
Baby weight (g)	3591.3 3 (71.95)	2253.1 8 (157.61)	< 0.0001*** (mean difference 1338.15, 95% CI 1664.98 - 1011.32)
Percentile ⁱ	60.79	3.05	< 0.0001***, mean difference -57.732, 95% CI -70.92 to -44.54)
Sex			
Female (%)	73.33	44.44	
Male (%)	26.67	55.55	
Placenta weight (trimmed, g)	456.22 (22.86)	298.78 (27.51)	p = 0.0004*** (mean difference 157.44, 95% CI -233.27 - 81.62)

Table 15. Patient samples used to generate the data presented in Figure 4.9 and Figure 4.10 Full details of each patient sample provided in Appendix 2. AGA group n = 15: LM4, LM7, LM8, LM9, LGI008, LGI011, LM23, LGI035, LGI037, LGI041 LGI045, LGI046, LGI069, LGI079, LGI096. SGA group n = 13: LM5, LM12, LM13, LM15, LGI016, LGI030, LGI038, LGI042, LGI051, LGI058, LGI063, LGI067, LGI075. Percentile: Where percentile was calculated as <0.4th, 0.4 was used in the comparison.

4.4 Piezo1 channel activity in placental ECs

4.4.1 Exposure to FSS increases the expression of Piezo1 mRNA and protein in FpECs

Given that messenger RNA encoding Piezo1 was readily detected in a variety of placental ECs and tissues, the next aim was to gain insight into the functional significance of these findings. As such, healthy FpECs were exposed to FSS and compared with those in a parallel static culture. The FpECs in flow conditions showed a significant increase in the expression of *PIEZO1* mRNA (Figure 4.11). This suggests that Piezo1 channels in FpECs are sensitive to flow over an extended time period. When the experiment was performed on SGA FpECs in parallel, the inference was the same, although there was no statistically significant difference (Figure 4.11A, C). These data also reconfirm the increased baseline level of *PIEZO1* expression in SGA FpECs versus AGA cells in static culture, as reported in section 4.3.3 (Figure 4.9). This raises the question of whether the lack of a significant rise in *PIEZO1* expression over and above the baseline is indicative of reduced responsiveness to FSS in the SGA placentas.

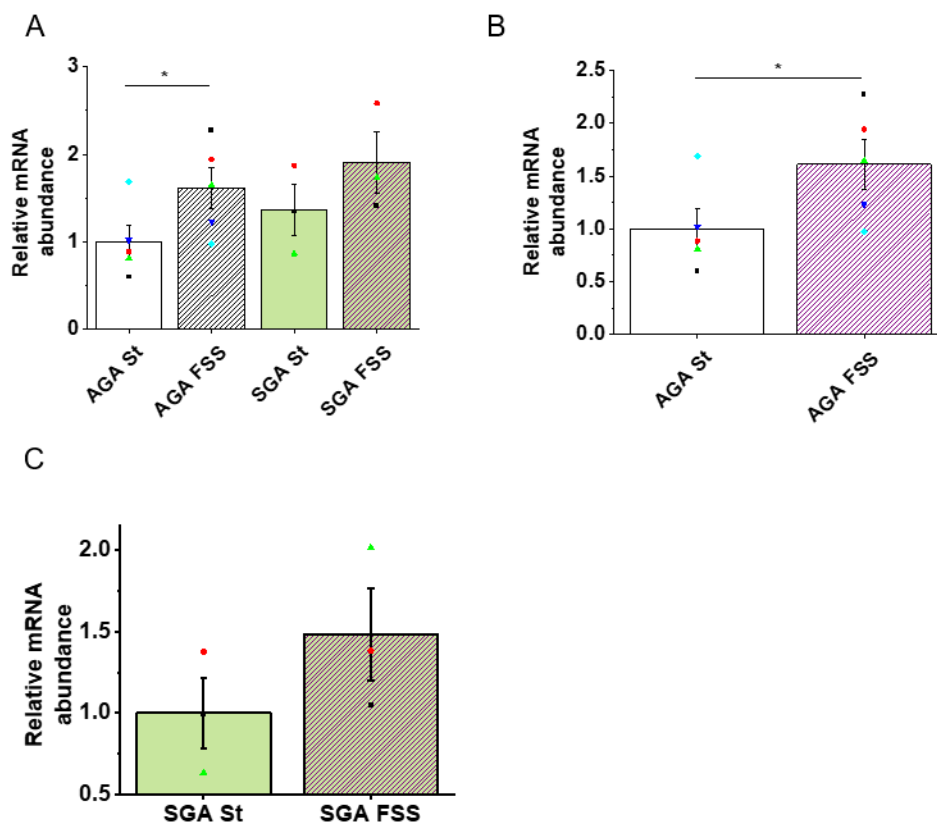


Figure 4.11. FSS induces upregulation of *Piezo1* mRNA that is significant in AGA samples but not SGA FpECs. A., Summarized mean \pm SEM QPCR data showing a significant increase in *PIEZO1* the AGA FpECs exposed to 48 hours of FSS, when normalised to the mean of three reference genes (*ACTB*, *CYC-1*, *YWHAZ*) ($p < 0.05$, $n = 5$: LGI034, LGI037, LGI020, LGI041, LGI049). Exposure to FSS does not significantly increase *PIEZO1* expression in the SGA FpECs, when normalised to the mean AGA FpEC static control ($n = 3$: LM12, LM15, LM16). B., Data as for A, normalised to the mean AGA FpEC static control. C., Data as for A, normalised to the mean SGA FpEC static control. A: ANOVA, B and C: Unpaired *t* test.

Given the increase in *PIEZO1* mRNA with exposure to FSS, lysate was also collected and probed with anti-Piezo1 antibody to determine whether flow resulted in increased Piezo1 protein expression. Due to the acknowledged lack of antibody specificity (Li et al., 2014), the experiment was attempted using two alternative antibodies – Proteintech and Bect4 (Figure 4.12 and Figure 4.13). Although unknown bands were still present

using the Proteintech antibody, these western blots showed greater clarity with bands visible at the expected mass of Piezo1. These data demonstrate the presence of Piezo1 protein in healthy FpECs, which appears increased when exposed to FSS.

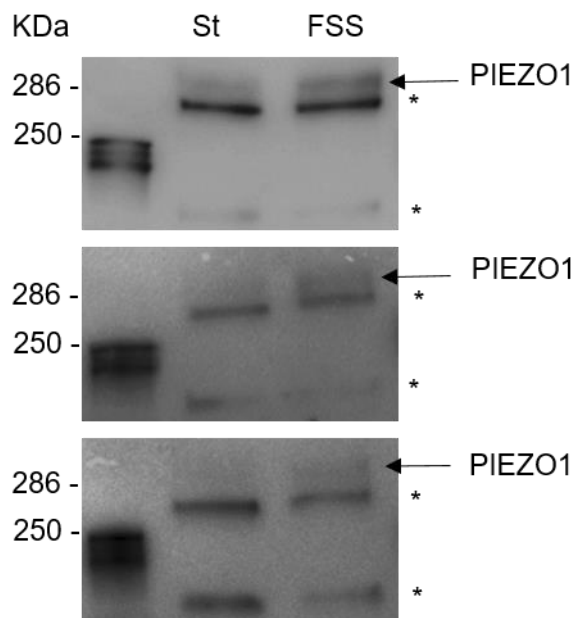


Figure 4.12 Western blot for FpEC lysate probed with Proteintech anti-Piezo1 antibody after exposure to FSS. FpECs were exposed to either FSS for 48 hours (orbital shaker at 153 rpm) or static culture conditions (St). The upper band represents Piezo1 with a predicted mass of 286 kDa. The bands highlighted with * are unknown proteins labelled non-specifically. Experiments were performed on an AGA sample LGI016. Three replicate experiments were performed – upper, middle and lower blots.

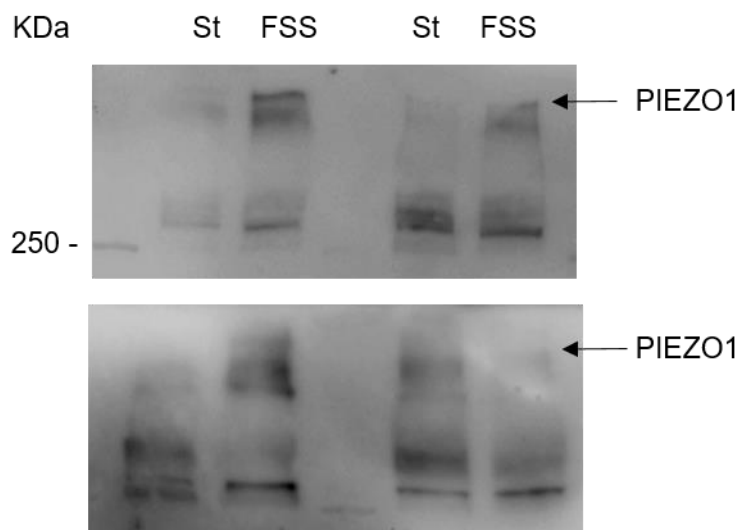


Figure 4.13 Western blot for FpEC lysate probed with Beec4 anti-Piezo1 antibody after exposure to FSS. Experiment performed as per Figure 4.12. Blot results showed more non-specific protein labelling and aggregation of proteins at higher than the predicted mass. Two independent experiments are shown: upper and lower blots, with two replicates per blot. That band which may be Piezo1 is indicated, however no quantitative analysis was performed on these images.

4.4.2 Endothelium freshly isolated from placental arterial ECs showed dominant FSS-activated Piezo1 channels

Differences in Piezo1 channel activity introduced by growing FpECs in culture was considered. As such, cell-detached outside-out membrane patch recordings were performed by laboratory member, Jian Shi to demonstrate and investigate Piezo1 channels in primary endothelium. These experiments were performed on arterial ECs freshly isolated from the chorionic plate. This allowed the identification of single channel currents and investigation of channel unitary conductance. Constitutive channel activity was observed which could be further enhanced by fluid flow and inhibited by Gd^{3+} (Figure 4.14). Measurement of unitary currents using amplitude histograms showed that the unitary current of the spontaneous channels was the same as that of the flow-activated channels (Figure 4.14D and E). Construction of a current–voltage relationship (IV) showed that the channel conductance was voltage-independent with amplitude of 26.6 pS (Figure 4.14). Statistical analysis further confirmed the channel sensitivity to Gd^{3+}

(Figure 4.14F). No other unitary current amplitudes were observed in response to fluid flow. These data provide further evidence that Piezo1 channels are present, and FSS-sensitive, in freshly isolated placental ECs. Furthermore, this suggests that Piezo1 channels are the dominant channel type activated by FSS in the chorionic plate arterial endothelium.

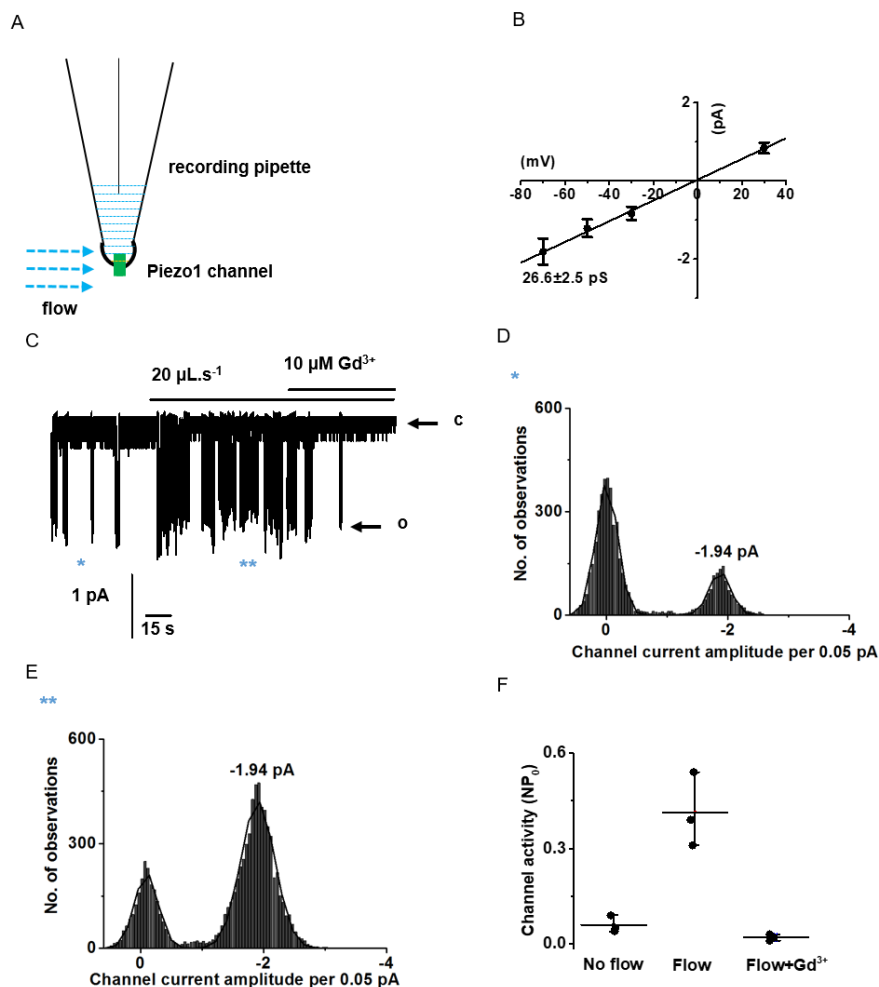


Figure 4.14. Piezo1 channels are membrane-delimited sensors of FSS in freshly-isolated endothelium of human placental artery.

A., Drawing illustrating the method of ionic current recording from outside-out patches excised from freshly isolated placental artery ECs. B., Mean unitary current amplitudes for channels activated by flow as shown in e (AGA samples $n = 3$: LM19, LM20, LM25, $n = 6$ FpECs from each, $N = 3$ replicates). C., Example recording at -70 mV. The patch was placed at the outlet of a capillary from which flowed ionic solution at $20 \mu\text{L}/\text{s}$. The letter c denotes the closed state of the channel and the letter o marks the open state. Subpanels D. and E. show the current amplitude histograms for the segments of trace indicated by * and **. F., Raw data and mean data for channel activity (NP_0 : channel number \times probability of opening) of the type shown in e ($n = 3/N = 3$). Flow $p = 0.007$, flow + Gd^{3+} $p = 0.004$. Figure produced from data collected by laboratory member Jian Shi.

4.5 Piezo1 channel activity can be investigated by *PIEZO1* silencing

In order to determine the significance of Piezo1 in FpECs, the effect of knocking down Piezo1 prior to performing functional experiments was investigated. Piezo1 was depleted in the FpECs using siRNA, and compared to cells treated with control siRNA or mock transfection (Lipofectamine™ only). The suppression of Piezo1 was confirmed using QPCR to demonstrate a significant mRNA reduction (Figure 4.15A). Piezo1 proteins were also depleted following the transfection protocol (Figure 4.15B).

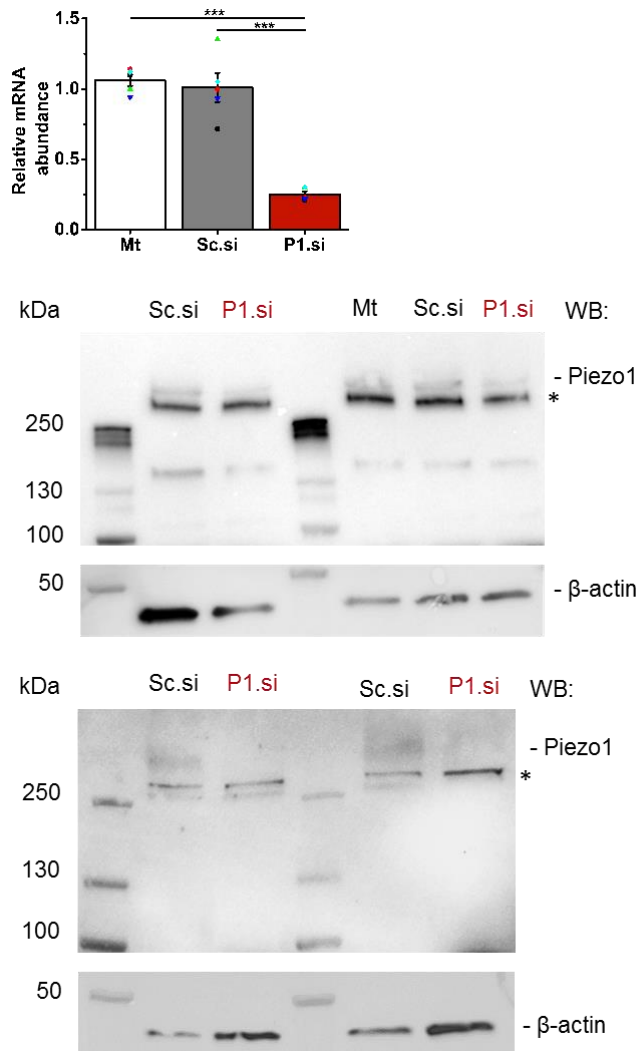


Figure 4.15 Piezo1 silencing confirmed by reduced mRNA and protein expression.

A., QPCR data for FpECs that underwent either mock transfection (Mt), transfection with control siRNA (Sc.si) or Piezo1 siRNA (P1.si). Significant difference in *PIEZO1* mRNA expression between both Mt and Sc.si transfected and P1.si ($p = 3.8 \times 10^{-6}$, 7.6×10^{-6} , respectively). No significant difference between Mt and Sc.si relative abundance of *PIEZO1*. Results normalised to the mean of three reference genes (*ACTB*, *CYC-1*, *YWHAZ*). AGA samples $n = 5/N = 2$: LGI011, LGI013, LGI046, LGI050, LGI079. ANOVA

B., Western blots for FpEC lysates probed with anti-Piezo1 antibody after transfection with Sc.si or P1.si.1, showing reduced Piezo1 band intensity after knockdown (predicted mass 286 KDa). Non-specific bands below Piezo1 indicated by *. β -actin was used as a protein loading control (predicted mass 37 KDa). Two independent experiments performed on AGA sample LGI016 (upper blot $N = 2$, and lower blot $N = 2$ replicates).

4.5.1 Piezo1 is required for FpEC alignment to FSS

Data demonstrating that FpECs are responsive to FSS by aligning in the direction that flow was applied was presented in Figure 3.10. This experiment was repeated comparing FpECs that had undergone with either Piezo1 siRNA or scrambled siRNA. Additional comparisons were made between cells that were exposed to flow but had not been transfected, and those in static culture conditions. After Piezo1 knockdown, the FpECs no longer aligned in the direction of flow (Figure 4.16). The degree of alignment was significantly different between the Piezo1-depleted and non-transfected samples. The lack of alignment after P1.si treatment was such that there was no significant difference compared to the non-transfected FpECs in static conditions. There was no evidence of a difference in alignment between the Sc.si-treated and NT cells. These data suggest that Piezo1 has an important role in the response of FpECs to fluidic force.

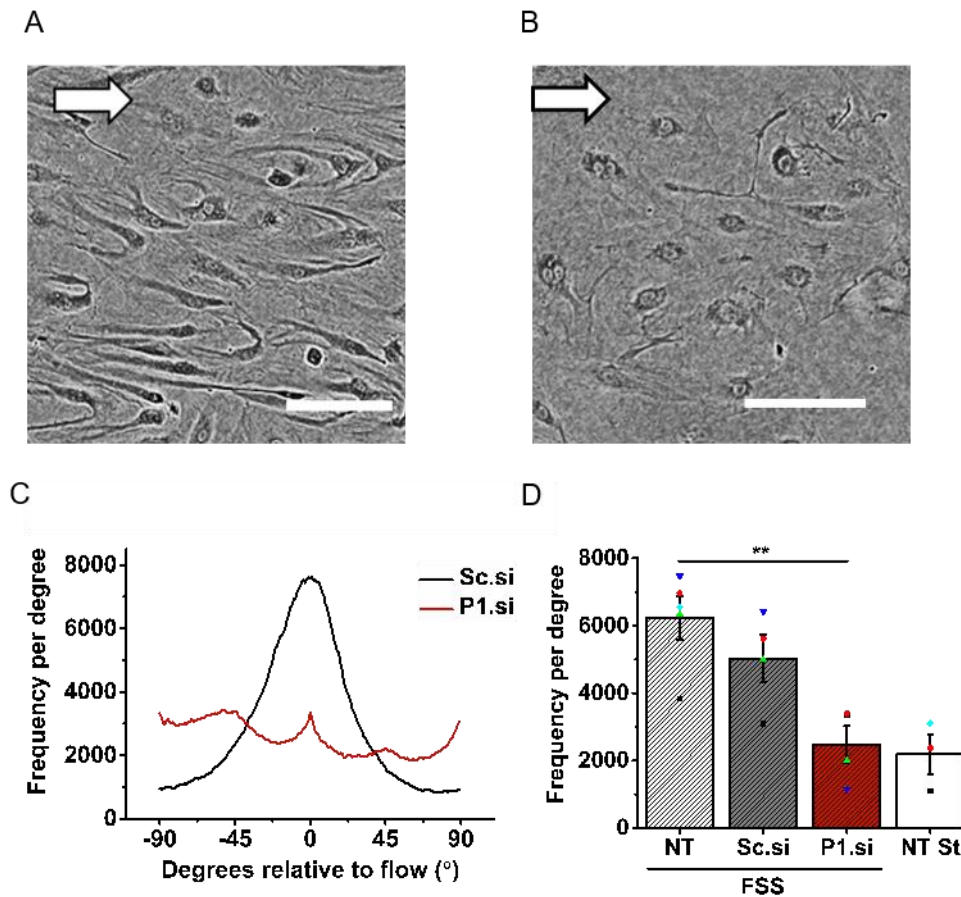


Figure 4.16 The response to FSS in FpECs is Piezo1 dependent.

A., FpECs transfected with Sc.si RNA after exposure to 48 hours of FSS (orbital shaker at 153 rpm), showing alignment in the direction of flow (arrow depicts direction of flow, scale bars 100 μ m). B., Lack of alignment in FpECs exposed to FSS after Piezo1 depletion with siRNA. C., Representative orientation analysis for images of the type shown in A and B, showing the frequency (number of angles) at the mode. D., Quantification of orientation analysis showing the mean peak height (SEM) after no transfection (NT) 6231.956 (629.153), Sc.si 5027.632 (708.53), P1.si 2478.065 548.786) or non-transfected static control (St) 2187.275 (586.011). Alignment was significantly reduced after P1.si transfection compared to the non-transfected (NT) control ($p = 0.0043$). The difference in alignment between Sc.si and P1.si did not quite reach statistical significance ($p = 0.06$). After Piezo1 knockdown there was no significant difference in alignment between these FpECs and that static control ($p = 0.99$) (AGA samples $n = 5/N = 1$: LM1, LM2, LM4, LM8, LM11. D: ANOVA.

To investigate the relationship between Piezo1 and FSS in more detail, single cells were used. Non-transfected and Piezo1 siRNA treated FpECs were seeded onto Ibidi slides prior to loading with Fura-2 AM dye. Cells were exposed to FSS at 15 dyne/cm² by a peristaltic pump. VEGF and Ca²⁺ were present in the flow solution. Single FpECs were identified using a microscope and Ca²⁺ entry recorded. Figure 4.17 demonstrates that in FpECs, the application of FSS induced Ca²⁺ entry into the cell. This was a single experiment and therefore these data are preliminary, although the lack of response to FSS after Piezo1 depletion was striking.

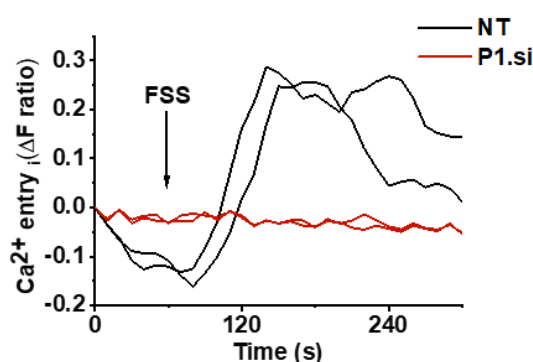


Figure 4.17 FSS induces a change in Ca²⁺ in FpECs, which is abolished by Piezo1 silencing. Single cell recordings of intracellular Ca²⁺ were made during exposure to flow (15 dyne/cm²) started at 60 seconds. Measurements were taken from two non-transfected (NT) cells and two Piezo-1 depleted (P1.si) FpECs, from an AGA sample (n = 1/N = 2 each group, LM2). Experiment performed with assistance from laboratory member Adam Hyman.

4.5.2 Piezo1 is not required for FpEC viability or substrate attachment

An imaging assay that recognises plasma membrane integrity was used to confirm that Piezo1 depletion using siRNA did not affect FpEC viability (Figure 4.18). Piezo1 knockdown had no effect on the percentage of cells which were viable or remained attached to the substrate. The application of staurosporine (SSP) to cause apoptosis was a positive control and led to significant decrease in FpEC viability (Figure 4.18C).

These data suggest that Piezo1 is unimportant for the viability or substrate attachment of FpECs.

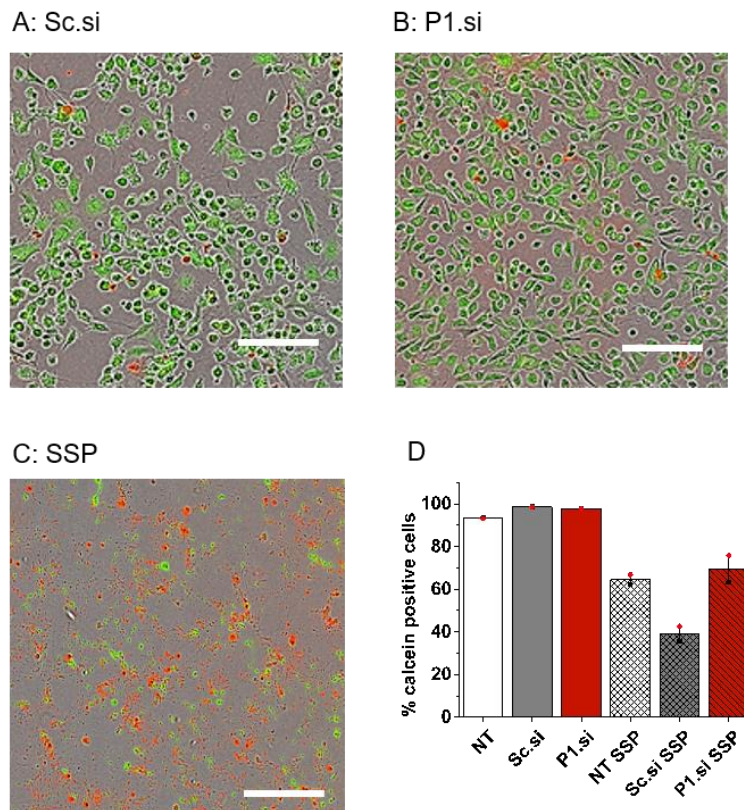


Figure 4.18 Piezo1 is not a requirement for cell viability or attachment to the substrate. Viability assay showing live FpECs of similar confluency in A., 48 hours post transfection with Sc.si, B., 48 hours after P1.si transfection, C., Dead cell control post treatment with 1 μ M staurosporine (SSP) (scale 300 μ m). D., Quantification showing no difference in viability between Sc.si and P1.si transfected cells ($p = \text{NS}$). Treatment with SSP results in cell apoptosis and detachment, verifying the viability assay. AGA FpECs used in this experiment ($n = 2/ N = 1$: LM10, LM14).

4.6 Chemical activation of Piezo1 using Yoda1

To further investigate whether the activation of Piezo1 channels leads to functional Ca^{2+} entry in FpECs, the synthetic Piezo1 agonist Yoda1 was applied during measurements of the intracellular Ca^{2+} concentration. Yoda1 caused a concentration-dependent increase in Ca^{2+} that was dose-dependent (Figure 4.19A, B). The 50% effect (EC_{50}) occurred at about 5.4 μM , although this is an approximation due to the aqueous solubility limitations of Yoda1. As such, 5 μM Yoda1 was used for the subsequent experiments of Piezo1 chemical activation.

Given the rise in intracellular Ca^{2+} occurring in response to Yoda1, whether this Ca^{2+} was released from intracellular stores, or entered the cell from outside was considered. If Yoda1 is activating Piezo1 on the ER, then Ca^{2+} will be released regardless of the extracellular Ca^{2+} concentration. In contrast, activating membrane Piezo1 is dependent on a degree of extracellular Ca^{2+} to pass through the open ion channel pore. As such, Yoda1 was applied to the cells in varying concentrations of Ca^{2+} solution. A minimal response to Yoda1 occurred in the 0 mM Ca^{2+} solution. With increasing Ca^{2+} concentration, the intracellular Ca^{2+} response to Yoda1 rose correspondingly (Figure 4.19C and D). These data suggest that Yoda1 is primarily stimulating membrane Piezo1 in FpECs, resulting in an influx of extracellular Ca^{2+} into the cell.

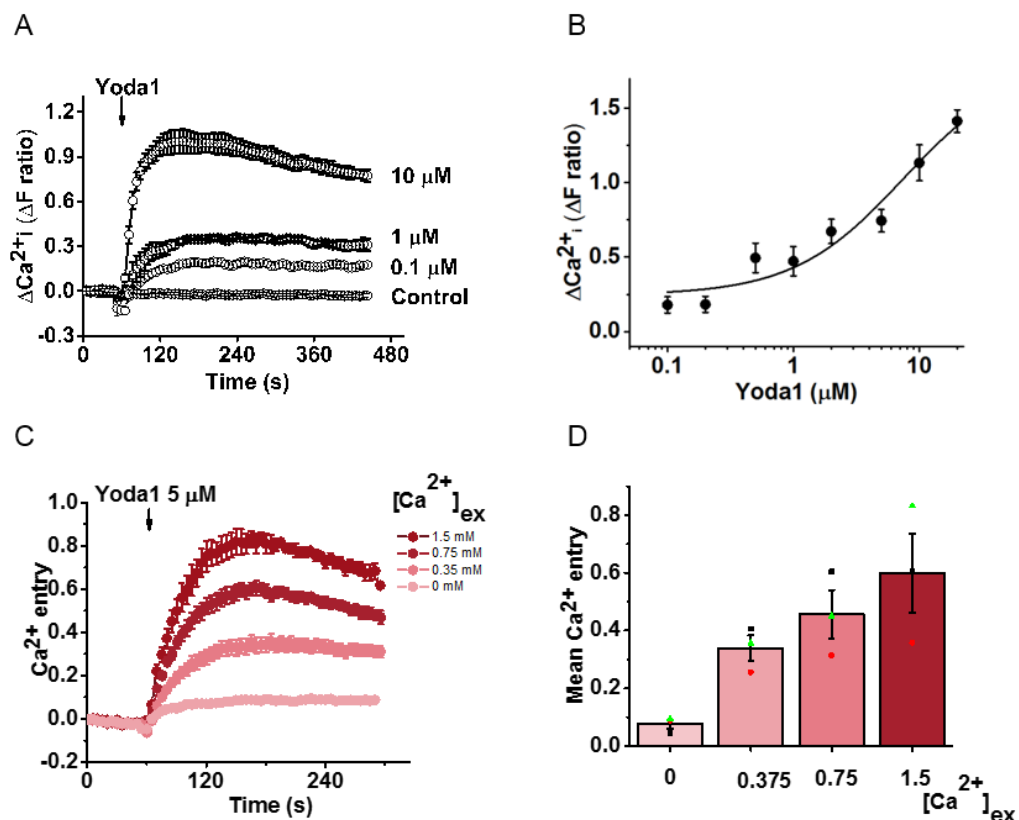


Figure 4.19 Dose-dependent Ca^{2+} entry occurs response to Yoda1 stimulation. A., Representative flex showing change (Δ) in intracellular Ca^{2+} in response to increasing concentrations of Yoda1 (μM) compared with vehicle control (DMSO) (LM14). B., mean \pm SEM responses to Yoda1 fitted with the Hill equation, suggesting an approximate EC_{50} of 5.36 μM ($n = 5/N = 3$: LM7, LM9, LM10, LM14, LM14). C., Representative flex showing calcium response to Yoda1 stimulation, which is dependent on concentration of extracellular calcium solution (LGI008). D., Pool mean data of the type shown in A., demonstrating minimal Yoda1 response in the presence of 0 mM extracellular stores ($n = 3/N = 1$: LGI008, LGI041, LGI046). This suggests that upon Yoda1 treatment, membrane Piezo1 channels are stimulated generating Ca^{2+} entry into the cell which is dependent on the availability of extracellular Ca^{2+} .

For comparison, the amplitude of the Yoda1 (5 μM) response was measured alongside that of ionomycin. Firstly, ionomycin alone was applied to FpECs during measurements of the intracellular Ca^{2+} concentration. This produced a concentration-dependent increase in Ca^{2+} that was dose-dependent (Figure 4.20). Ionomycin is a cation

ionophore, with a strong preference for Ca^{2+} . Treating a variety of cells types with ionomycin has been previously shown to induce a rapid, transient spike in cytosolic free Ca^{2+} (Albert and Tashjian, 1986, Morgan and Jacob, 1994). The initial increase is thought to result from the mobilisation of intracellular stores, followed by a more sustained influx across the membrane, as shown in Figure 4.20A. As such, this reproducible, and consistent, Ca^{2+} response to ionomycin was used to normalise the Yoda1-induced changes in Ca^{2+} concentration under different experimental conditions.

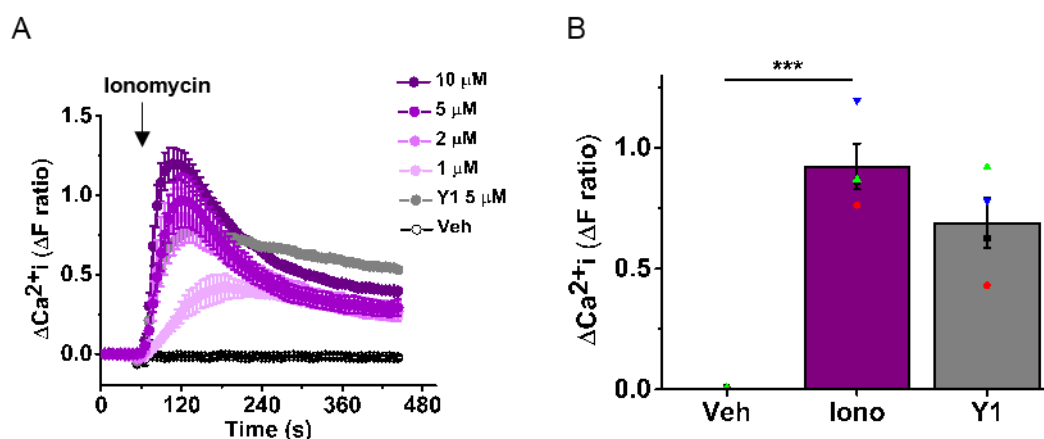


Figure 4.20 Dose-dependent Ca^{2+} entry occurs response to ionomycin stimulation.

A., Example Ca^{2+} measurement trace showing change (Δ) in intracellular Ca^{2+} in response to increasing concentrations of ionomycin (μM) compared with vehicle control (Veh, H_2O) (AGA sample LM25, $N = 3$). B., Mean \pm SEM responses to ionomycin (iono, 10 μM) demonstrating a consistent rise in intracellular Ca^{2+} compared to Veh ($p < 0.0001$). This increase was larger although not significantly different to the response to Yoda1 (Y1, 5 μM) (AGA samples, $n = 3/N = 3$: LM25, LM27, LGI039). Where indicated, 10 μM of ionomycin was used to normalise the responses to Yoda1 in subsequent experiments. B: ANOVA.

4.6.1 Piezo1-dependent Ca²⁺-entry in FpECs

After confirming that Yoda1 evokes Ca²⁺ entry in FpECs, acute chemical inhibition of Piezo1 was first used to determine if this was Piezo1 mediated. As such, the Ca²⁺ response to Yoda1 was measured in the presence or absence of gadolinium (Gd³⁺). This is a small molecule inhibitor of the Piezo1 channel pore (Coste et al., 2010). Pre-treatment with Gd³⁺ significantly inhibited the Yoda1-evoked Ca²⁺ entry. The response to Yoda1 was not completely abolished after Gd³⁺ at 30 or 100 μ M, although at the higher concentration the significant difference between Yoda1 stimulation and vehicle control was lost (Figure 4.21). This suggests that Yoda1-evoked change in intracellular Ca²⁺ is Piezo1-dependent. However, Gd³⁺ is non-specific and is a blocker of other cationic and Ca²⁺-selective channels, including Piezo2 (Coste et al., 2010). Given the lack of more specific Piezo1 channel antagonists, this was further investigated using Piezo1 siRNA for more selective inhibition.

Prior to performing the Ca²⁺ measurements, images of the FpECs after Piezo1 knockdown or control treatment were taken (Figure 4.22A-C). There were no visible morphological changes or differences in confluency between the conditions. After treating FpECs with an initial Piezo1 siRNA sequence, P1.91, the response to Yoda1 was once again strongly suppressed (Figure 4.22D and E). However, concerns were raised about off-target effects of this siRNA. Work performed in our laboratory by Marjolaine Debant and Vincenza Caolo identified P1.85 as being more specific. As such, the Yoda1 stimulation experiments were repeated using this sequence. After this Piezo1 knockdown the response to Yoda1 was similarly reduced, suggesting that the Yoda1 effect does indeed depend on Piezo1 (Figure 4.22F and G).

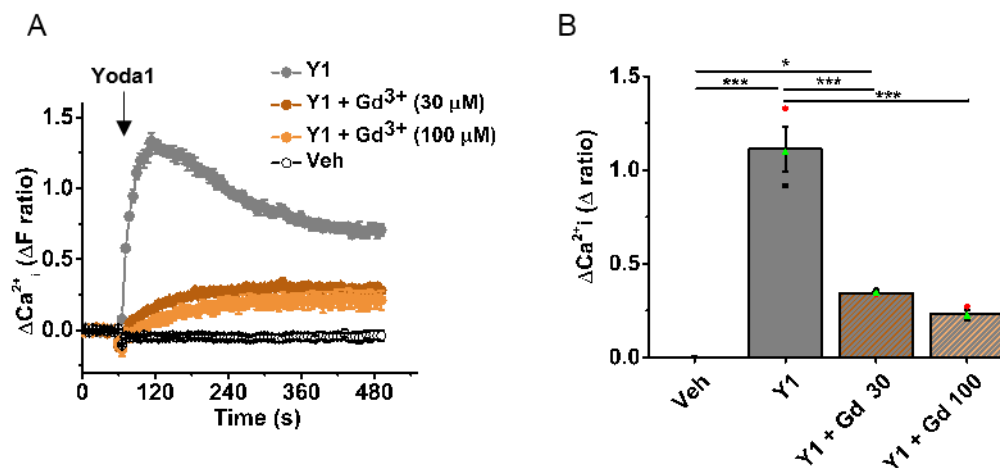


Figure 4.21. Yoda1 induced Ca^{2+} entry in FpECs is inhibited by the Piezo1 channel antagonist, Gd^{3+} . A., Example Ca^{2+} measurement trace showing reduced intracellular Ca^{2+} response to Yoda1 (Y1) after pre-treatment with the Ca^{2+} channel blocker Gd^{3+} at concentrations of 30 or 100 μM (AGA samples, $n = 3/N = 3$: LM27, LM33, LM35). B., Mean \pm SEM data for the type of experiment shown A, demonstrating a significant reduction in response between Yoda1 versus Yoda1 plus Gd^{3+} application at both concentrations (30 μM $p = 9.30 \times 10^{-5}$, 100 μM $p = 3.42 \times 10^{-5}$). No significant difference in intracellular Ca^{2+} response between vehicle control and Yoda1 plus Gd^{3+} 100 μM ($p = 0.08$). B: ANOVA.

Ionomycin was used as a positive control, evoking Ca^{2+} entry in both control siRNA- and Piezo1 siRNA-treated cells to the same degree (Figure 4.22H, I). This confirmed that the cells treated with Piezo1 siRNA are viable and have equivalent Ca^{2+} content. Furthermore, the responses to Yoda1 after Piezo1 knockdown remained significantly reduced after the peak intracellular Ca^{2+} entry data were normalised to that of ionomycin under each experimental condition. Taken together these data suggest that Piezo1 channels are a major Ca^{2+} entry mechanism in FpECs, that can be blocked by either genetic disruption of Piezo1 expression or chemical inhibition of channel function.

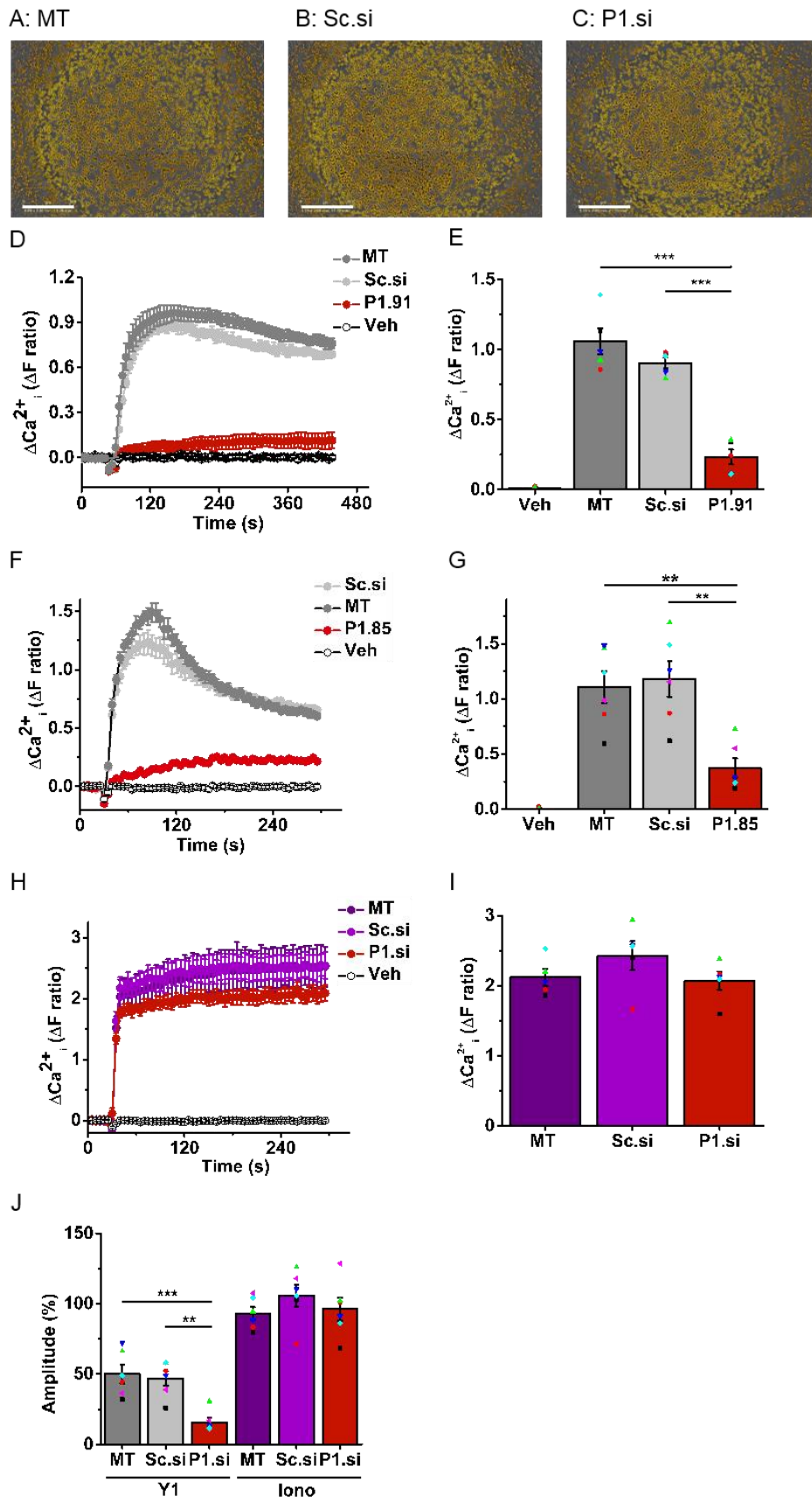


Figure 4.22. Yoda1 induced Ca²⁺-entry in FpECs is inhibited by Piezo1 knockdown.

A, B, C., Example images showing FpECs had the same morphological appearance and confluency at 48 hours post mock transfection (MT), control siRNA (Sc.si) or Piezo1 siRNA (P1.si) knockdown, respectively. Images taken prior to Ca²⁺ measurements (AG control sample LGI011, cell mask applied, scale bars 900 µM). D., Example Ca²⁺ measurement trace in FpECs showing reduced intracellular Ca²⁺ response to Yoda1 (5 µM, application at 30 seconds) after transfection with 20 nM of Piezo1 siRNA 91 (n = 3). E., Mean ± SEM data for the type of experiment shown in D, showing a significant difference in response to Yoda1 between the both the MT FpECs and P1.si.91 treated cells, and Sc.si versus Piezo1 knockdown (p = 9.11 x10⁻⁷, p = 1.02 x10⁻⁵, respectively, n = 3). F., As for D, showing a reduced response after transfection with 20 nM of Piezo1 siRNA 85, versus MT or Sc.si-transfected FpECs (LGI008, N = 3). G., Mean ± SEM data for the type of experiment shown in F, showing a significant difference in response to Yoda1 between the both the MT FpECs and P1.si.85 treated cells, and Sc.si versus Piezo1 knockdown (p = 0.0039, p = 0.0016, respectively (n = 6/N = 3: LGI079, LGI046, LGI050, LGI013, LGI011, LGI008). H., As in (D) but with application of 10 µM ionomycin or its vehicle (Veh.) I., Mean data for the type of experiment in H, showing no significant difference in the response ionomycin after treatment with Pi.si.85 (n = 5/N = 3: LGI079, LGI046, LGI050, LGI013, LGI011). J., The response to Yoda1 remains significantly reduced after Piezo1 knockdown when these data are normalised to ionomycin (versus MT p = 0.0039, versus Sc.si p = 0.0016, samples as for I). E, G, I, J: ANOVA.

4.6.2 Yoda1-induced Ca²⁺ is reduced in FpECs from SGA placentas

The change in intracellular Ca²⁺ after the application of Yoda1 was initially measured in FpECs cultured from the healthy placentas (AGA). Increasing doses of Yoda1 were applied to the cells, alongside ionomycin as a positive control (Figure 4.23). This experiment was repeated in FpECs from the SGA placentas, with Ca²⁺ traces for individual patient samples shown in Figure 4.24. The dose-dependent response appeared less consistent in the samples from the SGA group. To aid comparison

between the groups, the data presented in these figures has had the baseline subtracted, and is therefore zero. When the absolute baselines from the SGA and AGA groups were compared, there was no significant difference in baseline between the groups (Figure 4.25). The possibility of an interaction between the radiometric dye Fura-2 AM, extracellular Ca^{2+} solution, and the Yoda1 compound was considered. As such, a Ca^{2+} recording was made in the presence of two concentrations of Yoda1, but without any cells. In the absence of FpECs, Figure 4.25D demonstrates that there was no response to Yoda1.

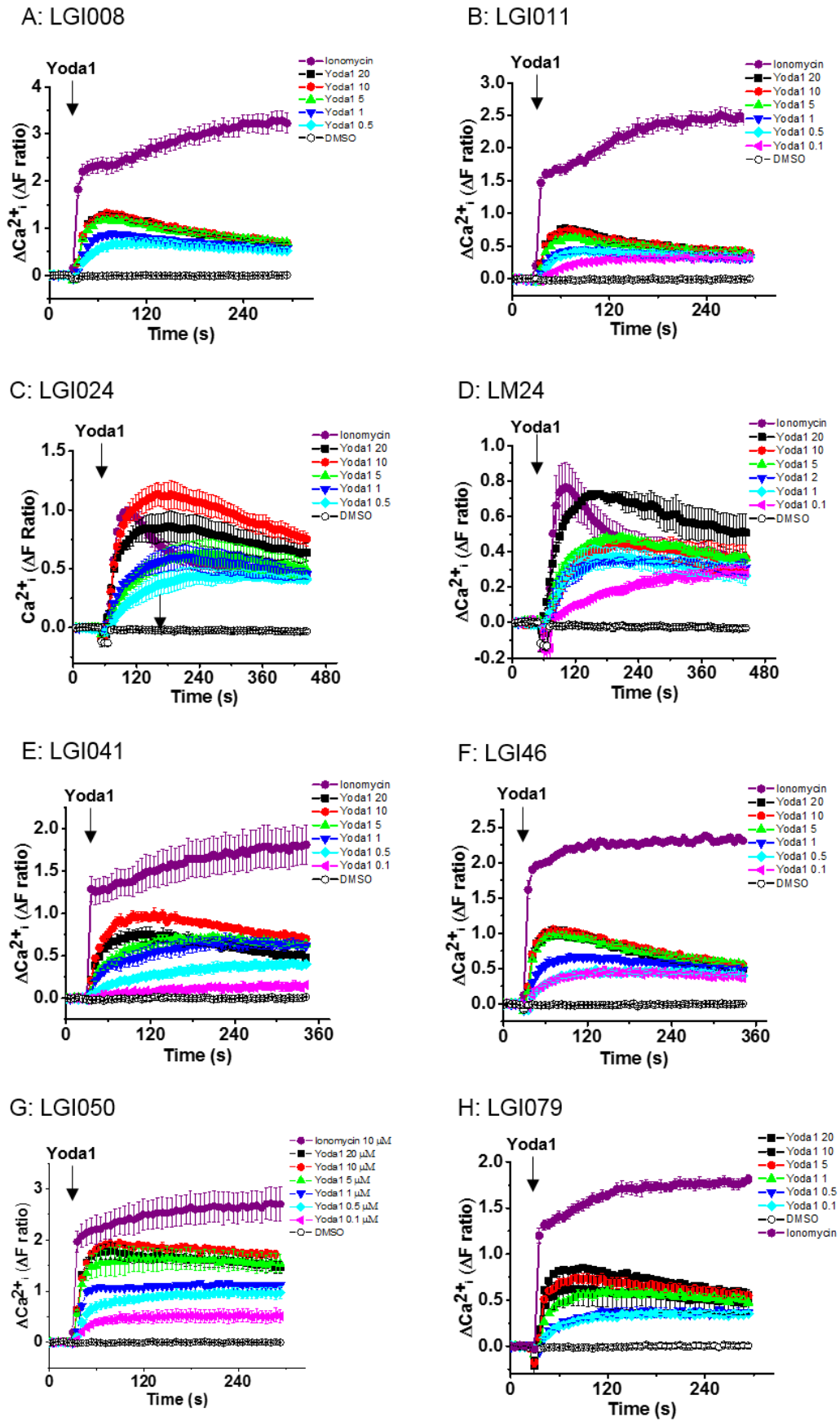


Figure 4.23 Example Ca^{2+} measurement traces from AGA FpECs in response to Yoda1 stimulation.

Data from eight individual patient samples in the AGA group, with three replicate wells per Ca^{2+} trace ($n = 1/N = 3$) per graph. These data show a consistent dose-dependent rise in intracellular Ca^{2+} in response to Yoda1, applied at 30 seconds. A large magnitude increase is observed in response to ionomycin ($10 \mu\text{M}$) applied at 30 seconds.

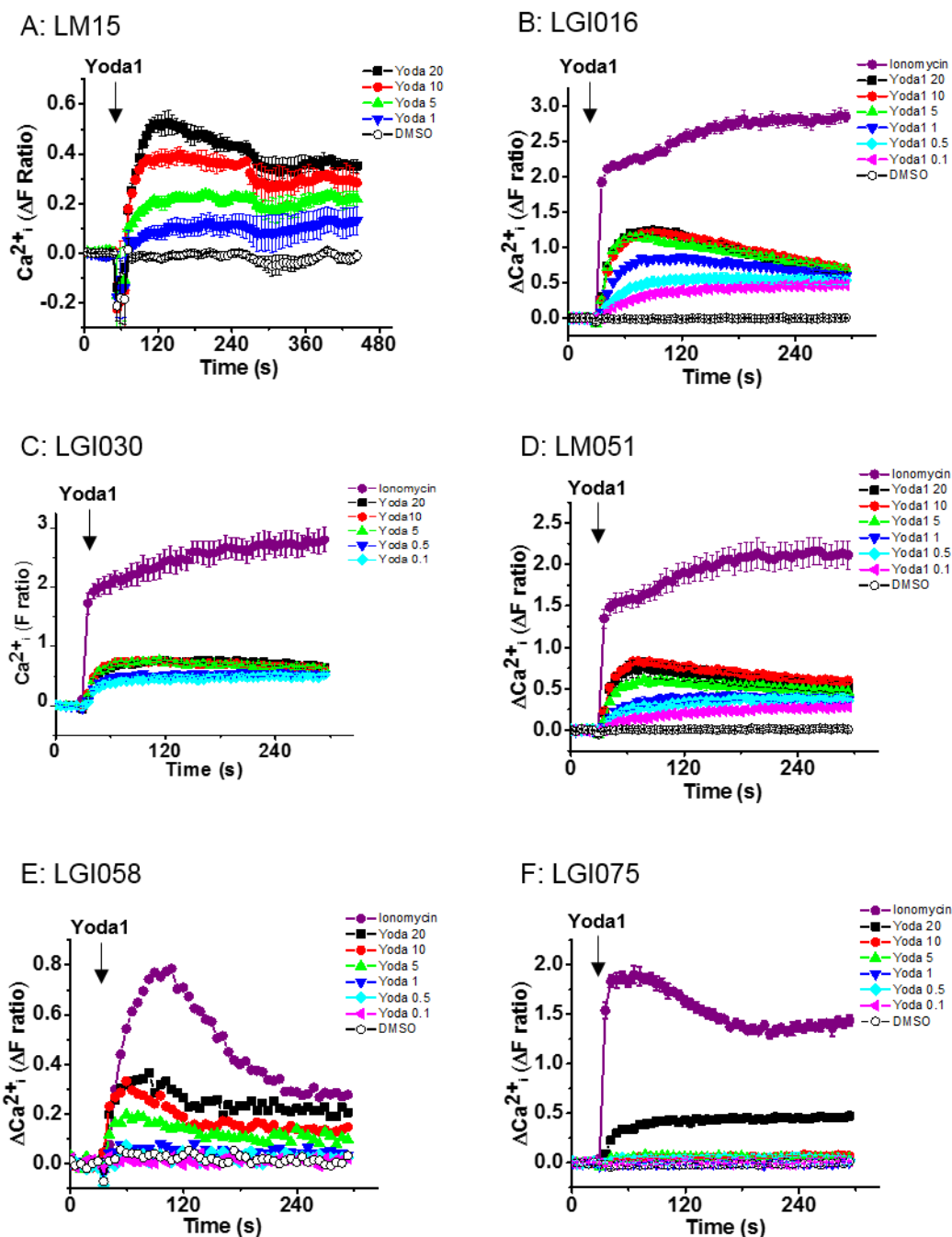


Figure 4.24 Example Ca^{2+} measurement traces from SGA FpECs in response to Yoda1 stimulation.

Data from six individual patient samples in the SGA group, with three replicate wells per Ca^{2+} trace ($n = 1/N = 3$) per graph. These data show a dose-dependent rise in intracellular Ca^{2+} in response to Yoda1 applied at 30 seconds, although with less consistency than the AGA samples shown in Figure 4.23. A larger magnitude of response is observed after the application of ionomycin ($10 \mu\text{M}$) at 30 seconds.

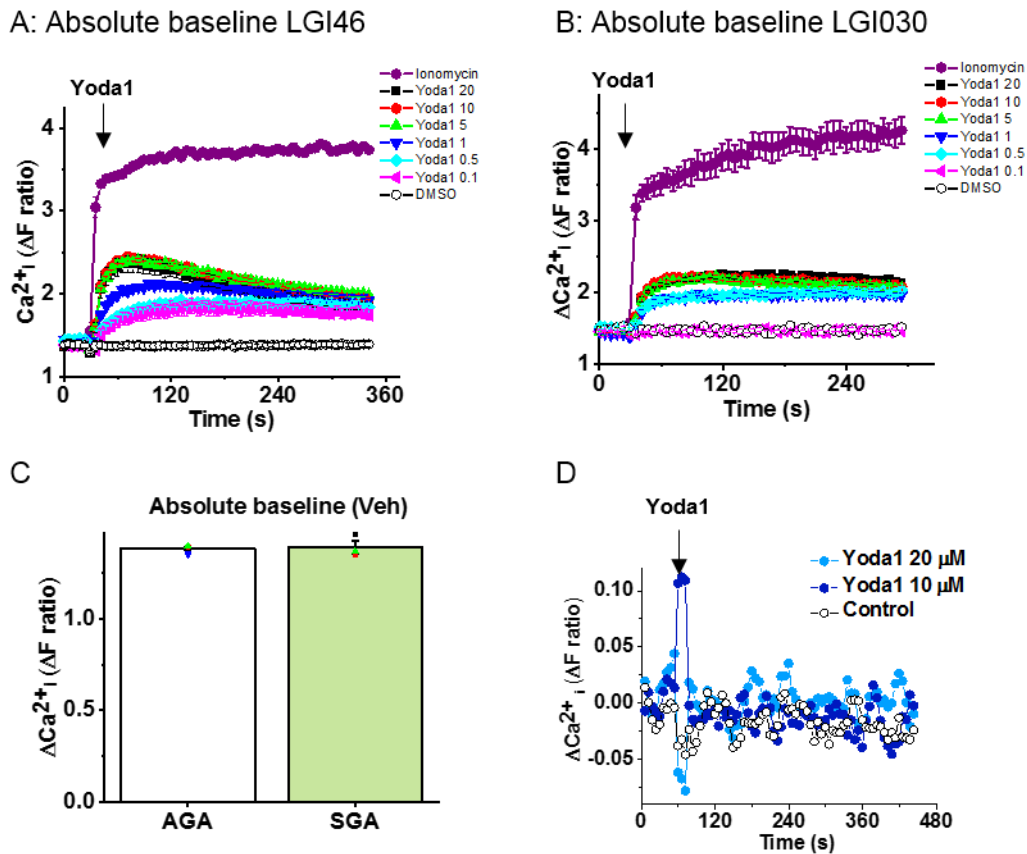


Figure 4.25. The baseline of Ca^{2+} measurement traces does not differ between healthy or SGA FpECs, and there is no Yoda1 response in the absence of FpECs.

A, and B., Example Ca^{2+} measurement traces from an AGA control (LGI046) and an SGA FpEC sample (LGI030) showing the absolute baseline. C., Pooled data showing no significant difference in absolute baseline (AGA $n = 8/N = 3$, SGA $n = 6/ N = 3$, ANOVA). This was determined by the mean baseline over 20 seconds of the experiment prior to Yoda1 application. D., No change in intracellular Ca^{2+} with Yoda1 stimulation in the absence of FpECs.

When these data were pooled, the response to all of the dose of Yoda1 in the SGA samples appeared reduced in comparison to the AGA controls (Figure 4.26A). This is highlighted in Figure 4.26B, which hints at a reduction in the response to 5 μM of Yoda1 response, although this is not significant ($p = 0.197$). These data were further investigated by normalising to the responses to ionomycin. The pattern again shows a reduction in the response to Yoda1 in the SGA group. This was significant at 5 μM and 1 μM of Yoda1 (indicated by the asterisks on Figure 4.26C, $p = 0.029$ and $p = 0.025$, respectively). As a positive control, there was no significant difference in the maximal response to ionomycin (10 μM) between the groups (Figure 4.26D).

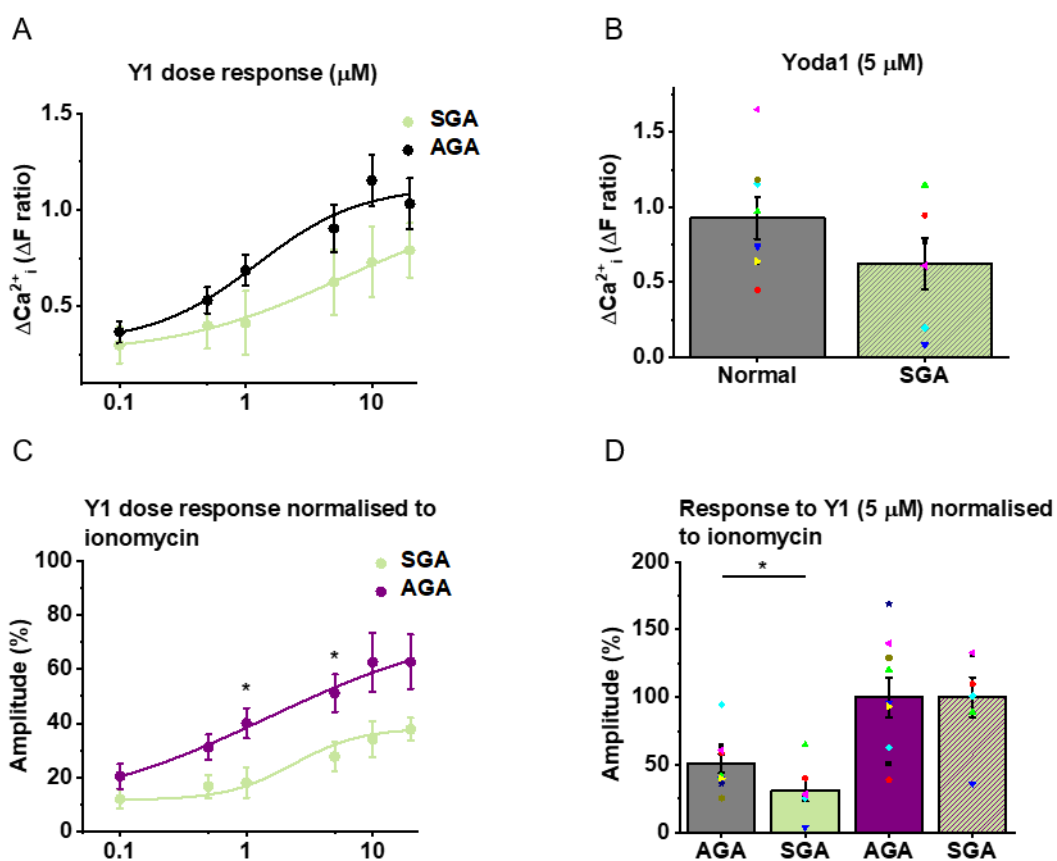


Figure 4.26 Pooled data showing reduced Yoda1-evoked Ca^{2+} entry in SGA FpECs.

A., Dose response curve showing no significant difference between AGA and SGA cells at each dose of Yoda1. B., Data as for A., showing the response to 5 μM of Yoda1, unpaired t test. C., Data as for A., normalised to the response to ionomycin 10 μM . Significant differences between AGA and SGA groups at 5 μM

and 1 μM of Yoda1 ($p = 0.029$ and 0.025 , respectively). D., No difference in response to ionomycin between the groups. Significant difference in response to Yoda1 5 μM between groups, when normalised to ionomycin. AGA $n = 8/N = 3$: LGI 008, LGI011, LM24, LGI024, LGI041, LGI046, LGI050, LGI079, SGA group $n = 6/N = 3$: LM15, LGI016, LGI030, LGI042, LGI051, LGI058, LGI075, ANOVA.

4.7 Expression of additional mechanosensors in the placenta

The aim of this PhD project has been to investigate mechanosensing in placental vasculature by focusing on Piezo1. Nonetheless, the presence of other mechanosensors in the placenta was considered, although these were not studied in detail as part of this project.

4.7.1 Expression of *PIEZO2* in the placenta

PIEZO1 expression was readily detected in FpECs and whole placental tissue, as presented in 4.3. As such, whether mRNA from *PIEZO2* was also expressed in the placenta was investigated. Amplified QPCR products from FpECs corresponding to the expected size of *PIEZO2* were initially demonstrated using gel electrophoresis (Figure 4.27A). Comparing the relative abundance of *PIEZO2* between the FpECs in AGA and SGA groups, suggested that expression may be lower in the SGA samples. However, the data had wide ranges, and the comparison was not significant.

In whole placental tissue, *PIEZO2* was detected at much later QPCR cycles compared to FpECs, indicative of low abundance (Figure 4.27D). This is reinforced by reviewing an example minus reverse transcriptase mean Ct value of 33.43 (AGA sample LGI096). The relative abundance of *PIEZO2* was found to be markedly lower than that of *PIEZO1*, in both FpECs and whole villous tissue (Figure 4.27G and H). As such, Piezo2 channels appear to present in fetoplacental endothelium, but no further conclusions regarding its potential role as a mechanosensor can be drawn.

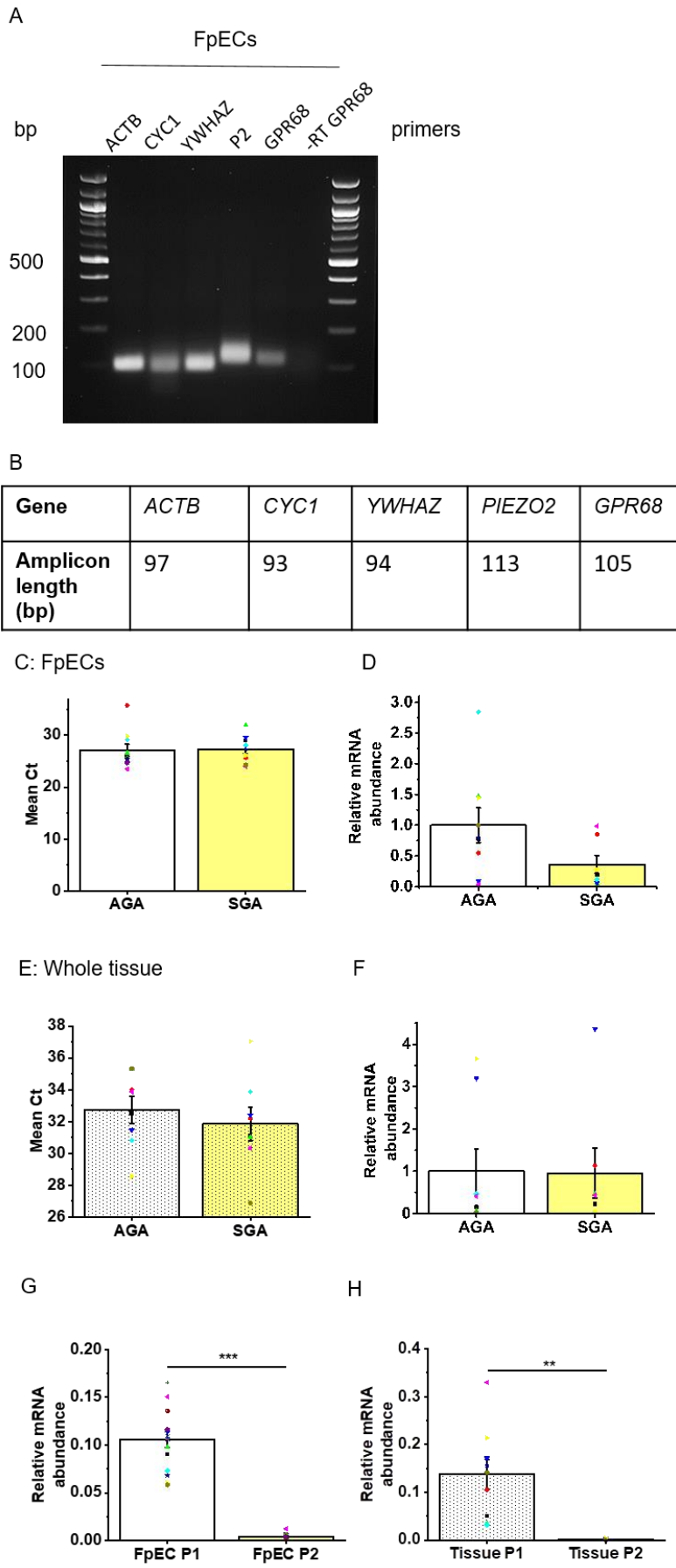


Figure 4.27 *PIEZO2* is expressed in FpECs and whole villous tissue.

A., Gel electrophoresis image of amplified products following QPCR, showing reference genes (*ACTB*, *CYC-1*, *YWHAZ*), *PIEZO1* and *GPR68*. Abbreviations: bp base pair, - RT minus reverse transcriptase control for *GPR68*. Gel produced from AGA sample LGI069.

B., Expected amplicon size (bp). C., Summarised mean \pm SEM Ct values for *PIEZO2* expression in FpECs. D., Summarized mean \pm SEM QPCR data showing no significant difference in *PIEZO2* between groups (AGA n = 9/N = 2: LM4, LM8, LGI009, LGI011, LGI037, LGI046, LGI069, LGI079, LGI096. SGA n = 7/N = 2: LM12, LGI016, LGI051, LGI067, LGI063, LGI075, LGI030, two additional samples were removed from the SGA group for being statistical outliers). E., As for C for *PIEZO2* expression in whole tissue. F., As for D, showing no significant difference in the expression of *PIEZO2* in whole tissue from AGA or SGA placentas (AGA n = 8/N = 2: LGI037, LGI043, LGI045, LGI065, LGI069, LGI071, LGI046, LGI082. SGA n = 7/N = 2: LGI004, LGI005, LGI026, LGI038, LGI051, LGI058, LGI063, one additional sample was removed for being a statistical outlier. G., Summarized mean \pm SEM QPCR data showing significantly less *PIEZO2* expression in FpECs, when compared to the relative abundance of *PIEZO1* ($p < 0.0001$). H., As for G., demonstrating that the relative abundance of *PIEZO2* is also less than *PIEZO1* in whole tissue ($p = 0.0025$). C-H: unpaired *t* test.

4.7.2 Expression of *GPR68* in the placenta

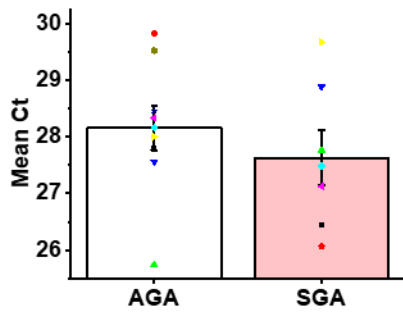
As discussed in the introduction to this chapter, *GPR68* is a G-protein coupled receptor which has been identified as a mechanosensor. After performing QPCR on FpECs, amplified products corresponding to the expected size of *GPR68* were demonstrated using gel electrophoresis (Figure 4.27A). This suggests that *GPR68* is expressed in the fetoplacental endothelium, and by extension, that there are mechanosensors present in FpECs in addition to Piezo1.

When FpECs from the AGA and SGA groups were compared, relative abundance was significantly higher in the SGA samples (Figure 4.28B). This supports the hypothesis that in the SGA placenta, elevated FSS leads to upregulation of mechanosensor expression.

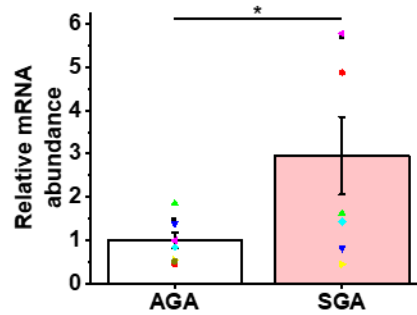
However, there was no significant difference in expression between whole villous tissue from AGA versus SGA placentas.

The relative abundance of *GPR68* was lower than that of *PIEZO1* in both FpECs and whole villous tissue (Figure 4.28E and F). The mean Ct values for *GPR68* in FpECs and whole villous tissue are shown in Figure 4.28A and C. For comparison, example minus reverse transcriptase Ct values were 43.72, or undetectable (AGA FpEC sample LGI096). This may suggest that although additional mechanosensors are present in the placenta, Piezo1 is dominant. However, further functional data on the role of GPR68 are required.

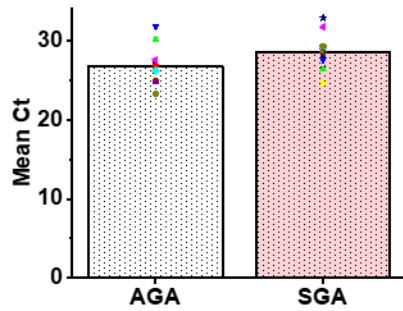
A. FpECs



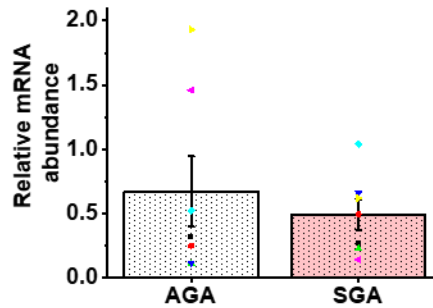
B.



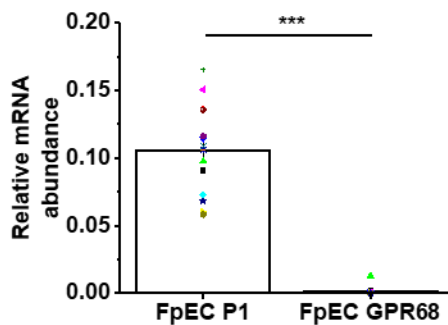
C: Whole villous tissue



D



E



F

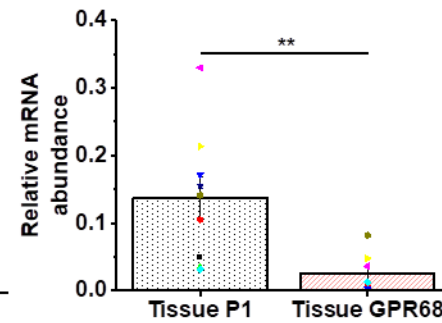


Figure 4.28. Increased mRNA expression of GPR68 in SGA FpECs

A., Summarised mean \pm SEM Ct values for *GPR68* expression (AGA $n = 8/N = 2$: LGI008, LGI037, LGI011, LGI035, LGI046, LGI079, LGI096, LGI103, LGI069 was removed for being a statistical outlier; SGA $n = 7/N = 2$: LM12, LGI016, LGI030, LGI038, LGI051, LGI063, LGI067). B., Summarized mean \pm SEM QPCR data for fold-change showing significant difference in *GPR68* between AGA and SGA FpECs ($p = 0.02$, samples as per 1.27A). C., As for A, showing mean Ct values for *GPR68* expression in whole villous tissue from AGA and SGA placentas. D., As for B, demonstrating no significant difference in *GPR68* relative abundance between AGA and SGA whole villous

tissue (AGA n = 8/N = 2: LGI022, LGI037, LGI043, LGI045, LGI046, LGI065, LGI069, LGI071. SGA n = 7/N = 2: LGI004, LGI005, LGI026, LGI038, LGI051, LGI055, LGI063). E., Summarized mean \pm SEM QPCR data showing significantly less *GPR68* expression in FpECs, when compared to the relative abundance of *PIEZO1* ($p < 0.0001$). F., As for E., demonstrating that the relative abundance of *GPR68* is also less than *PIEZO1* in whole tissue ($p = 0.0067$). A-F: Unpaired *t* test.

4.8 Discussion

PIEZO1 was consistently detected in all placental samples, including mRNA obtained from early as well as term pregnancy. Alongside the impact of flow on the endothelium, evidence is accumulating to suggest that FSS is critical for trophoblast migration and remodelling in early pregnancy. Trophoblast mechanosensitivity has been demonstrated by flow-induced production of PIGF from cells in culture (Lecarpentier et al., 2016a). A dose-dependent relationship between exposure to FSS and the trophoblastic response suggests that flow may be an important regulator of angiogenesis. As discussed in the Introduction, a careful balance of force is therefore required to enable the migration, remodelling and angiogenesis to take place without damaging delicate developing structures. The mechanisms underpinning how FSS is sensed, transduced and regulated by the trophoblast and endothelial cells in early pregnancy requires further understanding. A placental culture model using BeWo cells has also been used to demonstrate that FSS induces intracellular Ca^{2+} entry (Miura et al., 2015). The authors show that after knocking down the Ca^{2+} ion channel, TRPV6, a reduction in FSS-evoked Ca^{2+} entry occurs. However, the response was not completely abolished by TRPV6 depletion, raising the possibility of other flow-dependent mechanisms of Ca^{2+} influx into placental cells.

Piezo1 has previously been demonstrated in murine embryonic stem cells, with the implication that it has a developmental role in cell differentiation (Del Marmol et al., 2018). The research presented in this thesis determining the presence of *PIEZO1*, *PIEZO2* and

GPR68 mRNA in human early pregnancy tissue are novel findings. The subsequent experiments on term FpECs shown in Figure 4.16 and Figure 4.21 show that Piezo1 is a major Ca^{2+} entry mechanism and is important for the normal response to FSS. Future research is therefore required to establish the role of Piezo1 channels in early pregnancy.

Fundamental questions are to determine whether:

- *PIEZO1* mRNA is expressed in endometrial epithelial cells, and the implications for pregnancy implantation
- Piezo1 has a mechanosensory role in placental epithelial, as well as endothelial cells
- Piezo1 is important for angiogenesis in early placental development, including the interplay with VEGF activity
- Piezo2 and GPR68 are important mechanosensors in early pregnancy

If a suitable antibody were available, immunohistochemistry would have been performed to localise Piezo1 on placental tissue sections also stained for vascular and trophoblast markers. Previous attempts at immunohistochemistry using anti-Piezo1 in our laboratory resulted in widespread non-specific staining. This also meant that immunostaining could not be used to compare Piezo1 abundance and localisation in the AGA versus SGA tissue samples. To identify Piezo1 proteins using western blotting, two different anti-Piezo1 antibodies were tried (Proteintech and Beec4) which are presented in Figure 4.12 and Figure 4.13, respectively. Although the Piezo1 band is identifiable, other proteins were non-specifically labelled by the anti-Piezo1 antibody, as indicated. Future Piezo1 studies would therefore benefit from the development of a more specific antibody.

Alongside identifying *PIEZO1* mRNA in FpECs and whole villous tissue, laboratory member Sara Ibrahim measured the relative abundance of Piezo1 in tissue samples taken from the basal side of the placenta, the chorionic plate and chorionic membrane. In three samples from the AGA group, *PIEZO1* was consistently expressed at each site, with an appropriate band visible on gel electrophoresis. When normalised to the mean of *ACTB*, there were no significant differences in expression between the areas of

placenta sampled. The novel finding of *PIEZO1* in the chorionic membrane confirms that Piezo1 is present in placental epithelial tissue. The significance of this finding with regards to the functional importance of the chorionic membrane in withstanding mechanical pressure as pregnancy progresses, remains to be determined.

Without the use of immunohistochemistry, it was important to use other tools to demonstrate Piezo1 presence in the placenta. As such, ECs were freshly isolated from placental arteries, which showed dominant FSS-activated Piezo1 channels. Patch-clamp electrophysiology experiments on these cells enabled us to obtain the unitary conductance and thus Piezo1 signature of 25 pS. The freshly isolated cells were obtained through vessel dissection from the chorionic plate arteries and are therefore from larger capacity vessels than the cultured FpECs. The properties of these cell types may therefore differ. However, these data demonstrate consistency in finding Piezo1 presence and channel activity in the placenta.

The patch-clamp electrophysiology study showed that freshly isolated arterial cells respond to mechanical force. This is in addition to the results shown in Figure 3.10, demonstrating that the application of FSS to cultured FpECs results in their alignment in the direction that flow was applied. Using siRNA was therefore a useful tool for further investigating the functional significance of Piezo1 in cultured cells. When Piezo1 is depleted in FpECs, the response to FSS is diminished. As shown in Figure 4.16 and Figure 4.17, this was apparent when cells no longer aligned in the direction of flow, nor exhibited a flow-induced Ca^{2+} entry in single cells. This suggests the importance of Piezo1 channels in shear stress sensing and the associated Ca^{2+} entry of FpECs. This is supported by the data demonstrating that exposing FpECs to FSS increased *PIEZO1* expression (Figure 4.11).

Our group previously used tagging with green fluorescent protein (GFP) to demonstrate that exposure to FSS changes the subcellular location of Piezo1 in HUVECs. In static conditions, the channels were broadly distributed but when exposed to flow, there was accumulation at the leading apical lamellipodia (Figure 4.29). These apical processes

are characteristic of the early stage of endothelial cell alignment, necessary for EC migration as part of vascular remodelling. GFP tagging has previously been used to demonstrate that ECs under flow migrated and polarised to form new focal adhesions in the direction of flow (Li et al., 2002). The alignment data presented here are the first to demonstrate a role for Piezo1 in the molecular dynamics of 'mechanotaxis' in the placenta. I propose that FSS-sensing by Piezo1 channels promotes FpEC organization and alignment in the direction of flow. Future research is therefore required to determine whether mechanotaxis is dysregulated in FpECs from SGA placentas.

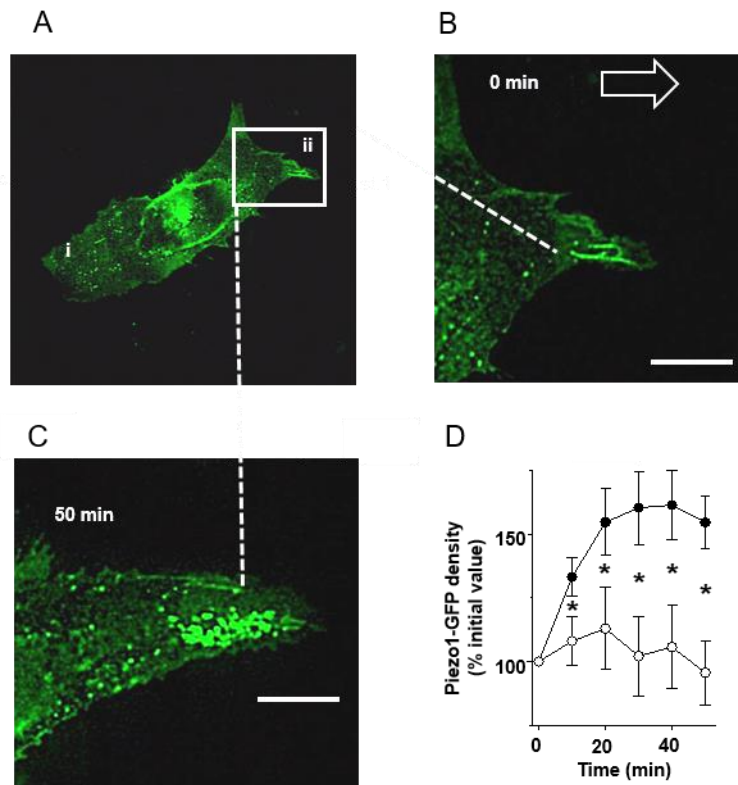


Figure 4.29 FSS-evoked redistribution of Piezo1 in HUVECs (adapted from Li et al., 2014, extended data Figure 6). A., Piezo1-GFP in a single HUVEC with a box indicating the region expanded in images B and C. Shear was applied at 15 dyne/cm² in a microfluidic chamber, with images taken at time point 0 (B) and 50 minutes (C). The direction of FSS is indicated by the open arrow. In image A, i indicates the part of the cell that became trailing after application of FSS and ii that which became leading. Scale bars 10 μ m. D., Analysis of experiments of the type shown in A, B and C (n=8 per data point except for n=7 at 50 min) where open, and closed circles represent the trailing and leading edges of the cell, respectively (Li et al., 2014).

To shed further light on the mechanism by which FSS and subsequent Piezo1 channel activation led to HUVEC alignment, our group previously sent lysates exposed to flow for proteomic analysis (Li et al., 2014). As anticipated, those exposed to FSS had higher cytoskeletal actin and focal adhesion proteins. Proteomic data also showed significant effects on calpain-2 and multiple substrates, including actinin, filamentin, integrin and

tubulin. These proteins are important for cytoskeletal structure and focal adhesions. In the Piezo1 knockout mouse used by our group, calpain activity was significantly less in Piezo1^{-/-} compared with Piezo1^{+/+} embryos. Furthermore, the increase in calpain activity in response to FSS was abolished by a Piezo1 channel inhibitor. HUVEC alignment was also inhibited in the absence of extracellular Ca²⁺ and the presence of calpain inhibitors. This suggests that calpain activation in coupling FFS-evoked Ca²⁺ entry through Piezo1 channels is important for endothelial organisation and alignment via proteolytic cleavage of cytoskeletal and focal adhesion proteins.

The importance of this Ca²⁺-activated proteolytic enzyme was also demonstrated in a mouse model, whereby calpain disruption resulted in abnormal vascular development in the yolk sac at mid-gestation (Arthur et al., 2000). Calpain may have also a role in embryo implantation, as demonstrated in a pregnant rat model. In this study, calpain-2 was found to be concentrated along the basal cell surface of rat uterine luminal epithelial cells, with a marked increase in activity during implantation. This coincided with disassembly of the focal adhesion proteins talin, paxillin, and integrin $\beta 1$ and $\beta 3$ (Kaneko et al., 2008). Equally, inhibiting calpain-2 significantly reduced the number of implantation sites in the uterine horns of the pregnant rats (Kaneko et al., 2014) (Figure 4.30). Calpain activation may therefore facilitate the detachment of uterine luminal epithelial cells for embryo invasion in implantation (Kaneko et al., 2014).



Figure 4.30 Effect of intra-peritoneal administration of Calpain-2 inhibitor on days 4-7 of pregnancy (Reproduced from Kaneko et al. 2014). Uterine horns from a rat model were excised on day 8 of pregnancy. Arrows point to implantation sites (left image), with no implantation sites seen when the inhibitor was used (right image) (Kaneko et al., 2014).

In human disease, dysregulated calpain proteolytic activity has been linked to atherosclerosis and inflammation in vascular disease, and tumorigenesis in breast cancer and glioblastoma (Miyazaki and Miyazaki, 2018, Vo et al., 2019, Grieve et al., 2016). Whether Piezo1 is involved in triggering calpain-2 activity in the placenta and/or uterine lining, and the relevance of these findings for implantation, early placentation and subsequent placental vascular function remains to be understood. It can therefore be hypothesised that abnormal Piezo1 channel activity and downstream alterations in calpain could result in abnormal implantation and placental insufficiency.

The evidence suggestive of increased FSS in the SGA placenta was discussed in Chapter 1, 1.6.3.2 of this thesis. Briefly, this is thought to occur due to abnormal architecture of the placental vascular tree, in combination with endothelial dysfunction, and other factors including hypoxia and circulating vasoconstrictors (Kingdom et al., 2000). This is supported by data from computerised models, which demonstrated

increased transmural pressure in small vessels, generating greater FSS forces (Tun et al., 2019). The data from FpECs displayed in Figure 4.9 shows that *PIEZO1* expression is increased in SGA. As such, I propose that the increased FSS occurring in SGA causes *PIEZO1* upregulation. This supports the hypothesis that Piezo1 is an important mechanosensor in placental vasculature. Furthermore, after probing FpEC lysates with Piezo1 antibody, increased band intensity was noted after FSS exposure (Figure 4.11). However, further western blotting to compare Piezo1 protein between the AGA and SGA samples was limited due to poor antibody specificity.

The lack of significant difference in *PIEZO1* expression between AGA and SGA whole villous tissue samples was observed, in contrast to the results in FpECs. This is alongside finding the same pattern of expression for the mechanosensor, GPR68, where the significant increase in expression in FpECs from SGA placentas was not replicated in whole tissue. The following hypotheses require consideration:

1. *Raised FSS associated with placental insufficiency predominantly affects the endothelium*

There is therefore an upregulation of mechanosensor mRNA in ECs, not seen in other placental cell types. As such, the significant increase in endothelial expression of *PIEZO1* and *GPR68* is lost in whole tissue samples.

2. *PIEZO1 gene expression is higher in endothelium than placental epithelial tissue*

The ability to detect changes between two clinical groups will also depend on the abundance of gene expressed. As such, I hypothesised that the relative abundance of *PIEZO1* was higher in FpECs than in whole villous tissue. Analysis revealed that *PIEZO1* was detected significantly earlier in the QPCR reaction in the endothelium ($p < 0.0001$). However, there was no evidence of a difference in the relative abundance of *PIEZO1* when comparing FpECs and whole villous tissue (Figure 4.31). This comparison is limited given that whole villous tissue comprises multiple cell types, and underwent a different experimental protocol to cultured FpECs.

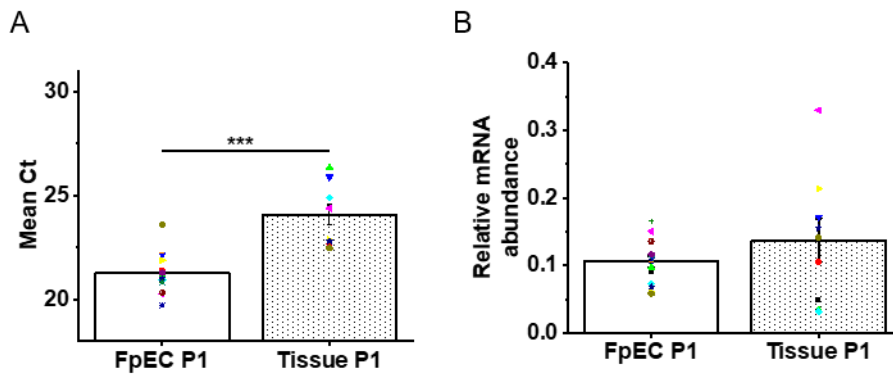


Figure 4.31 Expression of *PIEZO* in FpECs and whole villous tissue. A., Summarised mean \pm SEM Ct values for *PIEZO1* expression in FpECs and whole villous tissue from AG control samples, showing significantly lower Ct values for the cells, $p < 0.001$ (FpECs $n = 15/N = 2$: LM4, LM7, LM8, LM9, LM23, LGI008, LGI011, LGI035, LGI037, LGI041, LGI045, LGI046, LGI069, LGI079, LGI096. Tissue $n = 9/N = 2$: LGI022, LGI037, LGI043, LGI045, LGI046, LGI065, LGI069, LGI071, LGI082). B., Summarized mean \pm SEM QPCR data showing no significant difference in *PIEZO1* between FpECs and whole villous tissue. Samples as for A. A and B: unpaired *t* test.

3. *SGA placentas are less vascularised than AGA placentas, so the proportion of endothelial PIEZO1 expression is reduced*

In Figure 3.3, data were presented showing significantly reduced expression of the arterial and venous markers, ephrin-B2 (*EFNB2*) and ephrin-B4 (*EFNB4*) in the SGA tissue. This suggests that the SGA placental samples were less vascularised than the AGA controls. It follows that the abundance of Piezo1 would be lower in the presence of less endothelium. This is in comparison to the pure FpEC cultures. As such, in whole tissue samples from SGA, Piezo1 expression may still be upregulated, but this is masked by an overall reduction in vasculature. This hypothesis is supported by evidence discussed in Chapter 1, section 1.4.6 where placental insufficiency is characterised by reduced numbers of vascularised villi, impaired branching and distal villous hypoplasia on histology (Kingdom et al., 2000, Mifsud and Sebire, 2014). Although *CD31* expression

was not significantly different between the AGA and SGA placentas in my data, this could be demonstrative of villous immaturity and impaired angiogenesis in placental insufficiency (Mando et al., 2016, Junaid et al., 2014). For example, both placental endothelial progenitor cells and mature endothelium express CD31 (Gumina and Su, 2017). Furthermore, a small study of growth-restricted placentas found that human placental mesenchymal stem cells showed reduced ability to differentiate towards endothelial lineage when compared to cells from healthy controls (Mando et al., 2016). As such, similar *CD31* mRNA expression between groups may not reflect the altered vascular environment in placental insufficiency. As such, future research would benefit from immunohistochemistry with specific markers to identify the proportion of mature versus immature endothelial cells, and quantify nonvascular-associated CD31, such as stroma, and in vessels. This is alongside identifying Piezo1 on AGA and SGA placental samples using an appropriate antibody.

To compare Piezo1 channel activity in the normal versus SGA FpECs, Yoda1 was used as a chemical agonist. Despite an increase in *PIEZO1* mRNA in the SGA group, the response to Yoda1 was diminished, as shown in Figure 4.26. Potential hypotheses have been considered, and include:

1. *Abnormal Piezo1 channel function secondary to a mutation*

This could influence the subcellular localization of Piezo1, and subsequent signaling. As discussed in the Introduction chapter, both loss- and gain of function mutations in *PIEZO1* have been associated with miscarriage secondary to fetal hydrops (Lukacs et al., 2015, Fotiou et al., 2015). However, an isolated *PIEZO1* mutation may be unlikely given the broad clinical grouping of SGA used in this study. As such, future research could include sending tightly phenotyped samples for gene sequencing.

2. *Abnormal functioning of the endothelium in SGA*

For example, cells from growth-restricted placentas show reduced proliferation compared to healthy controls, despite maintained viability (Mando et al., 2016). Whether the FpECs from placental insufficiency are inherently less sensitive to stimuli remains to be determined. However, there was no difference in the response to ionomycin-evoked Ca^{2+} entry between the groups. In addition to functional changes in growth-restriction, FpECs from placental insufficiency may have structural alterations such as abnormal lipid composition of the membrane, which could therefore affect Piezo1 channel function.

3. Piezo1 channel activity being influenced by the placental environment

Placental oxygenation is known to be reduced in SGA. This has previously been demonstrated in a large data cohort ($n = 27,043$), where oxygen saturation values were calculated from umbilical cord partial pressures of oxygen (PO_2) and pH (Lackman et al., 2001). The authors found a stepwise reduction in PO_2 which correlated with birth centile. Correspondingly, the fractional oxygen extraction (OEF) values were stepwise higher in the SGA than in the AGA control group (Lackman et al., 2001). The OEF is defined as the ratio of oxygen that a tissue takes from blood in order to maintain function and morphological integrity, and is therefore a measure of the efficiency of oxygen utilization. As such, rising OEF corresponding to severity of SGA represents a compensatory drive to obtain adequate placental perfusion. This has been observed in the brain, where reduced cerebral blood flow is accompanied by a compensatory increase in the OEF to maintain normal neuronal function. However, once this capacity for compensation is utilized because the OEF is maximized, the risk of stroke is greatly increased (Liu and Li, 2016).

Whole placental vessels exhibit sensitivity to oxygen tension, which has been demonstrated on myography. In chorionic plate arteries from FGR pregnancies, increased arterial contraction was found (at 20% oxygen tension). Venous contraction was increased in hypoxia (7% and 2%) compared with veins from normal pregnancy placentas (Wareing et al., 2006b). These vessels showed enhanced thromboxane-induced contractility, which may also reflect the increase in vasoconstrictors, such as

thromboxane in growth-restricted placentas. This modified vasoreactivity of chorionic plate vessels could lead to the reduced perfusion and ischaemia-reperfusion affecting the downstream FpECs (Wareing et al., 2006b).

The effect of reduced oxygen saturation on placental endothelial cell components has been demonstrated in K⁺ channels, whose activity can be regulated by ROS and hypoxia (Wareing, 2014). The regulatory relationship between Piezo1 channel activity and hypoxia in the placenta remains to be investigated, although new data is emerging from research in other body systems, such as breast and gastric cancer (Zhang et al., 2018, Li et al., 2015). In colon cancer cell lines, Piezo1 depletion using siRNA reduced migration across a scratch wound. Correspondingly, treatment with Yoda1 enhanced cell migration, suggesting that Piezo1 may be important for tumour metastasis. As commonly found in tumour biology, HIF-1 was upregulated in the cancer cells, reflective of hypoxia. In the cancer cells treated with Yoda1, HIF-1 expression was significantly up-regulated, whereas HIF-1 α expression was significantly inhibited after Piezo1 knockdown. The authors propose that intercellular pressure in the tumour microenvironment leads to Piezo1 activation, which induces Ca²⁺-dependent signaling cascades associated with tumor cell migration.

The identification of GPR68 in FpECs and tissue from both the first and third trimester reveals that Piezo1 is not the sole placental mechanosensor. Although we do not have functional data regarding GPR68, it is possible that both Piezo1 and GPR68 contribute to FSS sensing in the placenta. Unlike *Piezo1*, *gpr*-deficient mice survive to adulthood, and the offspring appeared grossly normal. In cell lines, GPR68-dependent responses to FSS were still present after *PIEZO1* silencing, indicating that both mechanosensors can function independently (Xu et al., 2018). GPR68 is proton-dependent, whereby most activity occurs at pH 6.8 with inactivity when the pH reaches 7.8. As such, it could be expected that GPR68 would be upregulated in lactic acidosis. Figure 4.28 demonstrates increased *GPR68* mRNA in the FpECs from SGA placentas. I suggest that placental hypoxia may upregulate *GPR68* expression, alongside FSS. Whether Piezo1 and

GPR68 play additive/overlapping roles in FpECs and the functional significance of this finding remains to be determined.

4.9 Summary

- For the first time, Piezo1 has been shown to be present consistently in cultured and freshly isolated placental endothelium, and whole tissue from both early and term placenta.
- *PIEZO1* expression is increased in response to FSS, and is required for the normal response to flow in FpECs
- *PIEZO1* is upregulated in SGA FpECs. This may occur as a consequence of:
 - increased FSS secondary to vasoconstriction and altered vascular architecture in SGA
 - hypoxia in the SGA placenta – supported by finding an increase in the proton-dependent mechanosensor *GPR68* in SGA FpECs
 - reduced Piezo1 channel function in SGA FpECs, as evidenced by the reduced sensitivity to Yoda1
- *PIEZO1* upregulation may be a compensatory drive towards improving placental perfusion by increasing the fractional oxygen extraction. As such, further research is required to determine the signaling pathways downstream of Piezo1 in FpECs

Chapter 5 Interplay between Piezo1 activity, nitric oxide- and purinergic signalling in FpECs

5.1 Introduction

The data presented in Chapter 4 established the presence of Piezo1 mRNA and protein in the human placenta. Functional experiments demonstrated that Piezo1 mRNA was upregulated by FSS, and important for how FpECs respond to FSS. Our group previously investigated the downstream mechanisms using titanium dioxide trapping coupled with mass spectrometry to identify proteins affected by Piezo1 in HUVECs (Li et al., 2014). The process was performed for HUVECs cultured in both static and shear stress conditions. After Piezo1 depletion in these cells, there was a reduction in eNOS, suggesting that Piezo1 had a regulatory role in vasodilation through NO. Follow up experiments in HUVECs revealed that silencing Piezo1 also resulted in the reduction of VEGF-evoked phosphorylation of eNOS at serine 1177 - known to enhance eNOS activity (Figure 5.1) (Li et al., 2014). Similar findings were obtained in systemic endothelium, whereby VEGF-evoked phosphorylation of eNOS was abolished in aorta Piezo1 knock out mice (+/-).

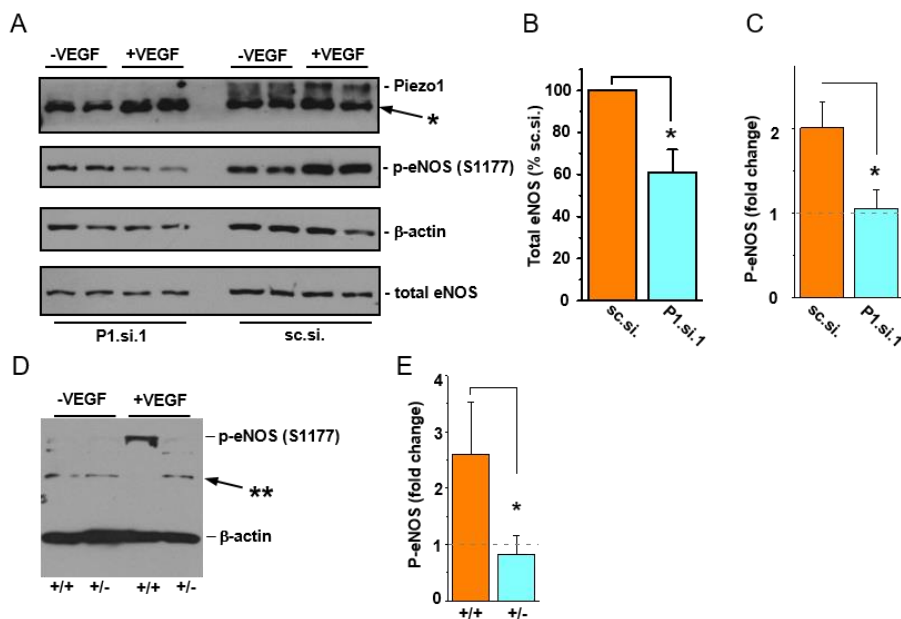


Figure 5.1 Piezo1 channel activity is coupled to eNOS.

A., Western blot for HUVEC lysates after transfection with Piezo1 siRNA (P1.si. left) or control siRNA (sc.si. right). HUVECs were treated with 30 ng/mL VEGF (+) or no VEGF (-) for 10 minutes. Lysates were probed with anti-Piezo1 antibody, antibody to phosphorylated S1177 in eNOS, anti- β -actin antibody, and antibody to total eNOS. A non-specific band in the anti-Piezo1 blot is highlighted with *. B., Quantitative data for the down-regulation of total eNOS after transfection of HUVECs with P1.si.1 (n = 6). C., Fold-change in S1177 eNOS phosphorylation (p-eNOS) evoked by VEGF as described in H. (n = 3 each). D., Western blot for VEGF (30 ng/mL) evoked S1177 eNOS phosphorylation (arrow) in aorta. Aorta was dissected from *Piezo1*^{+/+} or *Piezo1*^{+/-} littermates and allowed to equilibrate at 37 °C in culture medium without FSS for 3 hours. Aorta was exposed to VEGF (30 ng/mL) (+VEGF) or not (-VEGF) for 10 minutes, after which lysates were generated. Proteins were probed with antibody to phosphorylation at S1177 in eNOS. E, Mean data for the type of experiment shown in (D) (n = 5 for each genotype) and presented as in (C). Grey dashed line highlights 1-fold (no change). Highlights from Li et al., extended data Figure 7, A-D (Li et al., 2014).

As discussed in the Introduction chapter 1.6.3, NO is well-known as a potent vasodilator within placental vasculature (Boeldt et al., 2011). As such, the downstream response of FpECs to FSS may include activation of eNOS and subsequent NO production. This has been demonstrated in a placental perfusion model where changing haemodynamic factors (increasing viscosity or flow rate) stimulated NO release (Wieczorek et al., 1995). Increased eNOS expression was also found in ovine FpECs after exposure to FSS (Li et al., 2014).

In Chapter 4, section 4.8, I hypothesised that Piezo1 may have a role in mechanosensing in FpECs, which could be upregulated in a high FSS environment. The primary aim of this chapter was to determine whether Piezo1 channel activity leads to the downstream production of NO in FpECs from both AGA and SGA placentas.

Other extracellular or intracellular proteins may interact with, and regulate Piezo1 channels. For example, endothelial ATP release can be stimulated by flow (Wang et al., 2015). It has been suggested that Piezo1 is required for this ATP release, whereby FSS-activated Piezo1 leads to activation of the G protein-coupled receptor P2Y₂ and downstream NO production (Wang et al., 2016). Purinergic receptors have been previously been demonstrated in human placentas. P2X receptors have been identified in chorionic and umbilical vessels: P2X(4), P2X(7) and P2Y(2) in whole villous tissue, and P2X4, P2X7, P2Y₂, and P2Y6 receptors in trophoblast cells (Roberts et al., 2006, Roberts et al., 2007, Valdecantos et al., 2003). Functional activity has also been demonstrated, whereby the application of ATP caused an increase in Ca²⁺ in whole villous fragments (Roberts et al., 2007). Despite these findings, little is known about purinergic signalling in the fetoplacental endothelium. A secondary aim of this chapter was to determine whether there was commonality between Piezo1 channel activity and ATP activation in FpECs.

To further investigate Piezo1 activation by shearing forces, the impact of membrane tension on the channel was considered. As such, an assay utilising hypotonic solutions was used to induce osmotic cell swelling. This was developed by laboratory member

Melanie Ludlow, and adapted for use in FpECs. Here, the FlexStation fluorometer was used to measure the change in intracellular Ca^{2+} where Na^+ was replaced with decreasing concentrations of sucrose, rendering the solutions increasingly hypotonic. The increase in plasma membrane tension that results from this swelling causes stretching which should evoke Piezo1 channel activation. This experiment was used to test the hypothesis that Piezo1 contributes to stretch-induced Ca^{2+} influx caused by cell swelling in FpECs. The assay has been previously published in HUVECs where hypotonic stress was reported to mimic shear stress-mediated ATP release (Hirakawa et al., 2004). As such, this experiment was thought to be a useful tool to determine the relationship between Piezo1 and ATP in these FpECs.

5.2 Total eNOS and peNOS are increased in SGA placentas

In order to investigate whether Piezo1 channels are involved in the FSS-mediated signalling that induces eNOS phosphorylation, basal eNOS expression was first measured. As such, cultured FpECs from AGA and SGA samples were lysed. Basal levels of total eNOS and phosphorylated eNOS (Ser1177) were compared (Figure 5.2). This demonstrated a significant increase in peNOS in the SGA lysates, when normalised to both the total eNOS ($p = 0.031$). Total eNOS was also elevated in SGA samples (normalised to ACTB loading control, $p = 0.043$).

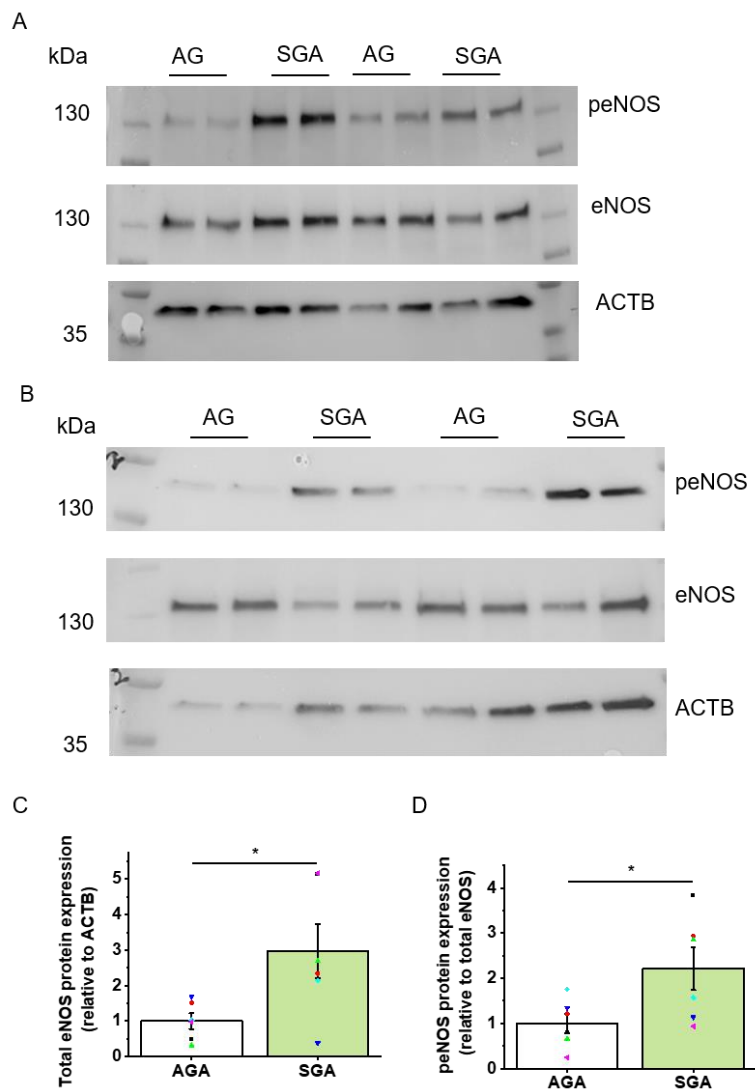


Figure 5.2 SGA placentas show raised expression of eNOS and phosphorylated eNOS proteins. A., Representative immunoblots for FpEC lysates from AGA and SGA samples probed with anti-phospho eNOS and anti-eNOS antibodies. The band in the upper blot represents Ser1177 phosphorylated eNOS (peNOS), with a predicted mass of 133 kDa. The band in the middle blot represents eNOS, with a predicted mass of 140 kDa. ACTB was included as a protein loading control, with a predicted mass of 42 kDa. Upper blot samples LGI045, LGI067, N = 2. B., Lower blot samples LGI041, LGI063, N = 2. C., Mean data from n = 6/N = 2 samples, showing a significant increase in total eNOS relative to ACTB. D., As for B, showing a significant increase in peNOS relative to eNOS. C and D: unpaired *t* test.

5.3 Chemical and FSS-evoked Piezo1 activation is coupled to eNOS phosphorylation

FpEC lysates from AGA samples that had been exposed to FSS were probed with antibody to phosphorylation at S1177 in eNOS. When compared to the proteins from cells in static conditions, those exposed to FSS had significantly greater peNOS expression, relative to the ACTB control and total eNOS ($p = 0.0019$ and $p = 0.0123$, respectively, Figure 5.3). The exposure to FSS did not significantly affect total eNOS or ACTB protein expression.

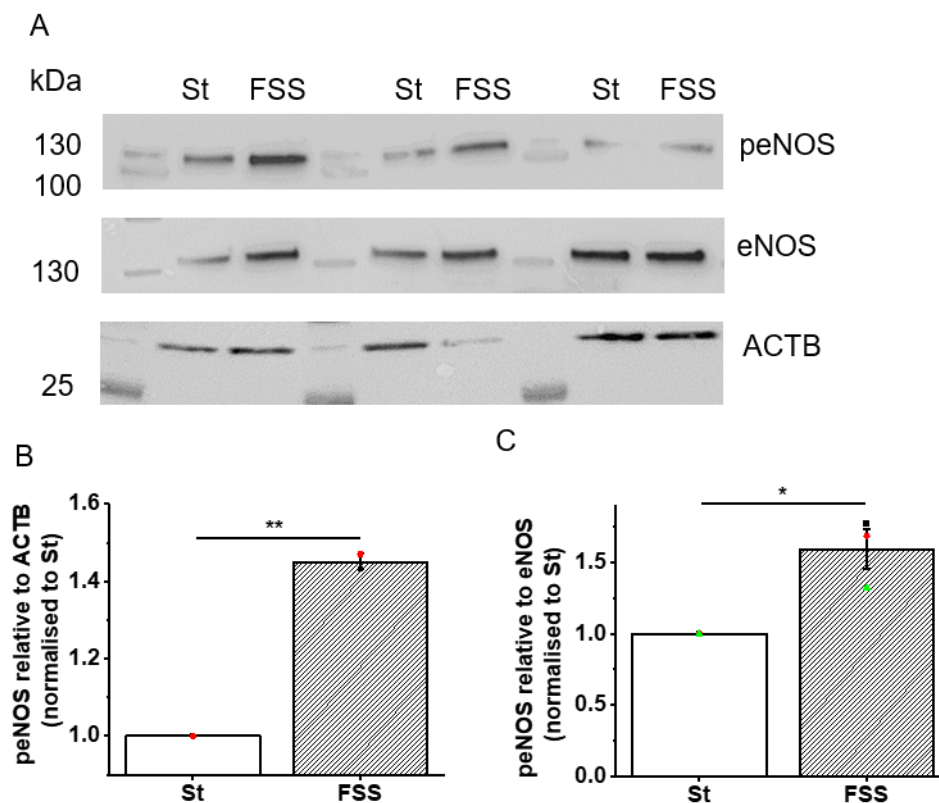


Figure 5.3 FSS evokes S1177 eNOS phosphorylation.

A., Immunoblots for FpEC lysates probed with anti-phospho eNOS and anti-eNOS antibodies after exposure to FSS. FpECs were exposed to either FSS for 48 hours (orbital shaker at 153 rpm) or static (St) culture conditions. The band in the upper blot represents Ser1177 phosphorylated eNOS (peNOS), with a predicted mass of 133 kDa. The band in the middle blot represents eNOS, with a predicted mass of 140 kDa. ACTB was included as a protein loading control, with a predicted mass of 42 kDa. Experiments were performed on three AGA samples, from left to right on the above blots: LGI037, LGI039, LGI041. B., Mean data from $n = 3$ samples, showing a significant increase in peNOS, relative to ACTB, after FSS. C., As for B, showing a significant increase in peNOS relative to eNOS. Data are displayed normalised to the St control. B and C: unpaired t test.

Previous experiments performed by Hannah Gaunt in our group demonstrated that in HUVECs treated with Piezo1 siRNA, scrambled siRNA, or mock transfection, basal

levels of peNOS were not affected by Piezo1 depletion. However, after the application of FSS, eNOS phosphorylation was increased in the control siRNA treated cells, when compared to the static control. However, this response was blunted in cells with Piezo1 depletion. These data add to the evidence presented in the Chapter 4, section 4.5.1, that Piezo1 is critical for FSS-sensing. Furthermore, these findings suggest that the channels are required for FSS-mediated downstream signalling commanding S1177 eNOS phosphorylation.

To investigate the relevance of these findings in clinical samples, Yoda1 was used to determine whether chemical activation of Piezo1 mimics the FSS-induced eNOS phosphorylation. The results from the intracellular Ca^{2+} measurement assays presented in the previous results chapter (Figure 4.19) demonstrated that Yoda1-evoked Piezo1 activation is rapid. Increased intracellular Ca^{2+} was evident within seconds of the Yoda1 application, at all doses used. Furthermore, the Ca^{2+} response was sustained throughout the six minutes of measurement. To investigate eNOS phosphorylation, a short treatment of 1 minute with 2 μM Yoda1 was initially used. This showed that in FpECs from healthy placentas, Yoda1 potently increased S1177 eNOS phosphorylation (Figure 5.4). The increase in peNOS was significantly higher after treatment with Yoda1 versus the vehicle control, relative to both total eNOS and ACTB ($p = 0.0003$ and $p = 0.0018$, respectively).

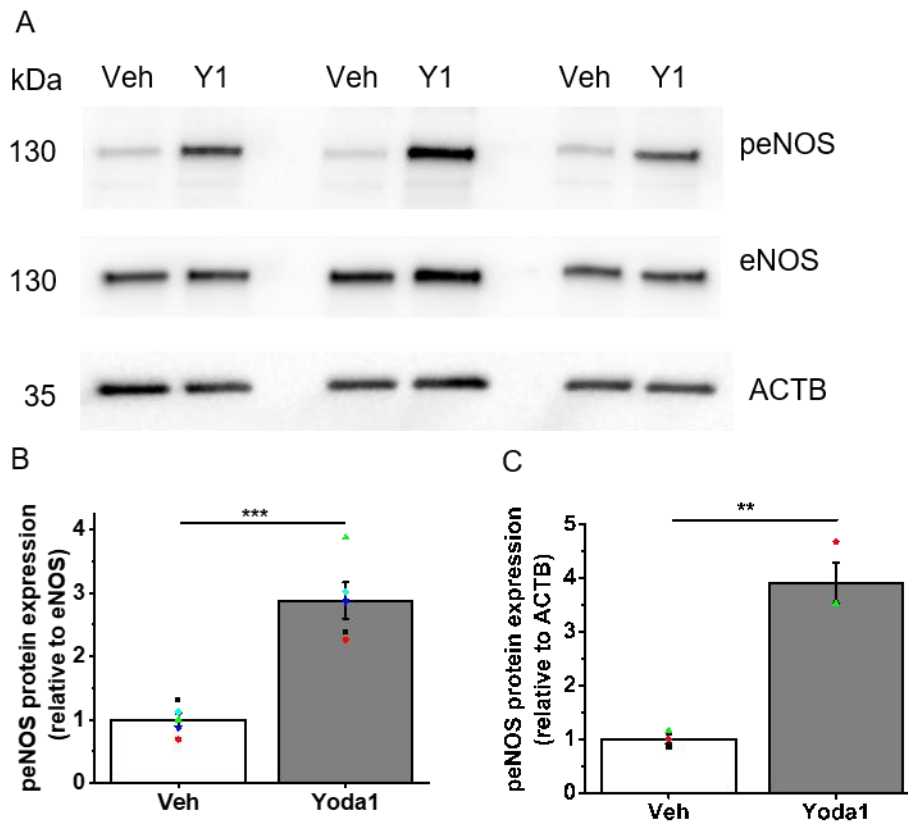


Figure 5.4 Yoda1 rapidly increases S1177 eNOS phosphorylation in FpECs. A., Immunoblots for anti-S1177 phospho-eNOS (upper blot), anti-eNOS (middle blot) in FpECs treated with 2 μ M Yoda1 (Y1) for 60 seconds or its vehicle, DMSO (Veh). ACTB was used as a protein loading control (lower blot). Three AGA sample lysates shown on the above blots: LGI008, LGI039, LGI041. B., Mean data from immunoblots, showing a significant increase in peNOS relative to total eNOS after Yoda1 application ($p = 0.0003$, $n = 5/N = 1$, AGA control samples: LGI008, LGI020, LGI037, LGI041, LGI045). C., As for B, relative to ACTB ($p = 0.0018$, $n = 3/N = 1$: LGI037, LGI039, LGI041). All data are displayed as normalised to the Veh. B and C: unpaired t test

Next, the effect of Piezo1 activation on eNOS phosphorylation in FpECs from SGA placentas was considered. As such, FpECs from the AGA and SGA groups were treated with Yoda1 or vehicle. Lysates were probed for anti-S1177 phospho-eNOS and anti-eNOS as described above. This demonstrated that treating FpECs from SGA placentas with Yoda1 resulted in eNOS phosphorylation that was significant compared to vehicle control, when normalised to both total eNOS and ACTB ($p = 0.001$ and $p = 0.029$, respectively, Figure 5.5). Visual inspection of the blots showed enhanced Yoda1-induced peNOS bands in the SGA samples compared to the AGA controls. Normalising these data to the AGA control vehicle in an ANOVA analysis demonstrated that there was no evidence of a difference in Yoda1-induced phosphorylation of eNOS in the SGA FpECs compared to those in the AGA group (Figure 5.5G). Taken together, these findings demonstrate that Yoda1 phosphorylates the Ser1177 regulatory site on eNOS in the fetoplacental endothelium in both AGA and SGA placentas. We therefore propose the pathway presented in Figure 5.6, whereby Yoda1 is a mimic of FSS-evoked Ca^{2+} entry in FpECs, leading to the downstream activation of eNOS.

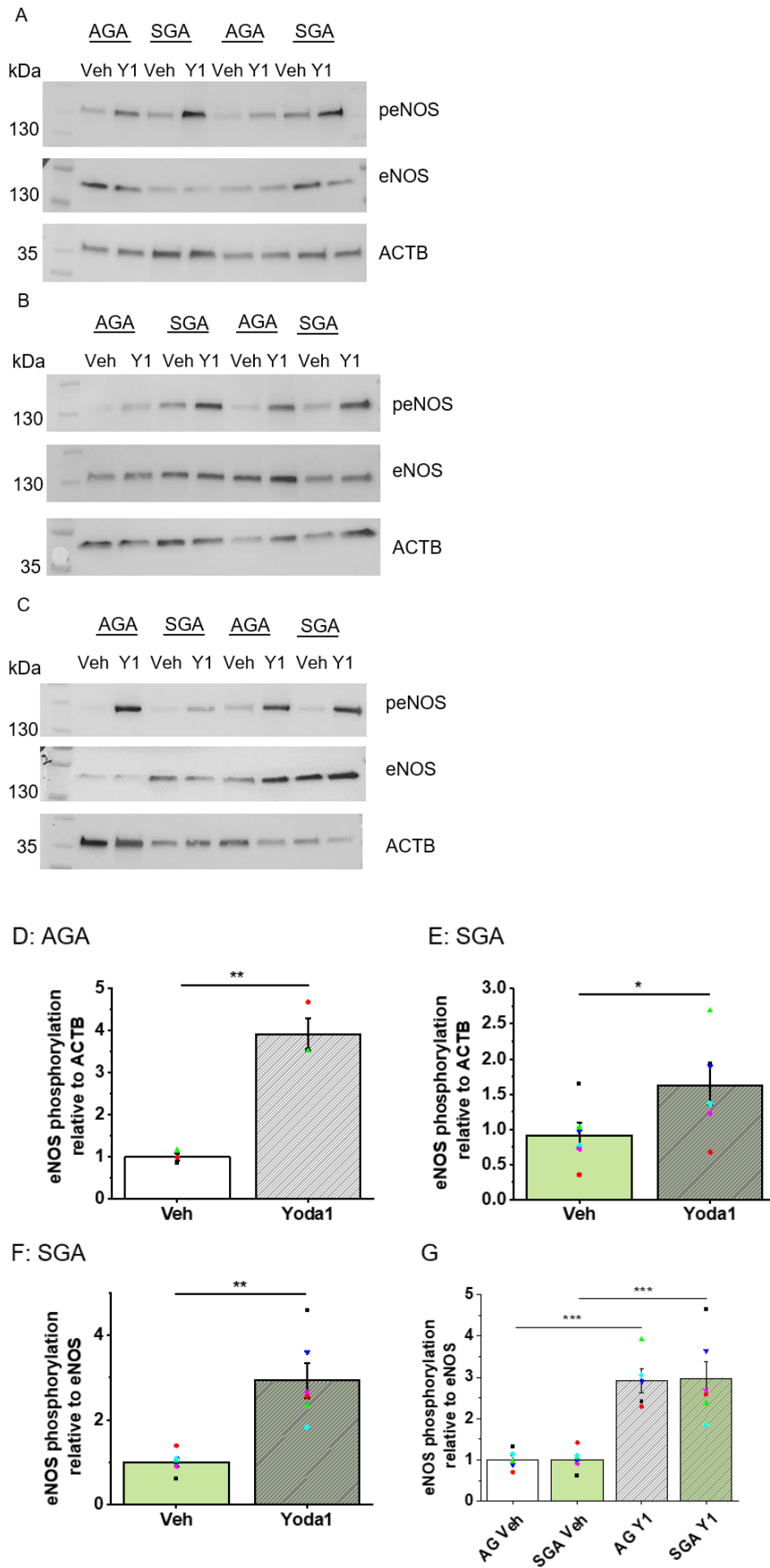


Figure 5.5 Yoda1 increases S1177 eNOS phosphorylation in FpECs from AGA and SGA placentas.

A., B. and C., Immunoblots for anti-S1177 phospho-eNOS (upper), anti-eNOS (middle) in FpECs treated with 2 μ M Yoda1 (Y1) for 60 seconds or its vehicle, DMSO (Veh). ACTB was used as a protein loading control (lower). $n = 6/N = 2$ in each group. Samples in blot A: LGI008, LGI016, LGI045, LGI051. Samples in blot B: LGI037, LGI067, LGI020, LGI075. Samples in blot C: LGI008, LGI030, LGI041, LGI063. D., Mean data from immunoblots, showing a significant increase in peNOS relative to ACTB after Yoda1 application in AGA control FpECs ($p = 0.0018$). E., As for D, showing a significant increase in peNOS relative to ACTB after Yoda1 application to SGA samples ($p = 0.0003$). F., As for E, showing significant increase in peNOS relative to total eNOS after Yoda1 application to SGA samples ($p=0.001$). G., ANOVA analysis of peNOS relative to eNOS data normalised to the AGA Veh. These data demonstrate a significant effect of Yoda1 application in both the AGA ($p = 8.5 \times 10^{-4}$) and SGA lysates ($p = 2.6 \times 10^{-4}$). There was no evidence of a difference in the magnitude of Yoda1-evoked peNOS between groups. D, E and F: unpaired t test, G: ANOVA.

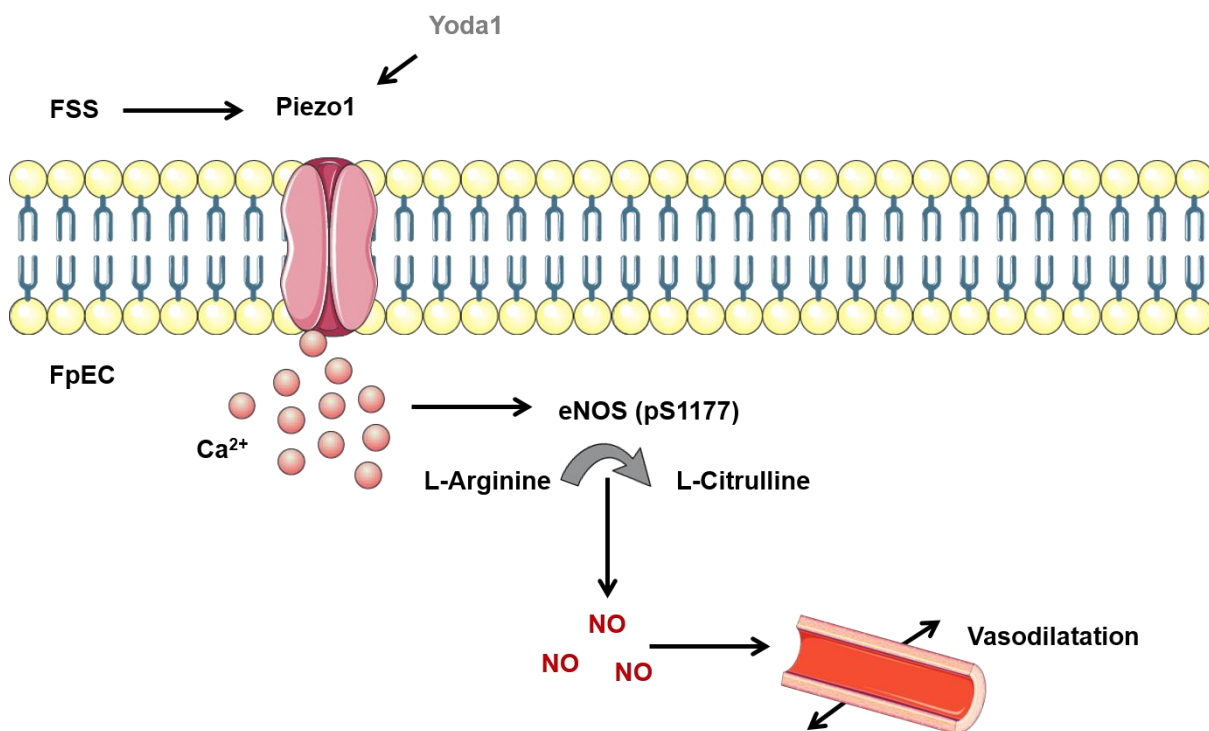


Figure 5.6 Schematic depicting Yoda1 activation of Piezo1 channels evoking Ca^{2+} entry and eNOS activation.

Yoda1 mimics the effect of FSS by inducing eNOS phosphorylation at serine site 1177. Subsequent release of NO is well-known to induce vasodilatation via smooth muscle relaxation. Abbreviations: FSS fluid shear stress, FpEC fetal placental endothelial cell, eNOS endothelial nitric oxide synthase, NO nitric oxide.

5.4 FpECs respond to ATP but P2Y₂ receptors are not a requirement for eNOS phosphorylation

As discussed in the introduction to this chapter, the vascular tone of blood vessels can be altered by purinergic signalling in the endothelium (Lohman et al., 2012). The release of ATP during conditions of increased shear stress has been well documented. This process has been linked to vasodilatation via endothelial NO production evoked by ATP. This is thought to occur via ATP activation of G_q/G₁₁-coupled purinergic P2Y₂ receptors subsequently inducing AKT mediated eNOS phosphorylation (Wang et al., 2015).

There are multiple mechanisms for ATP release depending on the cell type. For example, exocytosis via intracellular vesicles (Lohman et al., 2012). This has been demonstrated in HUVECs where a fluorescent labeller of intracellular ATP was used to demonstrate ATP within intracellular vesicles (Bodin and Burnstock, 2001). Stimulation by FSS at 10 or 25 dyne/cm² led to a rapid decrease in fluorescence and increase in ATP concentration in the extracellular media, which did not occur under static conditions. Other postulated mechanisms include ATP-binding cassette (ABC) transporters in the cell membrane, mitochondrial ATP synthase, connexin gap junction proteins and pannexin channels (Lohman et al., 2012). Pannexin proteins form membrane channels that allow transport of molecules between the intra- and extracellular space.

The Offermanns group suggested that Piezo1 is required for FSS-induced ATP release and subsequent downstream signalling that results in NO formation (Wang et al., 2016). They demonstrated that Piezo1-dependent ATP release was mediated in part by pannexin channels. Although evident that flow induces ATP release and is a mechanism upstream of NO production, there are few studies describing its role in placental physiology.

One previous study of purinergic signalling in the placenta identified connexin and pannexin mRNA and proteins in cultured placental explants from the first trimester (Xiao et al., 2020). P-glycoprotein (P-gp encoded by an ABC transporter) has also been identified in the syncytiotrophoblast layer of the placenta. P-gp was found to be reduced in severe PET, with the authors hypothesising that impaired ATP function may contribute to syncytiotrophoblast pathology (Dunk et al., 2018). In addition, reduced ATP generation has been demonstrated in trophoblasts isolated from placentas of obese women, suggestive of an association with inflammation.

The role of Piezo1 channel activation and ATP was therefore investigated in the AGA FpEC samples. The findings in Figure 4.19 in the previous results chapter, and Figure 5.4 in this chapter showed that Yoda1 application induced Ca²⁺ entry into FpECs and mimicked the FSS-evoked phosphorylation of eNOS. As such, Yoda1 was used in these

experiments as a specific tool to investigate Piezo1 signalling. The change in intracellular Ca^{2+} concentration was compared after the application of either Yoda1 (5 μM) or ATP (10 μM). The amplitude of response to Yoda1 was found to be larger, particularly after 3 min, and more sustained (Figure 5.7). When ATP and Yoda1 were used in combination, a larger Ca^{2+} response was initially observed but this early additive effect was later lost such that the combined response became indistinguishable from the response to Yoda1 alone (Figure 5.7).

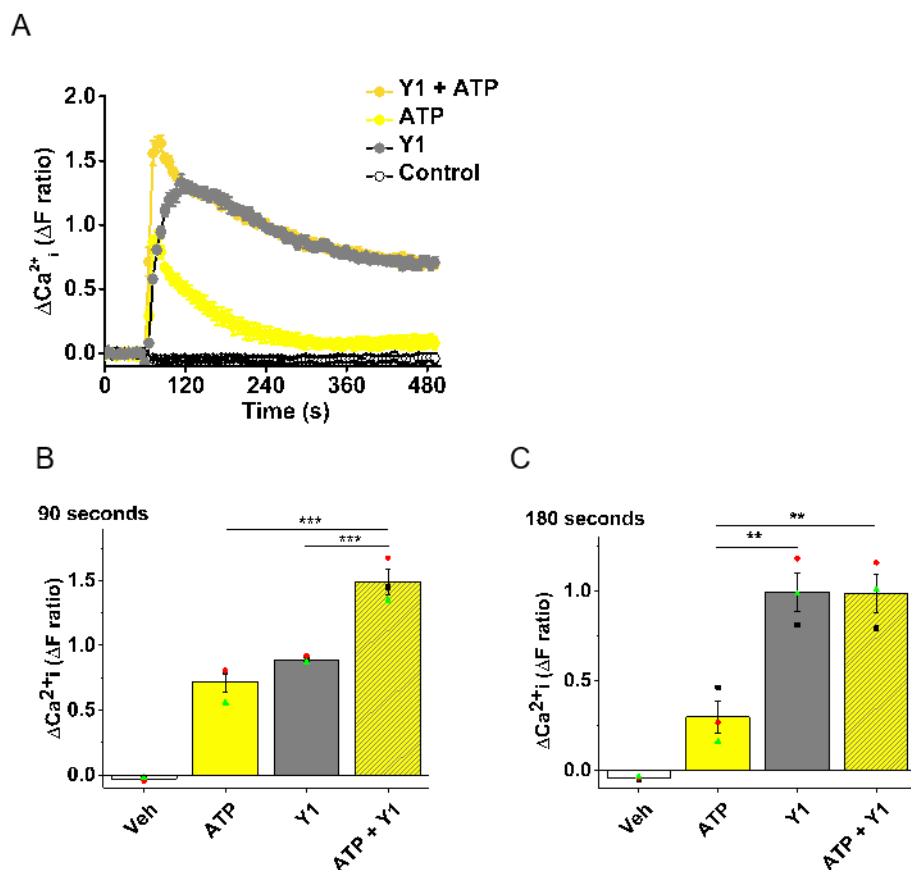


Figure 5.7 Intracellular Ca^{2+} increase is stimulated by Yoda1 and ATP, with an early additive effect when both are applied to FpECs in combination. A., Representative intracellular Ca^{2+} measurement tracing after stimulating FpECs with Yoda1 ($5 \mu\text{M}$, Y1), ATP ($10 \mu\text{M}$) or a combination of Yoda1 ($5 \mu\text{M}$) and ATP ($10 \mu\text{M}$), versus DMSO vehicle control (Veh) B, Mean \pm SEM data for the type of experiment shown in A, with values taken at 90 seconds (s) (drug application at 60 s), showing a significant difference for ATP ($p = 1.19 \times 10^{-4}$) or Yoda1 ($p = 7.02 \times 10^{-4}$) alone versus both agonists. C, as for B, with data taken at 180 s, demonstrating a significant difference between ATP and ATP plus Yoda1 ($p = 0.002$), but this was not significantly different to treatment with Yoda1 alone. AGA samples $n = 3/N = 3$: LGI034, LGI037, LGI039. B and C: ANOVA.

To investigate the coupling of ATP and Piezo1 channel activity, Ca^{2+} measurements were performed after the application of suramin. This is a non-selective P2Y_2 receptor inhibitor that inhibits ATP induced NO production (Silva et al., 2006, Beindl et al., 1996, Silva and Garvin, 2009). After a 30 minute pre-treatment with suramin, ATP evoked Ca^{2+}

entry was measured in FpECs. Suramin significantly suppressed the response to ATP ($p = 0.009$), consistent with its ability to antagonise P2Y₂ receptors (Figure 5.8).

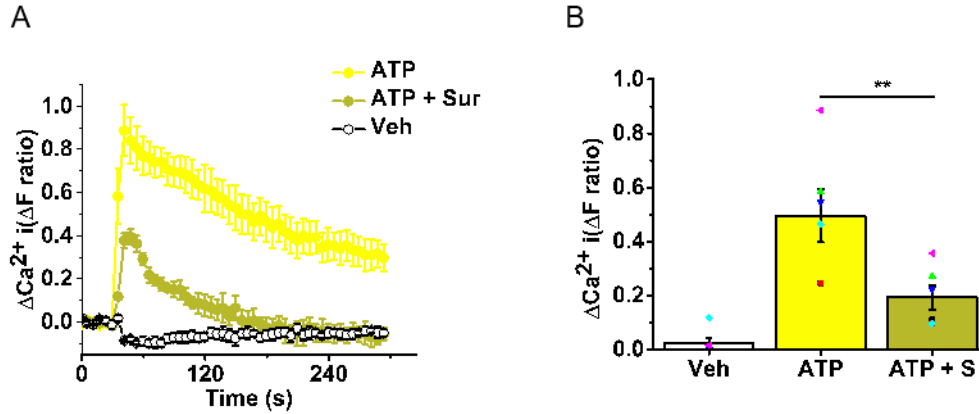


Figure 5.8 Suramin inhibits ATP evoked Ca²⁺ entry via an effect on P2Y₂ receptors.

A., Representative intracellular Ca²⁺ measurement tracing after stimulating FpECs with ATP following suramin pre-treatment or vehicle control (H₂O, Veh). AGA sample LGI034.

B., Mean \pm SEM of the peak responses in the type of experiment shown in A, demonstrating a significant reduction in response to ATP (10 μM) after suramin pre-treatment by about 60% (30 minutes, 10 μM), $p = 0.009$). AGA samples $n = 3/N = 3$: LGI034, LGI037 and LGI039, ANOVA.

Next, the effect of blocking P2Y₂ receptors on chemical-evoked Piezo1 channel activity was investigated. As such, suramin pre-treatment was used prior to treating FpECs with Yoda1. As seen in Figure 5.8A, there was a partial reduction in Yoda1-evoked Ca²⁺ entry in the cells treated with suramin. However, when data from each experiment were pooled, the inhibitory effect of suramin was not statistically significant (Figure 5.9B). To further investigate the interplay between Piezo1 channel activity and P2Y₂ receptor signalling, Yoda1 was again applied to cells, with or without a suramin pre-treatment. In this western blot, neither Yoda1-induced eNOS phosphorylation nor total eNOS appeared to be affected by suramin (Figure 5.9C). However, this experiment was limited to two AGA samples with two replicates each (LGI037, shown in Figure 5.9c and LGI039, data not shown), and therefore the results are preliminary.

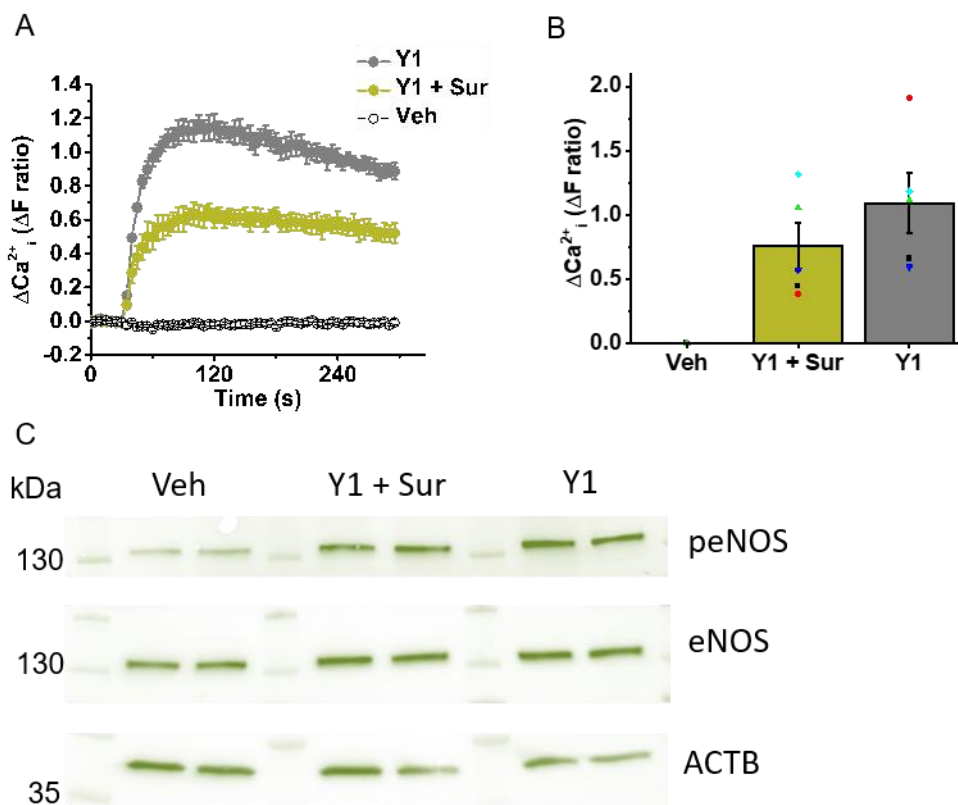
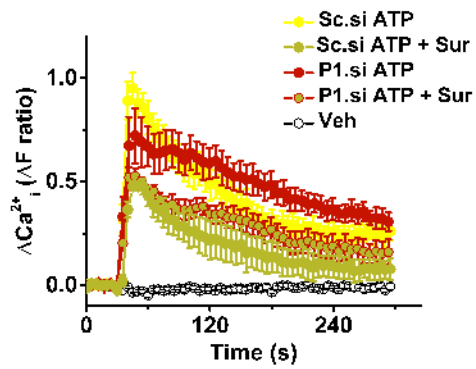


Figure 5.9 Suramin pre-treatment does not significantly reduce Yoda1-evoked Ca^{2+} entry or blunt eNOS phosphorylation. A., Representative intracellular Ca^{2+} measurement tracing after stimulating FpECs with Yoda1 (5 μM), Yoda1 following suramin pre-treatment (10 μM) or vehicle control (DMSO, Veh). AGA sample LGI034. B., Mean \pm SEM of the peak responses in the type of experiment shown in A, demonstrating no significant reduction in response to Yoda1 after suramin pre-treatment ($p = 0.278$). AGA samples $n = 3/N = 3$: LGI034, LGI037, LGI039, ANOVA. C., Representative immunoblot for anti-S1177 phospho-eNOS (upper), anti-eNOS (middle) in FpECs treated with 2 μM Yoda1 (Y1) for 60 seconds or Yoda1 after 30 minutes pre-treatment with suramin (Sur, 10 μM), or its vehicle (DMSO, Veh). ACTB was used as a protein loading control (lower). AGA sample LGI037, $n = 1/N = 2$.

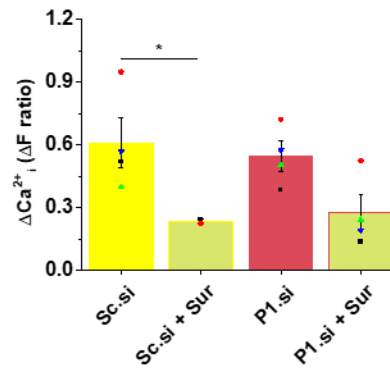
To further investigate these findings, the effect of suramin on ATP- and Yoda1-evoked Ca^{2+} entry was measured after Piezo1 knockdown using siRNA (Figure 5.10). As expected, after control siRNA transfection, suramin caused a significant reduction in the Ca^{2+} response to ATP ($p = 0.044$). Piezo1 depletion did not affect the response to ATP.

In addition, after P1.si transfection, suramin reduced the response to ATP by a comparable amount, indicating that there was no additive effect of Piezo1 silencing (Figure 5.10A and B). Once again, the addition of suramin caused a reduction in Yoda1-evoked Ca^{2+} entry in some experiments, but this was not significant when data were pooled. A small inhibitory response was seen after suramin was added to the Piezo1-depleted FpECs, but this was not significant (Figure 5.10C and D). Ionomycin-evoked Ca^{2+} entry was not affected by either suramin treatment, Piezo1 depletion or the combination, indicating that neither Piezo1 silencing or P2 receptor blockade compromised cell viability (Figure 5.10E and F). Taken together, these data suggest that treatment with Yoda1 evokes eNOS phosphorylation and intracellular Ca^{2+} entry that may involve ATP and P2Y₂ receptors but is largely independent of them.

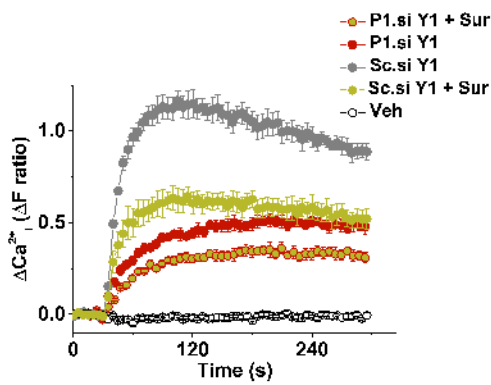
A: ATP (P1.si +/- suramin)



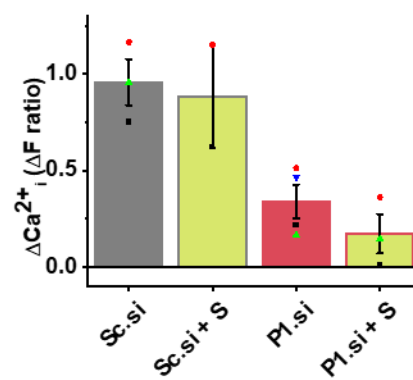
B



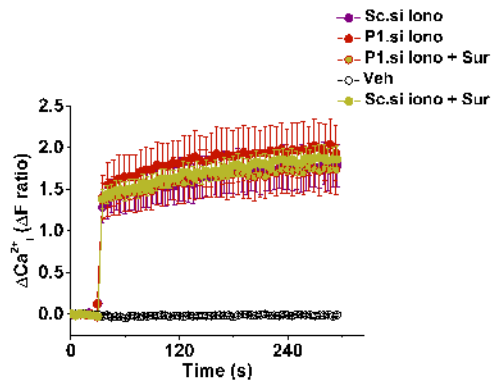
C: Yoda1 (P1.si +/- suramin)



D



E: Ionomycin (P1.si +/- suramin)



F

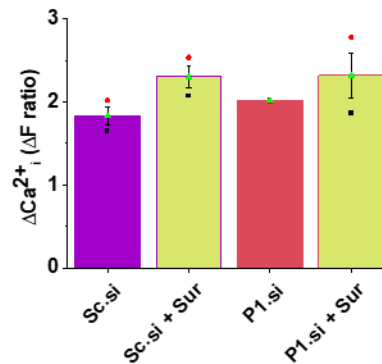


Figure 5.10 ATP evoked Ca^{2+} entry is not dependent on Piezo1 and nor does inhibition of $P2Y_2$ channels prevent Yoda1 induced Ca^{2+} entry in FpECs.

A., Representative intracellular Ca^{2+} measurement tracing after stimulating FpECs with ATP (10 μM), ATP following suramin pre-treatment (10 μM) or vehicle control (H_2O , Veh). As indicated, FpECs had undergone Piezo1 depletion (P1.si) or control siRNA (Sc.si) treatment. B., Mean \pm SEM of the peak responses in the type of experiment shown in A, demonstrating a significant reduction in response to ATP after suramin pre-treatment ($p = 0.044$), and no significant additive effect of Piezo1 depletion. C., As for A., where Ca^{2+} measurements were taken after stimulating transfected FpECs with Yoda1 (5 μM), Yoda1 following suramin pre-treatment (10 μM) or vehicle control (DMSO, Veh). D., As for B, demonstrating no significant reduction in response to Yoda1 after suramin pre-treatment, and no significant additive effect of Piezo1 depletion. E., As for A., where Ca^{2+} measurements were taken after stimulating transfected FpECs with ionomycin (10 μM), ionomycin following suramin pre-treatment (10 μM) or vehicle control (DMSO, Veh). F., As for B, demonstrating no significant reduction in response to ionomycin after suramin pre-treatment, and no additive effect of Piezo1 depletion. Data shown in A., C., E from AGA sample LGI034, N = 3 replicates. Mean data in B., D., F from AGA samples n = 3/N = 3:LGI034, LGI037, LGI039. B, D and F: ANOVA.

5.5 Hypotonic stress induces a rise in intracellular Ca^{2+} in FpECs

In order to further investigate the effect of mechanical force on Piezo1 channel activity in FpECs, membrane tension was produced by using extracellular hypotonic solutions. In this experiment, progressively hypotonic solutions induce cell swelling and therefore generate increasing membrane tension. Whether or not this would lead to Piezo1 channel activation in FpECs remained to be determined.

Firstly, the response of FpECs to hypotonic stress was examined by measuring the change in intracellular Ca^{2+} using the FlexStation fluorometer (Figure 5.11). Applying decreasing concentrations of sucrose caused a transient increase in the intracellular Ca^{2+} concentration. This was dose-dependent, with an EC_{50} of sucrose of 92.2 mM

(Figure 5.11B). 270 mM sucrose was used as an isotonic control throughout all experiments of this type.

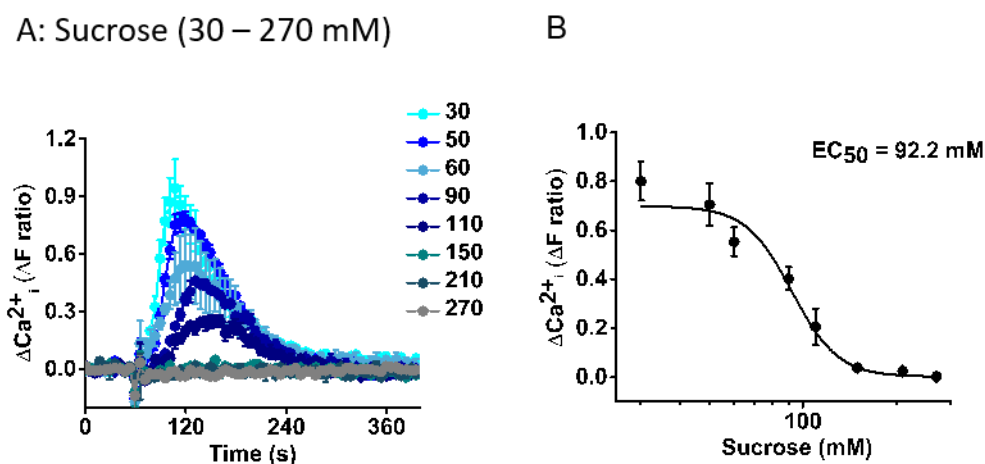


Figure 5.11 Hypotonic stress induces a change in the intracellular Ca^{2+} concentration of FpECs. A., Representative intracellular Ca^{2+} measurement tracing after applying sucrose solutions to FpECs (30 – 270 mM) (AGA sample LGI035). B., Mean \pm SEM responses to Yoda1 fitted with the Hill equation, suggesting an approximate EC_{50} of 92.2 mM (AGA samples $n = 5/N = 3$: LM11, LM37, LM38, LM39, LM41).

5.5.1 Hypotonic stress-induced intracellular Ca^{2+} mobilisation in FpECs is mediated, at least in part, by Piezo1 channels

After establishing that hypotonicity increased basal intracellular Ca^{2+} levels, whether this response involved Piezo1 channels was investigated. To this end, FpECs from individual patient samples were treated with either hypotonic solutions, Yoda1, or a combination of both (Figure 5.12). When the isotonic control solution (270 mM) was applied along with Yoda1, the peak intracellular Ca^{2+} matched that of Yoda1 alone. As solutions became increasingly hypotonic, there was an additive effect. The addition of Yoda1 increased the intracellular Ca^{2+} at each concentration of sucrose (other than the control), and the response was more sustained. The Ca^{2+} entry was higher at each hypotonic solution, other than the control, compared to when Yoda1 was applied in isolation.

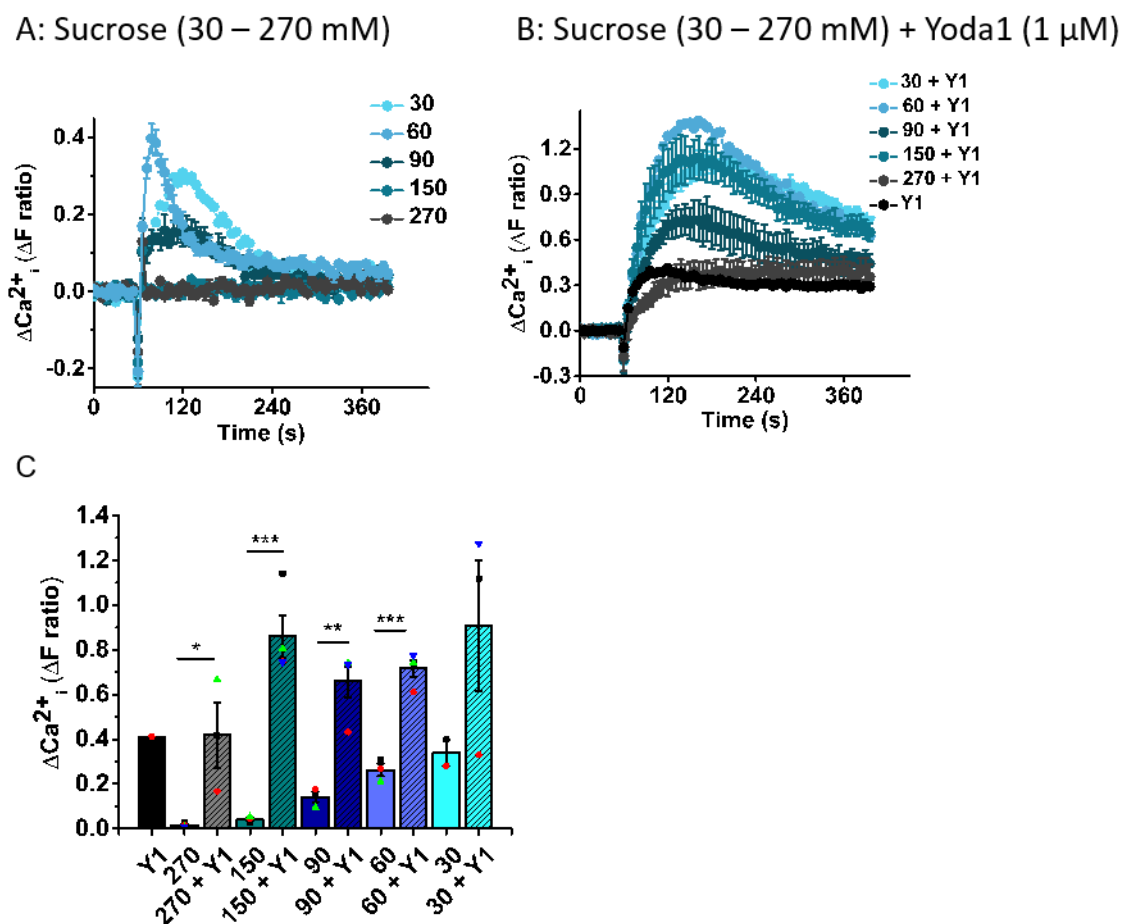


Figure 5.12 Yoda1 strongly potentiates hypotonic responses in FpECs. A., Representative intracellular Ca^{2+} measurement tracing after applying sucrose solutions to FpECs (30 – 270 mM) (AGA sample LM37). B., Representative intracellular Ca^{2+} measurement tracing of the same sample of FpECs as shown in A., after applying Yoda1 alone (1 μM) or hypotonic solutions (30 – 270 mM) plus Yoda1 (1 μM). C., Mean \pm SEM of the peak responses in the type of experiment shown in A and B, demonstrating an increase in Ca^{2+} concentration when Yoda1 pre-treatment was used prior to the application of hypotonic solutions. This additive effect was significant at the following sucrose concentrations: 270 mM $p = 0.02$, 150 mM $p = 0.0008$, 90 mM $p = 0.0024$, 60 mM $p = 0.0002$. No significant difference when Yoda1 was in combination with 30 mM sucrose, although the data were variable. AGA samples, $n = 3/N = 3$, ANOVA.

The additive effect of Yoda1 and cell swelling on Ca^{2+} concentration is consistent with functional Piezo1 channel activity in the FpECs. To determine whether this Ca^{2+} response was Piezo1 dependent, the cation channel ion pore blocker Gd^{3+} was used. In

this assay, FpECs were pre-treated for 30 minutes with 30 μM Gd^{3+} or its vehicle, and hypotonic induced Ca^{2+} entry was measured (Figure 5.13). In cells pre-treated with the vehicle of Gd^{3+} normal dose-dependent hypotonic responses were observed. These responses were almost completely abolished after the Gd^{3+} pre-treatment. These data suggest that mechanosensitive cation channels, including Piezo1 channels, are mediating the increase in intracellular Ca^{2+} evoked by cell swelling.

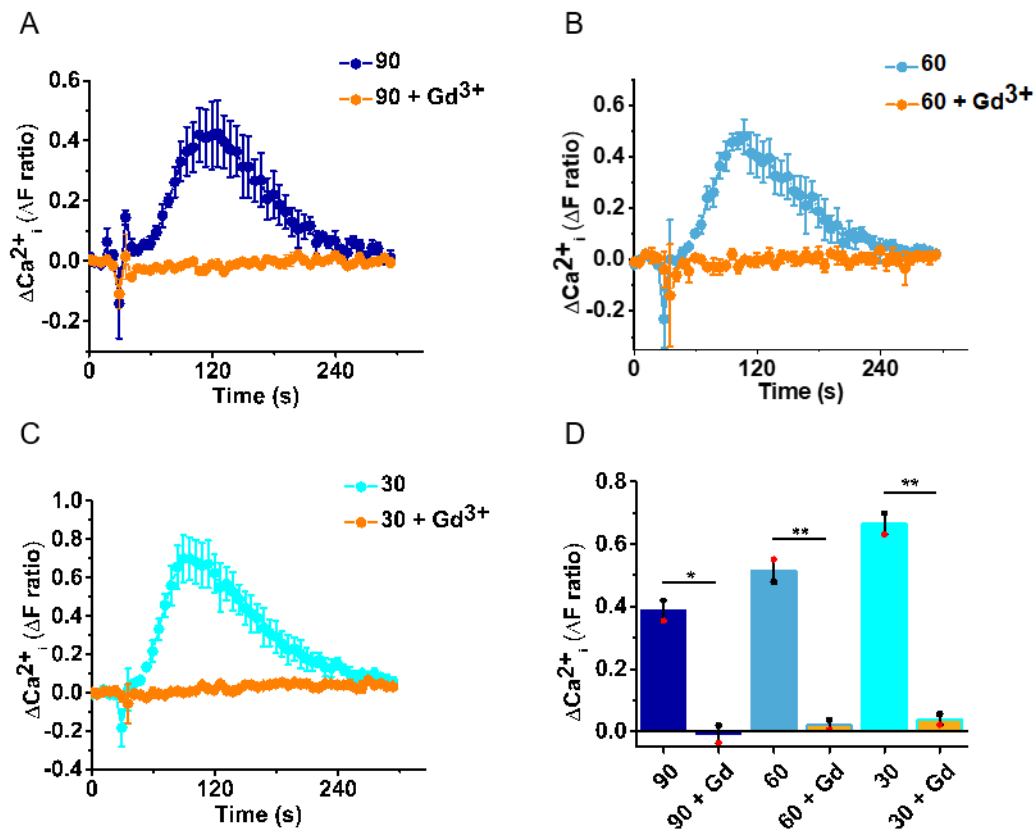


Figure 5.13 Hypotonicity-evoked increase in intracellular Ca^{2+} entry in FpECs is suppressed by gadolinium (Gd^{3+}).

A., Representative intracellular Ca^{2+} measurement tracing after applying a sucrose solution (90 mM) to FpECs in the presence or absence of Gd^{3+} pre-treatment (30 μM , 30 minutes). AGA sample LM33, N = 3. B., Representative intracellular Ca^{2+} measurement tracing of the same sample of FpECs as shown in A., after applying sucrose (60 mM) with or without Gd^{3+} pre-treatment. C., As for A and B, with sucrose (30 mM) with or without Gd^{3+} pre-treatment. D., Mean \pm SEM of the peak responses in the type of experiment shown in A, B and C demonstrating a lower intracellular Ca^{2+} concentration when Gd^{3+} pre-treatment was used prior to the application of hypotonic solutions. Unpaired *t* test performed on each pair showed a significant difference at each sucrose concentration: 90 mM ($p = 0.0117$), 60 mM ($p = 0.0063$), 30 mM ($p = 0.0037$).

Due to the non-selective properties of Gd^{3+} , transfection with Piezo1 siRNA was used to determine the dependency of this Ca^{2+} entry on Piezo1 channel function. Firstly, intracellular Ca^{2+} in response to Yoda1 was measured post transfection to confirm a significant Piezo1 knockdown (Figure 5.14A). After *PIEZO1* was strongly suppressed, there was a partial reduction in the intracellular Ca^{2+} concentration in response to hypotonic solutions. This was significant when 90 mM and 30 mM sucrose solutions were used (Figure 5.14). Given that a smaller rise in Ca^{2+} still occurred after Piezo1 depletion, whether additional cell components sensitive to mechanical tension were involved in this response was considered.

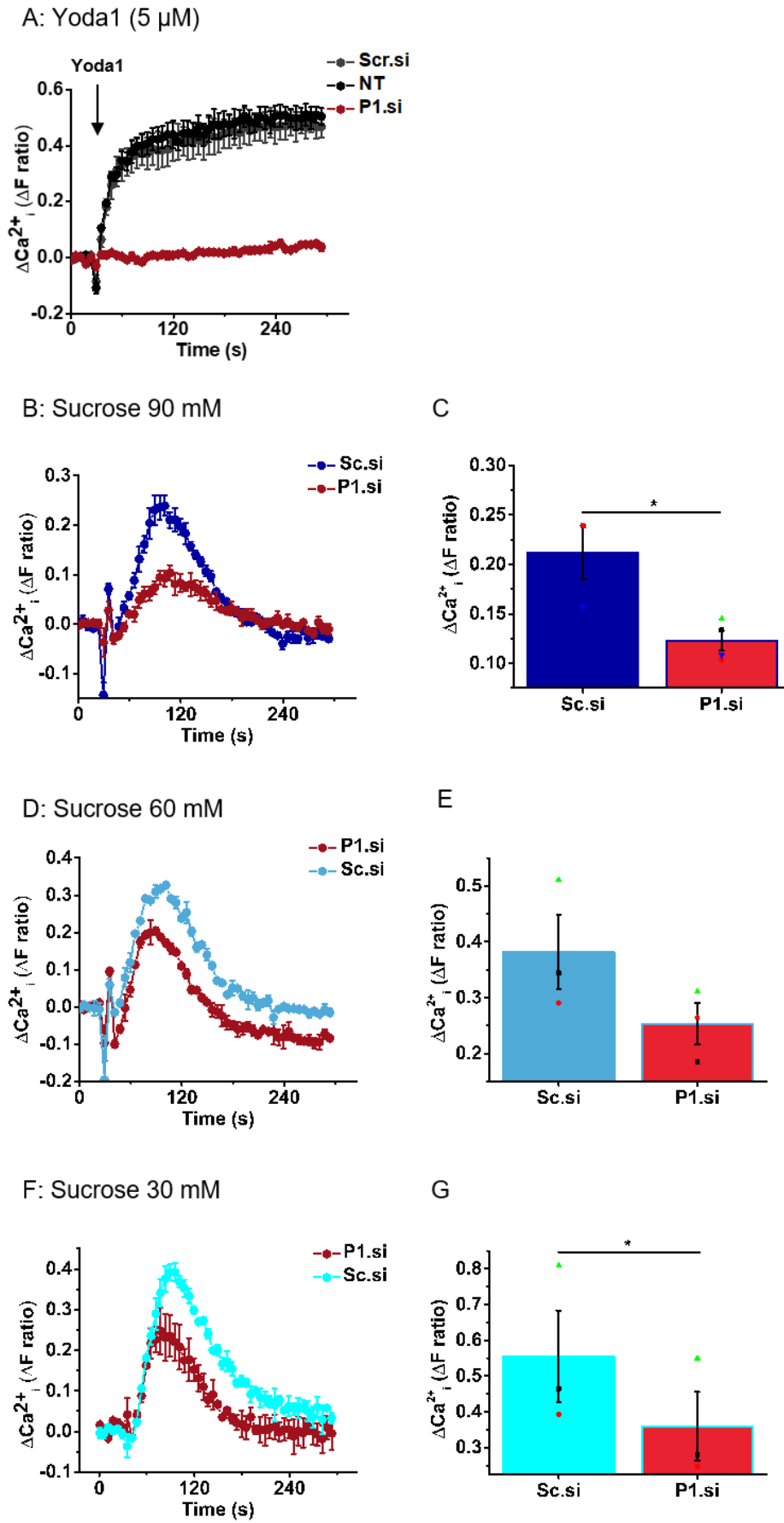


Figure 5.14 Piezo1 depletion reduces the hypotonicity-evoked rise in intracellular Ca^{2+} entry in FpECs.

A., Intracellular Ca^{2+} measurement in AGA FpECs after no transfection or transfection with either control siRNA (Sc.si) or Piezo1 siRNA (P1.si) confirming a lack of response to Yoda1 (5 μm) after Piezo1 depletion (LM33, N = 3) B., Representative intracellular Ca^{2+} measurement tracing after applying a sucrose solution (90 mM) to FpECs after transfection with either Sc.si or P1.si. C., Mean \pm SEM of the peak responses in the type of experiment shown in A, demonstrating a significantly lower intracellular Ca^{2+} concentration to sucrose (90 mM) after Piezo1 depletion ($p = 0.0177$), AGA samples $n = 3/N = 3$). D., As for B, after applying a sucrose solution (60 mM) to FpECs after transfection. D., As for C, showing no significant difference in response to sucrose (60 mM) after Piezo1 depletion ($p = \text{NS}$). E., As for B., after applying a sucrose solution (30 mM) to FpECs after transfection. F., As for C, showing a significant difference in response to sucrose (30 mM) after Piezo1 depletion ($p = 0.0276$). C, E and G: unpaired *t* test

5.5.2 Antagonising P2 receptors partially inhibits intracellular Ca^{2+} entry evoked by hypotonic stress

As discussed in section 5.4 of this chapter, FSS is known to stimulate endothelial ATP release. ATP activates G_q/G_{11} -coupled purinergic P2Y_2 receptors resulting in downstream signalling, such as AKT mediated eNOS phosphorylation. To determine whether mechanical tension on FpECs evoked purinergic signalling, the intracellular Ca^{2+} measurements were performed once again after the application of hypotonic solutions to generate cell swelling. As per previous experiments, the non-selective P2Y_2 receptor inhibitor suramin was used as a 30 minute pre-treatment.

The application of hypotonic sucrose solutions evoked an increase in intracellular Ca^{2+} levels (Figure 5.15). This appeared partially blunted by suramin, although the data are preliminary due to the small number of independent experiments. Overall, these data suggest that hypotonic stress is, at least in part, able to evoke activation of suramin sensitive receptors or channels.

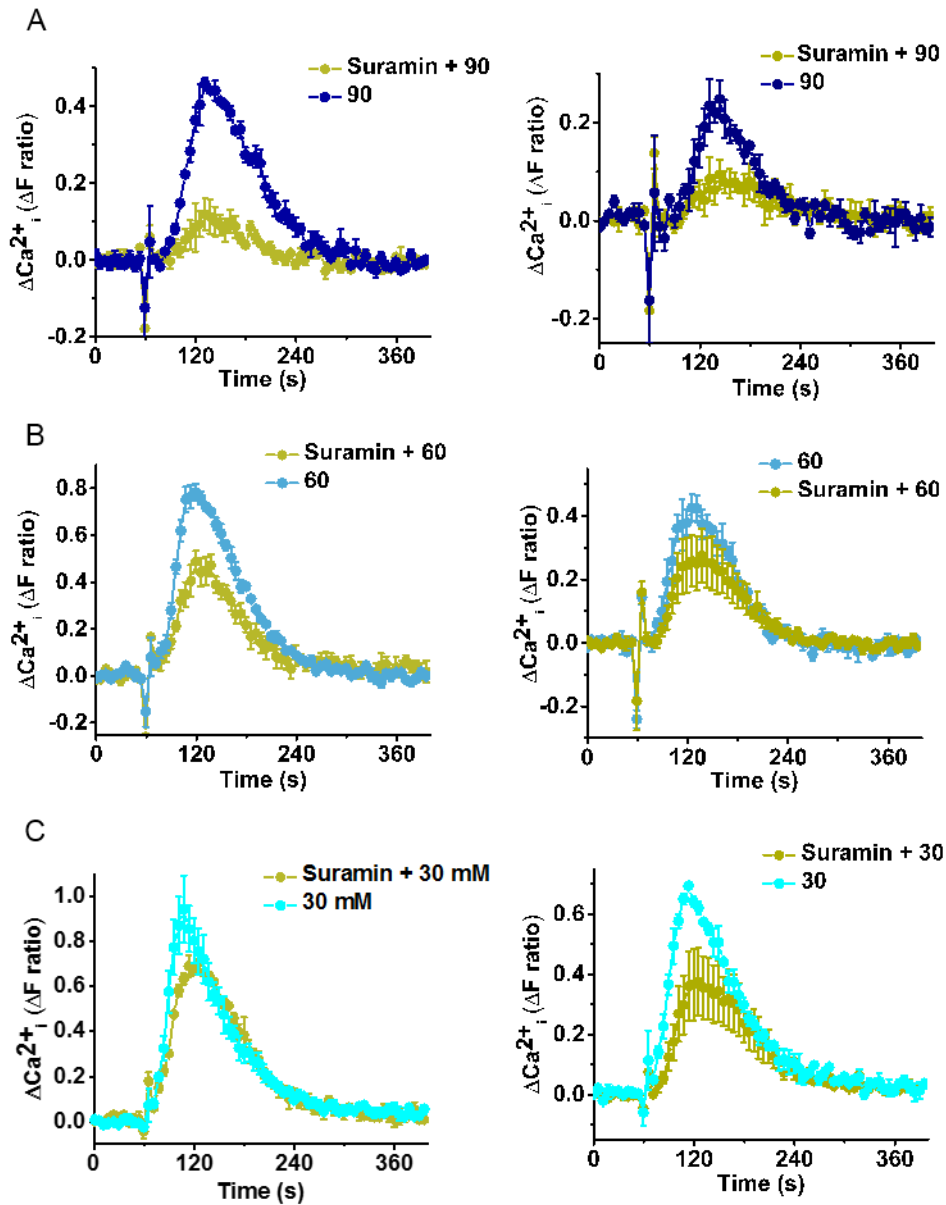


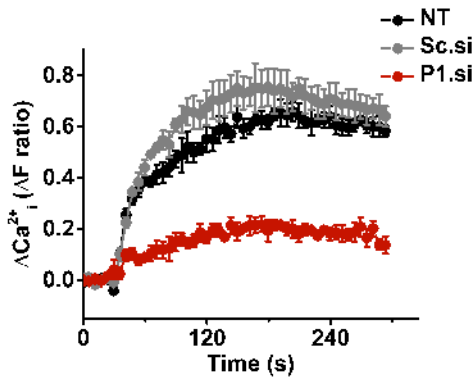
Figure 5.15 Hypotonicity mediated Ca^{2+} entry in FpECs is partially blunted by suramin.

A., Representative intracellular Ca^{2+} measurement traces after applying a sucrose solution (90 mM) to FpECs after pre-treatment with suramin (Sur, 10 μM), $n = 2/N=3$. B., Representative intracellular Ca^{2+} measurement traces after applying a sucrose solution (60 mM) to FpECs after pre-treatment with suramin, $n = 2/N = 3$. C., Representative intracellular Ca^{2+} measurement traces after applying a sucrose solution (30 mM) to FpECs after pre-treatment with suramin, $n = 2/N = 3$.

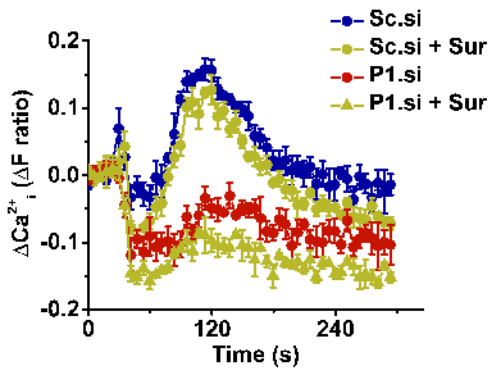
These findings are supported by previous work demonstrating that hypotonic stress induced ATP release which evoked a Ca^{2+} transient in HUVECs (Hirakawa et al., 2004). This group found that hypotonic stress resulted in the reorganisation of actin in the HUVECs, indicative of a response similar to that occurring after exposure of endothelial cells to FSS. However, disrupting the actin cytoskeleton did not suppress hypotonicity-induced ATP release. Furthermore, inhibition of the ATP-mediated Ca^{2+} response did not affect actin reorganization, indicating that these two responses are not interrelated. Hirakawa et al., (2004) found that suramin pre-treatment did significantly suppress the hypotonic response. However, similar to our data shown in Figure 5.15, the inhibition of ATP release did not abolish the hypotonicity-induced Ca^{2+} transients in HUVECs. As such, the partial reduction in response indicates that ATP release via P2Y_2 receptors is not the only mechanism for the hypotonic stress-induced Ca^{2+} mobilization in FpECs or HUVECs.

The findings presented in Figure 1.5.1 demonstrated that Piezo1 activation by hypotonic stress resulted in Ca^{2+} mobilisation, and that depletion of Piezo1 inhibits this response. Given the findings here suggesting that blocking ATP-evoked activation of P2 receptors partially blunted the hypotonic response, the effect of combining P1.si transfection with suramin pre-treatment was considered. Figure 5.16 shows a sequential reduction in the response to hypotonic stress. Here, Piezo1 depletion inhibited the Ca^{2+} elevation, a response which was almost totally abolished with the addition of suramin pre-treatment. These data are preliminary due to the small sample size, but suggest that a variety of mechanosensitive responses in endothelium may originate from a small number of intracellular signals operating either together or functioning independently, such as flow-induced ATP release and Piezo1 ion channel activity lead to downstream cellular effects.

A: Yoda1 (5 μ M)



B: Sucrose (90 mM), P1.si +/- suramin



C

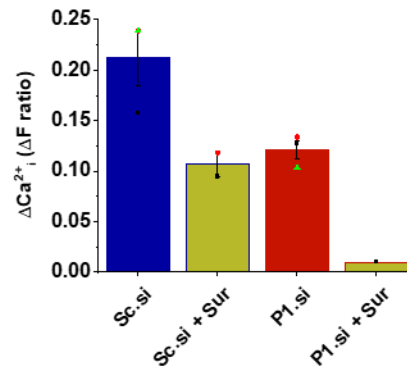


Figure 5.16 Depletion of Piezo1 and inhibition of P2 receptors prevented Ca^{2+} increase in response to hypotonic FpEC swelling. A., Representative intracellular Ca^{2+} measurement tracing after applying Yoda1 (5 μ M) to FpECs after either Sc.si or P1.si transfection confirming functional knockdown of Piezo1. B., Representative intracellular Ca^{2+} measurement tracing after applying a sucrose solution (90 mM) to FpECs after either Sc.si or P1.si transfection, with or without suramin pre-treatment (Sur, 10 μ M). AGA sample: LGI037. C., Mean \pm SEM of the peak responses in the type of experiment shown in B. This showed a reduction in intracellular Ca^{2+} concentration to sucrose (90 mM) after suramin pre-treatment or P1.si. Treating P1.si transfected FpECs with suramin caused a profound lack of rise in intracellular Ca^{2+} in response to hypotonicity. ANOVA analysis and quantification could not be performed due to insufficient sample numbers ($n = 3/N = 3$, only $n = 2$ for P1.si plus suramin, AGA samples: LGI034, LGI037, LGI039).

5.6 Summary of findings

- Exposure to FSS increases eNOS phosphorylation in FpECs
- Basal levels of total and phosphorylated eNOS are increased in SGA FpECs
- Yoda1 activates Piezo1 channels, rapidly increasing eNOS phosphorylation in AGA FpECs
- Yoda1 also evokes an increase in eNOS phosphorylation in SGA FpECs, indicating that activation of Piezo1 channels in SGA FpECs can lead to downstream NO signalling
- In the AGA FpECs, antagonising P2Y₂ receptors did not significantly reduce Yoda1-evoked Ca²⁺ entry nor peNOS, demonstrating that purinergic receptors are not a requirement for Piezo1 channel activity. Likewise Piezo1 depletion did not affect the ATP-evoked Ca²⁺ transient. Both purinergic signalling and Piezo1 channel activity occurred in the FpECs, but function, at least partly, independently of each other
- Hypotonic stress elevates intracellular Ca²⁺, which is potentiated by Yoda1, indicating that membrane tension activates Piezo1 channels in FpECs
- Both depletion of Piezo1 and antagonism of P2Y₂ receptors partially blunted the intracellular Ca²⁺ rise in response to hypotonic stress, which became abolished when both assays were used in conjunction. This supports our proposal that Piezo1 channel activity and purinergic signalling are both present, and may represent a small number of important intracellular signals operating either together or functioning independently for shear stress sensing in the fetoplacental endothelium

5.7 Discussion

5.7.1 Nitric oxide signalling in endothelial cells

In the introduction to this chapter, previous work from our group indicating that Piezo1 is important for eNOS phosphorylation was discussed. A key finding was that Piezo1 depletion in HUVECs reduced peNOS (Li et al., 2014). This was supported by murine model data where peNOS was reduced in aortic ECs from the Piezo1 knockout mice (Li et al., 2014). To confirm whether Yoda1 was sufficient to activate eNOS, laboratory member Hannah Gaunt measured the biochemical conversion of L-arginine to L-citrulline to measure eNOS activity in HUVECs (<http://etheses.whiterose.ac.uk/22684/>). In this experiment, application of Yoda1 was sufficient to evoke an increase in citrulline content, an indication of eNOS activation. VEGF was used a positive control in this assay, and was found to evoke a similar amplitude of increase in citrulline content compared to Yoda1. These data provide further evidence that chemical activation of Piezo1 evokes eNOS phosphorylation that leads to eNOS activation.

In this chapter I have presented the first evidence that Piezo1 may have a key role in regulating FSS-mediated vasodilation through NO signalling in the human placenta. Data presented here, and in Chapter 4 have demonstrated that Piezo1 channel activation by either FSS or Yoda1 leads to a rise in intracellular Ca^{2+} , and both stimuli result in eNOS phosphorylation at serine site 1177. We propose that the subsequent NO release contributes to placental vasodilatation via smooth muscle cell relaxation (Figure 5.17).

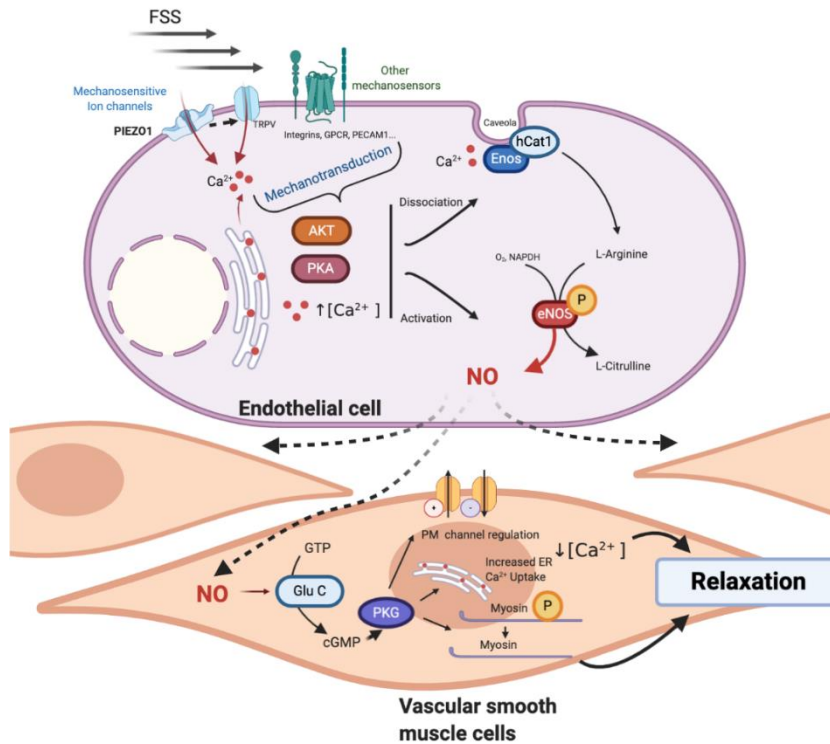


Figure 5.17 Schematic illustrating possible mechanisms by which FSS activation of Piezo1 and other mechanosensors in FpECs results in vasodilatation through the production of NO. Illustration showing that FSS-evoked activation of mechanosensors induces a rise in FpEC Ca^{2+} , either via Ca^{2+} entry or release from intracellular stores. Our focus is on Piezo1, but we acknowledge the potential role for other mechanosensors, having demonstrated G-protein coupled receptor 68 (*GPR68*) expression in FpECs. The resulting increase in intracellular Ca^{2+} drives eNOS phosphorylation. I have also included the contribution from FSS-evoked ATP inducing intracellular Ca^{2+} mobilisation, and AKT-mediated eNOS phosphorylation in FpECs, although the data suggest that this mechanism is largely independent of Piezo1-mediated Ca^{2+} entry and eNOS phosphorylation.

The subsequent NO production induces vasorelaxation via smooth muscle cells. In SGA FpECs, eNOS and phosphorylated eNOS are elevated, supporting the hypothesis that increased FSS results in compensatory production of NO. However, Piezo1 channel function may be reduced in SGA, decreasing the FSS-evoked Ca²⁺ entry. FSS-independent mechanisms of NO signalling may be enhanced, and mechanosensor gene expression upregulated (*PIEZO1* and *GPR68*) to drive the compensatory response. Abbreviations: NO nitric oxide, P phosphorylation, eNOS endothelial NO synthase, PK protein kinase, hCAT high affinity cationic amino acid transporter. Created with BioRender.com.

5.7.2 Nitric oxide signalling in fetal growth restriction

The data presented in Figure 5.2 show an increase in both total and phosphorylated eNOS in the FpECs from SGA placentas. These cells were cultured to passage 5 prior to lysing. This upregulation of peNOS has therefore persisted through passaging. This corresponds with prior reports in the literature showing increased peNOS in FGR (Myatt, 2006, Jones et al., 2015, Giannubilo et al., 2008). Earlier in this chapter we also showed that exposing FpECs to flow increases eNOS phosphorylation (Figure 5.3).

As discussed in Chapter 1, section 1.6.3 an increasing body of evidence from computer modelling is reporting higher shear stress in placental insufficiency (Tun et al., 2019). This corresponds to chorionic arteries from FGR placentas that show elevated baseline vascular resistance, alongside substantially reduced or absent flow mediated vasodilatation (Jones et al., 2015). Our data therefore supports the hypothesis that the fetoplacental endothelium in FGR attempts to compensate restricted blood flow by upregulating components of the NO system as an adaptive physiological mechanism. When endothelial dysfunction is severe enough to prevent this response to increased FSS, flow-induced NO compensation may be insufficient and vascular dysregulation may still progress (Jones et al., 2015, Morley et al., 2019, Giannubilo et al., 2008).

Jones et al., (2015) found increased nitrite in flow conditioned media from FGR chorionic plate arterial cells. This group also found raised levels of inducible NOS (iNOS) in the FGR group (Jones et al., 2015). iNOS is associated with turbulent flow conditions, and has been implicated in inflammatory vascular disease and obesity (Gliozzi et al., 2019, Torrisi et al., 2016). Here, vascular inflammation results in increased cytokine production, leading to dysregulation of the eNOS/iNOS enzymes. For example, overproduction of oxidized low-density lipoproteins in hyperlipidaemic patients leads to imbalanced activation of eNOS via upregulation of arginase (Gliozzi et al., 2019). Uncoupled eNOS is unable to produce NO effectively. In this context, the subsequent overproduction of reactive oxygen and nitrogen species (ROS and RNS, respectively) activates NADPH oxidase in the ECs. This results in a vicious circle, whereby the production of superoxide anions by NADPH oxidase, in turn, reduces NO bioavailability leading to further dysregulation of the eNOS/iNOS balance and worsening endothelial dysfunction (Gliozzi et al., 2019). Upregulated iNOS activity may therefore represent compensation for impaired NO bioavailability. Paradoxically, this iNOS-induced production of NO combines with the superoxide anions to form peroxynitrite. This is known to cause nitritative stress and has been correlated with EC death via apoptosis (Salvolini et al., 2019).

Krause et al., (2013) suggest that in FGR, despite the upregulated expression of eNOS, it has reduced biological activity. Their group found reduced gene expression for the hCAT proteins involved in eNOS activation (Casanello and Sobrevia, 2002). L-arginine transport and production of L-citrulline was also reduced in FGR (Casanello and Sobrevia, 2002). Furthermore, exposing HUVECs to hypoxia increased activity of arginase-2, the enzyme competitor of eNOS, thus influencing the bioavailability of L-arginine for NO production (Krause et al., 2013). Abnormal functioning of this part of the L-arginine-NO pathway (Figure 5.17) may also contribute to dysregulated NO in placental insufficiency. However, it should be noted that these data were obtained from basal, rather than flow conditions, therefore representing the FSS-independent state.

How the raised total and phosphorylated eNOS seen in the SGA samples in this project relate to the bioavailability of NO and production of iNOS remain to be determined. It is possible that rather than leading to effective compensatory vasodilatation, dysregulated activation of eNOS in placental insufficiency perpetuates endothelial dysfunction in a vicious circle. As such, determining the eNOS/iNOS balance and NO bioavailability alongside evidence of inflammation and nitrate stress in flow-conditioned samples from placental insufficiency is a research priority.

5.7.3 Piezo1 channel activity and ATP activation in FpECs

The secondary aim of this chapter was to determine whether there was commonality between Piezo1 channel activity and ATP activation in FpECs. This hypothesis was supported by our data showing that FpECs exhibit a Ca^{2+} mobilisation response to ATP, with an early additive effect when ATP and Yoda1 were used in combination (Figure 5.7).

The P2Y₂ receptor antagonist, suramin, has previously been used to demonstrate that ATP inhibition prevents AKT activity, resulting in blockade of ATP-induced NO (Silva et al., 2006). This has been demonstrated in the rat kidney, where in the presence of suramin, ATP-induced NO was blocked by 90% (Silva and Garvin, 2009). Likewise, in vivo transduction of nephrons with a dominant-negative *Akt1* decreased ATP-induced NO by 88%.

Suramin was therefore used to determine the dependence of ATP for Piezo1-evoked eNOS phosphorylation. These data showed that despite suramin effectively blocking ATP-induced Ca^{2+} transients, the impact on Yoda1-evoked Ca^{2+} entry was partial, and there was no evidence of a difference to eNOS phosphorylation in FpECs (Figure 5.8 and Figure 5.9). This was also investigated in HUVECs by another laboratory member, Hannah Gaunt. In assays using apyrase to catalyse the hydrolysis of ATP, Yoda1-evoked eNOS phosphorylation was seemingly unaffected in HUVECs (<http://etheses.whiterose.ac.uk/22684/>). In addition, treating HUVECs with siRNA

targeting *AKT* did not produce a difference in Yoda1-mediated eNOS phosphorylation. However, apyrase did significantly reduce the FSS-evoked Ca^{2+} response. Taken together with my findings, our data confirm that ATP has a role in the mechanosensory response in the human placenta. However, Yoda1 acts independently of extracellular ATP, P2Y_2 receptors and AKT. This suggests that in HUVECs and FpECs, purinergic signalling is not a requirement for Piezo1 channel function.

In addition, pre-treating FpECs with suramin did not fully block hypotonicity-induced Ca^{2+} entry (Figure 5.15). This indicates that the response to hypotonic stress is not only mediated by ATP release via P2 receptors, but by other ion channels as well. These data are in agreement with previous work using a similar assay whereby hypotonically-induced Ca^{2+} elevation was suppressed by the non-specific cation channel blockers nifedipine, amiloride, 2-aminoethoxydiphenylborate and ruthenium red, as well as Gd^{3+} . This study also found that Ca^{2+} elevation was not inhibited by suramin (Takii et al., 2006). The stimulatory effects of hypotonicity and Yoda1 were also lost in the presence of nonspecific Piezo1 inhibitors. This inhibition of Yoda1-induced Ca^{2+} entry by hypotonicity was maintained after Piezo1 knockdown. We therefore propose that hypotonic stress mechanically activates Piezo1 channels leading to Ca^{2+} entry and subsequent membrane depolarisation. However, certain experiments are lacking sufficient numbers to perform quantitative analysis (Figures 5.15 and 5.16C). Adding to these data would make the picture of Piezo1 and ATP contributions to flow-sensing clearer.

Similar to that described for FSS, it has also been suggested that the hypotonic stress response can be mediated by focal adhesion proteins (FAK/paxillin), integrins and Rho-kinases (Hirakawa et al., 2004). This group suggest that 'a variety of mechanosensitive responses in the endothelium in fact originate from a few common intracellular signals'. Whether Piezo1 FSS-sensing and intracellular Ca^{2+} entry is integrated with other mechanosensing components of FpECs remains to be determined. Preliminary data from HUVECS in our lab indicate that Piezo1 is involved with the mechanosensory triad

involving CD31. Whether this is true of FpECs, and whether the signalling differs in placental insufficiency requires further exploration.

It should be noted that the hypotonic solutions assay is not physiologically representative of shear stress on the endothelium. As such, data presented in the next chapter are from experiments exposing FpECs to flow conditions in a microfluidic chamber in order to better model physiological shearing forces.

Chapter 6 Notch signalling via Piezo1 in the placenta

6.1 Introduction

Earlier in the thesis (section 1.5) we considered the importance of FSS for normal vascular adaptation. The nature of the shearing force is also important for vascular health. For example, in the systemic circulation, FSS in the descending thoracic aorta is laminar, where the endothelium has an atheroprotective phenotype (Davies et al., 2013). However, in the aortic arch which is characterised as being atheroprone, flow is turbulent and oscillatory, altering the shearing forces (Davies et al., 2013). This is particularly important in the placenta, where due to the altered vascular anatomy in the FGR placenta, we propose that FSS is disturbed. Mechanosensors act as the 'initial responders' to changes in the mechanical environment (Mack et al., 2017). I have suggested that Piezo1 is a vital component of this process in FpECs, although the complete picture of mechano-signalling appears complex, with the potential for multiple dependent and independent pathways.

The Notch signalling pathway has also been demonstrated to be flow-sensitive. This has been demonstrated in human aortic ECs, where the application of FSS increased *NOTCH1* expression to a level comparable to CD31 in flow conditions (Mack et al., 2017). Furthermore, after *NOTCH1* depletion using siRNA, ECs lacked alignment to the direction of flow, and displayed a more proliferative phenotype (Mack et al., 2017). Given these findings, the role of Notch signalling in FpEC mechanosensation, and the potential for interplay with Piezo1, was investigated.

6.1.1 Notch signalling in endothelial cells

The Notch family of proteins are highly conserved across species, having first been identified in the fruit fly *Drosophila* (Wolf et al., 2019). In mammals, there are four Notch receptors, encoded by Notch genes 1-4. There are 5 ligands classified into two groups- the delta-like ligands (Dll)-1, -3, and -4, and Serrate-like ligands (Jagged-1 and -2) (Wolf et al., 2019, De Falco et al., 2007). The receptors are located at the cell surface, with an

extracellular domain that binds the ligands, and an intracellular domain. Both types of ligands are transmembrane proteins, with either a Delta, Serrate or Lag-2 (DSL) binding domain to enable the receptor interaction (De Falco et al., 2007). The predominant Notch signalling pathway is therefore canonical, where Notch receptors expressed on the surface of one cell interact with the ligands present on the surface of a neighbouring cell (Cuman et al., 2014). This signalling can occur between either equivalent or different cell types (trans-activation), or intracellular auto-inhibition within the same cell (cis-inhibition) (Cuman et al., 2014). Signalling is initiated when receptor-ligand binding results in proteolytic cleavage of the transmembrane subunit (Figure 6.1). This is performed by the proteases, ADAM10 (A Disintegrin and Metalloprotease) and γ -secretase. This releases the Notch intracellular domain (NICD), which translocates to the nucleus. NICD is activated by binding to Recombining Binding Protein Suppressor of Hairless (RBPSUH) in the nucleus, resulting in the transcription of Notch target genes. The downstream genes include members of the basic helix-loop-helix (Hes) and hairy/enhancer of split-related (Hey) families (Cuman et al., 2014). These genes are transcription regulators, which relates to the importance of Notch signalling for cell fate determination (De Falco et al., 2007).

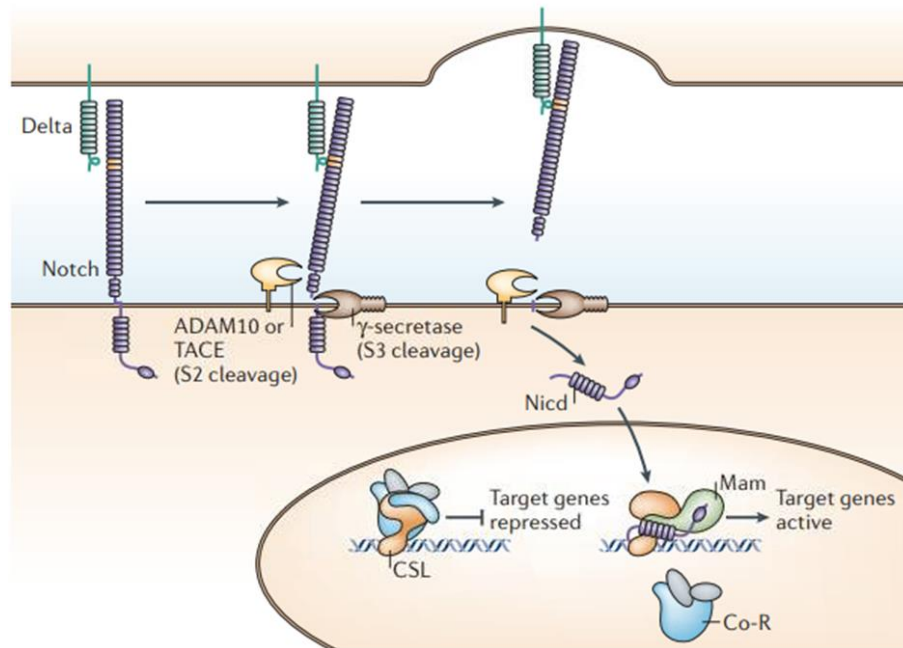


Figure 6.1 Notch signalling pathway schematic. Illustration showing binding of a Notch ligand (Delta, green) on the signal sending cell to a Notch receptor (purple) on another cell. This results in two proteolytic cleavages of the receptor. ADAM10 or TACE (TNF- α -converting enzyme; also known as ADAM17) metalloprotease (yellow) catalyses S2 cleavage, generating a substrate for S3 cleavage by the γ -secretase (brown). This proteolysis releases the Notch intracellular domain (NICD), which translocated to the nucleus. Here, NICD interacts with the DNA-binding CSL (CBF1, Suppressor of Hairless, Lag-1) proteins (orange). The co-activator Mastermind (Mam; green) and other transcription factors are recruited to the CSL complex, whereas co-repressors (Co-R; blue and grey) are released (Bray, 2006). This results in the transcription of Notch target genes. Figure from Bray et al., 2006.

Notch proteins can also participate in non-canonical signalling (Cuman et al., 2014). This can occur via membrane-bound ligands that lack the DSL domain, or independently. Ligand-independent signalling is thought to occur when Notch receptors localise to the cytoplasm. However, much remains to be understood about these non-canonical pathways and this has not been investigated in FpECs during this project.

6.1.2 Function and importance of Notch signalling

Several mouse models have been used to demonstrate that Notch signalling is important for vascular development from early in embryonic organo- and vasculogenesis, through to adult vascular function (Wolf et al., 2019). Examples include embryonic lethality in mice with haploinsufficiency of the Dll-4 ligand due to major vascular defects (Gale et al., 2004). Combined deletion of both *Notch1* and *Notch4*, or deletion of *Jag1* in mice resulted in haemorrhage and various disruptions to normal arterial development (De Falco et al., 2007).

During blood vessel formation, newly generated ECs undergo arterial-venous specification. This cell fate determination is thought to be regulated by Notch, and in particular, by the Dll-4 ligand. Differential expression of ligands and receptors therefore occurs, whereby Dll-4, Notch1, and Notch4 are solely expressed in arteries. In Chapter 3 which investigated the phenotype of placental tissue sampled in this project, the relative abundance of Ephrin genes was measured. Reduced expression of both the ephrin-B2 (arterial, *EFNB2*) and ephrin-B4 (venous, *EFNB4*) markers was found in the SGA whole villous tissue (Figure 3.3). This result raises the question of abnormalities in Notch signalling in placental insufficiency, given that Dll-4 induces expression of ephrin-B2.

Besides the control of cell fate, notch signalling is important for vascular homeostasis, through the regulation of angiogenesis (Wolf et al., 2019). During angiogenesis, ECs start sprouting and express Dll-4 downstream of VEGF (Caolo et al., 2015). This has been demonstrated in murine retina where VEGF-induced Dll-4 is a negative regulator of endothelial proliferation. Correspondingly, blockade of Dll-4 resulted in proliferation akin to pathological neovascularization (Lobov et al., 2007). Likewise, inhibition of ADAM10 or γ -secretase in the murine retina induced vascular sprouting and density (Caolo et al., 2015). Similarly, the expression pattern of the Hes component of Notch is temporal, whereby downregulation occurs at the initiation of new vessel sprouting to enable VEGF-mediated migration and proliferation (Henderson 2001). However, re-expression occurs later at tubular network formation to establish the mature, quiescent

vessel. These findings suggest that the Notch pathway is essential for the maturation and fine-tuning of a healthy vascular network.

6.1.3 Notch signalling in human disease

The role of Notch signalling in human disease was first recognised in 1991, when *NOTCH1* mutations were found to induce T-cell acute lymphoblastic leukaemia (Ellisen et al., 1991, Penton et al., 2012). Autosomal dominant mutations in the extracellular domains of *NOTCH3* were discovered to be the cause of an adult-onset vascular condition, CADASIL (for cerebral autosomal dominant arteriopathy with subcortical infarcts and leukoencephalopathy), characterised by strokes and dementia (Joutel et al., 1996). Autosomal dominant inheritance of a *JAG1* mutation has been identified in those with Alagille syndrome, which affects the organogenesis of liver, heart, skeleton, eye, face and kidney (Li et al., 1997). The importance of Notch signalling for organogenesis as well as vascular function has been further demonstrated in murine embryos, where studies of spontaneous or induced mutants revealed cell-lineage regulation in all primary germ layers: endoderm (pancreas), mesoderm (skeleton, mammary gland, vasculature, and hematopoietic cells), and ectoderm (neuronal lineages) (Penton et al., 2012).

6.1.4 Shear stress regulation of Notch signalling

The canonical Notch signalling pathway is activated by the binding of ligands to the Notch receptors. A further requirement of Notch activation is that the ligands need to be internalized by the signal-sending cell to activate Notch on the signal-receiving cell (D'Souza et al., 2010). In the absence of this endocytosis, ligands accumulate at the cell surface but fail to activate signalling. The ligand endocytosis is thought to generate a mechanical force which induces a conformational change in the Notch receptor (Kopan and Ilagan, 2009). This 'pulling' force exposes the ADAM10 cleavage site, thus acting as a lever for activating proteolysis. Supporting this hypothesis is the requirement for cell components involved in mechanosensing, such as the actin cytoskeleton, to enable alterations to membrane tension (D'Souza et al., 2010).

In addition to endocytosis-generated mechanical force triggering trans-activation, the effect of applying FSS on Notch signalling has been considered. This has been demonstrated in human aortic ECs, where the flow-induced upregulation of *NOTCH1* was prevented in the presence of a γ -secretase inhibitor (DAPT) (Mack et al., 2017). Flow-induced increased expression of the Notch target genes including *HES1* was also blocked by the DAPT. A separate study found an increase in NICD protein expression in HUVECs under flow conditions compared to static control. This FSS-evoked increase in NICD was also inhibited by DAPT (Fang et al., 2017). This study in HUVECs also showed that FSS (12 dyne/cm²) increased the expression of *HEY1* and *HES1*. However, these authors did not find that FSS increased *NOTCH1* (Fang et al., 2017).

Shear stress forces have been shown to induce EC differentiation into arterial or venous lineages (Masumura et al., 2009). This has been demonstrated in murine embryonic stem cells where exposure to FSS increased the expression of ephrin-B2, and decreased the expression of ephrin-B4, dose-dependently. FSS also induced Notch cleavage and translocation of NICD to the nucleus within 30 minutes of flow commencing. Furthermore, DAPT abolished the FSS-induced NICD translocation, which also prevented the upregulation of *Ephrin-B2* (Masumura et al., 2009). These findings therefore suggest that arterial-venous specification of ECs is, at least in part, regulated by Notch signalling pathways.

Our group have also shown that applying FSS (10 dyne/cm²) to human cardiac microvascular ECs increased the expression of the NICD protein (Caolo et al., 2020). Interestingly, after depletion of Piezo1 with siRNA, FSS-induced expression of NICD was reduced to levels of the static control. This raised the question of whether shear stress activation of Notch signalling is coupled to Piezo1. Our group went on to demonstrate that in adult mice with an endothelial-specific disruption of Piezo1, multiple notch target genes, including *Hes1*, *Hey1*, *Jag1* and *Dll4*, were suppressed in liver ECs, suggestive of functional importance *in vivo* (Caolo et al., 2020).

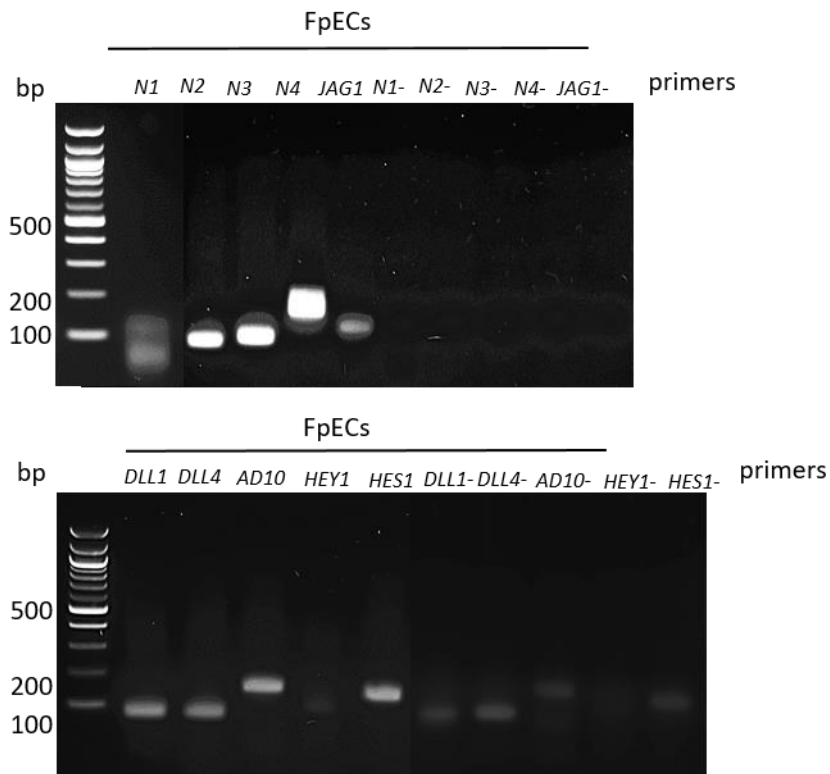
Given the importance of Notch signalling for embryonic organo- and vasculogenesis, the expression of Notch pathway genes in the human placenta was considered. As such, the potential for interplay between FSS-activated Piezo1 channels and Notch was investigated in the whole placental tissue samples and cultured FpECs used in this project.

6.2 Notch signalling gene expression in human placentas

6.2.1 Notch genes are expressed in FpECs from AGA and SGA placentas

Following on from the identification of Piezo1 mRNA in cultured FpECs, lysed cells from either the AGA group or the SGA samples were used to determine the expression of Notch pathway genes in the fetoplacental endothelium. QPCR was performed for the following genes: *NOTCH1*, *NOTCH2*, *NOTCH3*, *NOTCH4*, *JAG1*, *DLL1*, *DLL4*, *HEY1*, *HES1* and *ADAM10*. This expression was confirmed in an AGA sample (LGI096) by demonstrating the amplified QPCR products using gel electrophoresis (Figure 6.2).

In order to compare the relative abundance of each gene between the 10 AGA and 8 SGA samples, the expression data were normalised to the mean of the three reference genes used previously (*ACTB*, *CYC-1* and *YWHAZ*). A representative sample from the AGA and SGA groups was used for a minus reverse transcriptase (-RT) reaction. This demonstrated that *HEY1* was not expressed until a higher cycle threshold (Ct) compared to the other Notch genes, which was not different between the AGA or SGA sample (Table 16).



Gene	<i>N1</i>	<i>N2</i>	<i>N3</i>	<i>N4</i>	<i>JAG1</i>	<i>DLL1</i>	<i>DLL4</i>	<i>AD10</i>	<i>HEY1</i>	<i>HES1</i>
Amplicon length (bp)	119	111	121	116	146	76	77	153	85	133

Figure 6.2 Notch pathway genes are expressed in FpECs. Gel electrophoresis image of amplified products following QPCR, showing the following genes *N1* (*NOTCH1*), *N2* (*NOTCH2*), *N3* (*NOTCH3*), *N4* (*NOTCH4*), *AD10* (*ADAM10*). Samples suffixed with ‘-’ refers to minus reverse transcriptase. The lower panel shows expected amplicon sizes, bp (base pair). AGA control sample: LGI096.

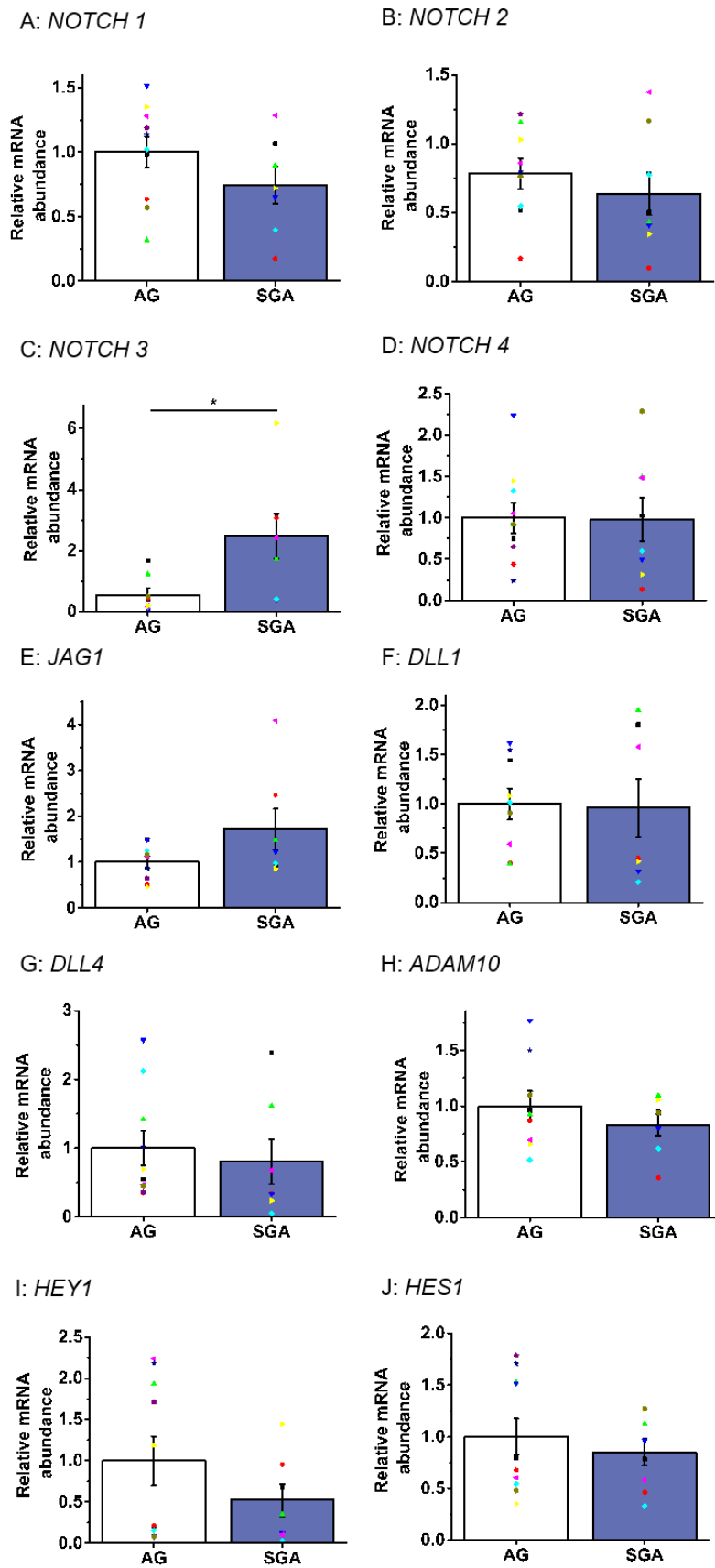


Figure 6.3 Notch signalling genes are present in FpECs from both AGA and SGA placentas, with increased expression of *NOTCH3* in SGA FpECs.

Summarized mean \pm SEM QPCR data for relative abundance of Notch signalling genes when normalised to the mean of three reference genes (*ACTB*, *CYC-1*, *YWHAZ*). *NOTCH3* was significantly upregulated in the SGA FpECs ($p < 0.02$). AGA control group $n = 10/N = 2$: LGI008, LGI011, LGI031*, LGI035, LGI037, LGI046, LGI069, LGI079, LGI096, LGI103. SGA group $n = 8/N = 2$: LM12, LGI016, LGI038, LGI042, LGI051, LGI058, LGI063, LGI067. *LGI031 was removed as a statistical outlier in the analyses of *NOTCH3* and *ADAM10*. A-J: unpaired *t* test.

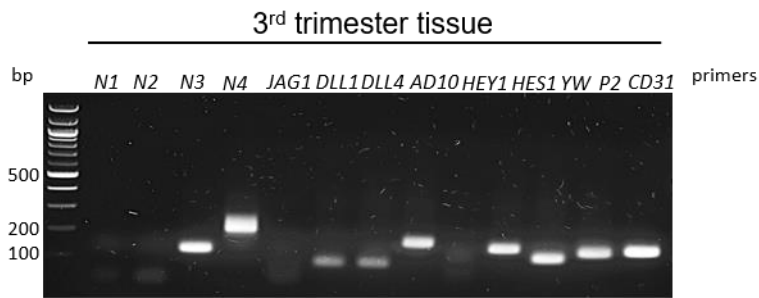
Gene	Mean Ct AGA LGI008	Mean - RT Ct AGA LGI008	Mean Ct SGA LGI051	Mean - RT Ct SGA LGI051
<i>N1</i>	21.5	31.95	21.94	32.275
<i>N2</i>	23.25	30.13	23.67	30.51
<i>N3</i>	28.90	36.19	28.59	35.95
<i>N4</i>	21.40	39.85	23.83	35.805
<i>DLL4</i>	22.35	34.59	22.47	36.22
<i>ADAM10</i>	19.65	30.2	20.92	32.425
<i>HEY1</i>	30.8	32.99	29.43	32.69
<i>HES1</i>	21.63	ND	22.29	ND
<i>JAG1</i>	22.045	34.485	22.82	34.215
<i>YWHAZ</i>	18.06	31.675	18.46	32.395

CYC1	20.88	ND	20.84	ND
BA	13.53	29.28	15.02	29.24

Table 16 Representative cycle threshold and minus reverse transcriptase values for Notch pathway and reference genes. Minus reverse transcriptase (-RT) was performed on one sample from the AGA group (LGI008) and one from the SGA group (LGI051), mean of two replicates. These data are presented alongside the positive reverse transcriptase cycle threshold (Ct) values. ND: not detected. When comparing the relative abundance of each of these genes, *NOTCH3* was upregulated in the SGA group, just meeting statistical significance ($p = 0.045$) (Figure 6.3C). To investigate this further, the demographic details of the patients in the SGA group were reviewed. Only one patient in the SGA group was a smoker (LGI038) and only one had abnormal placental blood flow Doppler recordings reported (LGI063), and therefore no subgroup analyses were performed.

6.2.2 Expression of notch genes in whole villous tissue from AG control and SGA placentas

Whole villous tissue was also used to investigate the expression of Notch genes in the placenta. QPCR for the genes shown in the previous section was performed on fresh frozen samples from AGA and SGA placentas. Gene expression was confirmed using gel electrophoresis on the amplified QPCR products from a representative AGA sample (Figure 6.4). The expected products for *NOTCH1*, *NOTCH2*, *JAG1* and *HEY1* were not shown clearly on this gel. I have nevertheless included quantitative data for the expression of these genes because the real-time QPCR methodology is more sensitive and specific than the gel-based approach. When reviewing the mean Ct values across all samples, the Ct values of *NOTCH1* and *NOTCH2* were 25.7 and 25.28, respectively. *JAG1* and *HEY1* were detected later (mean Ct of 31.8 and 31.26, respectively) indicative of low expression.



Gene	<i>N1</i>	<i>N2</i>	<i>N3</i>	<i>N4</i>	<i>JAG1</i>	<i>DLL1</i>	<i>DLL4</i>	<i>AD10</i>	<i>HEY1</i>	<i>HES1</i>
Amplicon length (bp)	119	111	121	116	146	76	77	153	85	133

Figure 6.4 Notch pathway gene expression in whole villous tissue. Gel electrophoresis image of amplified products following QPCR, showing the reference gene *YW* (*YWHAZ*), in addition to bands for *CD31* and Piezo 2 (*P2*). Abbreviations: *N1* (*NOTCH1*), *N2* (*NOTCH2*), *N3* (*NOTCH3*), *N4* (*NOTCH4*), *AD10* (*ADAM10*), bp (base pair). AGA sample: LGI069.

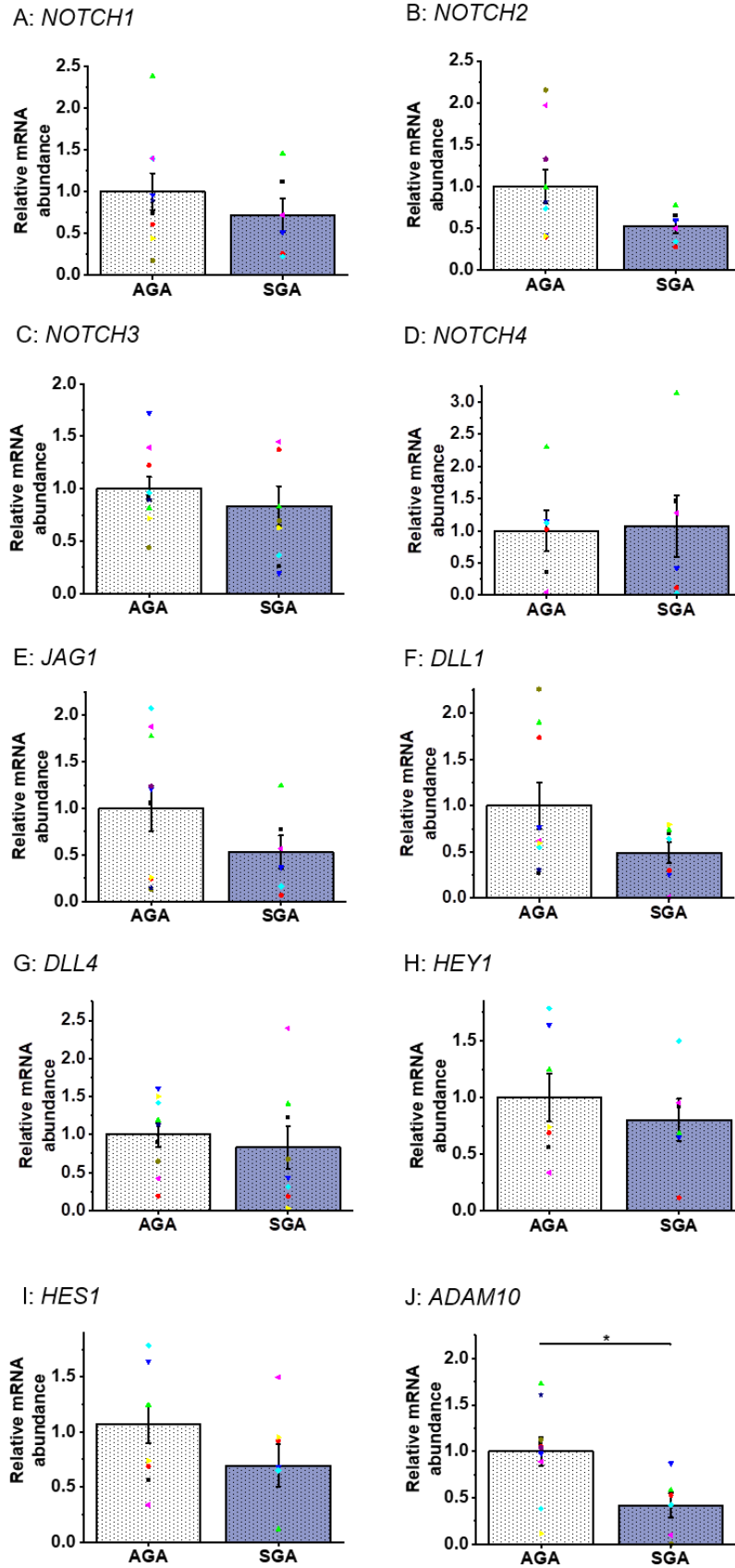


Figure 6.5 Notch signalling genes are present in whole villous tissue from AGA versus SGA placentas, with reduced expression of *ADAM10* in SGA samples.

Summarized mean \pm SEM QPCR data for relative abundance of Notch signalling genes when normalised to the mean of three reference genes (*ACTB*, *CYC-1*, *YWHAZ*). *ADAM10* was significantly downregulated in the SGA tissue ($p = 0.02$). AGA samples $n = 8/N = 2$: LGI036, LGI037, LGI041, LGI043, LGI045, LGI046, LGI065, LGI069, LGI071. SGA samples $n = 7/N = 2$: LGI026, LGI027*, LGI038, LGI051, LGI055, LGI058, LGI063. LGI027 was removed from the analysis for being a statistical outlier (relative abundance ($2\Delta\Delta CT$ 5.97)). A-J: unpaired t test.

The relative abundance of Notch genes normalised to the three reference genes was then compared between the fresh frozen placental tissue isolated from the AGA and SGA placentas. In contrast to the FpEC samples, there was no differential expression of *NOTCH3* between the AGA and SGA whole tissue samples, which may suggest that dysregulated *NOTCH3* occurs in the fetoplacental endothelium in placental insufficiency. There was, however, statistically significant downregulation of *ADAM10* in the SGA group ($p = 0.02$) (Figure 6.5J). This differential expression of *ADAM10* was only significant in whole tissue, as there was no evidence of difference in abundance in FpECs from AGA versus SGA placentas (Figure 6.3H). This raises questions about the expression of *ADAM10* in non-vascular placental cell types, or whether the culture of FpECs altered the expression phenotype compared to the fresh frozen villous tissue.

When reviewing the demographic details of patients included in this analysis, four women were smokers during the pregnancy (LGI026, LGI027, LGI038, LGI055). As such, a subgroup analysis was performed comparing the relative abundance of *ADAM10* between the AGA control group and SGA tissue with a maternal smoking history (Figure 6.6). The expression of *ADAM10* remained significantly lower in the SGA tissue compared to the AGA controls when those with a history of maternal smoking were included in the analysis ($n = 3$ patient samples, $p = 0.043$). Although the subgroup analysis including only non-smokers in the SGA group was not significant (Figure 6.6B), the inference was the same, and this analysis may be underpowered to detect an effect (Figure 6.6C). Within the SGA group, there was no significant difference in *ADAM10*

relative abundance between those with, and without a smoking history (Figure 6.6D). Given the endothelial dysfunction known to be caused by smoking (discussed in section 1.4.2.2), whether this impacts on Notch signalling function in placental vasculature remains an interesting question.

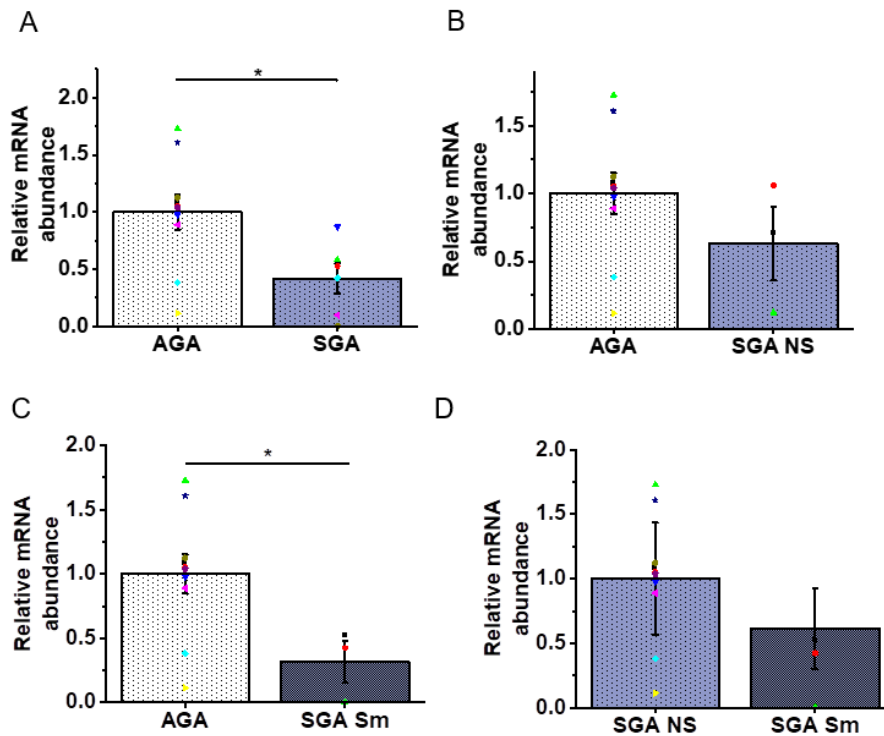
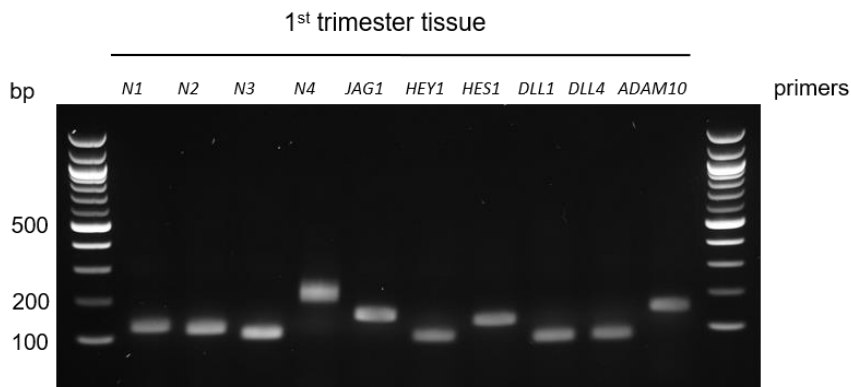


Figure 6.6. *ADAM10* relative mRNA abundance is downregulated in tissue from SGA placentas.

Summarized mean \pm SEM QPCR data for relative abundance of *ADAM10* when normalised to the mean of three reference genes (*ACTB*, *CYC-1*, *YWHAZ*). A., As per Figure 6.5J, *ADAM10* was significantly downregulated in the SGA whole villous tissue ($p = 0.02$). AGA samples $n = 8/N = 2$: LGI036, LGI037, LGI041, LGI043, LGI045, LGI046, LGI065, LGI069, LGI071. SGA samples $n = 7/N = 2$: LGI026, LGI027*, LGI038, LGI051, LGI055, LGI058, LGI063. LGI027 was removed from the analysis for being a statistical outlier (relative abundance ($2\Delta\Delta CT$) 5.97). B., Subgroup analysis comparing non-smokers (NS) in the SGA group ($n = 3/N = 2$: LGI051, LGI058, LGI063) with the AGA group (all NS), showing no significant difference. C., Subgroup analysis comparing those with a maternal history of smoking (Sm) in the SGA group (SGA Sm, $n = 3/N = 2$: LGI026, LGI038, LGI055) versus the AGA group, demonstrating significantly reduced expression of *ADAM10* in the SGA Sm tissue ($p = 0.043$). D., Data in the SGA Sm group were normalised to the SGA NS tissue, which demonstrated no significant difference in relative abundance. A-D: unpaired *t* test.

6.2.3 Notch genes are expressed in early pregnancy tissue

In the introduction to this chapter (section 6.1.2), the importance of Notch genes for vascular development and homeostasis was considered. Given the critical importance of angiogenesis and cell fate determination in human embryo- and vasculogenesis, we hypothesised that Notch signalling may be important in early pregnancy. Therefore, having established the expression of Notch pathway genes in FpECs and placental tissue, I next investigated Notch genes in the 1st trimester of pregnancy. As previously described, whole tissue mRNA samples were obtained from 1st trimester pregnancy terminations. QPCR was performed for the same panel of Notch genes. Expression was confirmed using gel electrophoresis on the amplified QPCR products from a representative sample (EP200) (Figure 6.7).



Gene	<i>N1</i>	<i>N2</i>	<i>N3</i>	<i>N4</i>	<i>JAG1</i>
Amplicon length (bp)	119	111	121	116	146
Gene	<i>HEY1</i>	<i>HES1</i>	<i>DLL1</i>	<i>DLL4</i>	<i>AD10</i>
Amplicon length (bp)	85	133	76	77	153

Figure 6.7 Notch pathway genes are expressed in 1st trimester pregnancy tissue.

Gel electrophoresis image of amplified products following QPCR, showing the following genes: *N1* (*NOTCH1*), *N2* (*NOTCH2*), *N3* (*NOTCH3*), *N4* (*NOTCH4*), *JAG1*, *HEY1*, *HES1*, *DLL1*, *DLL4*, *AD10* (*ADAM10*). bp (base pair). Early pregnancy sample: EP200.

The relative abundance of Notch genes was compared between the AGA tissue sampled from 3rd trimester placentas and pregnancy tissue obtained from the 1st trimester (Figure 6.8). These data revealed significantly higher expression of *JAG1* ligand and the *HEY1* signalling target mRNA. This corresponds with the low level of *JAG1* and *HEY1* expression in the control placental tissue from term pregnancies discussed in section 1.2.3. This can be illustrated by the significant difference in Ct values between the 1st and 3rd trimester samples for *JAG1* and *HEY1* (both $p < 0.0001$) (Figure 6.9).

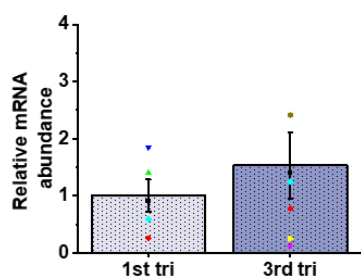
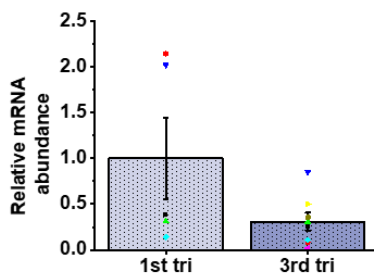
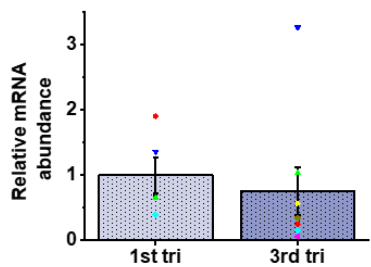
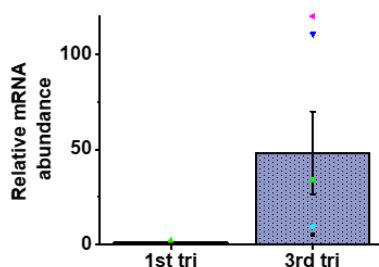
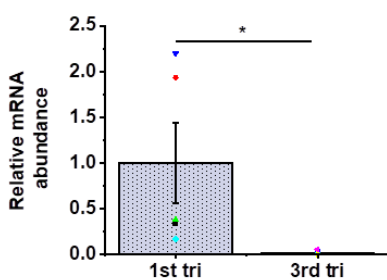
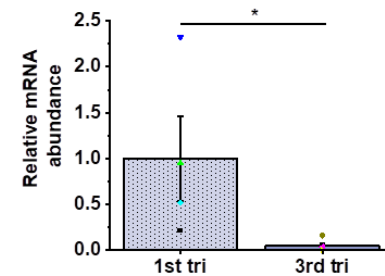
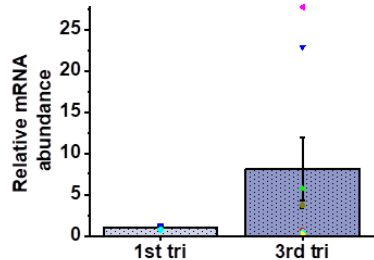
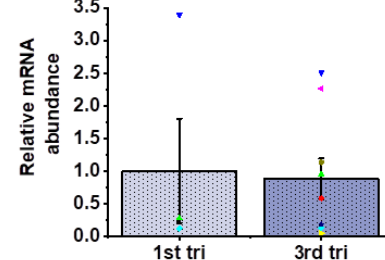
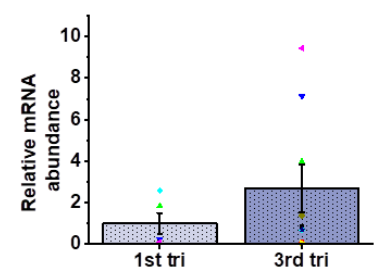
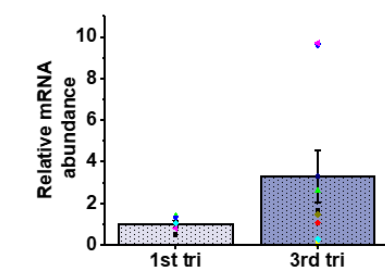
A: *NOTCH1*B: *NOTCH2*C: *NOTCH3*D: *NOTCH4*E: *JAG1*F: *HEY1*G: *HES1*H: *DLL1*I: *DLL4*J: *ADAM10*

Figure 6.8 Notch pathway genes are present in placentas from 1st and 3rd pregnancy trimesters with significant differential expression of *JAG1* and *HEY1*.

Summarized mean \pm SEM QPCR data for relative abundance of Notch signalling genes when normalised to the mean of 3 reference genes (*ACTB*, *CYC-1*, *YWHAZ*). A.-D., No significant difference in the relative abundance of Notch receptor genes, *NOTCH1*, *NOTCH2*, *NOTCH3*, *NOTCH4*, between the 1st and 3rd trimester tissue samples. E., Expression of *JAG1* is significantly higher in the 1st trimester samples ($p = 0.025$). F., Expression of *HEY1* is significantly higher in the 1st trimester samples ($p = 0.012$). G.-J., No significant difference in the relative abundance of *HES1*, *DLL1*, *DLL4* and *ADAM10* between groups. Early pregnancy samples $n = 5/N = 2$: EP188, EP189, EP200, EP201, EP202. AG control samples $n = 8/N = 2$: LGI022, LGI037, LGI043, LGI045, LGI046, LGI065, LGI069, LGI071. LGI071 was removed from the analyses for being a statistical outlier in all genes tested. A-H: unpaired *t* test.

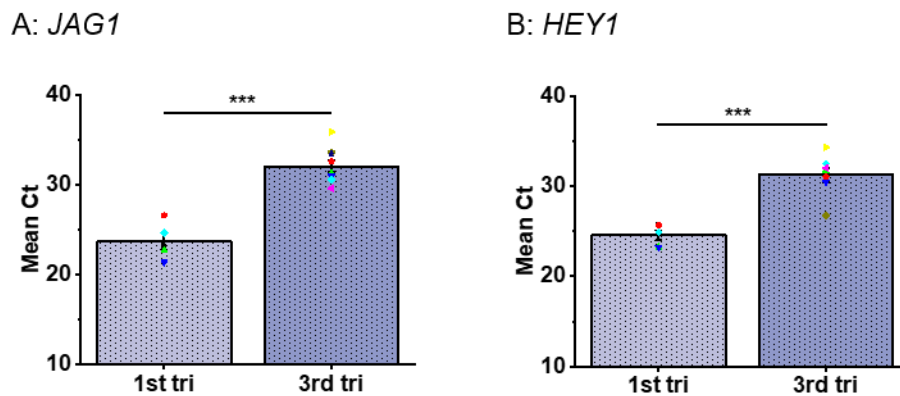


Figure 6.9 Threshold cycle of detection values for *JAG1* and *HEY1* are lower in the first trimester compared with the 3rd trimester. A., Significantly higher cycle threshold (Ct) in the 3rd trimester for *JAG1*. Mean 31.83 vs 23.7, $p < 0.0001$. B., As for A., for *HEY1*. Mean 31.26 vs 24.537, $p < 0.0001$. Samples as listed in Figure 6.8 legend, $n = 5/N = 2$ in 1st trimester group, $n = 8/N = 2$ in 3rd trimester group. A and B: unpaired *t* test

6.3 Chemical activation of Piezo1 upregulates parts of the Notch signalling pathway in FpECs

As discussed in the introduction to this chapter, FSS has been shown to upregulate aspects of the Notch signalling pathway, including *NOTCH1* and NICD mRNA and protein (Caolo et al., 2020, Mack et al., 2017). I have previously demonstrated that Yoda1 can activate Piezo1 channels, causing an influx of Ca^{2+} into the FpEC, without the need for applied exogenous force. As such, Yoda1 was used as tool to determine commonality between Yoda1-evoked Piezo1 channel activation and the Notch signalling pathway. Here, Yoda1 (0.2 μM) was applied to cells for a 30 minute pre-treatment. The results were compared to vehicle control (DMSO), and data from AGA and SGA groups were analysed.

Yoda1 had no effect on the expression of Notch receptor 1-4 genes in either the AGA or SGA groups (Figure 6.10). Strikingly, in these static conditions, Yoda1 stimulated an increase in the *DLL4* ligand, and *HEY1* and *HES1* effector genes in the FpECs from healthy placentas (Figure 6.11). In the SGA group, Yoda1 still potentiated a significant increase in *DLL4* (Figure 6.11J). However, the magnitude of increase was significantly less compared to that of the AGA group. After the application of Yoda1 to the SGA FpECs, there was no change in the expression of *HEY1* and *HES1* genes. The difference in *HEY1* and *HES1* evoked by Yoda1 was significant between the AGA and SGA FpECs (Figure 6.11D and F). There was no significant response to Yoda1 in any other Notch pathway genes tested (*JAG1*, *DLL1*, *ADAM10*), in either the AGA or SGA groups.

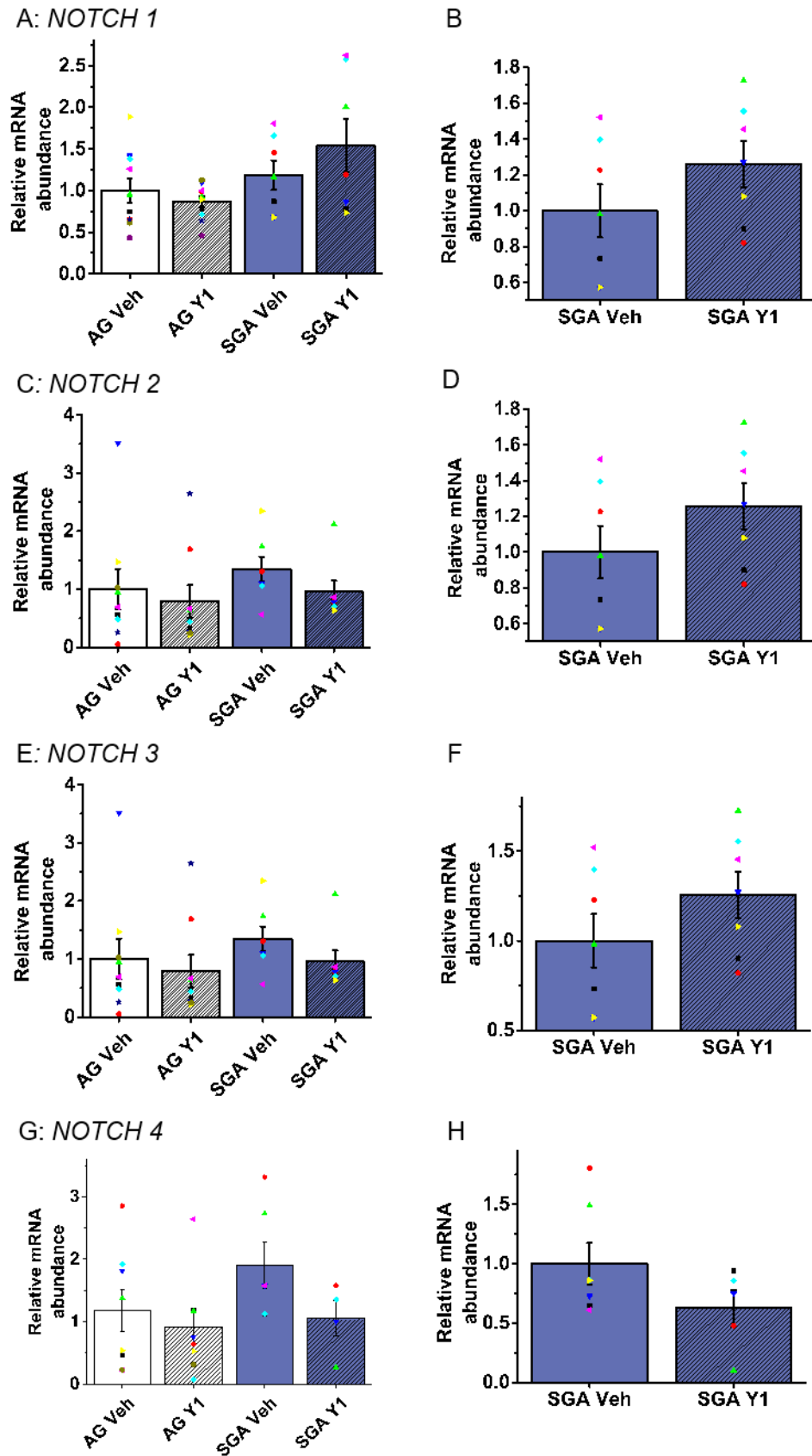
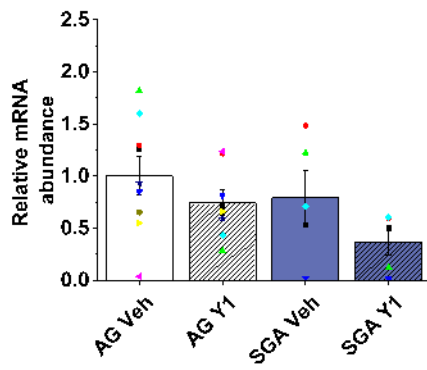


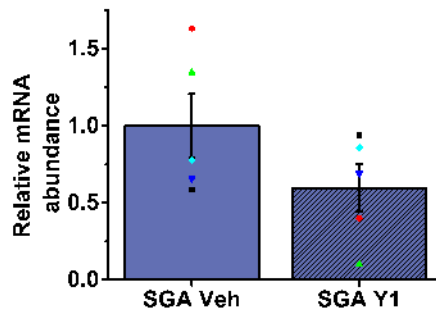
Figure 6.10 Yoda1 did not induce a significant difference in the expression of Notch receptor genes 1 to 4 in either AG for SGA FpECs.

Summarised mean \pm SEM QPCR data for relative abundance of Notch receptor genes 1-4, when normalised to the mean of 3 reference genes (*ACTB*, *CYC-1*, *YWHAZ*). A., C., E., G., Data normalised to the AGA vehicle (AG Veh, DMSO) control showing no significant difference in abundance after the application of Yoda1 (Y1, 0.2 μ M for 30 minutes), ANOVA. B., D., F., H., Data normalised to the SGA group vehicle (SGA Veh) showing no significant difference in abundance after the application of Y1. AG control samples, $n = 10/N = 2$: LGI011, LGI013, LGI031, LGI037, LGI041, LGI045, LGI046, LGI079, LGI096, LGI103. SGA samples, $n = 7/N = 2$: LGI016, LGI038, LGI051, LGI058, LGI063, LGI067, LGI075, unpaired *t* test.

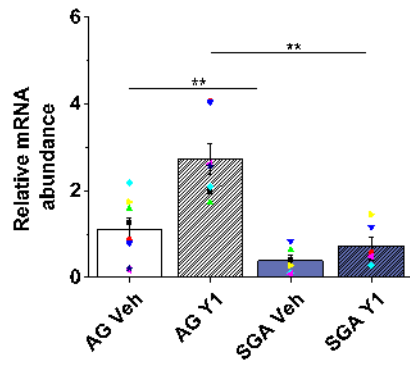
A: *JAG1*



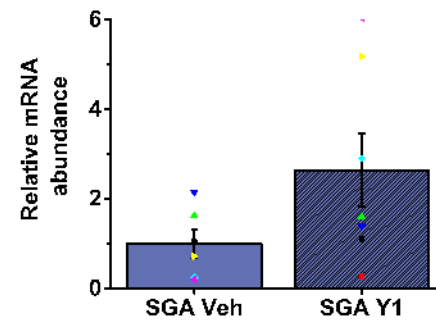
B



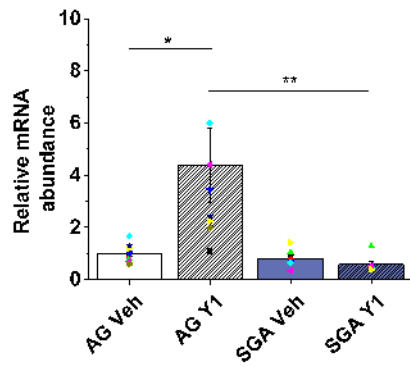
C: *HEY1*



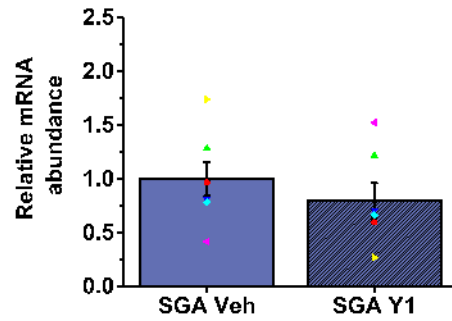
D

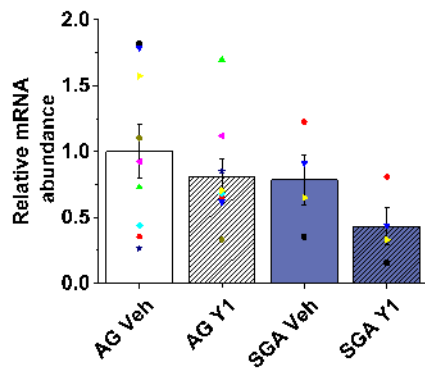


E: *HES1*

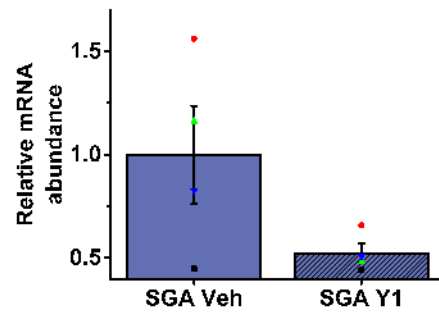
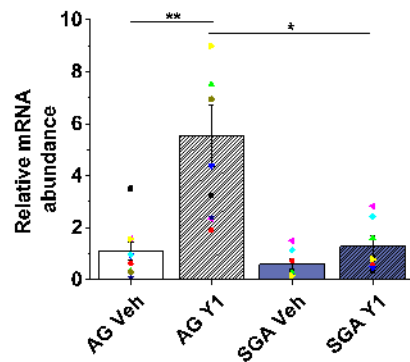


F

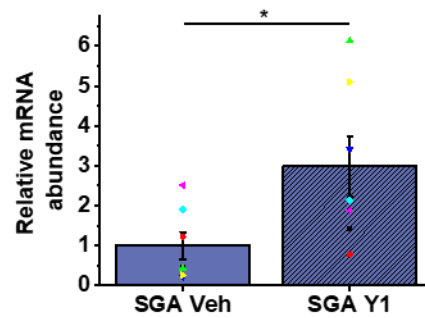
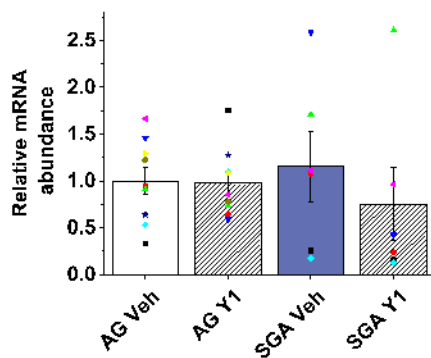


G: *DLL1*

H

I: *DLL4*

J

K: *ADAM10*

L

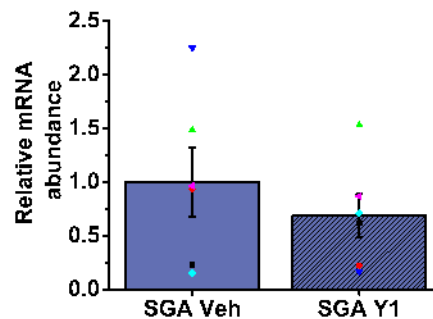


Figure 6.11 Yoda1 upregulates *HEY1*, *HES1* and *DLL4*, with differential expression between AG and SGA FpECs. Summarised mean \pm SEM QPCR data for relative abundance of Notch pathway ligand and effector genes, when normalised to the mean of 3 reference genes (*ACTB*, *CYC-1*, *YWHAZ*). FpECs from AGA or SGA groups were treated with either vehicle (Veh) or Yoda1 (Y1). A., C., E., G., I., K., Data normalised to the AGA vehicle (AG Veh) control, ANOVA. B., D., F., H., J., L., Data normalised to the SGA group vehicle (SGA Veh), unpaired *t* test. C., Y1 caused significant upregulation of

HEY1 in the AGA group ($p = 0.009$). Application of Yoda1 did not cause a significant increase in *HEY1* in the SGA group (C and D). The expression of *HEY1* was significantly greater after Y1 application in the AG control group versus Y1-treated SGA FpECs ($p = 0.005$). E., Y1 caused significant upregulation of *HES1* in the AG control group ($p = 0.01$). Application of Yoda1 did not cause a significant increase in *HES1* in the SGA group (E and F). The expression of *HES1* was significantly greater after Y1 application in the AGA group versus Y1-treated SGA FpECs ($p = 0.0065$). I., Y1 caused significant upregulation of *DLL4* in the AGA group ($p = 0.0036$). J., Y1 caused significant upregulation of *DLL4* in the SGA group ($p = 0.034$). The expression of *DLL4* was significantly greater after Y1 application in the AGA group versus Y1-treated SGA FpECs ($p = 0.0026$). Samples as per Figure 6.10 legend.

6.4 Effect of Piezo1 depletion on Yoda1-stimulated Notch gene expression in FpECs

Having established that Yoda1 evoked changes in the gene expression of parts of the Notch signalling pathway, I next sought to determine whether this response was Piezo1 dependent. As such, Piezo1 was depleted in FpECs using siRNA, as previously described. A scrambled siRNA sequence was used as a control, and cells were treated with either Yoda1 ($0.2 \mu\text{M}$) or vehicle (DMSO). After treatment with the control sequence, Yoda1 evoked a significant increase in the *NOTCH4* receptor, *DLL1* and *DLL4* ligands and effector genes, *HEY1* and *HES1* (Figure 6.12). It was noted however, that in this experiment series, the effect of Yoda1 was more marked than that evident in Figure 6.10 and Figure 6.11, when Yoda1 was applied to non-transfected AGA FpECs. Here, Yoda1 evoked a significant increase in *DLL4*, *HEY1* and *HES1* in 10 patient samples. Four of the 5 FpEC samples used for the transfection experiment were from the same patients as used for Figure 6.10 and Figure 6.11, with the addition of LGI050.

Of particular interest was the effect of Piezo1 depletion on the effect of Yoda1 on the expression of Notch genes. After Piezo1 siRNA transfection, there was no Yoda1-evoked change in the relative abundance of any Notch genes investigated (Figure 6.12). When quantified, the effect of Yoda1 was significantly different between the control and Piezo1-depleted FpECs for *DLL1*, *DLL4*, *HEY1*, and *HES1*. This indicates that the Yoda1-induced upregulation of ligand and effector gene components of Notch signalling, *DLL1*, *DLL4*, *HEY1*, and *HES1*, is Piezo1 dependent. Piezo1 depletion did not affect the basal expression of Notch genes in the absence of Yoda1 stimulation.

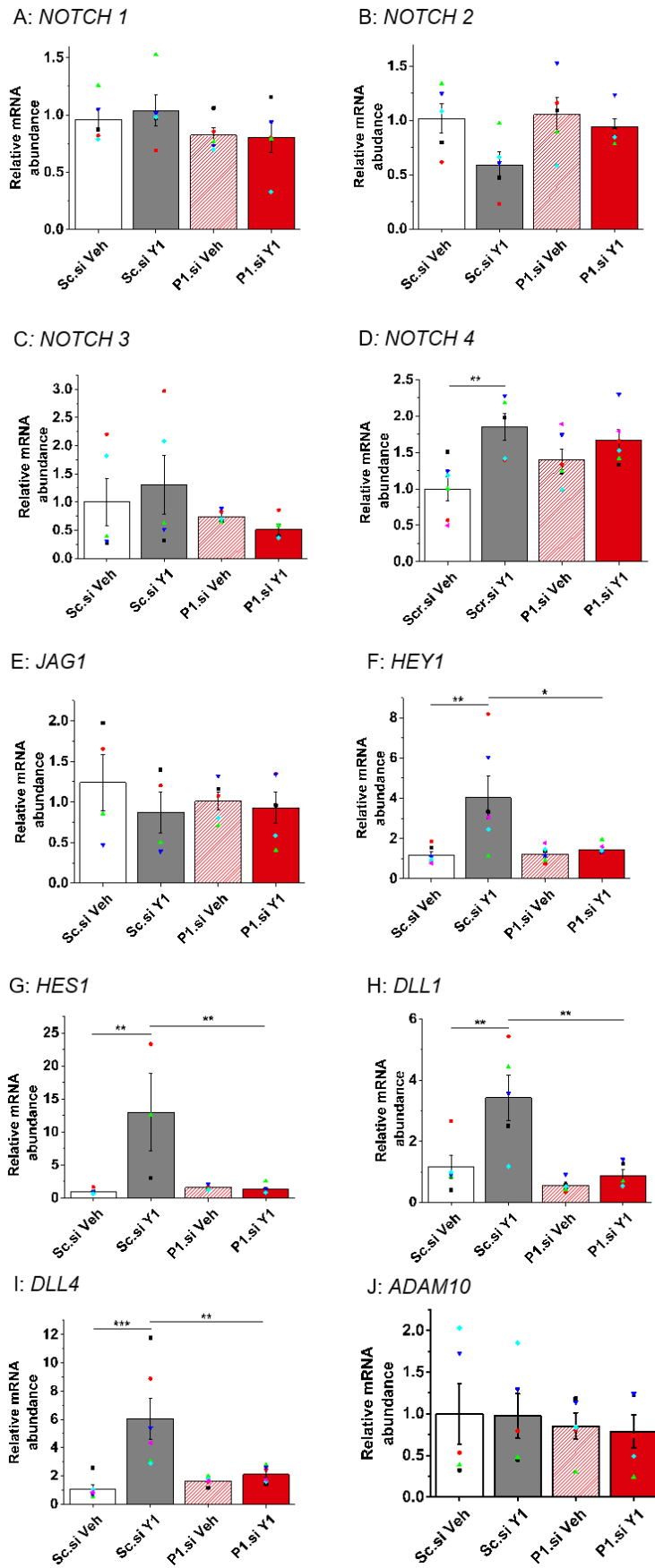


Figure 6.12 *PIEZO1* depletion blunts the effect of Yoda1 on the expression of *NOTCH4*, *HEY1*, *HES1*, *DLL1* and *DLL4*.

Summarised mean \pm SEM QPCR data for relative abundance of Notch pathway ligand and effector genes, when normalised to the mean of 3 reference genes (*ACTB*, *CYC1*, *YWHAZ*). FpECs from the AGA group were transfected with control sequence siRNA (Sc.si) or Piezo1-specific siRNA (P1.si), then treated with either Yoda1 (Y1) or vehicle (Veh, DMSO). A.-C., No significant difference in the relative abundance of Notch receptor genes 1-3. D., *NOTCH4* was increased after Y1 treatment in the Sc.si control group ($p = 0.007$), which was not significant after P1.si transfection. E., No significant difference in *JAG1* between Y1-treated Sc.si FpECs and Piezo1-depleted FpECs with Yoda1 applied. F., *HEY1* was increased after Y1 treatment in the Sc.si control group ($p = 0.007$), which was abolished after P1.si transfection. Significant difference between Y1-treated Sc.si FpECs and Piezo1-depleted FpECs with Yoda1 applied ($p = 0.015$). G., *HES1* was increased after Y1 treatment in the Sc.si control group ($p = 0.0009$), which was abolished after P1.si transfection. Significant difference between Y1-treated Sc.si FpECs and Piezo1-depleted FpECs with Y1 applied ($p = 0.0012$). H., *DLL1* was increased after Y1 treatment in the Sc.si control group ($p = 0.0096$), which was blunted after P1.si transfection. Significant difference between Y1-treated Sc.si FpECs and Piezo1-depleted FpECs with Y1 applied ($p = 0.0036$). I., *DLL4* was increased after Y1 treatment in the Sc.si control group ($p = 0.00076$), which was blunted after P1.si transfection. Significant difference between Yoda1-treated Sc.si FpECs and Piezo1-depleted FpECs with Y1 applied ($p = 0.007$). J: No significant difference in *ADAM10* between Y1-treated Sc.si FpECs and Piezo1-depleted FpECs with Yoda1 applied AG control samples $n = 5/N = 2$: LGI011, LGI013, LGI046, LGI050, LGI079. Data normalised to Sc.si Veh. A-J: ANOVA.

6.5 ADAM10 functional activity in FpECs can be stimulated by shear stress and Yoda1

After establishing that Yoda1 evoked changes in the expression of several Notch signalling genes in FpECs, we then showed that this potentiation was Piezo1 dependent. These data were obtained using Yoda1 as a specific activator of Piezo1 channels, to

mimic the effect of FSS. As such, we next sought to determine the impact of flow conditions in comparison to a static control. In addition, having previously using QPCR to detect gene expression, whether functional aspects of the Notch pathway could be demonstrated in FpECs was considered.

To test this, an assay developed by laboratory members, Vincenza Caolo and Marjolaine Debant, was adapted for use in FpECs. In this experiment, FpECs were seeded onto glass slides in a microfluidic chamber. They were exposed to FSS via a peristaltic pump (10 dyne/cm² for 30 minutes). Parallel microfluidic chambers were set up as static controls. Cells were lysed onto ice as quickly as possible in assay-specific buffer, prior to testing whether exposure to FSS affected ADAM10 functional activity. This experiment was also performed in static conditions using Yoda1 in order to investigate interplay between Piezo1 and ADAM10.

As discussed in the introduction to this chapter (section 6.1.1), ADAM10 is a metalloprotease that catalyses the proteolytic S2 cleavage of Notch1, prior to the S3 cleavage by γ -secretase (Figure 6.1). This releases NICD, which translocates to the nucleus triggering transcription of the Notch effector genes. The significant rise in ADAM10 activity in AGA FpECs after exposure to pulsatile FSS in the microfluidic chamber provides further evidence that FpECs are FSS-sensitive (Figure 6.13). Moreover, these functional data further suggest that ADAM10, and by inference the Notch signalling pathway, can be activated by FSS in FpECs.

A similar degree of ADAM10 activity occurred after treatment with Yoda1 for the same time period (Figure 6.13). This suggests that Piezo1 channel activity contributes to ADAM10 activation. ADAM10 has previously been shown to be regulated by Ca²⁺ (Nagano et al., 2004). We therefore propose that the intracellular Ca²⁺ entry induced by FSS, or Yoda1-mediated Piezo1 channel activation, contributes to ADAM10 activity. To further test this hypothesis Piezo1-specific siRNA could be used to determine the dependence of ADAM10 activity on Piezo1. In Figure 6.5 of this chapter, data was presented showing a significant downregulation of *ADAM10* mRNA in whole placental

tissue from SGA placentas. Future experiments should therefore also measure FSS- and Yoda1-evoked ADAM10 activity in normal compared to SGA FpECs, and other placental cell types.

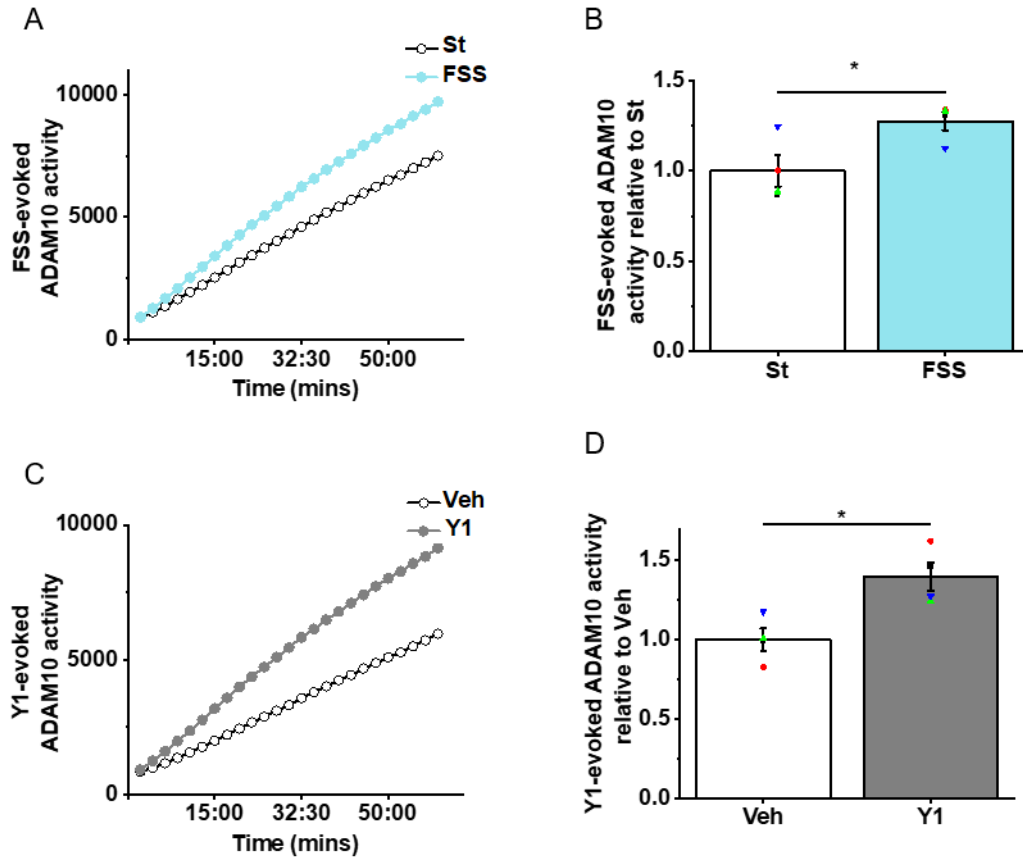


Figure 6.13 The application of shear stress and Yoda1 potentiate the activity of the ADAM10 enzyme in FpECs. A., Representative ADAM10 secretase activity assay showing readings taken every 2.5 minutes on a FlexStation fluorometer comparing FpECs exposed to fluidic shear stress (FSS) or static conditions (St) for 30 minutes. AGA sample: LGI096. B., Summarised mean \pm SEM ADAM10 secretase activity data showing a significant increase in activity after exposure to FSS ($p = 0.034$). C., As for A, showing FpECs pre-treated with either vehicle (Veh, DMSO) or Yoda1 (Y1, 0.2 μ M for 30 minutes). D., Summarised mean \pm SEM ADAM10 secretase activity data showing a significant increase in activity after exposure to Y1 ($p = 0.0125$). AGA samples $n = 4 / N = 1$: LGI041, LGI096, LGI103, LGI105. B and D: unpaired t test.

6.6 Summary of findings

- Notch pathway genes are present in the human placenta, having been identified in first trimester pregnancy tissue, 3rd trimester whole villous tissue and FpECs
- The expression of the *HEY1* target gene was low in 3rd trimester FpECs and tissue, but significantly higher in early pregnancy. *JAG1* ligand gene expression was also significantly higher in the 1st trimester
- Comparing SGA placentas with AGA controls revealed significantly higher basal expression of *NOTCH3* receptor mRNA in FpECs. *ADAM10* was downregulated in whole villous tissue from SGA placentas
- In static conditions, Yoda1 induced upregulation of *HEY1*, *HES1* and *DLL4*. This was dependent on Piezo1, since Piezo1 depletion blunted the response in these genes, plus *DLL1* and *NOTCH4*
- In SGA FpECs, the Yoda-induced potentiation of the *DLL4*, *HEY1* and *HES1* was blunted in comparison to AG controls, suggestive of an impaired response to Yoda1 in SGA
- Notch signalling is active in FpECs, whereby FSS evokes an increase in ADAM10 secretase activity. A similar increase after Yoda1 treatment suggests that there may be interplay between Piezo1 channel activity and ADAM10 activation

6.7 Discussion

6.7.1 Notch signalling in placental development and function

Notch pathway genes were readily detected in the early pregnancy tissue samples used in this project. Given the importance of Notch signalling for angiogenesis and cell fate regulation discussed section 6.1.2, I hypothesise that this pathway is important for the stages involved in establishing and sustaining pregnancy. A variety of murine studies support this proposal, demonstrating haploinsufficient lethality and placental arteriovenous malformations in Notch pathway mutants (Haider et al., 2017). Example

defects include impaired formation of the labyrinthine vascular network and reduced number of proliferative trophoblasts associated with disruption of *Notch1*, *Notch1/Notch4*, *Dll4*, *Hey*, *Hes/Hey* or *CSL* (Fischer et al., 2004, Xue et al., 1999, Duarte et al., 2004, Limbourg et al., 2007, Oka et al., 1995). In addition, a *Notch2* knockout model showed deficient arterial invasion with reduced placental perfusion (Hamada et al., 2007).

Previous studies of Notch in early human reproduction have found mRNA for all Notch receptors to be present in the endometrium, along with *DLL4* and *JAG1* ligands, *HEY* and *HES* signalling targets (Mikhailik et al., 2009). Interestingly, endometrial biopsies showed increased NOTCH1, DLL1 and JAG1 immunohistochemical staining during the receptive phase of the menstrual cycle (Van Sinderen et al., 2014). Furthermore, these proteins were significantly reduced in women with a history of unexplained infertility (Van Sinderen et al., 2014). In addition, blastocyst-conditioned media upregulated the epithelial expression of *NOTCH1* and *JAG1 in vitro* (Cuman et al., 2013). Notch1 can also be induced by hCG in primates, suggesting that angiogenic and vasculogenic regulation by Notch may have a role in endometrial preparation for implantation (Afshar et al., 2012). These data indicate that Notch signalling occurs in blastocyst-endometrial interaction and may therefore be important for endometrial receptivity (Cuman et al., 2014).

It is therefore unsurprising that Notch pathway genes were identified in the early pregnancy samples used in this project. Given the likely importance of Notch in early pregnancy establishment, our findings of significantly higher *JAG1* and *HEY1* in the 1st- compared to the 3rd trimester correspond. However, we do not have protein data to corroborate these gene expression results.

Only one previous study could be identified which sought to compare Notch pathway genes in early and late pregnancy. Herr et al., (2011) compared early pregnancy tissue with whole villous tissue sampled from placentas obtained from LSCS deliveries at term. In contrast to the data presented in this chapter, these authors showed an increase in

NOTCH3, *NOTCH4*, *JAG1*, *DLL1* and *DLL4* from the first to 3rd trimester (Herr et al., 2011). The number of samples per group was similar to my study, although the authors do not present results for *NOTCH1*, *NOTCH2*, *HEY1* or *HES1*, and data are only normalised to *ACTB*. This study reported no changes in the location or abundance of staining for these proteins on immunohistochemistry by gestation (Herr et al., 2011). However, a limitation of this type of analysis is that early pregnancy tissue from termination samples and term placental tissue are both composed of mixed cell types which may vary in proportion.

A small number of studies have sought to localise Notch to specific cell populations in the human placenta. For example, in the first trimester, Notch1 and Jagged-1 have been identified in the cytoplasm of the cytotrophoblast, with Notch1 also present in the syncytiotrophoblast on immunohistochemistry (De Falco et al., 2007). In the 3rd trimester both Notch1 and Jagged-1 have been identified in the syncytiotrophoblast and FpECs (De Falco et al., 2007). Dll-1 and Dll-4 are also expressed in villous FpECs (Herr et al., 2011). Notch receptors 2, 3 and 4 have previously been demonstrated in syncytiotrophoblasts (Herr et al., 2011, Sahin et al., 2011). Notch receptors 2, 3 and 4 have also been found on Hofbauer immune cells (Herr et al., 2011).

Notch protein localisation in placental villi, based on existing literature, is summarised in Figure 6.14 (Cuman et al., 2014). This corresponds to my data presented in this chapter, which confirmed the mRNA expression of *NOTCH1*, *JAG1*, *DLL1* and *DLL4* in FpECs (Figure 6.3). In addition, I have demonstrated the presence of mRNA for Notch receptors 2 and 3 in pure FpEC cultures. The presence of Notch genes in a combination of cytotrophoblast, Hofbauer cells and FpECs points towards involvement in placental vasculo- and angiogenesis, where canonical signalling may enable cell-cell communication (Cuman et al., 2014). The differential expression between cytotrophoblast and syncytiotrophoblast noted in the literature corresponds to the role of Notch in regulating cell fate decisions as discussed in the introduction to this chapter.

I have also demonstrated *ADAM10* expression in early pregnancy tissue, whole term villous tissue, and in FpECs. Furthermore, *ADAM10* activity could be stimulated in FpECs by FSS, which is the first functional demonstration of *ADAM10* in the placenta (Figure 6.13).

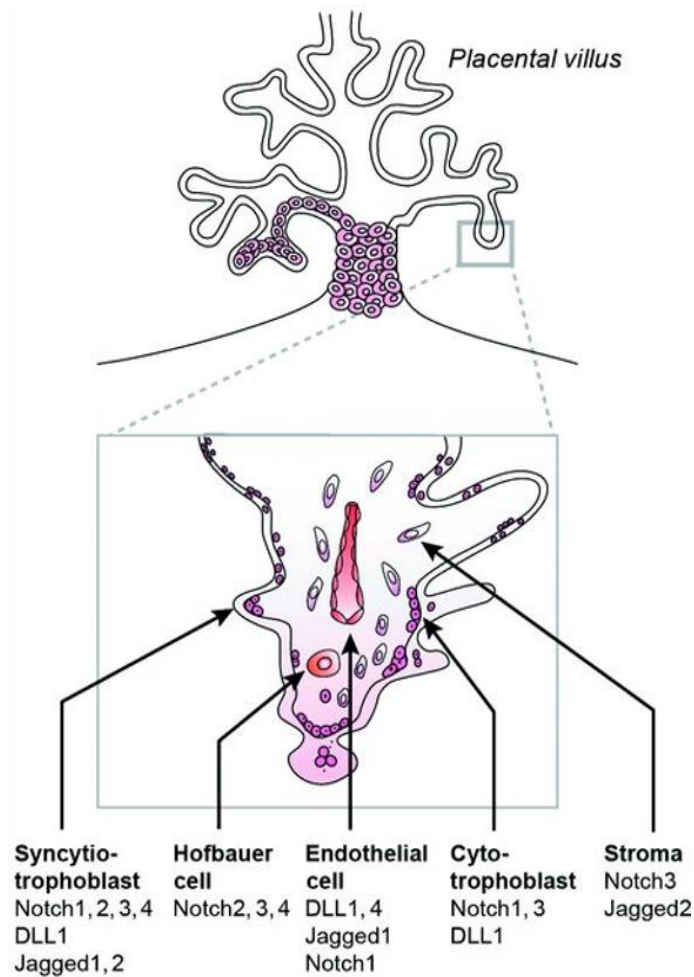


Figure 6.14 Localisation of Notch signalling proteins within the placental villi. Schematic adapted from Cuman et al., 2014, based on a review of studies using immunohistochemistry to identify Notch proteins in placental tissue specimens.

6.7.2 Notch signalling in pregnancy complications

In early pregnancy studies, Notch receptor and NICD proteins have been variously identified in cell column cytotrophoblast, endovascular extravillous trophoblast, interstitial

extravillous trophoblast, alongside uterine natural killer cells and the decidua (Cuman et al., 2014, Haider et al., 2017). Notch may therefore have as yet undefined roles in trophoblast differentiation, decidual invasion and subsequent spiral artery remodelling. As such, dysregulated Notch signalling may contribute to the abnormal placentation central to the pathogenesis of both PET and FGR.

In our study of AGA versus SGA placentas, we demonstrated that in FpECs, *NOTCH3* was significantly increased in the SGA samples. A study of severe early onset PET found similar distribution of Notch proteins compared to the normal placentas. However, NOTCH3 protein was significantly upregulated on western blotting (Zhao et al., 2014). The other findings in that study included reduced *NOTCH2* and *DLL4* mRNA expression in severe PET (Zhao et al., 2014).

Previous research using transmission electron microscopy to investigate the immunolocalisation of Notch receptors in tissue from term normal and pathological pregnancies demonstrated Notch 1, 2, 4 and Jagged-1 in the syncytiotrophoblast (Sahin et al., 2011). In placentas from FGR and pregnancy-induced hypertension, the immunoreactivity was reduced, and expression was localised more to the cytoplasm than the membrane. Downregulation of Notch1, Notch4 and Jagged-1 has also been demonstrated on immunostaining of placentas from PET pregnancies (Cobellis et al., 2007).

In whole villous tissue, our results found *ADAM10* to be downregulated in SGA. No prior studies could be identified that investigated ADAM10 gene or protein expression in FGR, although ADAM10 has been studied in PET. A characteristic feature of PET is increased secretion of sFlt-1 from the trophoblast. As discussed in the Introduction chapter, section 1.4.3, of this thesis, sFlt-1 antagonises VEGF and PlGF pro-angiogenic factors thereby contributing to placental vascular dysfunction in PET. A possible mechanism for the release of sFlt-1 is proteolysis mediated shedding. Immunohistochemistry has shown increased ADAM10 in the syncytiotrophoblasts in PET placentas compared to normal placentas (Hu et al., 2015). This is supported by data that have shown that siRNA

knockdown of ADAM10 leads to reduced sFlt-1 release from cultured human trophoblast cells (Hu et al., 2015). Given that sFlt release is not a feature of FGR pathology in the absence of hypertension, how these results relate to our findings is unclear.

Taken together, the expression of Notch genes from early to late pregnancy suggest that this signalling pathway is important for normal placentation and placental function. The most up to date evidence suggests that Notch signalling is dysregulated in placental dysfunction. However, further studies are required in FGR. These should include establishing protein abundance, localisation and functional studies, such as the ADAM10 secretase assay demonstrated here.

6.7.3 Notch signalling and Piezo1

In this chapter, I have presented the first evidence that Piezo1 channel activity influences Notch signalling in the placenta. This was demonstrated by the specific activator of Piezo1, Yoda1, upregulating the expression of *DLL4*, *HES1* and *HEY1*, with the addition of *NOTCH4* and *DLL1* in the transfection experiment. Multiple levels of the Notch pathway are therefore impacted by Piezo1 channel activation- receptor, ligands and effector genes.

A large magnitude of effect following the application of Yoda1 was seen in the relative abundance of *HES1* and *HEY1*. Murine studies showed that these Notch genes are highly expressed in the chorioallantoic layer that gives rise to the placental labyrinth (Fischer et al., 2004). Correspondingly, haploinsufficient *Hes/Hey* mice fail to undergo chorioallantoic branching. Although limited data exist in human studies, we can hypothesise that Yoda1 is influencing the expression of Notch genes that are of particular importance in placental vascular function.

In the FpECs from SGA placentas, the Yoda1-evoked increase in *HES1* and *HEY1* was blunted, an effect also noted for *DLL4*. In Chapter 4 section 4.6.2, data were presented showing reduced intracellular Ca^{2+} entry when Yoda1 was applied to FpECs from SGA placentas compared to AGA controls. I proposed that the SGA FpECs were less

responsive to Yoda1, which corresponds with the data presented in this chapter. Strikingly, the same pattern of genes was affected by Piezo1 knockdown. This was demonstrated in Figure 6.12, where Piezo1 depletion abolished the Yoda1-evoked upregulation of *DLL1*, *DLL4*, *HEY1* and *HES1*. Furthermore, *Dll4*, *Hey1* and *Hes1* were also the genes reduced in liver ECs of an EC-specific Piezo1 knockout mouse model (Caolo et al., 2020). This confirms that Piezo1 activation can regulate the Notch signalling from the ligand stage through to the effector genes. Furthermore, in placental insufficiency, we propose that altered Piezo1 channel activity impacts on Notch signalling.

These data were all obtained from experiments performed in static conditions, using Yoda1 as a tool to mimic FSS activation of Piezo1 channels. As such, a more physiologically representative experiment was sought to provide functional Notch data. Through the demonstration that FSS or Yoda1 applied to FpECs produced an increase ADAM10 enzyme activity, we can infer that Piezo1 is a requirement for ADAM10 activity. This is thought to occur via Piezo1-mediated intracellular Ca^{2+} . However, in flow conditions *in vivo*, the Ca^{2+} required for ADAM10 activation may be regulated by multiple sources, in addition to Piezo1. In the introduction to this chapter, we discussed that mechanical stress caused by endocytosis of Notch ligands produces membrane tension that triggers the signalling pathway. We previously showed that Piezo1 channels could be activated by membrane tension evoked by osmotic shear stress. As such, we can theorise that endocytosis-mediated membrane alterations are an FSS-independent mechanism of Piezo1 activation leading to downstream Notch signalling, although this hypothesis is yet to be tested.

The magnitude of impact of Yoda1 on the expression of *HEY1*, *HES1* and *DLL4* (3-, 4- and 5-fold change, respectively) is particularly striking given that studies of these conserved Notch genes in flies and worms have shown that Notch signalling is exquisitely sensitive to small changes in the abundance of Notch receptor or ligands (Harper 2003). These studies have demonstrated that multiple pathways may be

involved in the regulation of Notch signalling, such as Numb, LNX, Itch, and SEL-10 that can inhibit Notch, or Deltex and SHARP/MINT proteins that determine whether CSL activates or represses transcription (Harper et al., 2003). Little is known about the role of these regulatory pathways in the human placenta, but highlights the likely complexity of Notch signalling *in vivo*.

We therefore propose that in FpECs, Piezo1 is one mechanism of ADAM10 activation, which can be stimulated by either mechanical force or a chemical agonist. This results in the downstream production of Notch effector genes, which are known to be important for angio- and vasculogenic processes. As such our group have proposed the following model (Figure 6.15).

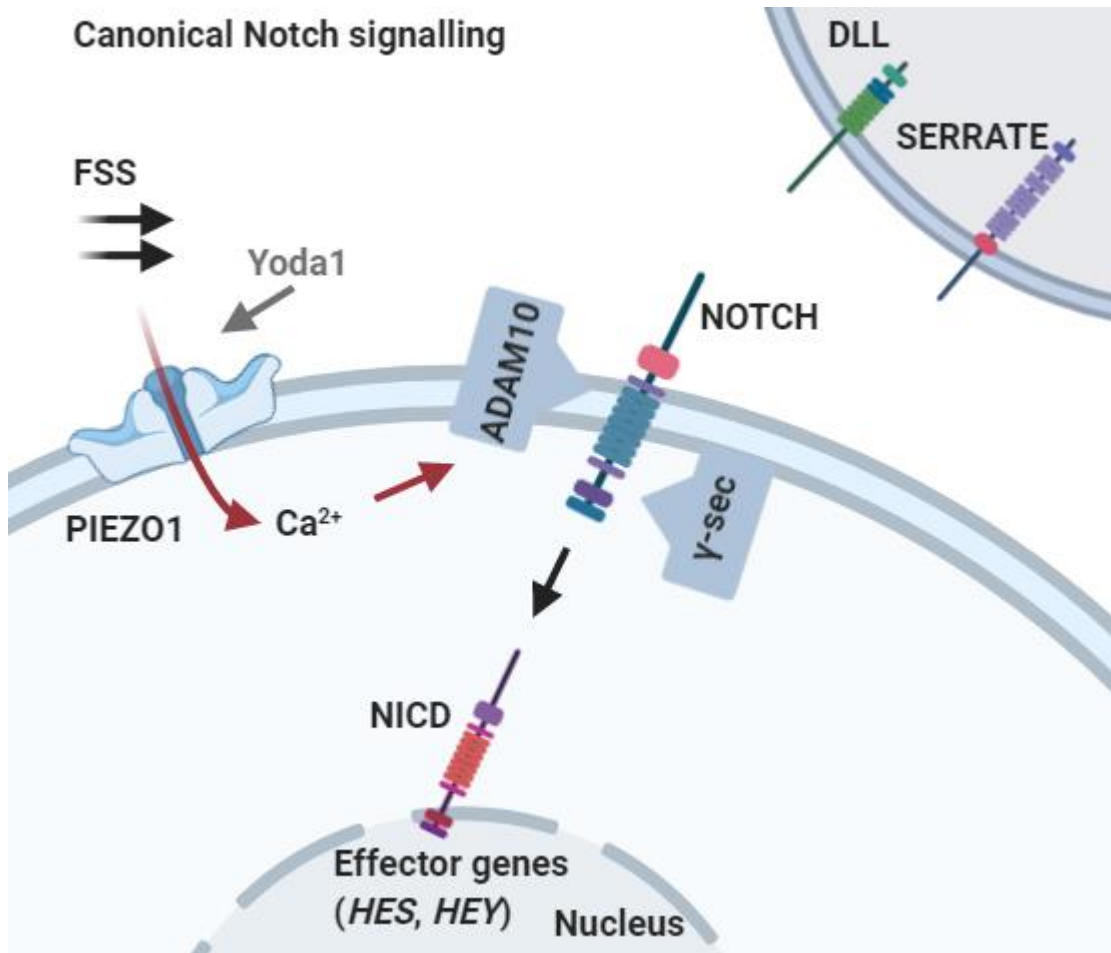


Figure 6.15 Schematic of proposed mechanism of Piezo1 interaction with the canonical Notch signalling pathway in FpECs. Activation of Piezo1 by FSS or Yoda1 causes an influx of cations into the cytoplasm, activating ADAM10, which was observed in FpECs. This proteolytic enzyme cleaves the Notch receptor, along with γ -secretase (γ -sec), which releases NICD to the nucleus. This drives the expression of the effector genes, *HES1* and *HEY1*. In FpECs, the application of Yoda1 resulting in the upregulation of *HES1*, *HEY1* and the ligand, *DLL4* (Delta-like 4). As discussed in the main text, intracellular Ca^{2+} present via other pathways independent of Piezo1 may also result in ADAM10 activity. In addition, Notch signalling can occur via a non-canonical pathway involving the Notch1 transmembrane domain which is not presented here.

Chapter 7 Conclusion and future directions

7.1 Summary of key findings

7.1.1 Significant findings in FpECs from AGA placentas

- Cultured FpECs expressed the protein and structural markers of ECs. FpECs were validated by demonstrating endothelial properties of migration, proliferation and tube formation (angiogenesis). Furthermore, FpECs demonstrated intracellular Ca^{2+} elevation in response to the application of VEGF
- *PIEZO1*, *PIEZO2* and *GPR68* mRNA was expressed in the FpECs. The relative abundance of *PIEZO1* was higher than either *PIEZO2* or *GPR68*
- Exposure to FSS increased *PIEZO1* expression
- In freshly isolated chorionic plate arterial ECs, constitutive Piezo1 channel activity was observed which was further enhanced by FSS, and inhibited by the non-specific channel blocker, Gd^{3+} . No other unitary current amplitudes were observed in response to fluid flow, suggesting that Piezo1 channels are the dominant channel type activated by flow in the chorionic plate arterial endothelium
- Confluent colonies of FpECs responded to FSS by aligning in the direction of flow. When Piezo1 was depleted, the FpECs no longer aligned in the direction of flow, indicating that Piezo1 is important for the response to FSS in the fetoplacental endothelium
- Exposing FpECs to FSS evoked S1177 eNOS phosphorylation, indicating that activation of Piezo1 channels can lead to downstream NO signalling in FpECs
- FpECs responded to the application of Yoda1, demonstrating a dose-dependent increase in intracellular Ca^{2+} entry. The response to Yoda1 was dependent upon Piezo1, whereby both Gd^{3+} and Piezo1 depletion inhibited the rise in Ca^{2+}
- The application of Yoda1 rapidly increased S1177 eNOS phosphorylation in FpECs

- The application of ATP to FpECs also evoked a Ca^{2+} elevation, with an additive effect of combined Yoda1 and ATP application in the first minute after application. Antagonising P2Y_2 receptors with suramin did not significantly reduce Yoda1-evoked Ca^{2+} entry nor peNOS, suggesting that purinergic receptors are not a requirement for Piezo1 channel activity. Piezo1 depletion did not significantly affect the ATP-evoked Ca^{2+} rise. Therefore, both purinergic signalling and Piezo1 channel activity occurred in the FpECs, but function, at least partly, independently of each other
- A rise in intracellular Ca^{2+} occurred after exposing FpECs to hypotonic stress. With the combined application of hypotonic solutions and Yoda1, the addition of Yoda1 strongly potentiated the change in Ca^{2+} . Moreover, application of Gd^{3+} abolished this response, indicating that hypotonic stress evokes a Ca^{2+} rise mediated by mechanosensory ion channels. A partial reduction in response to hypotonicity suggested that this effect may not be evoked by Piezo1 channels specifically. A similar margin of effect was noted after suramin treatment, indicating that ATP may be involved in this response. Notably, combining suramin with Piezo1 depletion was sufficient to abolish the Ca^{2+} rise, indicating that Piezo1 and ATP signalling are important for the response to shear stress in FpECs, although these data are preliminary
- mRNA for the following Notch pathway genes were identified in FpECs: *NOTCH1*, *NOTCH2*, *NOTCH3*, *NOTCH4*, *JAG1*, *DLL1*, *DLL4*, *HEY1*, *HES1* and *ADAM10*
- The application of Yoda1 upregulated the expression of Notch pathway ligand, *DLL4*, and the effector genes *HEY1* and *HES1*, suggesting that activating Piezo1 channels affects Notch signalling
- Strikingly, depletion of Piezo1 blunted the Yoda1-evoked upregulation of *NOTCH4*, *HEY1*, *HES1*, *DLL1* and *DLL4*

- FSS increased ADAM10 enzyme activity, further demonstrating that mechanosensing in FpECs results in Notch signalling
- The increase in enzyme activity evoked by the application of Yoda1 indicates that Piezo1 channel activity is linked to Notch signalling in FpECs

7.1.2 Differential results between AGA and SGA FpECs

- Mothers whose placentas were sampled were younger in the SGA group compared to those with AGA babies
- Gestation at delivery, birthweight and trimmed placental weight were reduced in the SGA group compared to the AGA FpECs
- The relative abundance of *PIEZO1* was increased in SGA FpECs compared to FpECs from AGA placentas. *PIEZO1* expression remained higher in a subgroup analysis comparing term-born SGA and AGA samples
- The highest relative abundance of Piezo1 mRNA was found in SGA samples, where emergency LSCS was the mode of delivery
- Ca²⁺ entry in response to Yoda1 was reduced in SGA FpECs, when data were normalised to the response to ionomycin (significant difference after application of 5 µM and 1 µM of Yoda1)
- The relative abundance of *GPR68* was higher in SGA FpECs, compared to the expression in the AGA group
- FpECs from SGA placentas showed raised basal expression of eNOS and phosphorylated eNOS proteins
- Yoda1 also evoked an increase in eNOS phosphorylation in the SGA FpECs, indicating that activation of Piezo1 channels in SGA FpECs can lead to downstream NO signalling in SGA placentas
- The relative abundance of *NOTCH3* was higher in SGA FpECs, compared to the expression in the AGA group

- The Yoda1-evoked increase in *DLL4* occurred in SGA FpECs. However, the effect of Yoda1 on *HEY1* and *HES1* was strikingly blunted in the SGA group

7.1.3 Significant findings in whole villous tissue from AGA placentas

- *PIEZO1* was expressed in whole villous tissue
- The relative abundance of *PIEZO1* in whole villous tissue was higher than that of *PIEZO2* and *GPR68*
- The relative abundance of *PIEZO2* was higher in pregnancy tissue from the first trimester than in whole villous tissue from the 3rd trimester
- The relative abundance of *JAG1* ligand, and *HEY1* effector genes in the Notch signalling pathway were higher in pregnancy tissue from the first trimester than in whole villous tissue from the 3rd trimester

7.1.4 Differential results between AGA and SGA whole villous tissue

- The weight of babies in the SGA group was significantly lower than those who were AGA. Placental weight, when trimmed of umbilical cord and membranes, was also significantly reduced in the SGA group
- *EFRNB2* (arterial) and *EFRNB4* (venous) were significantly reduced in SGA versus AGA tissue
- The relative abundance of *ADAM10* was lower in SGA whole villous tissue, compared to the expression in the AGA group

7.2 Hypotheses based on significant findings

In the AGA placenta

Piezo1 is a mechanosensitive Ca^{2+} channel present in the fetoplacental endothelium. *PIEZO1* is upregulated by FSS, and channel activity is required for the normal response of FpECs to FSS. Activation of Piezo1 by FSS causes an influx of Ca^{2+} into the FpEC that triggers downstream pathways. These include phosphorylation of eNOS, and Notch processing, including ADAM10 activation. Additional mechanosensory mechanisms are

present in FpECs, including GPR68, Piezo1 and flow-induced ATP production. However, FSS-induced channel activity in FpECs, and relative mRNA abundance demonstrate that Piezo1 is the dominant mechanosensor in the fetoplacental endothelium.

Changes in the SGA placenta

The increased mRNA expression of *PIEZO1*, *GPR68* and *NOTCH3* in SGA is indicative of compensatory gene upregulation in response to elevated FSS. Components of the NO signalling pathway, total- and phosphorylated eNOS undergo compensatory upregulation in placental insufficiency. Piezo1 function is compromised in SGA, whereby Ca^{2+} entry in response to channel activation is reduced. Piezo1 channel dysregulation affects downstream Notch signalling in FpECs, resulting in reduced mRNA expression of Notch effector genes after Piezo1 activation.

Early pregnancy

The increased relative mRNA abundance of components of the Notch pathway in the first trimester indicates that Notch is important for placental vascular development. The expression of both Notch and *PIEZO1* mRNA in the first trimester, and evidence of coupling between Notch signalling and Piezo1 in FpECs, suggests that Notch could be an important link between mechanosensing and downstream vascular homeostasis in early pregnancy.

7.3 Final discussion

7.3.1 Piezo1 is a functionally active mechanosensor in the human placenta

In my thesis I have shown that primary FpECs can be isolated from term placentas by tissue digestion and CD31 microbeads and can form functional colonies, as assessed

by morphological, biophysical and biochemical criteria. Establishing this *in vitro* system for studying the fetoplacental endothelium has provided novel insights into the presence and function of Piezo1 channels in the human placenta. Freshly obtained whole villous tissue and arterial ECs were also isolated. These were obtained through vessel dissection from the chorionic plate arteries and are therefore from larger capacity vessels than the cultured FpECs. Patch-clamp electrophysiology experiments on these cells enabled me to obtain the unitary conductance and thus Piezo1 signature of 25 pS. In FpECs I demonstrated the expression of Piezo1 mRNA and protein, both of which could be increased with exposure to FSS. These data display the consistent finding of Piezo1 channel activity in both fetoplacental cell types, and show that these cells respond to mechanical force. Activation of Piezo1 channels by either Yoda1 or alterations to membrane tension via hypotonic stress resulted in intracellular Ca²⁺ entry. When Piezo1 is depleted in FpECs, the response to FSS (alignment) and Yoda1-evoked Ca²⁺ entry was significantly diminished. This suggests the importance of Piezo1 channels in FSS sensing and associated Ca²⁺ entry in FpECs.

The study of signalling pathways downstream of Piezo1 activation in FpECs, demonstrated that both Yoda1 and exposure FSS caused a striking increase in the activation of eNOS. eNOS-derived NO is known to play a varied role throughout pregnancy, being involved in implantation, placental angiogenesis and the regulation of fetoplacental vascular tone (Cottrell et al., 2017). The identification of *PIEZO1* in early pregnancy as well as in term placentas, and the potential for Ca²⁺-evoked regulation of NO-mediated vasodilatation by Piezo1, suggests that Piezo1 may have important roles in multiple aspects of placental establishment and vascular function.

The data in my thesis demonstrate coupling between Piezo1 and Notch signalling in the human placenta for the first time. In static conditions, Yoda1 was found to upregulate components of the Notch signalling pathway: the ligand *DLL4*, and effector genes *HEY1*, *HES1*. This was Piezo1-dependent, since Piezo1 depletion blunted the response in these genes, plus *DLL1* and the receptor *NOTCH4*. We also demonstrated functional

activity of Notch signalling in FpECs, whereby FSS evoked an increase in ADAM10 secretase activity. This proteolytic enzyme cleaves the Notch receptor, releasing NICD to the nucleus, where transcription of the effector genes occurs. A similar increase after Yoda1 treatment suggests that there is interplay between Piezo1 channel activity and ADAM10 activation. As such, Piezo1 activation in response to FSS may not occur in isolation, and multiple downstream signalling pathways could be triggered.

It has been previously suggested that Piezo1 is required for FSS-induced ATP release (Wang et al., 2016). However, my data showed that Piezo1 depletion did not significantly affect ATP-evoked Ca^{2+} transients. Likewise, antagonising P2 receptors did not significantly reduce Yoda1-evoked Ca^{2+} entry or eNOS activation, demonstrating that purinergic receptors are not required for Piezo1 channel activity. This suggests that both purinergic signalling and Piezo1 channel activity occur in FpECs, but may function independently.

Alongside current research investigating the interplay between Piezo1 and other FSS-sensing components, new mechanosensors may be identified. For example, I have presented the novel finding of GPR68 presence in FpECs, and in placental tissue from both early and term pregnancy. GPR68 was recently discovered to be an important endothelial mechanosensor after being identified on a screening system that applied FSS to cultured cells (Xu et al., 2018). Follow-up studies found *Gpr68*-deficient mice to display markedly impaired FMV and remodelling abnormalities in mesenteric arterioles (Xu et al., 2018). In addition, the application of L-NAME profoundly inhibited FMV in small mesenteric arteries of both the *Gpr68*-deficient and wild-type mice, indicating that Gpr68 likely functions upstream of the NO pathway (Xu et al., 2018). Moreover, the vasodilatory response to SNP was greater in the transgenic vessels, suggesting that *Gpr68*-deficient mice could be more sensitive to NO-induced vasodilation. The presence of *GPR68* in FpECs, early pregnancy and villous tissue demonstrate that Piezo1 is not expressed in isolation as a sole mechanosensor in the human placenta. However the functional

significance of GPR68 in the placenta, including potential coupling to NO production, remains to be determined.

7.3.2 Shear stress sensing and Piezo1 signalling are dysregulated in placental insufficiency

Placental samples obtained in this project were selected to represent a group of SGA babies on the basis of birthweight <10th centile on WHO-based growth charts. The clinical and histopathological features were varied, but common findings were younger mothers, maternal smoking, and evidence of placental ischaemic and infarction. Whole villous tissue from this SGA group showed reduced relative abundance of *EFNB2* and *EFNB4*. These vascular markers are determinants of vascular identity linked to FSS signalling pathways (Masumura et al., 2009). The abundance of these ephrins could therefore reflect changes in vascular molecular identity corresponding to structural, flow, or other abnormalities in these placentas. This confirmed that the SGA phenotype in this project had macro- and microscopic changes, as well as alterations in gene expression.

Significant differences in the expression of my genes of interest were also found in FpECs and whole villous tissue from SGA placentas. The key findings were upregulation of FSS-sensing *PIEZO1* and *GPR68* in SGA FpECs. I propose that the dysregulated gene expression of these mechanosensors is secondary to elevated FSS in placental insufficiency, which occurs as a consequence of altered vascular architecture and vasoconstriction. In addition to being FSS-sensing, GPR68 is also proton sensitive and is upregulated in acidity (Xu et al., 2018). This has been demonstrated in a variety of cancers where the tumour microenvironment is hypoxic, and the expression of *GPR68* is increased (Wiley et al., 2019). As such the elevated *GPR68* expression presented in this thesis may be secondary to raised FSS and/or placental hypoxia.

Despite injury and senescence in pregnancy, the placenta retains a dynamic network, undergoing regional adaptation to sustain blood flow to the fetus. As such, I propose that the upregulation of *PIEZO1* and other mechanosensors is a compensatory drive towards improving placental perfusion, and thus improve fetal oxygenation. This is evidenced by

the increase in basal levels of total and phosphorylated eNOS protein in the SGA FpECs. Furthermore, my data demonstrate a profound increase in eNOS activation after Yoda1 application. Yoda1-evoked phosphorylation of eNOS occurred in both the AGA and SGA FpECs, indicating that in these SGA samples, NO activation still occurred. Similar effects have been described in the vascular biology of other body systems, including the cerebral circulation. Here, a reduction in cerebral blood flow in brain tissue was accompanied by a compensatory increase in the oxygen extraction fraction (OEF) to maintain normal neuronal function (Liu and Li, 2016).

I have also shown increased expression of *NOTCH3* receptor mRNA in SGA FpECs. This indicates that some parts of the Notch signalling pathway are upregulated in the fetoplacental endothelium in placental insufficiency. This finding is supported by a previous study that found increased *NOTCH3* in PET placentas (Zhao et al., 2014). Placental hypoxia secondary to hypoperfusion occurs in both FGR and PET, which is associated with chorangiogenesis – a compensatory increase in villous capillary EC proliferation. Given the importance of Notch in angiogenesis and vascular homeostasis, whether this abnormal vascularity could be driven by Notch signalling, is an interesting question.

Despite the increase in Piezo1 mRNA in the SGA FpECs, altered channel activity was observed, whereby the intracellular Ca^{2+} entry response to Yoda1 was diminished in the SGA group. Furthermore, the Yoda-induced potentiation of *DLL4*, *HEY1* and *HES1* was blunted in the SGA FpECs, suggestive of impaired sensitivity to Yoda1 in placental insufficiency. It was striking that the affected genes were the same ones whose Yoda1-evoked expression was suppressed by Piezo1 knockdown, indicating that Piezo1-evoked Notch signalling may be dysregulated in placental insufficiency. In addition, mRNA for a functional component of the Notch pathway, ADAM10 secretase, was downregulated in the SGA FpECs. Given the importance of Piezo1 for the morphological response to FSS demonstrated *in vitro* (alignment to flow), dysregulated Piezo1 channel activity will compromise the mechanism of flow sensing and response in FpECs.

In placental insufficiency, abnormal vascular architecture and hypoxia result in endothelial dysfunction, alongside increased vasoconstrictive and inflammatory mediators (Kingdom et al., 2000). There are a multitude of vasoactive circulating factors which have been discussed in brief in this thesis, including endothelin-1, TNF α , sFlt-1 and ROS. I therefore hypothesise that one cumulative effect of these insults on the fetoplacental endothelium is the altered function of Piezo1 channels, with subsequent dysregulation of downstream mechanotransduction pathways.

My hypothesis is that Piezo1 channel activity and downstream signaling, including the Notch pathway, may be adversely influenced by the placental environment and endothelial dysfunction in SGA (Figure 7.1). It remains to be determined whether additional compensatory NO may be derived from FSS-independent pathways in FpECs. Likewise, it is unclear whether the NO is at full capacity in FGR, and this combination of endothelial damage and vasoconstrictive factors prevents the elevated NO from effectively compensating for the increased resistance to flow (Figure 7.1). As such, the interplay between Piezo1 channel activity, modulators of FpEC function, and downstream signalling in placental insufficiency requires further investigation.

7.3.3 Limitations of the AGA versus SGA FpEC comparison

Biological comparisons have been made between AGA and SGA samples for the relative mRNA abundance of Piezo1, Piezo2 and GPR68, and Yoda1-evoked Ca²⁺ entry. The SGA samples are from a broad clinical spectrum, including well, term-born babies that may be constitutionally small with normal placental function. As such, it would be beneficial to have a larger sample size, with a greater number with evidence of abnormal placental blood flow and fetal redistribution. This would enable subgroup analysis of Piezo1 mRNA abundance and assessment of channel function in those with more severe disease.

The FpECs were obtained by digesting whole villous tissue and isolating CD31-positive cells. Although these cells were validated thoroughly as endothelial, this may be a mixed cell population, with varying proportions of capillary, arterial and venous endothelial cells,

which may impact on cell function and mRNA expression. Likewise, there is the potential for maternal EC contamination. In addition, during the culture period, the phenotype of cells could be altered, producing different functionality compared to *in vivo*.

Functional investigation of Piezo1 channels was limited to Yoda1-evoked Ca^{2+} entry (Figures 4.23 – 4.26). Comparing the response of AGA and SGA to other, known stimuli, such as VEGF- or ATP-evoked Ca^{2+} entry would be an important step towards determining if these data are indicative of globally reduced FpEC sensitivity or a specific change in Piezo1 channel response. Likewise, these data would be more robust with the addition of other functional measures of FpEC function. For example, the alignment data presented in Figure 4.16 demonstrated that Piezo1 was important to normal response to FSS. As such, measuring alignment in the SGA FpECs could be used to investigate whether dysfunctional Piezo1 channels in the SGA placenta are coupled to this functional response to flow. Furthermore, comparing Piezo1 protein detection and localisation would have been valuable to determining the impact of the increased relative mRNA abundance in the SGA samples on protein regulation.

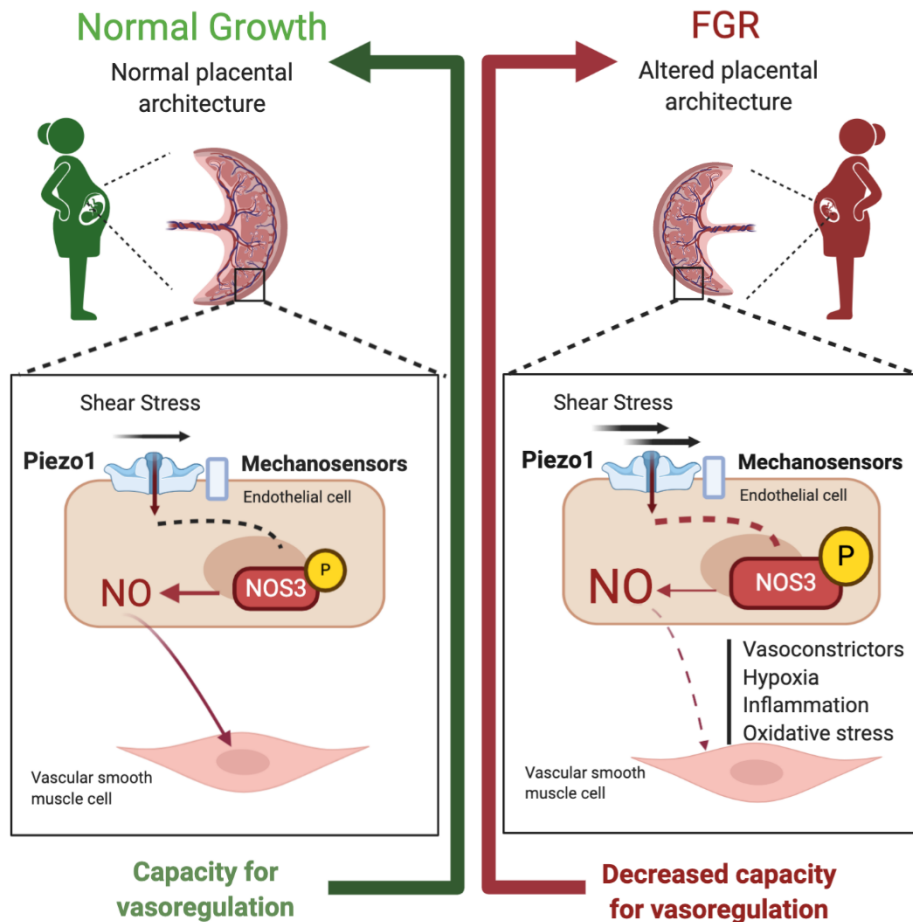


Figure 7.1. Schematic for our final hypothesis. Shear stress is elevated in FGR secondary to altered placental vascular architecture, and is sensed by Piezo1 and other mechanosensors, including gpr68. eNOS (NOS3) phosphorylation (P) is increased in FGR to generate increased NO-mediated vasodilation, which reaches maximal capacity. Vasoconstrictor and anti-angiogenic effects dominate, and flow responsiveness is attenuated. The normal capacity for placental haemodynamic autoregulation is lost, and vascular dysfunction worsens sequentially. Illustration produced by Marjolaine Debant after discussion. Created with BioRender.

7.4 Future direction

7.4.1 *Ex vivo* studies of placental villous tissue and FpECs

Leading directly on from this thesis, a number of specific follow up experiments could be performed to address our hypotheses, which are detailed in Table 17. The results obtained during this project have raised exciting questions which merit further scientific exploration. The rationale for these investigations, and examples of new directions in which to study mechanosensing in the placenta are discussed next.

Is there further evidence to support the hypothesis that Piezo1 is coupled to NO signaling in the placenta, which is dysregulated in placental insufficiency?		
Questions	Placental samples	Experiments
Does Piezo1 depletion prevent eNOS phosphorylation?	AGA FpECs	<ul style="list-style-type: none"> - Transfection (siRNA) - Western blotting
Is Piezo1 coupled to NO functional activity?		<ul style="list-style-type: none"> - Transfection (siRNA) - eNOS activity assay
Is NO functional activity dysregulated in SGA?	AGA and SGA FpECs	<ul style="list-style-type: none"> - iNOS protein expression (western blotting) - eNOS activity assay - Peroxynitrite formation assay (superoxide and NO combining, Chemiluminescence assay)
Can Piezo1 be accurately localized to cell types on placental histology, and is Piezo1 protein expression and localization altered in SGA?		

Is PIEZO1 protein expression altered in SGA?	AGA and SGA FpECs	<ul style="list-style-type: none"> - Antibody optimization/development - Western blotting
Where is Piezo1 localised in term and early pregnancy placenta?	<p>Whole villous tissue from AGA and SGA placentas</p> <p>Early pregnancy tissue</p>	<ul style="list-style-type: none"> - Antibody optimization/development - Western blotting - Immunohistochemistry
Is Piezo1 gene and protein expression altered by hypoxia?	AGA FpECs	<ul style="list-style-type: none"> - Hypoxic cell culture - QPCR - Western blotting
Is GPR68 a functional mechanosensor in FpECs?		
Does stimulating GPR68 with FSS or an agonist lead to an increase in expression, or intracellular Ca ²⁺ , respectively?	AGA FpECs	<ul style="list-style-type: none"> - FSS (microfluidic chamber) - FlexStation using GPR68 agonist (Ogerin) to measure intracellular Ca²⁺ - Transfection (GPR68 siRNA)
Where is GPR68 localised on placental specimens?	Whole villous tissue from AGA and SGA placentas	<ul style="list-style-type: none"> - Antibody testing - Immunohistochemistry
Is GPR68 protein expression altered in SGA?	AGA and SGA FpECs	<ul style="list-style-type: none"> - Western blotting
Does GPR68 activity alter in SGA?	AGA and SGA FpECs	<ul style="list-style-type: none"> - FlexStation using GPR68 agonist (Ogerin) to measure intracellular Ca²⁺

Is there further evidence to support the hypothesis that Notch signaling is coupled to Piezo1 in the placenta, and dysregulated in placental insufficiency		
Where are Notch pathway proteins localised in term and early pregnancy placenta?	Whole villous tissue from AGA and SGA placentas Early pregnancy tissue	<ul style="list-style-type: none"> - Antibody testing - Immunohistochemistry
Does FSS increase expression of Notch pathway genes and protein in FpECs, and is there differential expression in SGA?	AGA and SGA FpECs	<ul style="list-style-type: none"> - FSS (microfluidic chamber) - QPCR - Western blotting
Does FSS increase protein expression of NICD? Does Yoda1 increase expression of NICD? Is NICD expression Piezo1 dependent? Is NICD expression altered in SGA?	AGA and SGA FpECs	<ul style="list-style-type: none"> - Transfection (siRNA) - Yoda1 - FSS (microfluidic chamber) - Western blotting
Is ADAM10 activity Piezo1 dependent?	AGA FpECs	<ul style="list-style-type: none"> - Transfections (siRNA) - Piezo1 inhibitors - ADAM10 activity assay (FSS and Yoda1)
Is ADAM10 activity dysregulated in SGA?	AGA and SGA FpECs	<ul style="list-style-type: none"> - ADAM10 activity assay (FSS and Yoda1)

Is Piezo1 and Notch signaling important for angiogenesis in FpECs?		
Is angiogenesis Piezo1-dependent? Does Piezo1 stimulation with Yoda1 affect angiogenesis?	AGA FpECs	<ul style="list-style-type: none"> - Transfection (siRNA) - Tube formation (Matrigel and fibroblast co-culture) - Sprouting bead assay - Yoda1
Is angiogenesis dysregulated in SGA?	AGA and SGA FpECs	<ul style="list-style-type: none"> - Tube formation (Matrigel and fibroblast co-culture) - Sprouting bead assay - Yoda1
Is angiogenesis Notch pathway dependent? Is there evidence of coupling between Piezo1 and Notch in angiogenesis?	AGA FpECs	<ul style="list-style-type: none"> - Transfection (siRNA e.g. for <i>PIEZO1</i>, <i>NOTCH3</i>, and <i>ADAM10</i>). - Tube formation (Matrigel and fibroblast co-culture) - Sprouting bead assay

Table 17 A summary of key follow up experiments

7.4.1.1 Expression of mechanosensors in placental insufficiency and early pregnancy loss

One limitation with studies investigating the expression of endogenous Piezo1 protein, has been the lack of a specific antibody. However, given that Piezo1 bands were clearly identified in experiments in this study, further optimising the Proteintech antibody may be sufficient for use in immunohistochemistry. Complementary approaches to localising Piezo1 on tissue specimens would be to generate alternative Piezo1 antibodies, nanobodies and affimers. Should this be achieved, the relative abundance of PIEZO1 between AGA and SGA FpECs would be quantified by western blotting. Immunohistochemistry would be performed to localise PIEZO1 on placental villous tissue

specimens from AGA and SGA samples. Given my findings of altered gene expression of Notch pathway components, and *GPR68* in SGA whole villous tissue and FpEC samples, these data would also be further investigated by determining protein expression (Table 17).

I also demonstrated *PIEZO1* expression in first trimester pregnancy tissue. An important first step would be localising and quantifying Piezo1 protein expression in first trimester samples using immunohistochemistry (Table 17). The impact of *PIEZO1* mutations on the lymphovascular system supports the importance of the channel for human development (Martin-Almedina et al., 2018). Important translational research has recently correlated *PIEZO1* variants with clinical US and autopsy findings from cases of fetal hydrops (Mastromoro et al., 2020). As such, a future study should correlate the presence of *PIEZO1* mutations in similar cases with placental investigation and immunohistochemistry. In addition, whether *PIEZO1* variants have a role in the pathogenesis of cases of recurrent miscarriage of unknown aetiology, remains to be determined.

Given the evidence supporting an important role for Piezo1 and Notch in angiogenesis, their expression could be investigated in decidual tissue biopsies. My hypothesis would be that cross talking between Piezo1 and Notch is important for mechanosensing and transduction that results in downstream decidual vascular adaptations for pregnancy. Furthermore, dysregulated FSS sensing could be a contributor to abnormal endometrial receptivity, affecting subsequent implantation.

7.4.1.2 Functional studies

Determining the effect of hypoxia on FSS sensing

A well-documented feature of FGR is placental hypoxia, signs of which are present on placental pathology. Hypoxia associated with FGR is also evident clinically, such as reduced umbilical vein oxygen saturation and increased risk of hypoxic-ischaemic encephalopathy (Rossi and Prefumo, 2019, Kingdom, 1998, Lackman et al., 2001).

Whether there is a relationship between hypoxia, FSS and mechanosensory signalling pathways is an interesting question. *Ex vivo* placental perfusion data suggest that hypoxia increases vascular resistance. However, observing villous chorangiogenesis on histology indicates that hypoxia induces a chronic compensatory drive towards increasing trophoblast proliferation and angiogenesis (Schoots et al., 2018, Kingdom and Kaufmann, 1997). Correspondingly, a failure of this adaptive capacity could lead to worsening fetal hypoxia (Sandovici et al., 2012).

There are currently no published data on the effect of low oxygen tension on the function of Piezo1 channels. However, various other factors involved in mechanosensing have been shown to undergo alterations in response to hypoxia. For example, in the systemic circulation, a decreased concentration of oxygen triggers the release of ATP from erythrocytes. This initiates ATP signalling, as described in Chapter 5, section 5.4, leading to subsequent production of NO that results in vasodilation (Wang et al., 2016). As well as showing that cultured FpECs respond to ATP, I have demonstrated the presence of *GPR68* in placental tissue and FpECs. As previously described, *GPR68* is proton-sensitive, and therefore upregulated in hypoxia. As such, low oxygen-induced activation of ATP signalling, *GPR68* and potentially Piezo1, could lead to NO-mediated vasodilatation. Further exploration is therefore required to determine whether differential function of these mechanosensors occurs in response to low oxygen tension in the placenta, and whether the hypoxic placental environment in FGR contributes to dysregulated FSS sensing.

The role of Piezo1 and Notch in placental angiogenesis

As part of the validation of the cultured FpECs, I demonstrated that FpECs readily form tubes – a measure of early angiogenesis. This tube formation occurred both on a Matrigel substrate, with endothelial changes occurring within the first hour of the assay, and on a longer fibroblast co-culture model. In the placenta, dominant inducers of angiogenesis are VEGF proteins, including PlGF. FSS has been recognised as a critical stimulus of

angiogenesis, as evidenced by a dose-dependent rise in PIGF associated with increasing flow (Brugger et al., 2020, Lecarpentier et al., 2016a). Compromised angiogenesis disrupts villous vascularisation, leading to increased capillary-mediated vascular resistance and abnormal FSS (Shah and Khalil, 2015). Given my data demonstrating altered *PIEZO1* expression and channel function in fetoplacental endothelium from placental insufficiency, the role of Piezo1 in placental angiogenesis should be determined. Previous data from our laboratory has indicated that Piezo1 depletion suppressed VEGF-induced tube formation and migration (Li et al., 2014). These data were obtained from cell line HUVECs, and it will therefore be important to perform these experiments in FpECs from normal pregnancies to establish Piezo1-dependence in angiogenesis, followed by comparisons with those from placentally-mediated pregnancy complications (Table 17).

The presence and functional activity of Notch genes and ADAM10 secretase in FpECs demonstrated in this project also warrants further investigation into the relevance of these findings for angiogenesis (Table 17). This is in the context of Notch signalling being a known regulator of angiogenesis and cell fate determination, as described in Chapter 6, section 6.1.2 (Wolf et al., 2019). This may be particularly applicable to a new study of endometrial receptivity in early pregnancy.

Whole vessel implications of Piezo1 modulation

My results showed that a short treatment of FpECs with Yoda1 induced eNOS activation. I therefore propose that Piezo1 channel activation either by FSS, or by Yoda1, is upstream of NO-mediated vasodilatory effects in fetoplacental blood vessels. A limitation of this work was a lack of data establishing the effect of applying Yoda1, or other blood flow mimetics, on whole placental vessels. This is important given the potential for differential effects of Piezo1 in whole vessels versus single cell type colonies. Our group have previously demonstrated that the role of Piezo1 channels may differ *in vivo* between vascular beds. For example, we previously found Piezo1 to be an important

mechanosensor in the murine mesenteric artery. This myography study found Piezo-dependent vasoconstriction generated through opposition of EDHF (Rode et al 2017). We propose that this mechanism enabled the redistribution of blood flow away from the gut in response to exercise. This suggests that Piezo1 channels are widely found in the endothelium and have multiple important roles in vascular biology. It also suggests that Piezo1 may have different roles under certain circumstances, specific to the vascular bed.

In one previous study, the role of Piezo1 in uterine arteries was investigated (John et al., 2018). This research used pressure myography of rat uterine artery, comparing pregnant and non-pregnant dams. These data demonstrated that the application of Yoda1 induced profound vasodilatation. Furthermore, this vasodilatation was blunted by the Piezo1 inhibitor, GsMTx-4, as well as L-NAME. These findings support our hypothesis that Piezo1 activation leads to vasodilation via NO, and that Yoda1 affects whole vessel function. Given that this study used an animal model and investigated the uterine artery, further research is required to determine the dependence of vasodilatation on Piezo1 expression, and the effect of Piezo1 channel modulators on vasomotor tone in *ex vivo* human fetoplacental blood vessels.

7.4.2 Animal models

A significant proportion of the data demonstrating the importance of Piezo1 for vascular development and function has been obtained through the use of animal models. This also presents an opportunity for determining the global effect of modulating this mechanosensing channel. As discussed in the Introduction to this thesis, global or endothelial-specific disruption of Piezo1 in a mouse model profoundly disturbed the developing vasculature and was lethal within days of the heart beating (Li et al., 2014). Haploinsufficiency was not lethal, and therefore studies of Piezo1 +/- deficiency could be performed on adult mice. Imaging of ECs in mature vessels revealed striking abnormalities, such as a lack of alignment to flow. As such, the developmental of a

placental-specific Piezo1-deficient mouse model would be an exciting step towards definitive understanding of the global effects of Piezo1 in the placenta.

Animal models may also have utility for determining the response to modulators of mechanosensory function. This was previously described where vasodilatation of *ex vivo* rat uterine arteries was confirmed after the direct application of Yoda1 (John et al., 2018). To further the concept of mechanosensory modulators as a potential therapeutic, animal models of both normal pregnancy and placental insufficiency will be of great importance. Numerous pregnant animal models are in use to determine potential beneficial effects, maternal and fetal complications, and teratogenicity (Vuguin, 2007). Each model has relative pros and cons, and a comparison between the placental development, vascular and endocrine functions between the species is required. Examples include rodent models, such as pregnant dams administered with a phosphodiesterase inhibitor, which is discussed in more detail in section 1.4.1.3 (Dilworth et al., 2013). Larger ovine models have been used to explore targeted therapy for FGR, namely VEGF gene therapy mediated by an adenovirus vector directed at the maternal uterine artery (David, 2017).

7.4.3 Modelling shear stress in the placenta

Accurately representing *in vivo* SS conditions in the *in vitro* setting remains a challenge. This is particularly apparent in the placenta due to the complex vascular architecture. Indeed variations in shear may occur between vascular beds, type and size of vessel, and even at each bifurcation (Sprague et al., 2010). As such, results obtained from pure laminar SS exposure may not be representative (Sprague et al., 2010). This has consequences for determining the downstream pathways modulated by FSS. This was highlighted by a study which demonstrated that both laminar and disturbed flow were found to activate the same initial pathways involving Piezo1, P2Y₂ and GPCRs. However, only disturbed flow resulted in the downstream activation of integrins and focal adhesion proteins (Albarran-Juarez et al., 2018).

To overcome this, Sprague et al., (2010) suggested using mathematical models and computer simulation to better reflect the complexity of SS and improve the congruency

of current experimental models with *in vivo* vasculature. The utility of this approach has been demonstrated using micro-computerised tomography-derived images of the rat fetoplacental vascular network to generate a 3D computational fluid dynamics model (Bappoo et al., 2017). This was able to determine physiologically-relevant shear stress magnitudes, patterns and gradients, demonstrating the heterogeneous nature of shear in the placenta with gradients at vessel bifurcations.

The primary aim of this PhD project was to establish whether Piezo1 channels were present and functionally active in the human fetoplacental vasculature. As such, we chose to isolate a pure EC fraction to focus on the relative abundance and function of Piezo1 in FpECs. To obtain a more 'global' view of the placenta, we also performed QPCR on whole villous tissue. However, in the *in vivo* setting, there may be cross talk between the multiple placental cell types, influencing local gene expression and functional activity. This was demonstrated in a co-culture model of human FpECs and BeWo choriocarcinoma cells (Troja et al., 2014). Here, co-culture altered the expression profile of angiogenic genes (*ANG1*, *ANG2*, *VEGF-A*, *PLGF*) when compared to the FpECs in monoculture. This suggests that trophoblastic factors also have a regulatory role in fetoplacental angiogenesis (Troja et al., 2014). As such, the potential interplay between FSS activation of signalling in the trophoblast and endothelium and whether this produces an orchestrated response requires further investigation (Brugger et al., 2020).

The development of multi-compartmental, multi-cell 3D microfluidic cell culture devices facilitates the study of FSS-evoked signalling through the application of targeted shear rates in these 'Organs-on-a-Chip' (OOC) systems. Key advantages of these OOC systems are the capacity for real-time imaging in these long term cultures (minimum of 4 weeks), and analysis of secretion and metabolism of individual cell types by sampling conditioned media from each compartment (Gnecco et al., 2017). This approach has been demonstrated in Leeds with the development of an endometrial stromal - endothelial cell model (Gnecco et al., 2017). Future 'Placenta-on-a-Chip' models may

enable the study of FSS-evoked cell-cell interactions and the impact on Piezo1, GPR68, and Notch signalling.

To ensure the accuracy of such models, the FSS must accurately reflect *in vivo* placental conditions, both in healthy pregnancy and placental insufficiency. As such, the precise nature of FSS at different stages of human placental development needs to be characterised. Furthermore, the detection of localised areas of flow abnormality, and the degree of inter-person variation requires consideration. High fidelity *in silico* models of human fetoplacental haemodynamics will therefore be a valuable tool for providing metrics that can be correlated with *in vivo* fetoplacental assessment (Clark et al., 2020).

One multiscale computational model of fetoplacental blood flow has been described (Clark et al., 2015). Here, the authors used a combination of *in vivo* assessments and histopathological measurements to calculate, for example, placental volume, chorionic branching pattern and number, and umbilical artery resistance. Blood flow was simulated to predict resistance and heterogeneity of flow at each level of vasculature, which was then used to estimate FSS. Although there are currently limitations with the model, namely steady state rather than pulsatile flow, and lack of differentiation at the capillary level, this does provide an important link between macro-scale vascular structure and shear stress in the micro-vasculature (Clark et al., 2015). The authors have since used this model to predict elevated FSS in the microvasculature in FGR, as discussed in section 1.6.3 (Tun et al., 2019).

These multilevel computational models allow inference of local tissue properties where direct measurement is not possible (Clark et al., 2015). As such, an individual patient's clinically-assessed *in vivo* measurements, such as umbilical artery Doppler flow resistance indices and placental volume assessment could feed into a computational model which would then estimate microvascular level abnormalities in FSS. Given our increased understanding of the importance of FSS for placental vascular function, these could provide an additional tool in fetoplacental haemodynamic assessment to better predict clinical outcome and thus guide timing of intervention and/or delivery.

7.5 Clinical placental research considerations

A limitation of this research was the inclusion of SGA infants with normal placental blood flow alongside those with abnormal umbilical Doppler measurements and evidence of cerebral redistribution. Pregnancies exhibiting both early- and late-onset growth restriction were recruited. As such, the likely inclusion of constitutionally small fetuses alongside those with pathological growth restriction may have added to the heterogeneity of results. The research was also complicated by variations in maternal characteristics, such as smoking status, and mode of delivery. Future research would benefit from tighter clinical phenotyping of placental samples. In order to achieve an appropriate number of samples, this may require a multi-centre study. This would enable additional subgroup analyses, such as determining whether sexual dimorphism in the placenta was important for the response to FSS and subsequent mechanotransduction signalling.

In Chapter 1, section 1.3.2, the long term consequences of placental dysfunction were described, including an increased risk of obesity, cardiovascular and metabolic disease in later life. Central to the DOHaD hypothesis is the concept that fetal hemodynamic adaptations *in utero* lay the foundation for organ structure and function in the neonatal period and beyond. Evidence of vascular maladaptation may be present from early in the neonatal period. This includes altered cerebral oximetry and discordant left and right brachial artery blood flow (Sepulveda et al., 1995, Cohen et al., 2019). Furthermore, FGR infants demonstrate left ventricular hypertrophy and dilatation, altered cardiac morphology, and reduced myocardial reserve compared to AGA controls (Tan and Lewandowski, 2020). A six year European multicentre prospective cohort study (EVERREST) plans to follow up the neurodevelopmental outcomes of infants born growth restricted (Spencer et al., 2017). Follow up of the participants is planned at 3, 6, 12 and 24 months, and includes a variety of growth, health and neurodevelopmental assessments. These outcome data will improve knowledge of the natural history and sequelae of FGR, which will also be important when evaluating the efficacy and safety of any future placental therapeutics. As such, future studies of the biological mechanisms

of FGR should aim to incorporate meaningful clinical outcome measures in addition to birthweight.

7.6 Targeting mechanosensory pathways for FGR

Enhancement of physiological FSS through exercise has shown beneficial effects in the systemic circulation, whereby flow-induced increased NO is associated with improved cardiovascular disease outcomes (Rodriguez and Gonzalez, 2014). One study of maternal exercise on placental NO found higher eNOS expression in whole villous homogenates, along with reduced superoxide anions in a mitochondrial fraction (Ramirez-Velez et al., 2013). As such, the potential for pharmacological modulators of mechanosensing to ameliorate endothelial dysfunction, and improve blood flow, is of great clinical interest both in the systemic circulation and placental biology.

7.6.1 Blood flow mimetics

One therapeutic strategy is to develop mimetics targeting specific mechanosensors. For example, in addition to FSS, the small molecule GSK1016790A is an agonist of TRPV4 channels. The application of GSK1016790A to human coronary artery endothelial cells increased eNOS phosphorylation (Xu et al., 2016). Furthermore, oral administration of GSK1016790A reduced plaque formation in a mouse model of atherosclerosis (Xu et al., 2016).

We have discussed finding *GPR68* expression in the placenta with upregulation in whole villous tissue. Determining the significance of GPR68 requires functional studies, which could be performed using the positive modulator of GPR68, Ogerin. This compound was identified through screening, and can potentiate low-pH induced cAMP release (Wiley et al., 2019, Xu et al., 2018). Given the evidence for GPR68 involvement in FSS-sensing and tumourigenesis, the potential role of Ogerin as a flow mimetic warrants further investigation (Wiley et al., 2019).

The small molecule activator of Piezo1 channel, Yoda1, has been discussed widely in this thesis. FpECs responded to Yoda1 exhibited a dose-dependent increase in intracellular Ca^{2+} that was Piezo1-dependent, and blunted in SGA. Furthermore, Yoda1 application induced eNOS activation. Yoda1 has also been shown to mimic the effect of laminar flow on HUVECs (Davies et al., 2019). Here, Yoda1 applied to HUVECs in static conditions and with laminar flow had similar effects in reducing the ability of $\text{TNF-}\alpha$ to induce the expression of inflammatory intercellular adhesion molecule 1 (ICAM-1) and vascular cell adhesion molecule-1 (VCAM-1) (Davies et al., 2019). Given the atheroprotective phenotype of endothelium under laminar flow, this suggests that stimulating Piezo1 channels with an agonist could have an additional anti-inflammatory benefit. However, Yoda1 itself does not have the physico-chemical properties of a drug suitable for therapeutic use.

More recently, a new set of Piezo1 chemical activators (Jedi) has been developed, with the aim of generating agonists with improved pharmacokinetic properties. Interestingly, activation by Jedi required the presence of the force-sensing architectural components of the Piezo1 channel to be effective (Wang et al., 2018). Likewise, new inhibitors are also being developed by medicinal chemists, such as Dooku1, which counteracts the effects of Yoda1 (Evans et al., 2018). In section 7.4.1.2, the potential for Piezo1 channels to have differing roles dependent on the vascular bed and haemodynamic circumstance was discussed. As such, a significant challenge to developing therapeutics is specificity of effect. Excitingly, newly published research has also shown that Piezo1 in HUVECs can be activated by shear stress induced using an ultrasound probe (1 MHz stimulation for 10 seconds). These findings highlight the possibility of new interventions to modulate specific FSS-sensing targets (Zhang et al., 2020).

The potential for, and consequences of, these mechanosensor modulators crossing the placenta and their effect on the baby remains to be determined. For example, we do not yet know if such agents would have vascular bed specificity within uteroplacental and/or fetoplacental circulations, nor the effect this would have on maternal and fetal wellbeing

given the importance of maintaining a balanced pressure gradient between the two circulations.

7.6.2 Downstream modulators

Transduction of flow-induced biomechanical signals leads to a variety of signalling pathways, some of which have been described during this thesis. Downstream effects include altered activity of transcription factors leading to changes in gene expression, and epigenetic modification, thereby generating biological response (Xu, 2020). As such, targeting modifiers of the transcription factors downstream of flow transduction is an alternative therapeutic strategy (Xu, 2020).

A current example in the systemic circulation is the use of lipid-lowering statins (HMG-CoA reductase inhibitors), which activate KLF₂ (Kruppel-Like Factor 2) expression (Slegtenhorst et al., 2018). KLF₂ is regarded as a 'master regulator of flow-induced gene expression in endothelial cells' upstream of both eNOS and endothelin 1 activity, thereby regulating endothelial function (Xu, 2020). FSS also modulates epigenetic enzymes, such as those involved in DNA methylation (DNMT). When used in an atherosclerotic mouse model, a DNMT inhibitor improved endothelial function (Xu, 2020).

We have demonstrated that flow induces ADAM10 secretase activity, a component of the Notch pathway. Given the importance of Notch as a regulator of angiogenesis and cell fate determination, modulating Notch signalling has been considered in the field of cancer biology. Notch signalling is dysregulated in a number of cancers, including breast and cervical tumours (Rodrigues et al., 2019, Kontomanolis et al., 2018). As such, agents that block Notch receptor cleavages (γ -secretase inhibitors), or interfere with Notch ligand-receptor interaction, such as monoclonal antibodies, are under development (Takebe et al., 2014).

7.6.3 Approaches to target the NO pathway

In pregnancy research, efforts to enhance NO bioavailability have included maternal L-arginine supplementation. In a trial of women presenting with severe vascular FGR, there was no significant improvement in birthweight nor fetal outcomes following treatment (Winer et al., 2009). It has been suggested the lack of effect may be in part due to rapid metabolism by liver and gastrointestinal arginases (Cottrell et al., 2017). Interestingly, administration of L-citrulline in a rat model of FGR increased fetal growth. Furthermore, placental expression of growth factor genes (e.g. *Igf*) was increased, suggesting that an effect on vascular function was occurring within the placenta (Tran et al., 2017). No studies of L-citrulline supplementation in human pregnancy have been identified.

In addition to endogenous NO production from L-arginine, significant NO can be derived from dietary nitrate, particularly abundant in leafy green vegetables and beetroot (Cottrell et al., 2017). As such, maternal nitrate supplementation has been investigated, with the aim of improving uteroplacental vascular function and thus increasing fetal growth. In a feasibility trial of 40 hypertensive pregnant women given either placebo or nitrate (beetroot juice), there was no significant reduction in blood pressure (Ormesher et al., 2018). However, there was an inverse correlation between plasma nitrite concentrations and diastolic blood pressure. In this study, placental function and fetal growth was normal between the groups, and as such the impact of this intervention in the context of FGR warrants further investigation.

In clinical trials of hypertensive non-pregnant patients undergoing similar treatment with dietary nitrate, short-term lowering of blood pressure was noted (Bahadoran et al., 2017). However, meta-analysis of medium-term data, as measured by 24 hour ambulatory blood pressure recordings following a minimum of seven days treatment showed no significant difference (Ashor et al., 2017). With regards to the vasodilatory effect of nitrate on small vessels, supplements have also been given to individuals with Raynaud's phenomenon and cold hypersensitivity disorder. However, the results of these trials were mixed, where increases in blood flow, enhanced endothelium-dependent vasodilatation

and anti-inflammatory effect found in one study could not be replicated in another (Eglin et al., 2017, Shepherd et al., 2019). As such, the long-term effect of nitrates on systemic vascular pathology remains unclear.

A small study of using transdermal nitroglycerin and intravenous plasma volume expansion found that this increased fetal weight in pregnancies affected by maternal hypertension and FGR (Valensise et al., 2008). The increase in maternal cardiac output and reduction in total vascular resistance suggested that this effect was primarily due to alterations in maternal haemodynamics. In studies of pregnancies with normal placental function and fetal growth, nitroglycerin administration reduces uterine vascular impedance, with no effect on fetal perfusion (Kahler et al., 2004). As such, the mechanistic effect and clinical utility of these interventions on fetoplacental vasculature remains to be determined.

Efforts to develop therapies for FGR are also considering repurposing drugs that have been used in the systemic circulation. For example, pentaerythrityl tetranitrate (PETN) is a long-acting nitrate used for the chronic treatment of angina pectoris. This NO donor has a vasodilatory effect on myocardial vasculature, increasing perfusion and enhancing the expression of antioxidants (Kahler et al., 2004). A multi-centre trial in Germany comparing the effect of PETN versus placebo on fetal growth was started in 2017. Their inclusion criteria are women with abnormal uterine Doppler blood flow measurements at 19 - 22 weeks of gestation in singleton pregnancies (Groten et al., 2019). In their pilot study, these authors recruited 111 women with abnormal uterine resistance at mid-gestation. Resistance in uterine artery Doppler and umbilical artery Doppler were improved in the treatment arm. Developing absent umbilical artery end diastolic flow was delayed in the PETN group, suggestive of a beneficial effect in both the fetoplacental and uteroplacental circulations (Bowkalow et al., 2018).

Sildenafil citrate has also been repurposed as a potential rescue therapy for FGR. This vasodilating molecule increases NO concentrations by inhibiting phosphodiesterase-5 activity (Lopez-Tello et al., 2017). In several experimental models of FGR, there has

been apparent benefit following the administration of sildenafil (Dilworth et al., 2013, Stanley et al., 2012). In an ovine model of FGR sildenafil resulted in greater fetal and placental weights, suggesting that changes to fetal growth are at least partly related to fetoplacental modification (Oyston et al., 2016).

Few studies have focussed on the effect of sildenafil on the fetoplacental vasculature. Phosphodiesterase-5 mRNA and protein have been demonstrated in human chorionic arteries (Maharaj et al., 2009). Sildenafil produced dose-dependent vasodilatation of chorionic arteries which was dependent on cGMP. Moreover, sildenafil-induced vasodilatation enhanced the vasodilation produced by the NO donor sodium nitroprusside (Maharaj et al., 2009). In a rabbit model of FGR, sildenafil was associated with increased numbers of dilated placental small capillaries, venules, arterioles and arterial sinuses (Lopez-Tello et al., 2017). As such, sildenafil appears to have an effect on fetoplacental vasculature with an impact on fetal weight in multiple models. A large multicentre international clinical trial has evaluated the use of sildenafil in patients with FGR (Sharp et al., 2018). The inclusion criteria for the STRIDER (Sildenafil TheRapy In Dismal prognosis Early-onset fetal growth Restriction) trial were women from 22 weeks of gestation with an SGA baby (EFW <5th centile) and placental insufficiency, as defined by abnormal uterine artery Doppler, umbilical or middle cerebral artery Doppler measurements, maternal hypertension and/or low PIGF. Patients were administered sildenafil (25mg orally, three times per day) or placebo, from randomisation until delivery. There was no significant difference in the primary outcome, delay of delivery, between groups. Furthermore, a Doppler measurement indicative of fetal wellbeing, examining flow within the ductus venosus, worsened in the treatment arm. A range of other secondary outcomes were reported, but the summary effect was no benefit from sildenafil. However, questions still remain regarding dosage required for effect, and the critical nature of this clinical cohort (~45% perinatal mortality) prohibiting any potential benefit.

7.7 Conclusion

Mechanosensing by FpECs ultimately regulates NO bioavailability, thus impacting upon vasomotor tone. Mechanisms of FSS sensing are compromised in FGR, allowing vasoconstrictor and anti-angiogenic effects to dominate. The fetoplacental endothelium in FGR attempts to compensate restricted blood flow by upregulating components of the NO system but this of course lacks flow responsiveness and is already maximal, which may explain why efforts to boost NO have not yielded clinically significant results. Critical to the success of a therapy for placental insufficiency will be a more nuanced understanding of how FSS is transduced by the fetoplacental endothelium, the interplay with stressors such as hypoxia, and ensuring that target vessels are responsive to NO-driven vasodilatation. Furthermore, FGR is a heterogeneous condition, even within the majority of cases that are of placental origin. As such, tight clinical phenotyping will be required in future studies to determine the interplay between mechanosensory signalling and the clinical and genetic risk factors for placental insufficiency.

We suggest that Piezo1 is an entry point to this new understanding and presents an opportunity for targeted intervention. The availability of new small molecule channel modulators such as Yoda1, Jedi and Dooku1 which specifically target the Piezo1 channel offer opportunities for further fundamental research into this important mechanosensor. In addition, new *in silico* and *ex vivo* models of FSS may be used to better identify and study fetoplacental circulatory deficiency, bridging the gap between better understanding fetoplacental haemodynamics and useful clinical interventions.

List of references

- ADAIR, T. H. M., J.P. 2010. Angiogenesis. San Rafael (CA): Morgan & Claypool Life Sciences.
- AFSHAR, Y., JEONG, J. W., ROQUEIRO, D., DEMAYO, F., LYDON, J., RADTKE, F., RADNOR, R., MIELE, L. & FAZLEABAS, A. 2012. Notch1 mediates uterine stromal differentiation and is critical for complete decidualization in the mouse. *FASEB J*, 26, 282-94.
- ALBARRAN-JUAREZ, J., IRING, A., WANG, S., JOSEPH, S., GRIMM, M., STRILIC, B., WETTSCHURECK, N., ALTHOFF, T. F. & OFFERMANN, S. 2018. Piezo1 and Gq/G11 promote endothelial inflammation depending on flow pattern and integrin activation. *J Exp Med*, 215, 2655-2672.
- ALBERT, P. R. & TASHJIAN, A. H., JR. 1986. Ionomycin acts as an ionophore to release TRH-regulated Ca²⁺ stores from GH4C1 cells. *Am J Physiol*, 251, C887-91.
- ALCAINO, C., FARRUGIA, G. & BEYDER, A. 2017. Mechanosensitive Piezo Channels in the Gastrointestinal Tract. *Curr Top Membr*, 79, 219-244.
- ALFIREVIC, Z., STAMPALIJA, T. & DOWSWELL, T. 2017. Fetal and umbilical Doppler ultrasound in high-risk pregnancies. *Cochrane Database Syst Rev*, 6, CD007529.
- ALFIREVIC, Z., STAMPALIJA, T. & MEDLEY, N. 2015. Fetal and umbilical Doppler ultrasound in normal pregnancy. *Cochrane Database Syst Rev*, CD001450.
- AMERICAN COLLEGE OF, O. & GYNECOLOGISTS 2013. ACOG Practice bulletin no. 134: fetal growth restriction. *Obstet Gynecol*, 121, 1122-33.
- ANDO, J. & YAMAMOTO, K. 2013. Flow detection and calcium signalling in vascular endothelial cells. *Cardiovasc Res*, 99, 260-8.
- ARNAOUTOVA, I., GEORGE, J., KLEINMAN, H. K. & BENTON, G. 2009. The endothelial cell tube formation assay on basement membrane turns 20: state of the science and the art. *Angiogenesis*, 12, 267-74.
- ARTHUR, J. S., ELCE, J. S., HEGADORN, C., WILLIAMS, K. & GREER, P. A. 2000. Disruption of the murine calpain small subunit gene, *Capn4*: calpain is essential for embryonic development but not for cell growth and division. *Mol Cell Biol*, 20, 4474-81.
- ASHOR, A. W., LARA, J. & SIERVO, M. 2017. Medium-term effects of dietary nitrate supplementation on systolic and diastolic blood pressure in adults: a systematic review and meta-analysis. *J Hypertens*, 35, 1353-1359.
- AUDETTE, M. C. & KINGDOM, J. C. 2018. Screening for fetal growth restriction and placental insufficiency. *Semin Fetal Neonatal Med*, 23, 119-125.
- BAHADORAN, Z., MIRMIRAN, P., KABIR, A., AZIZI, F. & GHASEMI, A. 2017. The Nitrate-Independent Blood Pressure-Lowering Effect of Beetroot Juice: A Systematic Review and Meta-Analysis. *Adv Nutr*, 8, 830-838.
- BAKHASHAB, S., LARY, S., AHMED, F., SCHULTEN, H. J., BASHIR, A., AHMED, F. W., AL-MALKI, A. L., JAMAL, H. S., GARI, M. A. & WEAVER, J. U. 2014. Reference genes for expression studies in hypoxia and hyperglycemia models in human umbilical vein endothelial cells. *G3 (Bethesda)*, 4, 2159-65.
- BAPPOO, N., KELSEY, L. J., PARKER, L., CROUGH, T., MORAN, C. M., THOMSON, A., HOLMES, M. C., WYRWOLL, C. S. & DOYLE, B. J. 2017. Viscosity and haemodynamics in a late gestation rat feto-placental arterial network. *Biomech Model Mechanobiol*, 16, 1361-1372.
- BARATCHI, S., KHOSHMANESH, K., WOODMAN, O. L., POTOCHNIK, S., PETER, K. & MCINTYRE, P. 2017a. Molecular Sensors of Blood Flow in Endothelial Cells. *Trends Mol Med*, 23, 850-868.
- BARATCHI, S., KNOERZER, M., KHOSHMANESH, K., MITCHELL, A. & MCINTYRE, P. 2017b. Shear Stress Regulates TRPV4 Channel Clustering and Translocation from Adherens Junctions to the Basal Membrane. *Sci Rep*, 7, 15942.
- BARKER, D. J. 2007. The origins of the developmental origins theory. *J Intern Med*, 261, 412-7.

- BEECH, D. J. & KALLI, A. C. 2019. Force Sensing by Piezo Channels in Cardiovascular Health and Disease. *Arterioscler Thromb Vasc Biol*, 39, 2228-2239.
- BEINDL, W., MITTERAUER, T., HOHENEGGER, M., IJZERMAN, A. P., NANOFF, C. & FREISSMUTH, M. 1996. Inhibition of receptor/G protein coupling by suramin analogues. *Mol Pharmacol*, 50, 415-23.
- BELKACEMI, L., BEDARD, I., SIMONEAU, L. & LAFOND, J. 2005. Calcium channels, transporters and exchangers in placenta: a review. *Cell Calcium*, 37, 1-8.
- BELMOKHTAR, C. A., HILLION, J. & SEGAL-BENDIRDJIAN, E. 2001. Staurosporine induces apoptosis through both caspase-dependent and caspase-independent mechanisms. *Oncogene*, 20, 3354-62.
- BIGONNESSE, E., SICOTTE, B. & BROCHU, M. 2018. Activated NO pathway in uterine arteries during pregnancy in an IUGR rat model. *Am J Physiol Heart Circ Physiol*, 315, H415-H422.
- BODIN, P. & BURNSTOCK, G. 2001. Evidence that release of adenosine triphosphate from endothelial cells during increased shear stress is vesicular. *J Cardiovasc Pharmacol*, 38, 900-8.
- BOELDT, D. S., YI, F. X. & BIRD, I. M. 2011. eNOS activation and NO function: pregnancy adaptive programming of capacitative entry responses alters nitric oxide (NO) output in vascular endothelium--new insights into eNOS regulation through adaptive cell signaling. *J Endocrinol*, 210, 243-58.
- BOWKALOW, S., SCHLEUSSNER, E., KAHLER, C., SCHNEIDER, U., LEHMANN, T. & GROTEN, T. 2018. Pentaerythrityltetranitrate (PETN) improves utero- and fetoplacental Doppler parameters in pregnancies with impaired utero-placental perfusion in mid-gestation - a secondary analysis of the PETN-pilot trial. *J Perinat Med*, 46, 1004-1009.
- BRAKEMEIER, S., EICHLER, I., HOPP, H., KOHLER, R. & HOYER, J. 2002. Up-regulation of endothelial stretch-activated cation channels by fluid shear stress. *Cardiovasc Res*, 53, 209-18.
- BRAY, S. J. 2006. Notch signalling: a simple pathway becomes complex. *Nat Rev Mol Cell Biol*, 7, 678-89.
- BRUGGER, B. A., GUETTLER, J. & GAUSTER, M. 2020. Go with the Flow-Trophoblasts in Flow Culture. *Int J Mol Sci*, 21.
- BURTON, G. J. & JAUNIAUX, E. 2018. Development of the Human Placenta and Fetal Heart: Synergic or Independent? *Front Physiol*, 9, 373.
- BURTON, G. J., REDMAN, C. W., ROBERTS, J. M. & MOFFETT, A. 2019. Pre-eclampsia: pathophysiology and clinical implications. *BMJ*, 366, l2381.
- CAOLO, V., DEBANT, M., ENDESH, N., FUTERS, T. S., LICHTENSTEIN, L., BARTOLI, F., PARSONAGE, G., JONES, E. A. & BEECH, D. J. 2020. Shear stress activates ADAM10 sheddase to regulate Notch1 via the Piezo1 force sensor in endothelial cells. *Elife*, 9.
- CAOLO, V., SWENNEN, G., CHALARIS, A., WAGENAAR, A., VERBRUGGEN, S., ROSE-JOHN, S., MOLIN, D. G., VOOIJS, M. & POST, M. J. 2015. ADAM10 and ADAM17 have opposite roles during sprouting angiogenesis. *Angiogenesis*, 18, 13-22.
- CASANELLO, P. & SOBREVIA, L. 2002. Intrauterine growth retardation is associated with reduced activity and expression of the cationic amino acid transport systems y⁺/hCAT-1 and y⁺/hCAT-2B and lower activity of nitric oxide synthase in human umbilical vein endothelial cells. *Circ Res*, 91, 127-34.
- CHATTERJEE, S. 2018. Endothelial Mechanotransduction, Redox Signaling and the Regulation of Vascular Inflammatory Pathways. *Front Physiol*, 9, 524.
- CHOW, S., SHAO J, WANG H. 2008. Sample Size Calculations in Clinical Research 2nd Edition. *CRC Biostatistics Series*. Chapman & Hall.
- CINDROVA-DAVIES, T. 2009. Gabor Than Award Lecture 2008: pre-eclampsia - from placental oxidative stress to maternal endothelial dysfunction. *Placenta*, 30 Suppl A, S55-65.

- CLARK, A. R., LEE, T. C. & JAMES, J. L. 2020. Computational modeling of the interactions between the maternal and fetal circulations in human pregnancy. *Wiley Interdiscip Rev Syst Biol Med*, e1502.
- CLARK, A. R., LIN, M., TAWHAI, M., SAGHIAN, R. & JAMES, J. L. 2015. Multiscale modelling of the fetoplacental vasculature. *Interface Focus*, 5, 20140078.
- COBELLIS, L., MASTROGIACOMO, A., FEDERICO, E., SCETTINO, M. T., DE FALCO, M., MANENTE, L., COPPOLA, G., TORELLA, M., COLACURCI, N. & DE LUCA, A. 2007. Distribution of Notch protein members in normal and preeclampsia-complicated placentas. *Cell Tissue Res*, 330, 527-34.
- COHEN, E., BAERTS, W., CAICEDO DORADO, A., NAULAERS, G., VAN BEL, F. & LEMMERS, P. M. A. 2019. Cerebrovascular autoregulation in preterm fetal growth restricted neonates. *Arch Dis Child Fetal Neonatal Ed*, 104, F467-F472.
- COON, B. G., BAEYENS, N., HAN, J., BUDATHA, M., ROSS, T. D., FANG, J. S., YUN, S., THOMAS, J. L. & SCHWARTZ, M. A. 2015. Intramembrane binding of VE-cadherin to VEGFR2 and VEGFR3 assembles the endothelial mechanosensory complex. *J Cell Biol*, 208, 975-86.
- COSTE, B., MATHUR, J., SCHMIDT, M., EARLEY, T. J., RANADE, S., PETRUS, M. J., DUBIN, A. E. & PATAPOUTIAN, A. 2010. Piezo1 and Piezo2 are essential components of distinct mechanically activated cation channels. *Science*, 330, 55-60.
- COTTRELL, E., TROPEA, T., ORMESHER, L., GREENWOOD, S., WAREING, M., JOHNSTONE, E., MYERS, J. & SIBLEY, C. 2017. Dietary interventions for fetal growth restriction - therapeutic potential of dietary nitrate supplementation in pregnancy. *J Physiol*, 595, 5095-5102.
- CRISPI, F., MIRANDA, J. & GRATACOS, E. 2018. Long-term cardiovascular consequences of fetal growth restriction: biology, clinical implications, and opportunities for prevention of adult disease. *Am J Obstet Gynecol*, 218, S869-S879.
- CUMAN, C., MENKHORST, E., WINSHIP, A., VAN SINDEREN, M., OSIANLIS, T., ROMBAUTS, L. J. & DIMITRIADIS, E. 2014. Fetal-maternal communication: the role of Notch signalling in embryo implantation. *Reproduction*, 147, R75-86.
- CUMAN, C., MENKHORST, E. M., ROMBAUTS, L. J., HOLDEN, S., WEBSTER, D., BILANDZIC, M., OSIANLIS, T. & DIMITRIADIS, E. 2013. Preimplantation human blastocysts release factors that differentially alter human endometrial epithelial cell adhesion and gene expression relative to IVF success. *Hum Reprod*, 28, 1161-71.
- D'SOUZA, B., MELOTY-KAPPELLA, L. & WEINMASTER, G. 2010. Canonical and non-canonical Notch ligands. *Curr Top Dev Biol*, 92, 73-129.
- DARDIK, A., CHEN, L., FRATTINI, J., ASADA, H., AZIZ, F., KUDO, F. A. & SUMPIO, B. E. 2005. Differential effects of orbital and laminar shear stress on endothelial cells. *J Vasc Surg*, 41, 869-80.
- DAVID, A. L. 2017. Maternal uterine artery VEGF gene therapy for treatment of intrauterine growth restriction. *Placenta*, 59 Suppl 1, S44-S50.
- DAVIES, J. E., LOPRESTO, D., APTA, B. H. R., LIN, Z., MA, W. & HARPER, M. T. 2019. Using Yoda-1 to mimic laminar flow in vitro: A tool to simplify drug testing. *Biochem Pharmacol*, 168, 473-480.
- DAVIES, P. F., CIVELEK, M., FANG, Y. & FLEMING, I. 2013. The atherosusceptible endothelium: endothelial phenotypes in complex haemodynamic shear stress regions in vivo. *Cardiovasc Res*, 99, 315-27.
- DE FALCO, M., COBELLIS, L., GIRALDI, D., MASTROGIACOMO, A., PERNA, A., COLACURCI, N., MIELE, L. & DE LUCA, A. 2007. Expression and distribution of notch protein members in human placenta throughout pregnancy. *Placenta*, 28, 118-26.
- DE ONIS, M., BLOSSNER, M. & VILLAR, J. 1998. Levels and patterns of intrauterine growth retardation in developing countries. *Eur J Clin Nutr*, 52 Suppl 1, S5-15.

- DEL MARMOL, J. I., TOUHARA, K. K., CROFT, G. & MACKINNON, R. 2018. Piezo1 forms a slowly-inactivating mechanosensory channel in mouse embryonic stem cells. *Elife*, 7.
- DELA PAZ, N. G., WALSH, T. E., LEACH, L. L., SAINT-GENIEZ, M. & D'AMORE, P. A. 2012. Role of shear-stress-induced VEGF expression in endothelial cell survival. *J Cell Sci*, 125, 831-43.
- DILWORTH, M. R., ANDERSSON, I., RENSHALL, L. J., COWLEY, E., BAKER, P., GREENWOOD, S., SIBLEY, C. P. & WAREING, M. 2013. Sildenafil citrate increases fetal weight in a mouse model of fetal growth restriction with a normal vascular phenotype. *PLoS One*, 8, e77748.
- DREWLO, S., LEVYTSKA, K. & KINGDOM, J. 2012. Revisiting the housekeeping genes of human placental development and insufficiency syndromes. *Placenta*, 33, 952-4.
- DUARTE, A., HIRASHIMA, M., BENEDITO, R., TRINDADE, A., DINIZ, P., BEKMAN, E., COSTA, L., HENRIQUE, D. & ROSSANT, J. 2004. Dosage-sensitive requirement for mouse Dll4 in artery development. *Genes Dev*, 18, 2474-8.
- DUNK, C. E., PAPPAS, J. J., LYE, P., KIBSCHULL, M., JAVAM, M., BLOISE, E., LYE, S. J., SZYF, M. & MATTHEWS, S. G. 2018. P-Glycoprotein (P-gp)/ABCB1 plays a functional role in extravillous trophoblast (EVT) invasion and is decreased in the pre-eclamptic placenta. *J Cell Mol Med*, 22, 5378-5393.
- EGLIN, C. M., COSTELLO, J. T., BAILEY, S. J., GILCHRIST, M., MASSEY, H. & SHEPHERD, A. I. 2017. Effects of dietary nitrate supplementation on the response to extremity cooling and endothelial function in individuals with cold sensitivity. A double blind, placebo controlled, crossover, randomised control trial. *Nitric Oxide*, 70, 76-85.
- ELLISEN, L. W., BIRD, J., WEST, D. C., SORENG, A. L., REYNOLDS, T. C., SMITH, S. D. & SKLAR, J. 1991. TAN-1, the human homolog of the Drosophila notch gene, is broken by chromosomal translocations in T lymphoblastic neoplasms. *Cell*, 66, 649-61.
- ESSENBIOSCIENCE 2020. IncuCyte®96-Well Scratch Wound: Cell Migration & Invasion Assays
User Manual Sartorius.
- EVANS, E. L., CUTHBERTSON, K., ENDESH, N., RODE, B., BLYTHE, N. M., HYMAN, A. J., HALL, S. J., GAUNT, H. J., LUDLOW, M. J., FOSTER, R. & BEECH, D. J. 2018. Yoda1 analogue (Dooku1) which antagonizes Yoda1-evoked activation of Piezo1 and aortic relaxation. *Br J Pharmacol*, 175, 1744-1759.
- FANG, J. S., COON, B. G., GILLIS, N., CHEN, Z., QIU, J., CHITTENDEN, T. W., BURT, J. M., SCHWARTZ, M. A. & HIRSCHI, K. K. 2017. Shear-induced Notch-Cx37-p27 axis arrests endothelial cell cycle to enable arterial specification. *Nat Commun*, 8, 2149.
- FEARNLEY, G. W., SMITH, G. A., ODELL, A. F., LATHAM, A. M., WHEATCROFT, S. B., HARRISON, M. A., TOMLINSON, D. C. & PONNAMBALAM, S. 2014. Vascular endothelial growth factor A-stimulated signaling from endosomes in primary endothelial cells. *Methods Enzymol*, 535, 265-92.
- FELS, B. & KUSCHE-VIHROG, K. 2020. It takes more than two to tango: mechanosignaling of the endothelial surface. *Pflugers Arch*, 472, 419-433.
- FISCHER, A., SCHUMACHER, N., MAIER, M., SENDTNER, M. & GESSLER, M. 2004. The Notch target genes Hey1 and Hey2 are required for embryonic vascular development. *Genes Dev*, 18, 901-11.
- FOTIOU, E., MARTIN-ALMEDINA, S., SIMPSON, M. A., LIN, S., GORDON, K., BRICE, G., ATTON, G., JEFFERY, I., REES, D. C., MIGNOT, C., VOGT, J., HOMFRAY, T., SNYDER, M. P., ROCKSON, S. G., JEFFERY, S., MORTIMER, P. S., MANSOUR, S. & OSTERGAARD, P. 2015. Novel mutations in PIEZO1 cause an autosomal recessive generalized lymphatic dysplasia with non-immune hydrops fetalis. *Nat Commun*, 6, 8085.

- FRUSCA, T., TODROS, T., LEES, C., BILARDO, C. M. & INVESTIGATORS, T. 2018. Outcome in early-onset fetal growth restriction is best combining computerized fetal heart rate analysis with ductus venosus Doppler: insights from the Trial of Umbilical and Fetal Flow in Europe. *Am J Obstet Gynecol*, 218, S783-S789.
- GACCIOLI, F. & LAGER, S. 2016. Placental Nutrient Transport and Intrauterine Growth Restriction. 7.
- GAGNÉ, F. 2014. Tissue Preparation and Subcellular Fractionation Techniques. *Biochemical Ecotoxicology*. Elsevier.
- GALE, N. W., DOMINGUEZ, M. G., NOGUERA, I., PAN, L., HUGHES, V., VALENZUELA, D. M., MURPHY, A. J., ADAMS, N. C., LIN, H. C., HOLASH, J., THURSTON, G. & YANCOPOULOS, G. D. 2004. Haploinsufficiency of delta-like 4 ligand results in embryonic lethality due to major defects in arterial and vascular development. *Proc Natl Acad Sci U S A*, 101, 15949-54.
- GARCIA-GONZALEZ, M. A., OUTEDA, P., ZHOU, Q., ZHOU, F., MENEZES, L. F., QIAN, F., HUSO, D. L., GERMINO, G. G., PIONTEK, K. B. & WATNICK, T. 2010. Pkd1 and Pkd2 are required for normal placental development. *PLoS One*, 5.
- GARDOSI, J., KADY, S. M., MCGEOWN, P., FRANCIS, A. & TONKS, A. 2005. Classification of stillbirth by relevant condition at death (ReCoDe): population based cohort study. *BMJ*, 331, 1113-7.
- GAUSTER, M., MAJALI-MARTINEZ, A., MANINGER, S., GUTSCHI, E., GREIMEL, P. H., IVANISEVIC, M., DJELMIS, J., DESOYE, G. & HIDEN, U. 2017. Maternal Type 1 diabetes activates stress response in early placenta. *Placenta*, 50, 110-116.
- GIANNUBILO, S. R., MENEGAZZI, M., TEDESCHI, E., BEZZECCHERI, V., SUZUKI, H. & TRANQUILLI, A. L. 2008. Doppler analysis and placental nitric oxide synthase expression during fetal growth restriction. *J Matern Fetal Neonatal Med*, 21, 617-22.
- GLIOZZI, M., SCICCHITANO, M., BOSCO, F., MUSOLINO, V., CARRESI, C., SCARANO, F., MAIUOLO, J., NUCERA, S., MARETTA, A., PAONE, S., MOLLACE, R., RUGA, S., ZITO, M. C., MACRI, R., OPPEDISANO, F., PALMA, E., SALVEMINI, D., MUSCOLI, C. & MOLLACE, V. 2019. Modulation of Nitric Oxide Synthases by Oxidized LDLs: Role in Vascular Inflammation and Atherosclerosis Development. *Int J Mol Sci*, 20.
- GLOGOWSKA, E., SCHNEIDER, E. R., MAKSIMOVA, Y., SCHULZ, V. P., LEZONGEYDA, K., WU, J., RADHAKRISHNAN, K., KEEL, S. B., MAHONEY, D., FREIDMANN, A. M., ALTURA, R. A., GRACHEVA, E. O., BAGRIANTSEV, S. N., KALFA, T. A. & GALLAGHER, P. G. 2017. Novel mechanisms of PIEZO1 dysfunction in hereditary xerocytosis. *Blood*, 130, 1845-1856.
- GNECCO, J. S., PENSABENE, V., LI, D. J., DING, T., HUI, E. E., BRUNER-TRAN, K. L. & OSTEEEN, K. G. 2017. Compartmentalized Culture of Perivascular Stroma and Endothelial Cells in a Microfluidic Model of the Human Endometrium. *Ann Biomed Eng*, 45, 1758-1769.
- GORDIJN, S. J., BEUNE, I. M., THILAGANATHAN, B., PAPAGEORGHIOU, A., BASCHAT, A. A., BAKER, P. N., SILVER, R. M., WYNIA, K. & GANZEVOORT, W. 2016. Consensus definition of fetal growth restriction: a Delphi procedure. *Ultrasound Obstet Gynecol*, 48, 333-9.
- GREENBERG, H. Z., SHI, J., JAHAN, K. S., MARTINUCCI, M. C., GILBERT, S. J., VANESSA HO, W. S. & ALBERT, A. P. 2016. Stimulation of calcium-sensing receptors induces endothelium-dependent vasorelaxations via nitric oxide production and activation of IKCa channels. *Vascul Pharmacol*, 80, 75-84.
- GRIEVE, S., GAO, Y., HALL, C., HU, J. & GREER, P. A. 2016. Calpain Genetic Disruption and HSP90 Inhibition Combine To Attenuate Mammary Tumorigenesis. *Mol Cell Biol*, 36, 2078-88.
- GROTEN, T., LEHMANN, T., SCHLEUSSNER, E. & GROUP, P. S. 2019. Does Pentaerythryltetranitrate reduce fetal growth restriction in pregnancies complicated by uterine mal-perfusion? Study protocol of the PETN-study: a randomized controlled multicenter-trial. *BMC Pregnancy Childbirth*, 19, 336.

- GUMINA, D. L. & SU, E. J. 2017. Endothelial Progenitor Cells of the Human Placenta and Fetoplacental Circulation: A Potential Link to Fetal, Neonatal, and Long-term Health. *Front Pediatr*, 5, 41.
- GUO, Y. R. & MACKINNON, R. 2017. Structure-based membrane dome mechanism for Piezo mechanosensitivity. *Elife*, 6.
- GUZMAN-GUTIERREZ, E., ARROYO, P., SALSOSO, R., FUENZALIDA, B., SAEZ, T., LEIVA, A., PARDO, F. & SOBREVIA, L. 2014. Role of insulin and adenosine in the human placenta microvascular and macrovascular endothelial cell dysfunction in gestational diabetes mellitus. *Microcirculation*, 21, 26-37.
- HAIDER, S., POLLHEIMER, J. & KNOFLER, M. 2017. Notch signalling in placental development and gestational diseases. *Placenta*, 56, 65-72.
- HAMADA, Y., HIROE, T., SUZUKI, Y., ODA, M., TSUJIMOTO, Y., COLEMAN, J. R. & TANAKA, S. 2007. Notch2 is required for formation of the placental circulatory system, but not for cell-type specification in the developing mouse placenta. *Differentiation*, 75, 268-78.
- HARPER, J. A., YUAN, J. S., TAN, J. B., VISAN, I. & GUIDOS, C. J. 2003. Notch signaling in development and disease. *Clin Genet*, 64, 461-72.
- HARTMANNGRUBER, V., HEYKEN, W. T., KACIK, M., KAISTHA, A., GRGIC, I., HARTENECK, C., LIEDTKE, W., HOYER, J. & KOHLER, R. 2007. Arterial response to shear stress critically depends on endothelial TRPV4 expression. *PLoS One*, 2, e827.
- HERR, F., SCHREINER, I., BAAL, N., PFARRER, C. & ZYGMUNT, M. 2011. Expression patterns of Notch receptors and their ligands Jagged and Delta in human placenta. *Placenta*, 32, 554-63.
- HIRAKAWA, M., OIKE, M., KARASHIMA, Y. & ITO, Y. 2004. Sequential activation of RhoA and FAK/paxillin leads to ATP release and actin reorganization in human endothelium. *J Physiol*, 558, 479-88.
- HU, T., WANG, G., ZHU, Z., HUANG, Y., GU, H. & NI, X. 2015. Increased ADAM10 expression in preeclamptic placentas is associated with decreased expression of hydrogen sulfide production enzymes. *Placenta*, 36, 947-50.
- HUANG, C., SHEIKH, F., HOLLANDER, M., CAI, C., BECKER, D., CHU, P. H., EVANS, S. & CHEN, J. 2003. Embryonic atrial function is essential for mouse embryogenesis, cardiac morphogenesis and angiogenesis. *Development*, 130, 6111-9.
- HUANG, Z., SUN, Z., ZHANG, X., NIU, K., WANG, Y., ZHENG, J., LI, H. & LIU, Y. 2019. Loss of stretch-activated channels, PIEZO1s, accelerates non-small cell lung cancer progression and cell migration. *Biosci Rep*, 39.
- HYMAN, A. J., TUMOVA, S. & BEECH, D. J. 2017. Piezo1 Channels in Vascular Development and the Sensing of Shear Stress. *Curr Top Membr*, 79, 37-57.
- ILIODROMITI, S., MACKAY, D. F., SMITH, G. C., PELL, J. P., SATTAR, N., LAWLOR, D. A. & NELSON, S. M. 2017. Customised and Noncustomised Birth Weight Centiles and Prediction of Stillbirth and Infant Mortality and Morbidity: A Cohort Study of 979,912 Term Singleton Pregnancies in Scotland. *PLoS Med*, 14, e1002228.
- INTERNATIONAL STILLBIRTH ALLIANCE COLLABORATIVE FOR IMPROVING CLASSIFICATION OF PERINATAL, D., FLENADY, V., WOJCIESZEK, A. M., ELLWOOD, D., LEISHER, S. H., ERWICH, J., DRAPER, E. S., MCCLURE, E. M., REINEBRANT, H. E., OATS, J., MCCOWAN, L., KENT, A. L., GARDENER, G., GORDON, A., TUDEHOPE, D., SIASSAKOS, D., STOREY, C., ZUCCOLLO, J., DAHLSTROM, J. E., GOLD, K. J., GORDIJN, S., PETTERSSON, K., MASSON, V., PATTINSON, R., GARDOSI, J., KHONG, T. Y., FROEN, J. F. & SILVER, R. M. 2017. Classification of causes and associated conditions for stillbirths and neonatal deaths. *Semin Fetal Neonatal Med*, 22, 176-185.
- JAMES, J. L., CARTWRIGHT, J. E., WHITLEY, G. S., GREENHILL, D. R. & HOPPE, A. 2012. The regulation of trophoblast migration across endothelial cells by low shear stress: consequences for vascular remodelling in pregnancy. *Cardiovasc Res*, 93, 152-61.

- JAMES, J. L., SAGHIAN, R., PERWICK, R. & CLARK, A. R. 2018. Trophoblast plugs: impact on utero-placental haemodynamics and spiral artery remodelling. *Hum Reprod*, 33, 1430-1441.
- JAUNIAUX, E., WATSON, A. L., HEMPSTOCK, J., BAO, Y. P., SKEPPER, J. N. & BURTON, G. J. 2000. Onset of maternal arterial blood flow and placental oxidative stress. A possible factor in human early pregnancy failure. *Am J Pathol*, 157, 2111-22.
- JOHN, L., KO, N. L., GOKIN, A., GOKINA, N., MANDALA, M. & OSOL, G. 2018. The Piezo1 cation channel mediates uterine artery shear stress mechanotransduction and vasodilation during rat pregnancy. *Am J Physiol Heart Circ Physiol*, 315, H1019-H1026.
- JONES, S., BISCHOF, H., LANG, I., DESOYE, G., GREENWOOD, S. L., JOHNSTONE, E. D., WAREING, M., SIBLEY, C. P. & BROWNBILL, P. 2015. Dysregulated flow-mediated vasodilatation in the human placenta in fetal growth restriction. *J Physiol*, 593, 3077-92.
- JOUTEL, A., CORPECHOT, C., DUCROS, A., VAHEDI, K., CHABRIAT, H., MOUTON, P., ALAMOWITCH, S., DOMENGA, V., CECILLION, M., MARECHAL, E., MACIAZEK, J., VAYSSIERE, C., CRUAUD, C., CABANIS, E. A., RUCHOUX, M. M., WEISSENBAACH, J., BACH, J. F., BOUSSER, M. G. & TOURNIER-LASSERVE, E. 1996. Notch3 mutations in CADASIL, a hereditary adult-onset condition causing stroke and dementia. *Nature*, 383, 707-10.
- JUNAID, T. O., BROWNBILL, P., CHALMERS, N., JOHNSTONE, E. D. & APLIN, J. D. 2014. Fetoplacental vascular alterations associated with fetal growth restriction. *Placenta*, 35, 808-15.
- KADAM, P. & BHALERAO, S. 2010. Sample size calculation. *Int J Ayurveda Res*, 1, 55-7.
- KAHLER, C., SCHLEUSSNER, E., MOLLER, A. & SEEWALD, H. J. 2004. Nitric oxide donors: effects on fetoplacental blood flow. *Eur J Obstet Gynecol Reprod Biol*, 115, 10-4.
- KANEKO, Y., LINDSAY, L. A. & MURPHY, C. R. 2008. Focal adhesions disassemble during early pregnancy in rat uterine epithelial cells. *Reprod Fertil Dev*, 20, 892-9.
- KANEKO, Y., MURPHY, C. R. & DAY, M. L. 2014. Calpain 2 activity increases at the time of implantation in rat uterine luminal epithelial cells and administration of calpain inhibitor significantly reduces implantation sites. *Histochem Cell Biol*, 141, 423-30.
- KINGDOM, J. 1998. Adriana and Luisa Castellucci Award Lecture 1997. Placental pathology in obstetrics: adaptation or failure of the villous tree? *Placenta*, 19, 347-51.
- KINGDOM, J., HUPPERTZ, B., SEAWARD, G. & KAUFMANN, P. 2000. Development of the placental villous tree and its consequences for fetal growth. *Eur J Obstet Gynecol Reprod Biol*, 92, 35-43.
- KINGDOM, J. C. & KAUFMANN, P. 1997. Oxygen and placental villous development: origins of fetal hypoxia. *Placenta*, 18, 613-21; discussion 623-6.
- KISERUD, T., PIAGGIO, G., CARROLI, G., WIDMER, M., CARVALHO, J., NEERUP JENSEN, L., GIORDANO, D., CECATTI, J. G., ABDEL ALEEM, H., TALEGAWKAR, S. A., BENACHI, A., DIEMERT, A., TSHEFU KITOTO, A., THINKHAMROP, J., LUMBIGANON, P., TABOR, A., KRIPLANI, A., GONZALEZ PEREZ, R., HECHER, K., HANSON, M. A., GULMEZOGLU, A. M. & PLATT, L. D. 2017. The World Health Organization Fetal Growth Charts: A Multinational Longitudinal Study of Ultrasound Biometric Measurements and Estimated Fetal Weight. *PLoS Med*, 14, e1002220.
- KO, N. L., MANDALA, M., JOHN, L., GELINNE, A. & OSOL, G. 2018. Venoarterial communication mediates arterial wall shear stress-induced maternal uterine vascular remodeling during pregnancy. *Am J Physiol Heart Circ Physiol*, 315, H709-H717.

- KOHLER, R., SCHONFELDER, G., HOPP, H., DISTLER, A. & HOYER, J. 1998. Stretch-activated cation channel in human umbilical vein endothelium in normal pregnancy and in preeclampsia. *J Hypertens*, 16, 1149-56.
- KONTOMANOLIS, E. N., KALAGASIDOU, S., POULILIOU, S., ANTHOULAKI, X., GEORGIU, N., PAPAMANOLIS, V. & FASOULAKIS, Z. N. 2018. The Notch Pathway in Breast Cancer Progression. *ScientificWorldJournal*, 2018, 2415489.
- KOPAN, R. & ILAGAN, M. X. 2009. The canonical Notch signaling pathway: unfolding the activation mechanism. *Cell*, 137, 216-33.
- KRAUSE, B. J., CARRASCO-WONG, I., CANIUGUIR, A., CARVAJAL, J., FARIAS, M. & CASANELLO, P. 2013. Endothelial eNOS/arginase imbalance contributes to vascular dysfunction in IUGR umbilical and placental vessels. *Placenta*, 34, 20-8.
- KUBLICKIENE, K. R., LINDBLOM, B., KRUGER, K. & NISELL, H. 2000. Preeclampsia: evidence for impaired shear stress-mediated nitric oxide release in uterine circulation. *Am J Obstet Gynecol*, 183, 160-6.
- LACKMAN, F., CAPEWELL, V., GAGNON, R. & RICHARDSON, B. 2001. Fetal umbilical cord oxygen values and birth to placental weight ratio in relation to size at birth. *Am J Obstet Gynecol*, 185, 674-82.
- LANG, I., PABST, M. A., HIDEN, U., BLASCHITZ, A., DOHR, G., HAHN, T. & DESOYE, G. 2003. Heterogeneity of microvascular endothelial cells isolated from human term placenta and macrovascular umbilical vein endothelial cells. *Eur J Cell Biol*, 82, 163-73.
- LAUSMAN, A., KINGDOM, J. & MATERNAL FETAL MEDICINE, C. 2013. Intrauterine growth restriction: screening, diagnosis, and management. *J Obstet Gynaecol Can*, 35, 741-748.
- LEARMONT, J. G. & POSTON, L. 1996. Nitric oxide is involved in flow-induced dilation of isolated human small fetoplacental arteries. *Am J Obstet Gynecol*, 174, 583-8.
- LECARPENTIER, E., ATALLAH, A., GUIBOURDENCHE, J., HEBERT-SCHUSTER, M., VIEILLEFOSSE, S., CHISSEY, A., HADDAD, B., PIDOUX, G., EVAÏN-BRION, D., BARAKAT, A., FOURNIER, T. & TSATSARIS, V. 2016a. Fluid Shear Stress Promotes Placental Growth Factor Upregulation in Human Syncytiotrophoblast Through the cAMP-PKA Signaling Pathway. *Hypertension*, 68, 1438-1446.
- LECARPENTIER, E., BHATT, M., BERTIN, G. I., DELOISON, B., SALOMON, L. J., DELORON, P., FOURNIER, T., BARAKAT, A. I. & TSATSARIS, V. 2016b. Computational Fluid Dynamic Simulations of Maternal Circulation: Wall Shear Stress in the Human Placenta and Its Biological Implications. *PLoS One*, 11, e0147262.
- LERTKIATMONGKOL, P., LIAO, D., MEI, H., HU, Y. & NEWMAN, P. J. 2016. Endothelial functions of platelet/endothelial cell adhesion molecule-1 (CD31). *Curr Opin Hematol*, 23, 253-9.
- LI, C., REZANIA, S., KAMMERER, S., SOKOLOWSKI, A., DEVANEY, T., GORISCHEK, A., JAHN, S., HACKL, H., GROSCHNER, K., WINDPASSINGER, C., MALLE, E., BAUERNHOFER, T. & SCHREIBMAYER, W. 2015. Piezo1 forms mechanosensitive ion channels in the human MCF-7 breast cancer cell line. *Sci Rep*, 5, 8364.
- LI, J., HOU, B., TUMOVA, S., MURAKI, K., BRUNS, A., LUDLOW, M. J., SEDO, A., HYMAN, A. J., MCKEOWN, L., YOUNG, R. S., YULDASHEVA, N. Y., MAJEED, Y., WILSON, L. A., RODE, B., BAILEY, M. A., KIM, H. R., FU, Z., CARTER, D. A., BILTON, J., IMRIE, H., AJUH, P., DEAR, T. N., CUBBON, R. M., KEARNEY, M. T., PRASAD, R. K., EVANS, P. C., AINSCOUGH, J. F. & BEECH, D. J. 2014. Piezo1 integration of vascular architecture with physiological force. *Nature*, 515, 279-282.
- LI, L., KRANTZ, I. D., DENG, Y., GENIN, A., BANTA, A. B., COLLINS, C. C., QI, M., TRASK, B. J., KUO, W. L., COCHRAN, J., COSTA, T., PIERPONT, M. E., RAND, E. B., PICCOLI, D. A., HOOD, L. & SPINNER, N. B. 1997. Alagille syndrome is

- caused by mutations in human Jagged1, which encodes a ligand for Notch1. *Nat Genet*, 16, 243-51.
- LI, S., BUTLER, P., WANG, Y., HU, Y., HAN, D. C., USAMI, S., GUAN, J. L. & CHIEN, S. 2002. The role of the dynamics of focal adhesion kinase in the mechanotaxis of endothelial cells. *Proc Natl Acad Sci U S A*, 99, 3546-51.
- LIANG, J., HUANG, B., YUAN, G., CHEN, Y., LIANG, F., ZENG, H., ZHENG, S., CAO, L., GENG, D. & ZHOU, S. 2017. Stretch-activated channel Piezo1 is up-regulated in failure heart and cardiomyocyte stimulated by AngII. *Am J Transl Res*, 9, 2945-2955.
- LIMBOURG, A., PLOOM, M., ELLIGSEN, D., SORENSEN, I., ZIEGELHOEFFER, T., GOSSLER, A., DREXLER, H. & LIMBOURG, F. P. 2007. Notch ligand Delta-like 1 is essential for postnatal arteriogenesis. *Circ Res*, 100, 363-71.
- LIU, Z. & LI, Y. 2016. Cortical Cerebral Blood Flow, Oxygen Extraction Fraction, and Metabolic Rate in Patients with Middle Cerebral Artery Stenosis or Acute Stroke. *AJNR Am J Neuroradiol*, 37, 607-14.
- LOBOV, I. B., RENARD, R. A., PAPADOPOULOS, N., GALE, N. W., THURSTON, G., YANCOPOULOS, G. D. & WIEGAND, S. J. 2007. Delta-like ligand 4 (Dll4) is induced by VEGF as a negative regulator of angiogenic sprouting. *Proc Natl Acad Sci U S A*, 104, 3219-24.
- LOHMAN, A. W., BILLAUD, M. & ISAKSON, B. E. 2012. Mechanisms of ATP release and signalling in the blood vessel wall. *Cardiovasc Res*, 95, 269-80.
- LOPEZ-TELLO, J., ARIAS-ALVAREZ, M., JIMENEZ-MARTINEZ, M. A., BARBERO-FERNANDEZ, A., GARCIA-GARCIA, R. M., RODRIGUEZ, M., LORENZO, P. L., TORRES-ROVIRA, L., ASTIZ, S., GONZALEZ-BULNES, A. & REBOLLAR, P. G. 2017. The effects of sildenafil citrate on fetoplacental development and haemodynamics in a rabbit model of intrauterine growth restriction. *Reprod Fertil Dev*, 29, 1239-1248.
- LUKACS, V., MATHUR, J., MAO, R., BAYRAK-TOYDEMIR, P., PROCTER, M., CAHALAN, S. M., KIM, H. J., BANDELL, M., LONGO, N., DAY, R. W., STEVENSON, D. A., PATAPOUTIAN, A. & KROCK, B. L. 2015. Impaired PIEZO1 function in patients with a novel autosomal recessive congenital lymphatic dysplasia. *Nat Commun*, 6, 8329.
- MACK, J. J., MOSQUEIRO, T. S., ARCHER, B. J., JONES, W. M., SUNSHINE, H., FAAS, G. C., BRIOT, A., ARAGON, R. L., SU, T., ROMAY, M. C., MCDONALD, A. I., KUO, C. H., LIZAMA, C. O., LANE, T. F., ZOVEIN, A. C., FANG, Y., TARLING, E. J., DE AGUIAR VALLIM, T. Q., NAVAB, M., FOGELMAN, A. M., BOUCHARD, L. S. & IRUELA-ARISPE, M. L. 2017. NOTCH1 is a mechanosensor in adult arteries. *Nat Commun*, 8, 1620.
- MAHARAJ, C. H., O'TOOLE, D., LYNCH, T., CARNEY, J., JARMAN, J., HIGGINS, B. D., MORRISON, J. J. & LAFFEY, J. G. 2009. Effects and mechanisms of action of sildenafil citrate in human chorionic arteries. *Reprod Biol Endocrinol*, 7, 34.
- MALEK, A. M., ALPER, S. L. & IZUMO, S. 1999. Hemodynamic shear stress and its role in atherosclerosis. *JAMA*, 282, 2035-42.
- MALHOTRA, A., ALLISON, B. J., CASTILLO-MELENDZ, M., JENKIN, G., POLGLASE, G. R. & MILLER, S. L. 2019. Neonatal Morbidities of Fetal Growth Restriction: Pathophysiology and Impact. *Front Endocrinol (Lausanne)*, 10, 55.
- MANDO, C., RAZINI, P., NOVIELLI, C., ANELLI, G. M., BELICCHI, M., ERRATICO, S., BANFI, S., MEREGALLI, M., TAVELLI, A., BACCARIN, M., ROLFO, A., MOTTA, S., TORRENTE, Y. & CETIN, I. 2016. Impaired Angiogenic Potential of Human Placental Mesenchymal Stromal Cells in Intrauterine Growth Restriction. *Stem Cells Transl Med*, 5, 451-63.
- MARTIN-ALMEDINA, S., MANSOUR, S. & OSTERGAARD, P. 2018. Human phenotypes caused by PIEZO1 mutations; one gene, two overlapping phenotypes? *J Physiol*, 596, 985-992.
- MASTROMORO, G., GUADAGNOLO, D., GIANCOTTI, A., DI GREGORIO, M. G., MARCHIONNI, E., VENA, F., LEPRI, F. R., BARGIACCHI, L., VENTRIGLIA, F., DI GIOIA, C., NOVELLI, A. & PIZZUTI, A. 2020. Recurrent prenatal PIEZO1-

- RELATED lymphatic dysplasia: Expanding molecular and ultrasound findings. *Eur J Med Genet*, 104106.
- MASUMURA, T., YAMAMOTO, K., SHIMIZU, N., OBI, S. & ANDO, J. 2009. Shear stress increases expression of the arterial endothelial marker ephrinB2 in murine ES cells via the VEGF-Notch signaling pathways. *Arterioscler Thromb Vasc Biol*, 29, 2125-31.
- MELLER, M., VADACHKORIA, S., LUTHY, D. A. & WILLIAMS, M. A. 2005. Evaluation of housekeeping genes in placental comparative expression studies. *Placenta*, 26, 601-7.
- MIFSUD, W. & SEBIRE, N. J. 2014. Placental pathology in early-onset and late-onset fetal growth restriction. *Fetal Diagn Ther*, 36, 117-28.
- MIKHAILIK, A., MAZELLA, J., LIANG, S. & TSENG, L. 2009. Notch ligand-dependent gene expression in human endometrial stromal cells. *Biochem Biophys Res Commun*, 388, 479-82.
- MILLER, S. L., HUPPI, P. S. & MALLARD, C. 2016. The consequences of fetal growth restriction on brain structure and neurodevelopmental outcome. *J Physiol*, 594, 807-23.
- MILLS, T. A., WAREING, M., BUGG, G. J., GREENWOOD, S. L. & BAKER, P. N. 2005. Chorionic plate artery function and Doppler indices in normal pregnancy and intrauterine growth restriction. *Eur J Clin Invest*, 35, 758-64.
- MIRANDA, J., RODRIGUEZ-LOPEZ, M., TRIUNFO, S., SAIRANEN, M., KOURU, H., PARRA-SAAVEDRA, M., CROVETTO, F., FIGUERAS, F., CRISPI, F. & GRATACOS, E. 2017. Prediction of fetal growth restriction using estimated fetal weight vs a combined screening model in the third trimester. *Ultrasound Obstet Gynecol*, 50, 603-611.
- MIURA, S., SATO, K., KATO-NEGISHI, M., TESHIMA, T. & TAKEUCHI, S. 2015. Fluid shear triggers microvilli formation via mechanosensitive activation of TRPV6. *Nat Commun*, 6, 8871.
- MIYAZAKI, T. & MIYAZAKI, A. 2018. Dysregulation of Calpain Proteolytic Systems Underlies Degenerative Vascular Disorders. *J Atheroscler Thromb*, 25, 1-15.
- MONTEITH, C., FLOOD, K., PINNAMANENI, R., LEVINE, T. A., ALDERDICE, F. A., UNTERSCHIEDER, J., MCAULIFFE, F. M., DICKER, P., TULLY, E. C., MALONE, F. D. & FORAN, A. 2019. An abnormal cerebroplacental ratio (CPR) is predictive of early childhood delayed neurodevelopment in the setting of fetal growth restriction. *Am J Obstet Gynecol*, 221, 273 e1-273 e9.
- MORGAN, A. J. & JACOB, R. 1994. Ionomycin enhances Ca²⁺ influx by stimulating store-regulated cation entry and not by a direct action at the plasma membrane. *Biochem J*, 300 (Pt 3), 665-72.
- MORLEY, L. C., BEECH, D. J., WALKER, J. J. & SIMPSON, N. A. B. 2019. Emerging concepts of shear stress in placental development and function. *Mol Hum Reprod*, 25, 329-339.
- MORLEY, L. C., SHI, J., GAUNT, H. J., HYMAN, A. J., WEBSTER, P. J., WILLIAMS, C., FORBES, K., WALKER, J. J., SIMPSON, N. A. B. & BEECH, D. J. 2018. Piezo1 channels are mechanosensors in human fetoplacental endothelial cells. *Mol Hum Reprod*, 24, 510-520.
- MORLEY, L. T.-R., AW. 2012. Understanding How Plasmodium falciparum Binds to the Placenta and Produces Pathology Provides a Rationale for Pregnancy-Associated Malaria Vaccine Development. *The open vaccine journal*, 5, 8-27.
- MYATT, L. 2006. Placental adaptive responses and fetal programming. *J Physiol*, 572, 25-30.
- MYATT, L. & THORNBURG, K. L. 2018. Effects of Prenatal Nutrition and the Role of the Placenta in Health and Disease. *Methods Mol Biol*, 1735, 19-46.
- NAGANO, O., MURAKAMI, D., HARTMANN, D., DE STROOPER, B., SAFTIG, P., IWATSUBO, T., NAKAJIMA, M., SHINOHARA, M. & SAYA, H. 2004. Cell-matrix interaction via CD44 is independently regulated by different metalloproteinases activated in response to extracellular Ca(2+) influx and PKC activation. *J Cell Biol*, 165, 893-902.

- NELSON, S. H., STEINSLAND, O. S., WANG, Y., YALLAMPALLI, C., DONG, Y. L. & SANCHEZ, J. M. 2000. Increased nitric oxide synthase activity and expression in the human uterine artery during pregnancy. *Circ Res*, 87, 406-11.
- NICE 2019. Hypertension in pregnancy: diagnosis and management (NG133). NICE.
- OKA, C., NAKANO, T., WAKEHAM, A., DE LA POMPA, J. L., MORI, C., SAKAI, T., OKAZAKI, S., KAWAICHI, M., SHIOTA, K., MAK, T. W. & HONJO, T. 1995. Disruption of the mouse RBP-J kappa gene results in early embryonic death. *Development*, 121, 3291-301.
- ORMESHER, L., MYERS, J. E., CHMIEL, C., WAREING, M., GREENWOOD, S. L., TROPEA, T., LUNDBERG, J. O., WEITZBERG, E., NIHLEN, C., SIBLEY, C. P., JOHNSTONE, E. D. & COTTRELL, E. C. 2018. Effects of dietary nitrate supplementation, from beetroot juice, on blood pressure in hypertensive pregnant women: A randomised, double-blind, placebo-controlled feasibility trial. *Nitric Oxide*, 80, 37-44.
- OSOL, G. & MOORE, L. G. 2014. Maternal uterine vascular remodeling during pregnancy. *Microcirculation*, 21, 38-47.
- OYSTON, C., STANLEY, J. L., OLIVER, M. H., BLOOMFIELD, F. H. & BAKER, P. N. 2016. Maternal Administration of Sildenafil Citrate Alters Fetal and Placental Growth and Fetal-Placental Vascular Resistance in the Growth-Restricted Ovine Fetus. *Hypertension*, 68, 760-7.
- PAPAPETROPOULOS, A., GARCIA-CARDENA, G., MADRI, J. A. & SESSA, W. C. 1997. Nitric oxide production contributes to the angiogenic properties of vascular endothelial growth factor in human endothelial cells. *J Clin Invest*, 100, 3131-9.
- PARK, Y. G., CHOI, J., JUNG, H. K., SONG, I. K., SHIN, Y., PARK, S. Y. & SEOL, J. W. 2017. Fluid shear stress regulates vascular remodeling via VEGFR-3 activation, although independently of its ligand, VEGF-C, in the uterus during pregnancy. *Int J Mol Med*, 40, 1210-1216.
- PENTON, A. L., LEONARD, L. D. & SPINNER, N. B. 2012. Notch signaling in human development and disease. *Semin Cell Dev Biol*, 23, 450-7.
- PEREIRA, L., PETITT, M., FONG, A., TSUGE, M., TABATA, T., FANG-HOOVER, J., MAIDJI, E., ZYDEK, M., ZHOU, Y., INOUE, N., LOGHAVI, S., PEPKOWITZ, S., KAUVAR, L. M. & OGUNYEMI, D. 2014. Intrauterine growth restriction caused by underlying congenital cytomegalovirus infection. *J Infect Dis*, 209, 1573-84.
- QUINN, J. A., MUNOZ, F. M., GONIK, B., FRAU, L., CUTLAND, C., MALLETT-MOORE, T., KISSOU, A., WITTKE, F., DAS, M., NUNES, T., PYE, S., WATSON, W., RAMOS, A. A., CORDERO, J. F., HUANG, W. T., KOCHHAR, S., BUTTERY, J. & BRIGHTON COLLABORATION PRETERM BIRTH WORKING, G. 2016. Preterm birth: Case definition & guidelines for data collection, analysis, and presentation of immunisation safety data. *Vaccine*, 34, 6047-6056.
- RAMIREZ-VELEZ, R., BUSTAMANTE, J., CZERNICZYNIENEC, A., AGUILAR DE PLATA, A. C. & LORES-ARNAIZ, S. 2013. Effect of exercise training on eNOS expression, NO production and oxygen metabolism in human placenta. *PLoS One*, 8, e80225.
- RANADE, S. S., QIU, Z., WOO, S. H., HUR, S. S., MURTHY, S. E., CAHALAN, S. M., XU, J., MATHUR, J., BANDELL, M., COSTE, B., LI, Y. S., CHIEN, S. & PATAPOUTIAN, A. 2014. Piezo1, a mechanically activated ion channel, is required for vascular development in mice. *Proc Natl Acad Sci U S A*, 111, 10347-52.
- RCOG 2014. The Investigation and Management of the Small-for-Gestational-Age Fetus. London: Royal College of Obstetricians and Gynaecologists.
- REEVES, S. & BERNSTEIN, I. 2008. Effects of maternal tobacco-smoke exposure on fetal growth and neonatal size. *Expert Rev Obstet Gynecol*, 3, 719-730.
- ROBERTS, V. H., GREENWOOD, S. L., ELLIOTT, A. C., SIBLEY, C. P. & WATERS, L. H. 2006. Purinergic receptors in human placenta: evidence for functionally active P2X4, P2X7, P2Y2, and P2Y6. *Am J Physiol Regul Integr Comp Physiol*, 290, R1374-86.

- ROBERTS, V. H., WATERS, L. H. & POWELL, T. 2007. Purinergic receptor expression and activation in first trimester and term human placenta. *Placenta*, 28, 339-47.
- ROBERTS, V. H. J., MORGAN, T. K., BEDNAREK, P., MORITA, M., BURTON, G. J., LO, J. O. & FRIAS, A. E. 2017. Early first trimester uteroplacental flow and the progressive disintegration of spiral artery plugs: new insights from contrast-enhanced ultrasound and tissue histopathology. *Hum Reprod*, 32, 2382-2393.
- RODE, B., SHI, J., ENDESH, N., DRINKHILL, M. J., WEBSTER, P. J., LOTTEAU, S. J., BAILEY, M. A., YULDASHEVA, N. Y., LUDLOW, M. J., CUBBON, R. M., LI, J., FUTERS, T. S., MORLEY, L., GAUNT, H. J., MARSZALEK, K., VISWAMBHARAN, H., CUTHBERTSON, K., BAXTER, P. D., FOSTER, R., SUKUMAR, P., WEIGHTMAN, A., CALAGHAN, S. C., WHEATCROFT, S. B., KEARNEY, M. T. & BEECH, D. J. 2017. Piezo1 channels sense whole body physical activity to reset cardiovascular homeostasis and enhance performance. *Nat Commun*, 8, 350.
- RODRIGUES, C., JOY, L. R., SACHITHANANDAN, S. P. & KRISHNA, S. 2019. Notch signalling in cervical cancer. *Exp Cell Res*, 385, 111682.
- RODRIGUEZ, I. & GONZALEZ, M. 2014. Physiological mechanisms of vascular response induced by shear stress and effect of exercise in systemic and placental circulation. *Front Pharmacol*, 5, 209.
- ROMAC, J. M., SHAHID, R. A., SWAIN, S. M., VIGNA, S. R. & LIDDLE, R. A. 2018. Piezo1 is a mechanically activated ion channel and mediates pressure induced pancreatitis. *Nat Commun*, 9, 1715.
- ROSSI, A. C. & PREFUMO, F. 2019. Antepartum and intrapartum risk factors for neonatal hypoxic-ischemic encephalopathy: a systematic review with meta-analysis. *Curr Opin Obstet Gynecol*, 31, 410-417.
- ROTH, V. 2006. *Doubling Time Computing* [Online]. Available: Doubling Time Computing [Accessed 01.02.2017 2017].
- SAHIN, Z., ACAR, N., OZBEY, O., USTUNEL, I. & DEMIR, R. 2011. Distribution of Notch family proteins in intrauterine growth restriction and hypertension complicated human term placentas. *Acta Histochem*, 113, 270-6.
- SAK, M. E., DEVECI, E., TURGUT, A., SAK, S., EVSEN, M. S., GUL, T. & KALKANLI, S. 2013. Placental expression of vimentin, desmin and ultrastructural changes in the villi in patients with HELLP syndrome. *Eur Rev Med Pharmacol Sci*, 17, 874-8.
- SALVOLINI, E., VIGNINI, A., SABBATINELLI, J., LUCARINI, G., POMPEI, V., SARTINI, D., CESTER, A. M., CIAVATTINI, A., MAZZANTI, L. & EMANUELLI, M. 2019. Nitric oxide synthase and VEGF expression in full-term placentas of obese women. *Histochem Cell Biol*, 152, 415-422.
- SANDOVICI, I., HOELLE, K., ANGIOLINI, E. & CONSTANCIA, M. 2012. Placental adaptations to the maternal-fetal environment: implications for fetal growth and developmental programming. *Reprod Biomed Online*, 25, 68-89.
- SAOTOME, K., MURTHY, S. E., KEFAUVER, J. M., WHITWAM, T., PATAPOUTIAN, A. & WARD, A. B. 2018. Structure of the mechanically activated ion channel Piezo1. *Nature*, 554, 481-486.
- SCHNEIDER, C. A., RASBAND, W. S. & ELICEIRI, K. W. 2012. NIH Image to ImageJ: 25 years of image analysis. *Nat Methods*, 9, 671-5.
- SCHOOTS, M. H., GORDIJN, S. J., SCHERJON, S. A., VAN GOOR, H. & HILLEBRANDS, J. L. 2018. Oxidative stress in placental pathology. *Placenta*, 69, 153-161.
- SCIENTIFIC, T. 2009. NanoDrop 2000/2000c Spectrophotometer V1.0 User Manual Thermo Fisher Scientific.
- SEPULVEDA, W., BOWER, S., NICOLAIDIS, P., DE SWIET, M. & FISK, N. M. 1995. Discordant blood flow velocity waveforms in left and right brachial arteries in growth-retarded fetuses. *Obstet Gynecol*, 86, 734-8.

- SERVIN-VENCES, M. R., MORONI, M., LEWIN, G. R. & POOLE, K. 2017. Direct measurement of TRPV4 and PIEZO1 activity reveals multiple mechanotransduction pathways in chondrocytes. *Elife*, 6.
- SHAH, D. A. & KHALIL, R. A. 2015. Bioactive factors in uteroplacental and systemic circulation link placental ischemia to generalized vascular dysfunction in hypertensive pregnancy and preeclampsia. *Biochem Pharmacol*, 95, 211-26.
- SHARP, A., CORNFORTH, C., JACKSON, R., HARROLD, J., TURNER, M. A., KENNY, L. C., BAKER, P. N., JOHNSTONE, E. D., KHALIL, A., VON DADELSZEN, P., PAPAGEORGHIOU, A. T., ALFIREVIC, Z. & GROUP, S. 2018. Maternal sildenafil for severe fetal growth restriction (STRIDER): a multicentre, randomised, placebo-controlled, double-blind trial. *Lancet Child Adolesc Health*, 2, 93-102.
- SHEPHERD, A. I., COSTELLO, J. T., BAILEY, S. J., BISHOP, N., WADLEY, A. J., YOUNG-MIN, S., GILCHRIST, M., MAYES, H., WHITE, D., GORCZYNSKI, P., SAYNOR, Z. L., MASSEY, H. & EGLIN, C. M. 2019. "Beet" the cold: beetroot juice supplementation improves peripheral blood flow, endothelial function, and anti-inflammatory status in individuals with Raynaud's phenomenon. *J Appl Physiol (1985)*, 127, 1478-1490.
- SHIHATA, W. A., MICHELL, D. L., ANDREWS, K. L. & CHIN-DUSTING, J. P. 2016. Caveolae: A Role in Endothelial Inflammation and Mechanotransduction? *Front Physiol*, 7, 628.
- SILVA, G., BEIERWALTES, W. H. & GARVIN, J. L. 2006. Extracellular ATP stimulates NO production in rat thick ascending limb. *Hypertension*, 47, 563-7.
- SILVA, G. B. & GARVIN, J. L. 2009. Akt1 mediates purinergic-dependent NOS3 activation in thick ascending limbs. *Am J Physiol Renal Physiol*, 297, F646-52.
- SLATOR, P. J., HUTTER, J., MCCABE, L., GOMES, A. D. S., PRICE, A. N., PANAGIOTAKI, E., RUTHERFORD, M. A., HAJNAL, J. V. & ALEXANDER, D. C. 2018. Placenta microstructure and microcirculation imaging with diffusion MRI. *Magn Reson Med*, 80, 756-766.
- SLEGTENHORST, B. R., FAJARDO RAMIREZ, O. R., ZHANG, Y., DHANERAWALA, Z., TULLIUS, S. G. & GARCIA-CARDENA, G. 2018. A Mechano-Activated Cell Reporter System as a Proxy for Flow-Dependent Endothelial Atheroprotection. *SLAS Discov*, 23, 869-876.
- SPENCER, R., AMBLER, G., BRODSZKI, J., DIEMERT, A., FIGUERAS, F., GRATACOS, E., HANSSON, S. R., HECHER, K., HUERTAS-CEBALLOS, A., MARLOW, N., MARSAL, K., MORSING, E., PEEBLES, D., ROSSI, C., SEBIRE, N. J., TIMMS, J. F., DAVID, A. L. & CONSORTIUM, E. 2017. EVERREST prospective study: a 6-year prospective study to define the clinical and biological characteristics of pregnancies affected by severe early onset fetal growth restriction. *BMC Pregnancy Childbirth*, 17, 43.
- SPRAGUE, B., CHESLER, N. C. & MAGNESS, R. R. 2010. Shear stress regulation of nitric oxide production in uterine and placental artery endothelial cells: experimental studies and hemodynamic models of shear stresses on endothelial cells. *Int J Dev Biol*, 54, 331-9.
- STAMPALIJA, T., THORNTON, J., MARLOW, N., NAPOLITANO, R., BHIDE, A., PICKLES, T., BILARDO, C. M., GORDIJN, S. J., GYSELAERS, W., VALENSISE, H., HECHER, K., SANDE, R. K., LINDGREN, P., BERGMAN, E., ARABIN, B., BREEZE, A. C., WEE, L., GANZEVOORT, W., RICHTER, J., BERGER, A., BRODSZKI, J., DERKS, J., MECACCI, F., MARUOTTI, G. M., MYKLESTAD, K., LOBMAIER, S. M., PREFUMO, F., KLARITSCH, P., CALDA, P., EBBING, C., FRUSCA, T., RAIIO, L., VISSER, G. H. A., KROFTA, L., CETIN, I., FERRAZZI, E., CESARI, E., WOLF, H., LEES, C. C. & GROUP, T.-. 2020. Fetal cerebral Doppler changes and outcome in late preterm fetal growth restriction: prospective cohort study. *Ultrasound Obstet Gynecol*, 56, 173-181.
- STANLEY, J. L., ANDERSSON, I. J., POUDEL, R., RUEDA-CLAUSEN, C. F., SIBLEY, C. P., DAVIDGE, S. T. & BAKER, P. N. 2012. Sildenafil citrate rescues fetal

- growth in the catechol-O-methyl transferase knockout mouse model. *Hypertension*, 59, 1021-8.
- STORCH, U., MEDEROS Y SCHNITZLER, M. & GUDERMANN, T. 2012. G protein-mediated stretch reception. *Am J Physiol Heart Circ Physiol*, 302, H1241-9.
- SU, E. J. 2015. Role of the fetoplacental endothelium in fetal growth restriction with abnormal umbilical artery Doppler velocimetry. *Am J Obstet Gynecol*, 213, S123-30.
- SYEDA, R., XU, J., DUBIN, A. E., COSTE, B., MATHUR, J., HUYNH, T., MATZEN, J., LAO, J., TULLY, D. C., ENGELS, I. H., PETRASSI, H. M., SCHUMACHER, A. M., MONTAL, M., BANDELL, M. & PATAPOUTIAN, A. 2015. Chemical activation of the mechanotransduction channel Piezo1. *Elife*, 4.
- TABERNER, F. J., PRATO, V., SCHAEFER, I., SCHRENK-SIEMENS, K., HEPPESTALL, P. A. & LECHNER, S. G. 2019. Structure-guided examination of the mechanogating mechanism of PIEZO2. *Proc Natl Acad Sci U S A*, 116, 14260-14269.
- TAKEBE, N., NGUYEN, D. & YANG, S. X. 2014. Targeting notch signaling pathway in cancer: clinical development advances and challenges. *Pharmacol Ther*, 141, 140-9.
- TAKII, M., ISHIKAWA, T., TSUDA, H., KANATANI, K., SUNOUCHI, T., KANEKO, Y. & NAKAYAMA, K. 2006. Involvement of stretch-activated cation channels in hypotonically induced insulin secretion in rat pancreatic beta-cells. *Am J Physiol Cell Physiol*, 291, C1405-11.
- TAN, C. M. J. & LEWANDOWSKI, A. J. 2020. The Transitional Heart: From Early Embryonic and Fetal Development to Neonatal Life. *Fetal Diagn Ther*, 47, 373-386.
- THOMPSON, J. M., IRGENS, L. M., SKJAERVEN, R. & RASMUSSEN, S. 2007. Placenta weight percentile curves for singleton deliveries. *BJOG*, 114, 715-20.
- TORRISI, J. S., HESPE, G. E., CUZZONE, D. A., SAVETSKY, I. L., NITTI, M. D., GARDENIER, J. C., GARCIA NORES, G. D., JOWHAR, D., KATARU, R. P. & MEHRARA, B. J. 2016. Inhibition of Inflammation and iNOS Improves Lymphatic Function in Obesity. *Sci Rep*, 6, 19817.
- TRAN, N. T., AMARGER, V., BOURDON, A., MISBERT, E., GRIT, I., WINER, N. & DARMAUN, D. 2017. Maternal citrulline supplementation enhances placental function and fetal growth in a rat model of IUGR: involvement of insulin-like growth factor 2 and angiogenic factors. *J Matern Fetal Neonatal Med*, 30, 1906-1911.
- TROJA, W., KIL, K., KLANKE, C. & JONES, H. N. 2014. Interaction between human placental microvascular endothelial cells and a model of human trophoblasts: effects on growth cycle and angiogenic profile. *Physiol Rep*, 2, e00244.
- TROPEA, T., WAREING, M., GREENWOOD, S. L., FEELISCH, M., SIBLEY, C. P. & COTTRELL, E. C. 2018. Nitrite mediated vasorelaxation in human chorionic plate vessels is enhanced by hypoxia and dependent on the NO-sGC-cGMP pathway. *Nitric Oxide*, 80, 82-88.
- TUN, W. M., YAP, C. H., SAW, S. N., JAMES, J. L. & CLARK, A. R. 2019. Differences in placental capillary shear stress in fetal growth restriction may affect endothelial cell function and vascular network formation. *Sci Rep*, 9, 9876.
- TZIMA, E., IRANI-TEHRANI, M., KIOSSES, W. B., DEJANA, E., SCHULTZ, D. A., ENGELHARDT, B., CAO, G., DELISSER, H. & SCHWARTZ, M. A. 2005. A mechanosensory complex that mediates the endothelial cell response to fluid shear stress. *Nature*, 437, 426-31.
- UKGOV. 2011. *List of ethnic groups* [Online]. Available: <https://www.ethnicity-facts-figures.service.gov.uk/style-guide/ethnic-groups> [Accessed].
- ULRICH-MERZENICH, G., METZNER, C., BHONDE, R. R., MALSCH, G., SCHIERMEYER, B. & VETTER, H. 2002. Simultaneous isolation of endothelial and smooth muscle cells from human umbilical artery or vein and their growth response to low-density lipoproteins. *In Vitro Cell Dev Biol Anim*, 38, 265-72.

- VALDECANTOS, P., BRIONES, R., MOYA, P., GERMAIN, A. & HUIDOBRO-TORO, J. P. 2003. Pharmacological identification of P2X1, P2X4 and P2X7 nucleotide receptors in the smooth muscles of human umbilical cord and chorionic blood vessels. *Placenta*, 24, 17-26.
- VALENSISE, H., VASAPOLLO, B., NOVELLI, G. P., GIORGI, G., VERALLO, P., GALANTE, A. & ARDUINI, D. 2008. Maternal and fetal hemodynamic effects induced by nitric oxide donors and plasma volume expansion in pregnancies with gestational hypertension complicated by intrauterine growth restriction with absent end-diastolic flow in the umbilical artery. *Ultrasound Obstet Gynecol*, 31, 55-64.
- VAN BEIJNUM, J. R., ROUSCH, M., CASTERMANS, K., VAN DER LINDEN, E. & GRIFFIOEN, A. W. 2008. Isolation of endothelial cells from fresh tissues. *Nat Protoc*, 3, 1085-91.
- VAN SINDEREN, M., CUMAN, C., GAMAGE, T., RAINCZUK, K., OSIANLIS, T., ROMBAUTS, L. & DIMITRIADIS, E. 2014. Localisation of the Notch family in the human endometrium of fertile and infertile women. *J Mol Histol*, 45, 697-706.
- VANDESOMPELE, J., DE PRETER, K., PATTYN, F., POPPE, B., VAN ROY, N., DE PAEPE, A. & SPELEMAN, F. 2002. Accurate normalization of real-time quantitative RT-PCR data by geometric averaging of multiple internal control genes. *Genome Biol*, 3, RESEARCH0034.
- VEERBEEK, J. H., TISSOT VAN PATOT, M. C., BURTON, G. J. & YUNG, H. W. 2015. Endoplasmic reticulum stress is induced in the human placenta during labour. *Placenta*, 36, 88-92.
- VILLAR, J., PAPAGEORGHIOU, A. T., PANG, R., OHUMA, E. O., CHEIKH ISMAIL, L., BARROS, F. C., LAMBERT, A., CARVALHO, M., JAFFER, Y. A., BERTINO, E., GRAVETT, M. G., ALTMAN, D. G., PURWAR, M., FREDERICK, I. O., NOBLE, J. A., VICTORA, C. G., BHUTTA, Z. A., KENNEDY, S. H., INTERNATIONAL, F. & NEWBORN GROWTH CONSORTIUM FOR THE 21ST, C. 2014. The likeness of fetal growth and newborn size across non-isolated populations in the INTERGROWTH-21st Project: the Fetal Growth Longitudinal Study and Newborn Cross-Sectional Study. *Lancet Diabetes Endocrinol*, 2, 781-92.
- VO, T. M., JAIN, S., BURCHETT, R., MONCKTON, E. A. & GODBOUT, R. 2019. A positive feedback loop involving nuclear factor IB and calpain 1 suppresses glioblastoma cell migration. *J Biol Chem*, 294, 12638-12654.
- VUGUIN, P. M. 2007. Animal models for small for gestational age and fetal programming of adult disease. *Horm Res*, 68, 113-23.
- WANG, S., CHENNUPATI, R., KAUR, H., IRING, A., WETTSCHURECK, N. & OFFERMANN, S. 2016. Endothelial cation channel PIEZO1 controls blood pressure by mediating flow-induced ATP release. *J Clin Invest*, 126, 4527-4536.
- WANG, S., IRING, A., STRILIC, B., ALBARRAN JUAREZ, J., KAUR, H., TROIDL, K., TONACK, S., BURBIEL, J. C., MULLER, C. E., FLEMING, I., LUNDBERG, J. O., WETTSCHURECK, N. & OFFERMANN, S. 2015. P2Y(2) and Gq/G(1)(1) control blood pressure by mediating endothelial mechanotransduction. *J Clin Invest*, 125, 3077-86.
- WANG, Y., CHI, S., GUO, H., LI, G., WANG, L., ZHAO, Q., RAO, Y., ZU, L., HE, W. & XIAO, B. 2018. A lever-like transduction pathway for long-distance chemical- and mechano-gating of the mechanosensitive Piezo1 channel. *Nat Commun*, 9, 1300.
- WANG, Y. & ZHAO, S. 2010. *Vascular Biology of the Placenta*. San Rafael (CA).
- WAREING, M. 2012. Effects of oxygenation and luminal flow on human placenta chorionic plate blood vessel function. *J Obstet Gynaecol Res*, 38, 185-91.
- WAREING, M. 2014. Oxygen sensitivity, potassium channels, and regulation of placental vascular tone. *Microcirculation*, 21, 58-66.
- WAREING, M., BAI, X., SEGHER, F., TURNER, C. M., GREENWOOD, S. L., BAKER, P. N., TAGGART, M. J. & FYFE, G. K. 2006a. Expression and function of potassium channels in the human placental vasculature. *Am J Physiol Regul Integr Comp Physiol*, 291, R437-46.

- WAREING, M., GREENWOOD, S. L., FYFE, G. K. & BAKER, P. N. 2006b. Reactivity of human placental chorionic plate vessels from pregnancies complicated by intrauterine growth restriction (IUGR). *Biol Reprod*, 75, 518-23.
- WIECZOREK, K. M., BREWER, A. S. & MYATT, L. 1995. Shear stress may stimulate release and action of nitric oxide in the human fetal-placental vasculature. *Am J Obstet Gynecol*, 173, 708-13.
- WILEY, S. Z., SRIRAM, K., SALMERON, C. & INSEL, P. A. 2019. GPR68: An Emerging Drug Target in Cancer. *Int J Mol Sci*, 20.
- WINER, N., BRANGER, B., AZRIA, E., TSATSARIS, V., PHILIPPE, H. J., ROZE, J. C., DESCAMPS, P., BOOG, G., CYNOBER, L. & DARMAUN, D. 2009. L-Arginine treatment for severe vascular fetal intrauterine growth restriction: a randomized double-blind controlled trial. *Clin Nutr*, 28, 243-8.
- WOLF, K., HU, H., ISAJI, T. & DARDIK, A. 2019. Molecular identity of arteries, veins, and lymphatics. *J Vasc Surg*, 69, 253-262.
- XIAO, X., TANG, Y., WOOFF, Y., SU, C., KANG, M., O'CARROLL, S. J., CHEN, Q. & CHAMLEY, L. 2020. Upregulation of pannexin-1 hemichannels explains the apparent death of the syncytiotrophoblast during human placental explant culture. *Placenta*, 94, 1-12.
- XIE, Y., WANG, F., PUSCHECK, E. E. & RAPPOLEE, D. A. 2007. Pipetting causes shear stress and elevation of phosphorylated stress-activated protein kinase/jun kinase in preimplantation embryos. *Mol Reprod Dev*, 74, 1287-94.
- XIE, Y., WANG, F., ZHONG, W., PUSCHECK, E., SHEN, H. & RAPPOLEE, D. A. 2006. Shear stress induces preimplantation embryo death that is delayed by the zona pellucida and associated with stress-activated protein kinase-mediated apoptosis. *Biol Reprod*, 75, 45-55.
- XU, J., MATHUR, J., VESSIERES, E., HAMMACK, S., NONOMURA, K., FAVRE, J., GRIMAUD, L., PETRUS, M., FRANCISCO, A., LI, J., LEE, V., XIANG, F. L., MAINQUIST, J. K., CAHALAN, S. M., ORTH, A. P., WALKER, J. R., MA, S., LUKACS, V., BORDONE, L., BANDELL, M., LAFFITTE, B., XU, Y., CHIEN, S., HENRION, D. & PATAPOUTIAN, A. 2018. GPR68 Senses Flow and Is Essential for Vascular Physiology. *Cell*, 173, 762-775 e16.
- XU, S. 2020. Therapeutic potential of blood flow mimetic compounds in preventing endothelial dysfunction and atherosclerosis. *Pharmacol Res*, 155, 104737.
- XU, S., LIU, B., YIN, M., KOROLEVA, M., MASTRANGELO, M., TURE, S., MORRELL, C. N., ZHANG, D. X., FISHER, E. A. & JIN, Z. G. 2016. A novel TRPV4-specific agonist inhibits monocyte adhesion and atherosclerosis. *Oncotarget*, 7, 37622-37635.
- XUE, Y., GAO, X., LINDSELL, C. E., NORTON, C. R., CHANG, B., HICKS, C., GENDRON-MAGUIRE, M., RAND, E. B., WEINMASTER, G. & GRIDLEY, T. 1999. Embryonic lethality and vascular defects in mice lacking the Notch ligand Jagged1. *Hum Mol Genet*, 8, 723-30.
- YE, J., COULOURIS, G., ZARETSKAYA, I., CUTCUTACHE, I., ROZEN, S. & MADDEN, T. L. 2012. Primer-BLAST: a tool to design target-specific primers for polymerase chain reaction. *BMC Bioinformatics*, 13, 134.
- ZARYCHANSKI, R., SCHULZ, V. P., HOUSTON, B. L., MAKSIMOVA, Y., HOUSTON, D. S., SMITH, B., RINEHART, J. & GALLAGHER, P. G. 2012. Mutations in the mechanotransduction protein PIEZO1 are associated with hereditary xerocytosis. *Blood*, 120, 1908-15.
- ZEITLIN, J., ANCEL, P. Y., SAUREL-CUBIZOLLES, M. J. & PAPIERNIK, E. 2000. The relationship between intrauterine growth restriction and preterm delivery: an empirical approach using data from a European case-control study. *BJOG*, 107, 750-8.
- ZHANG, J., ZHOU, Y., HUANG, T., WU, F., LIU, L., KWAN, J. S. H., CHENG, A. S. L., YU, J., TO, K. F. & KANG, W. 2018. PIEZO1 functions as a potential oncogene by promoting cell proliferation and migration in gastric carcinogenesis. *Mol Carcinog*, 57, 1144-1155.

- ZHANG, L., LIU, X., GAO, L., JI, Y., WANG, L., ZHANG, C., DAI, L., LIU, J. & JI, Z. 2020. Activation of Piezo1 by ultrasonic stimulation and its effect on the permeability of human umbilical vein endothelial cells. *Biomed Pharmacother*, 131, 110796.
- ZHAO, Q., ZHOU, H., CHI, S., WANG, Y., WANG, J., GENG, J., WU, K., LIU, W., ZHANG, T., DONG, M. Q., WANG, J., LI, X. & XIAO, B. 2018. Structure and mechanogating mechanism of the Piezo1 channel. *Nature*, 554, 487-492.
- ZHAO, Q., ZHOU, H., LI, X. & XIAO, B. 2019. The mechanosensitive Piezo1 channel: a three-bladed propeller-like structure and a lever-like mechanogating mechanism. *FEBS J*, 286, 2461-2470.
- ZHAO, W. X., HUANG, T. T., JIANG, M., FENG, R. & LIN, J. H. 2014. Expression of notch family proteins in placentas from patients with early-onset severe preeclampsia. *Reprod Sci*, 21, 716-23.
- ZHENG, W., NIKOLAEV, Y. A., GRACHEVA, E. O. & BAGRIANTSEV, S. N. 2019. Piezo2 integrates mechanical and thermal cues in vertebrate mechanoreceptors. *Proc Natl Acad Sci U S A*, 116, 17547-17555.

Appendix 1: Data collection proforma

Patient ID:

Sample ID:

Date:

Maternal age	
BMI at booking (height & weight)	
Smoking status	Non smoker Stopped in pregnancy Smoked during pregnancy
Ethnicity	
Hb at booking	
Health issues / medication	
Gravidity / parity	
Mode of delivery	
Gestation at delivery	
Baby weight	
Baby sex	
Placenta weight (trimmed)	
Placenta appearance	
Tissue sample weight	
Latest US scan	SGA AGA

Doppler	S/D ratio Evidence of reversal of flow
Diagnosis	AGA Severe early onset PET Late onset PET Hypertensive SGA Idiopathic SGA
Tissue used for:	Snap freezing FpEC isolation HUVEC isolation Myography SJUH group Forbes group Other:

Appendix 2: Sample databases

ID	Cons.	Grp	Age	BMI	Sm.	Ethnicity	P & G	MOD	Gest	Sex	Birth wt	Centile
LM1	LM	AGA						EI LSCS	39			
LM2	LM	AGA						EI LSCS	39			
LM3	LM	SGA						Em LSCS	39			
LM4	LM	AGA	22		NS	white	1+2	EI LSCS	39+0	F	4050	99
LM5	LM	SGA	26		NS	Asian	1+2	Em LSCS	37+0	F	1850	<0.4
LM6	LM	AGA						Em LSCS	39			
LM7	LM	AGA	29	36.7	NS	white	1+2	EI LSCS	39	F	3615	68
LM8	LM	AGA	37	24.7	NS	white	1+2	EI LSCS	39	F	3590	66
LM9	LM	AGA	31		NS	Asian	1+2	EI LSCS	39	F	3870	85
LM10	LM	AGA			NS			EI LSCS	39			

Table 18 Mother and baby details for samples collected for pilot study (2016)

ID	Cons.	Grp	Age	BMI	Sm	Ethnicity	Med hx	Meds	Obs hx	P + G	Doppler	MOD	Gest	Sex	Birth wt	Centile	PI wt
10	LM	AGA		25	NS	Asian	β thal trait	ferrous	1x LSCS	1+2	NA	EI LSCS		F		95	
11	LM	AGA		26	NS	White	IVF		NA	0+1	NA	EI LSCS (praevia)	39+1	F		75	
12	LM	SGA		34		White	anaemia	ferrous	1x LSCS, SVD	1+2		EI LSCS	37+5	M	2670	2	311
13	LM	SGA	26		NS	Asian	NAD			0+1	abn	EI LSCS	30+0	M	910	2	550
14	LM	AGA		20	NS	White	NAD		1x LSCS (twins)	1+2	NA	EI LSCS	39+5	F	3630	69	750
15	LM	SGA	39	26	NS	White	NAD		NA	0+1	NAD	Em LSCS (IOL)	38+3	M	2750	4	320
16	LM	SGA	38	23	NS	White	NAD		praevia, APH	0+1		Em LSCS	34+2	F	1700	9	550
17	LM	SGA	42	26	NS	White	NAD		praevia, IVF	2+3	NAD	EI LSCS	38+5	F	2370	<0.4	670
18	LM	SGA		26	NS	White	NAD		1x LSCS	1+2	NAD	EI LSCS	35+6	M	2300	18	680
19	LM	AGA	41	24	NS	White	NAD		1x LSCS	1+2	NA	EI LSCS	39+5	F	3560	63	

36	LM	AGA	31	38	NS	White	NAD		1x LSCS	1+2	NA	EI LSCS (twins)	37+2	M/F	2900 / 3300	NAD	
37	LM	AGA	27	25	NS	White	NAD		1x LSCS	1+2	NA	EI LSCS (breech)	38+3	F	3335	43	960
38	LM	AGA	32	21	NS	White	NAD		1x LSCS	1+2	NA	EI LSCS	39+1	F	3300	40	880
39	LM	AGA	25	22.5	NS	Asian	NAD		1x LSCS	1+2	NA	EI LSCS	41+1	F	4850	99	900
40	LM	SGA + PET	39	39	NS	Black	PET	labetal ol	2x LSCS	3+4	NAD	EI LSCS	37+0	F	2750	5	
41	LM	AGA	32	23.8	NS	White	NAD		3rd tear	1+2	NA	EI LSCS	39+5	F	3275	37	750
42	LM	AGA	35	22.5	NS	White	asthma	salbuta mol	2x LSCS	2+3	NA	EI LSCS	39+2	F	3800	NAD	800

Table 19 Mother and baby details for samples collected in 2017 (ethics: 13/YH/03/44)

ID	Cons	Grp	Age	BMI	Sm.	Ethnicity	Med hx	Meds	Obs hx	*P + G	Dopp	MOD	Gest	Sex	Birth wt	Centile	Pl wt
LGI001	LM	AGA	36	27	NS	White	NAD	none	x1 LSCS	1+2	NA	EI LSCS	39+3	F			
LGI002	LM	AGA	40	27	NS	White	hypothyroid	levothyroxine	x1 LSCS	1+2	NA	EI LSCS	39+0	M	3560	50	750

LGI015	LM	discarded															
LGI016	LM	SGA	29	27.6	NS	White	low PAPP-A	aspirin	NA	0+1	NAD	Em LSCS (distress)	37+4	M	2340	<0.4	515
*LGI017	LM																
LGI018	LM	Not AGA	29	19	Sm	White	NAD	NA	x1 Em LSCS	1+2	NA	EI LSCS	39+5	F	2685	4	640
LGI019	LM	not AGA	32	NAD	NS	White	HTN	labetalol	NA	0+1	NA	Em LSCS (IOL, distress)	40+5	F	3160	27	600
LGI020	LM	AGA	30	NAD	NS	White	NAD	none	3rd tear	1+2	NAD	EI LSCS	39+5	F	3260	36	420
LGI021	LM	AGA	39	27	NS	White	IVF	none	x1 LSCS	0+1	NA	Em LSCS (failed IOL)	40+5	M	2995	11	500
LGI022	LM	AGA	25	26	NS	White	NAD	none	x1 LSCS	0+1	NA	EI LSCS	39+0	M	3600	54	760
LGI023	LM	AGA	30	33	NS	White	NAD	none	SVDs	2+3	NA	SVD (spont labour)	39+4	F	3250	35	800
LGI024	LM	AGA	28	25	NS	White	NAD	none	previous FGR	1+2	NA	SVD (spont labour)	39+4	F	3415	50	705

LGI025	LM	AGA	36	31	NS	White	hypothyroid	levothyroxine	2x LSCS	2+3	NA	EI LSCS	39+0	M	3360	33	565
LGI026	LM	SGA	30	18	Sm	White	NAD	none	3x LSCS	3+4	NAD	EI LSCS	39+0	M	2960	9	700
LGI027	LM	SGA	28	17	Sm	White	NAD	none	SVD	1+2	abn	SVD (IOL for FGR)	38+3	F	2275	1.4	690
LGI028	LM	GDM + HTN	37	30	NS	White	HTN	metformin, labetalol	1x LSCS	1+2	NAD	EI LSCS	39+0	M	3475	50	745
LGI029	LM	GDM	29	25.4	NS	Asian	GDM	Metformin	NA	0+2	NAD	Em LSCS (cat 2)	39+0	F	3135	25	
LGI030	SI	SGA	28	23.98	NS	White	NAD	none	NA	0+1	NAD	SVD	40+0	F	2680	3	362
LGI031	LM MK KW	AGA	29	24.6	NS	Black	NAD	none	x1 LSCS	1+2	NA	EI ESCS	39+5	F	2895	11	760
LGI032	LM	AGA		NAD	NS	Black	NAD	none	x1 Em LSCS	1+2	NA	Em LSCS (7cm)	39+0	F			433(T)
LGI033	SI	SGA	18	NAD	Sm	White	asthma	salbutamol	NA	0+1	NAD	SVD (spont labour)	39+0	F	2500	1.2	391(T)

LGI034	LM MK KW	GDM	32	22.6	NS	White	GDM, IVF	metformin	NA	0+1	>90th	EI LSCS (EFW >90th)	39+1	M	3540	49	560(T)
LGI035	LM MK KW	AGA	37	28	NS	other	NAD	none	x5 LSCS	5+6	NA	EI LSCS	39+3	M	3295	28	401(T)
LGI036	SI	AGA	39	25.2	NS	White	Fabrys	none	x1 Em LSCS	1+1	NA	EI LSCS	39+3	M	4640	99	804(T)
LGI037	SI	AGA	23	26.5	NS	White	neuroge nic bladder	none	NA	0+1	NA	EI LSCS	38+0	F	3315	41	483(T)
LGI038	SI	SGA	19	18	Sm	White	NAD	none	NA	0+1	NAD	SVD	37+3	F	2300	<0.4	444(T)
LGI039	SI	AGA	32	25.5	NS	Black	NAD	none	x1 Em LSCS	1+2	normal	EI LSCS	39+0	M	3405	37	586(T)
LGI040	LM	SGA	18	NAD	NS	White	PET	nifedipin e, labetalol , MgSO ⁴		0+2	absent EDF	Em LSCS (cat 3 FTP)	26+2	F	500	1	103(T)
LGI041	SI	AGA	30	28	NS	White	NAD	none	NA	0+1	normal	EI LSCS	40+10	F	4100	94	478(T)
LGI042	KW	SGA	20	23	Sm	White	NAD	none	SVDs	2+3	NA	SVD	39+1	F	2900	9	375(T)
LGI043	KW	AGA	36	24.4	NS	White	NAD	none	SVDs	0+1	NAD		37+0	M	3280	27	398(T)

LGI044	MK	GDM	35	38	NS	Black	NIDDM	metformin		1+2	NAD		36+0	F	3390	97	477 (T)
LGI045	SI	AGA	41	24	NS	White	NAD	none	unknown	2+3	NAD	EI LSCS	39+5	M	3860	75	509(T)
LGI046	MK	AGA	36	34.2 6	NS	White	asthma	none	unknown	2+3	NAD	EI LSCS	39+4	F	3430	52	380(T)
LGI047	SI	AGA	23	19.5	NS	White	anxiety	none	GBS	1+2	NAD	EI LSCS	39+4	M	3340	32	434(T)
LGI048	KW	AGA	33	21.5	NS	White	NAD	none		1+2	NAD	mat request	38+6	F	3090	22	454(T)
LGI049	SI	GDM	37	52	Sm	White	IDDM, sleep apnoea	insulin, metformin		1+2	NAD		39+0	M	3680	62	400(T)
LGI050	MK	SGA	27	32	NS	White	low PAPP-A, depression	aspirin, sertraline	SVD	1+2	NAD	SVD (IOL for FGR)	37+5	F	2360	2.2	280(T)
LGI051	NS	SGA	30	27	NS	other	NAD	none	prev FGR, LSCS	1+2	NAD	previous LSCS	37+3	F	2590	2.1	242(T)
LGI052	KW	SGA	36	19	NS	White	NAD	none		?	NA		37+6	F	2835	8	407(T)
LGI053	KW	AGA	27	27.7	NS	White	NAD	none		?							

LGI054	SI	discarded															
LGI055	SI	SGA	23	27.8	Sm	White	NAD	none	prev FGR	1+2	NAD	SVD (IOL for FGR)	37+2	F	2405	1	217(T)
LGI056	SI	discarded			Sm												
LGI057	KW	discarded		48													
LGI058	SI	SGA	40		NS	White	HTN	labetalol	x1 LSCS	2+3		EI LSCS	37+4		2255	<0.4	220(T)
LGI059	SI	GDM	32	35.38	NS	Black	NIDDM, hypothyroid	thyroxine, metformin		3+4	NAD	EI LSCS	38+1	F	3865	85	520(T)
LGI060	SI	AGA	28	23.52	NS	White	none	none	x1 LSCS	1+2	NA	EI LSCS	39+0	M	3335	31	485(T)
LGI061	SI	GDM	22	32.7	NS	White	IDDM	metformin, insulin	NA	0+1		SVD (IOL)	39+1	M	3935	80	502(T)
LGI062	SI	discarded															
LGI063	SI	SGA	34	NAD	NS	White	tetralogy of fallot	MgSO ⁴ , warfarin, bisoprol	prev FGR	1+2	absent EDF	Prem FGR	28+2	M	850	5	100(T)

								ol, diazepa m									
LGI064	SI	GDM	35	33	NS	Asian	IDDM	insulin, metformi n		1+2	NAD	EI LSCS	38+2	M	3595	54	462(T)
LGI065	SI	AGA	31	30	NS	White	NAD	none		1+2	NA	EI LSCS	40+0	M	3845	74	567(T)
LGI066	MK	AGA	35	22.4 5	NS	White	NAD	none		1+1	NA		39+4	M	3478	43	422(T)
LGI067	SI	SGA	19	20	NS	White	anxiety, depressi on	none		0+1	NAD	SVD (IOL FGR)	38+3		2665	5	332(T)
LGI068	KW	not AGA															
LGI069	KW	AGA	40	25	NS	White	NAD	none		1+2		EL LSCS	39+0	F	3475		
LGI070	MK	disca r d															
LGI071	MK	AGA	23	28.2	NS	White	NAD	none	normal	2+3	normal	EI LSCS	39+1	M	3540	49	499(T)
LGI072	SI	GDM	42	31	NS	Black	NIDDM	metformi n		3+4	NAD	EI LSCS	38	M	3700		473(T)

LGI073	SI	fetal distres s															
LGI074	KW, KT	disca r d															
LGI075	SI	SGA	25	30.4 1	Sm	White	NAD	none		1+2		SVD	37+5	M	2585	6	341(T)
LGI076	MK	LGA	30	19.5 2	NS	White	epilepsy		NA	0+1	>95th	EI LSCS	39+0	M	4340	95	533(T)
LGI077	MK	LGA	28	27		White	none	none		1+1	>95th	EI LSCS	39+0	M	3830	73	674(T)
LGI078	KW	disca r d															
LGI079	SI	AGA	35	NAD	NS	Asian	asthma	salbuta mol		3+4		EI LSCS	39+0	M	3735	65	
LGI080	MK	AGA	40	26	NS	White	NAD	none		1+2		EI LSCS	38+3	M	3110	16	356(T)
LGI081	KW	AGA	28	27.5	NS	White	NAD	none	NND	0+2	NAD	EI LSCS (mat choice)	38+0	M	3680	61	493(T)
LGI082	KT	AGA	28	NAD	NS	White	NAD	none		5+6		EI LSCS	39+0	M	3185	21	464(T)
LGI083	KW	AGA	30	26	NS	Asian	NAD	none		1+3	NA	EI LSCS	39+4	M	3455	41	507(T)

LGI084	MK	not AGA	34	NAD	NS	White	NAD	none	NA	0+1	NA	EI LSCS	37+0	F	2390	10	381(T)
LGI085	KT	AGA	30	23.6 6	NS	White	NAD	none		1+2		EI LSCS	38+6	M	3310	29	463(T)
LGI086	KW	AGA	34	23	NS	White	NAD	none		1+2	NA	EI LSCS	39+0	M	3445	40	486(T)
LGI087	KW	AGA	37	29	NS	Asian	NAD	none		3+4	NA	EI LSCS	39+0	M	3820	72	586(T)
LGI088	KW	AGA	40	25		White	NAD	none		1+2	NA	EI LSCS	39+0	M	3620	56	482(T)
LGI089	KW	SGA	35	31	Sm	White	NAD	none		1+3	NAD	EI LSCS	39+0	M	2955	9	490(T)
LGI090	KW	SGA	32	26.5	Sm	White	NAD	none		1+2	NAD	EI LSCS	39+3	F	2740	5	506(T)
LGI091	KW	AGA	32	28	Sm	White	NAD	none		4+5	NAD	EI LSCS	39+0	F	2940	13	474(T)
LGI092	KW	AGA	41	NAD	NS		NAD	none		1+2	NA	EI LSCS	39+2	M	3290	28	475(T)
LGI093	KW	AGA	28	25.8	NS	White	NAD	none		1+2	NA	EI LSCS	39+1	F	3795	81	550(T)
LGI094	RQ	AGA	32	NAD	NS	White	NAD	none		0+1	NA	EI LSCS	39+3	F	3075	21	497(T)
LGI095	RQ	AGA	34	21.5 1	NS	White	NAD	ferrous		1+2	NA	EI LSCS	39+3	M	3603	54	488(T)
LGI096	KT	AGA	36	29.1 7		White	NAD	none		2+3	NA	EI LSCS	39+1	F	3610	68	350(T)
LGI097	LM	SGA	31	NAD		White	NAD	none		0+1		Em LSCS (failed IOL)	37+6	F	1950	<0.4	300(T)

LGI098	LM	SGA	34	15.7	Sm	White	NAD	none		2+4	abn	SVD (IOL for SGA)	37+4	M	2495	1	352(T)
*LGI099	LM	discar ded															
LGI100	LM	SGA									abn						>10th
LGI101	KT	AGA	22	23		White	NAD	none		1+2	NA	EI LSCS	39+1	F	3215	23	382(T)
LGI102	RQ	AGA	31			White	NAD	none				EI LSCS		M	4200		538(T)
LGI103	RQ	AGA	27			White	NAD	none				EI LSCS		M	3586		580(T)
LGI104	KT	AGA	34			other	NAD	none							3265		625(T)
LGI105	KT	AGA	28			White	NAD	none		0+1		EI LSCS	39+4	M	4375	96	599(T)
LGI106	RQ	LGA	39							1+2		EI LSCS	39+1	M	4300	95	746(T)
LGI107	RQ	GDM	28					insulin		2+3		EI LSCS	38+6	M			458(T)
LGI108	MK	AGA	38				NAD	none				EI LSCS		F	3585		505(T)
LGI109	AS	AGA		52													
LGI110	AS	AGA	27		Sm	White	NAD	none		3+3		EI LSCS	39+0	F	3025	17	376(T)

Table 20. Mother and baby details for samples collected in 2018-2020 (ethics: 18/LO/0067)

Key to tables

Excluded samples shown in red (reason for exclusion shown in red), Samples not included in this study but used in other research projects shown in green. *Original copy of consent form not found in patient notes, and therefore sample was destroyed.

Consent taken by Lara Morley (LM), Sara Ibrahim (SI), Maggie Kennedy (MK), Katy Walsh (KW), Kate Timms (KT), Abbie Stead (AS), Nigel Simpson (NS).

Abbreviations used in tables

Headings: consent (Cons), group (Grp), Medical history (Med hx), obstetric history (Obs hx), parity and gravidity at time of consent (P+G), Doppler (Dopp), mode of delivery (MOD), gestation (Gest), birth weight (Birth wt), placenta weight (PI wt), smoking status (Sm)

Not applicable (NA), No abnormality detected (NAD), induction of labour (IOL), miscarriage (misc.), hypertension (HTN), gestational diabetes mellitus (GDM), insulin dependent diabetes mellitus (IDDM), trimmed weight (T), elective lower segment caesarean section (EI LSCS), emergency lower segment caesarean section (Em LSCS), large for gestational age (LGA), smoker (Sm), non-smoker (NS), pregnancy-associated plasma protein A (PAPP-A), SVD (spontaneous vaginal delivery), preterm birth (PTB), group B streptococcus GBS), previous (prev).

